DOCTORAL THESIS

QUALITY-BY-DESIGN APPROACH FOR THE DEVELOPMENT OF LIPID-BASED NANOSYSTEMS FOR ANTI-MYCOBACTERIAL THERAPY

Helena Rouco Taboada

INTERNACIONAL DOCTORAL SCHOOL

DOCTORAL PROGRAM IN DRUG RESEARCH AND DEVELOPMENT

SANTIAGO DE COMPOSTELA

2020

USC
UNIVERSIDADE
DE SANTIAGO
DE COMPOSTELA

TESIS DE DOCTORADO

EMPLEO DE ESTRATEGIAS DE CALIDAD POR DISEÑO PARA EL DESARROLLO DE NANOSISTEMAS BASADOS EN LÍPIDOS PARA TERAPIA ANTIMICOBACTERIANA

Helena Rouco Taboada

ESCUELA DE DOCTORADO INTERNACIONAL

PROGRAMA DE DOCTORADO EN INVESTIGACIÓN Y DESARROLLO DE MEDICAMENTOS

SANTIAGO DE COMPOSTELA

2020

USC
UNIVERSIDADE
DE SANTIAGO
DE COMPOSTELA

PhD CANDIDATE STATEMENT

Quality-by-design approach for the development of lipid-based nanosystems for anti-mycobacterial therapy

Miss Helena Rouco Taboada

I submit my Doctoral thesis, following the procedure according to the Regulation, stating that:

1) This thesis gathers the results corresponding to my work.
2) When applicable, explicit mention is given to the collaborations the work may have had.
3) The present document is the final version submitted for its defense and coincide with the document sent in electronic format.
4) I confirm that this thesis does not incur in any plagiarism of any other authors or documents submitted by me for obtaining other degrees.

Santiago de Compostela, on ……..... 2020

Sgd. Helena Rouco Taboada

USC
UNIVERSIDADE
DE SANTIAGO
DE COMPOSTELA

DECLARACIÓN DEL AUTOR DE LA TESIS

Empleo de estrategias de calidad por diseño para el desarrollo de nanosistemas basados en lípidos para terapia antimicobacteriana

Dña. Helena Rouco Taboada

Presento mi tesis, siguiendo el procedimiento adecuado al Reglamento, y declaro que:

1) La tesis abarca los resultados de la elaboración de mi trabajo.
2) En su caso, en la tesis se hace referencia a las colaboraciones que tuvo este trabajo.
3) La tesis es la versión definitiva presentada para su defensa y coincide con la versión enviada en formato electrónico.
4) Confirmo que la tesis no incurre en plagio de otros autores, ni de trabajos presentados por mí para la obtención de otros títulos.

Santiago de Compostela, a ……de 2020

Fdo. Helena Rouco Taboada

USC
UNIVERSIDADE
DE SANTIAGO
DE COMPOSTELA

AUTHORIZATION OF THE THESIS SUPERVISORS

Quality-by-design approach for the development of lipid-based nanosystems for anti-mycobacterial therapy

Prof. Mariana Landín Pérez, as director and tutor

Prof. María del Carmen Remuñán López, as director

REPORT:

That the present thesis, corresponds to the work carried out by Miss **Helena Rouco Taboada**, under our supervision, and that we authorize its presentation considering that it gathers the necessary requirements of the USC Doctoral Studies Regulation, and that as supervisors of this thesis, it does not incur in the abstention causes established by the Law 40/2015.

According to the Regulation of Doctorate Studies, we also declare that the present doctoral thesis is suitable to be defended on the basis of the Monographic modality with reproduction of publications, in which the participation of the doctoral student was decisive for its elaboration and that the publications correspond to the research plan.

At Santiago de Compostela, on …… 2020

Sgd. Mariana Landín Pérez

Sgd. María de Carmen Remuñán López

USC
UNIVERSIDADE
DE SANTIAGO
DE COMPOSTELA

AUTORIZACIÓN DEL DIRECTOR / TUTOR DE LA TESIS

Empleo de estrategias de calidad por diseño para el desarrollo de nanosistemas basados en lípidos para terapia antimicobacteriana

Dña. Mariana Landín Pérez, como directora y tutora

Dña. María del Carmen Remuñán López, como directora

INFORMAN:

Que la presente tesis, corresponde con el trabajo realizado por Dña. **Helena Rouco Taboada**, bajo nuestra dirección, y autorizamos su presentación, considerando que reúne los requisitos exigidos en el Reglamento de Estudios de Doctorado de la USC, y que como directoras de ésta no incurre en las causas de abstención establecidas en Ley 40/2015.

De acuerdo con lo indicado en el Reglamento de Estudios de Doctorado, declaran también que la presente tesis de doctorado es idónea para ser defendida en base a la modalidad Monográfica con reproducción de publicaciones, en los que la participación de la doctoranda fue decisiva para su elaboración y que las publicaciones se ajustan al plan de investigación.

En Santiago de Compostela, a ……de 2020

Fdo. Mariana Landín Pérez

Fdo. María de Carmen Remuñán López

USC
UNIVERSIDADE
DE SANTIAGO
DE COMPOSTELA

"To live a creative life, we must
lose our fear of being wrong"

Joseph Chilton Pearce

USC
UNIVERSIDADE
DE SANTIAGO
DE COMPOSTELA

ACKNOWLEDGEMENTS/AGRADECIMIENTOS

USC
UNIVERSIDADE
DE SANTIAGO
DE COMPOSTELA

Me gustaría agradecer la contribución de todas aquellas personas que han estado en mi vida durante estos últimos años, y que, de una forma u otra, han aportado su granito de arena para que este trabajo fuese posible:

En primer lugar, me gustaría dar las gracias a mis directoras de tesis por darme esta maravillosa oportunidad. A Mariana Landín por su cercanía, su apoyo desde el momento en el que inicié este camino hasta el día de hoy y por haberme ayudado a crecer durante estos años, tanto desde el punto de vista profesional como personal. A Carmen Remuñán, por su confianza, y sus buenos consejos.

A Patricia, por haber puesto su cerebro a mi disposición durante estos años, por haber sido un auténtico salvavidas para mí en los momentos de crisis y por haber conseguido contagiarme su pasión por este trabajo.

A todos los profesores del Departamento de Farmacología, Farmacia y Tecnología Farmacéutica por su cercanía y amabilidad.

A todos mis compañeros de laboratorio y doctorado, en especial a Estefanía y a Cristina, por los inolvidables momentos compartidos. Como no podría ser de otra forma, me gustaría dar las gracias a todos aquellos que durante estos años han sido mi familia del laboratorio: Lorena, Leticia, Víctor y Jesús. Os agradezco muchísimo vuestro apoyo y amistad, sin vosotros esto no hubiese sido lo mismo.

A Mirian, por su cariño y simpatía, y a Rebeca, por recordarme ese entusiasmo característico de las etapas iniciales de la tesis.

También a Santi y a Alba, por ser el mejor apoyo técnico en el laboratorio que hubiera podido desear.

Al Profesor António Almeida por su gran apoyo, y por darme la oportunidad de realizar una estancia en la Universidad de Lisboa. A Joana Marto, Lídia Gonçalves y, en especial, a Diana Gaspar, por su amabilidad, paciencia y su dedicación.

A Filipa, por hacer que me sintiera como en casa desde el primer día, por enseñarme hasta el último rincón de Lisboa y por hacer que no pasara ni un solo fin de semana aburrido.

A Marta Alonso-Hearn, por acogerme amablemente en el Departamento de Sanidad Animal de Neiker, y a María Canive, por su paciencia y su tiempo.

Y, como también existe vida más allá de trabajo, a Raquel, a María y, de forma especial, a Ana, porque su churrascada anual y nuestros planes del sábado noche son ya toda una institución, y me han ayudado a sobrellevar más de una época dura. También a Nere, porque nuestros viajecillos por España adelante han sido un auténtico oasis en el medio del desierto, y a Clara, por aguantarme desde que entramos en la carrera y por no faltar nunca a nuestra señalada cita anual.

A Jorge, por ser mi mejor amigo y mi soporte fundamental, por estar a mi lado, escucharme y aguantarme cuando nadie más lo hubiese hecho.

A mi familia, en especial a mis padres, Luís y Eva, por su gran paciencia, sus consejos, su sentido del humor, su cariño y por todas las oportunidades que me han proporcionado a lo largo de todos estos años. También a Sara, por su alegría contagiosa. Y, por último, pero no menos importante, a Jose, sin él este trabajo seguro que no habría sido posible porque todavía seguiría estudiando fisicoquímica.

¡Muchas gracias a todos!

TABLE OF CONTENT

USC
UNIVERSIDADE
DE SANTIAGO
DE COMPOSTELA

LIST OF ABBREVIATIONS

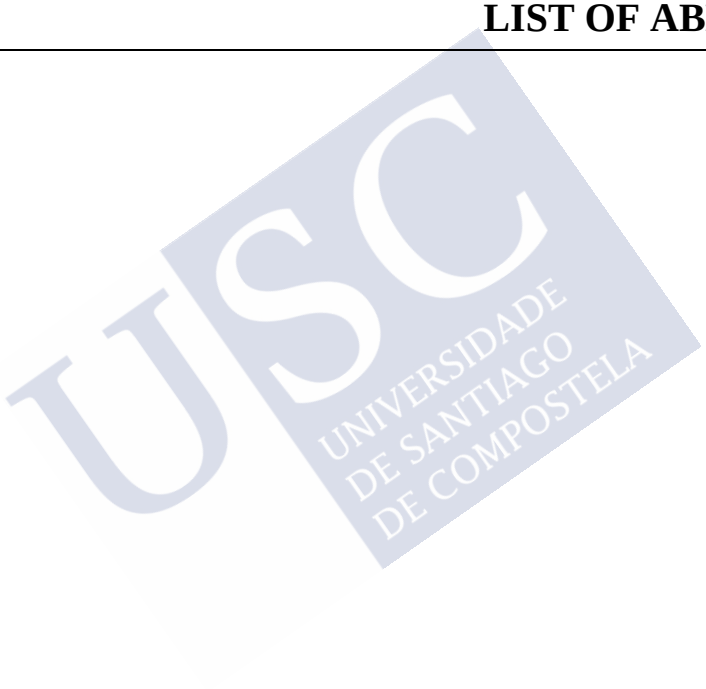

USC
UNIVERSIDADE
DE SANTIAGO
DE COMPOSTELA

Act-NLC: Acitretin-loaded nanostructured lipid carriers/Transportadores lipídicos nanoestructurados cargados con acitretina

AFM: Atomic force microscopy/Microscopía de fuerza atómica

AI: Artificial Intelligence/Inteligencia Artificial

ANN: Artificial Neural Networks/Redes Neuronales Artificiales

ANOVA: Analysis of variance/Análisis de varianza

C: Carbon atoms/Átomos de carbono

C6: Coumarin 6/Cumarina 6

CD: Crohn's disease/Enfermedad de Crohn

CDAI: Crohn´s Disease Active Index/Índice de Actividad de la Enfermedad de Crohn

CFU: Colony forming units/Unidades formadoras de colonias

CP: Cryoprotectant/Crioprotector

CPs: Cryoprotectants/Crioprotectores

Cryo-FESEM: Cryo field emission scanning electron microscopy/Criomicroscopía electrónica de barrido de emisión de campo

DL: Drug loading/Carga de fármaco

DLS: Dynamic light scattering/Dispersión dinámica de luz

DMEM: Dulbecco´s modified Eagle´s medium/Medio Eagle modificado de Dulbecco

DMSO: Dimethyl sulfoxide/Dimetilsulfóxido

DSC: Differential scanning calorimetry/Calorimetría diferencial de barrido

DNA: Deoxyribonucleic acid/Ácido desoxirribonucleico

EE: Encapsulation efficiency/Eficiencia de encapsulación

FBS: Foetal bovine serum/Suero fetal bovino

FTIR: Fourier-transform infrared spectroscopy/Espectroscopía de infrarrojos por transformada de fourier

GAMA: Gas-assisted melting atomization/Atomización por fusión asistida por gas

GI: Gastrointestinal

GRAS: Generally regarded as safe/Generalmente reconocido como seguro

HIV: Human Immunodeficiency Virus/Virus de la Inmunodeficiencia Humana

HLB: Hydrophilic-lipophilic balance/Balance hidrofílico-lipofílico

HPLC: High performance liquid chromatography/Cromatografía líquida de alta resolución

HSH: Hot high shear homogenization/Homogenización a alta cizalla en caliente

IC_{50}: Inhibitory concentration 50/Concentración inhibitoria 50

LD: Laser difraction/Difracción láser

LL: Liquid Lipid/Lípido líquido

LN: Lipid nanoparticles/Nanopartículas lipídicas

LP: Lyophilized Powders/Polvos liofilizados

MAC: *Mycobacterium avium complex*

MAP: *Mycobacterium avium paratuberculosis*

MAPUS: MAP US study/Estudio estadounidense de MAP

MAs: Mycolic acids/Ácidos micólicos

MD: Membership degree/Grado de pertenencia

α-MEM: Minimum essential media/Medio mínimo esencial

MGIT: Mycobacterial growth indicator tubes/Tubos indicadores de crecimiento micobacteriano

MIC: Minimum inhibitory concentration/Concentración mínima inhibitoria

MW: Molecular weight/Peso molecular

MWCO: Molecular weight cut off/Corte de peso molecular

MW_{CP}: Cryoprotectant´s molecular weight/ Peso molecular del crioprotector

NFL: Neurofuzzy logic/Lógica neurodifusa

NLC: Nanostructured lipid carriers/Transportadores lipídicos nanoestructurados

OA: Oleic acid/Ácido oleico

OADC: Oleic acid-albumin-dextrose-catalase/Ácido oleico-albúmina-dextrosa-catalasa

O/F/W: Oil-in-solid fat-in-water/Aceite-en-grasa sólida-en-agua

O/W: Oil-in-water/Aceite-en-agua

Papp: Apparent permeability coefficient/Coeficiente de permeabilidad aparente

PBS: Phosphate buffered saline/Tampón fosfato salino

PCR: Polymerase chain reaction/Reacción en cadena de la polimerasa

PCS: Photon correlation spectroscopy/Espectroscopía de correlación fotónica

PDI: Polydispersity index/Índice de polidispersión

P-gp: Glycoprotein-P/Glicoproteína-P

PLGA: Poly (lactic-co-glycolic acid)/Ácido poli (láctico-co-glicólico)

PMA: Phorbol 12-myristate 13-acetate/Forbol 12-miristato 13-acetato

QbD: Quality by design/Calidad por diseño

RFB: Rifabutin/Rifabutina

RPM: Revolutions per minute/Revoluciones por minuto

RPMI 1640: Roswell park memorial institute 1640 medium/Medio 1640 Roswell park memorial institute

SEM: Scanning electron microscopy/Microscopía electronica de barrido

SCF: Supercritical fluid/Fluido supercrítico

SCFEE: Supercritical fluid extraction of emulsions/Extracción de emulsiones por fluidos supercríticos

SIF: Simulated intestinal fluid/Fluido intestinal simulado

SiRNA: Small interfering ribonucleic acid/Ácido ribonucleico pequeño de interferencia

SLN: Solid Lipid Nanoparticles/Nanopartículas Lipídicas Sólidas

SP: Spirololactone/Espironolactona

TB: Tuberculosis

TEER: Transepithelial electric resistance/Resistencia eléctrica transepitelial

TEM: Transmission electron microscopy/Microscopía electronica de transmisión

Tg: Glass transition temperature/Temperatura de transición vítrea

Tg´: Glass transition temperature of the maximum cryo-concentrated solution/Temperatura de transición vítrea de la solución de máxima crio-concentración

TNF: Tumor necrosis factor/Factor de necrosis tumoral

TOF SIMS Static time-of-flight secondary ion mass spectrometry/Espectrometría de masas de iones secundarios de tiempo de vuelo estático

TTD: Time to detection/Tiempo de detección

USP: United States Pharmacopeia/Farmacopea Estadounidense

UV: Ultraviolet/Ultravioleta

WHO: World Health Organization/Organización mundial de la salud

W/O: Water-in-oil/Agua-en-aceite

W/O/W: Water-in-oil-in-water/Agua-en-aceite-en-agua

XPS: X-ray photoelectron spectroscopy/Espectroscopía de fotoelectrones emitidos por rayos X

XRD: X-ray diffraction/Difracción de rayos X

ZP: Zeta potential/Potencial zeta

II: Osmolarity/Osmolaridad

ABSTRACT/RESUMEN

USC
UNIVERSIDADE
DE SANTIAGO
DE COMPOSTELA

ABSTRACT

One of the main obstacles in the development and usage of numerous drugs is their reduced aqueous solubility, which greatly limits their bioavailability and, therefore, their clinical applicability. An example of the limitations associated to poorly soluble drugs is the anti-mycobacterial therapy of Crohn's Disease, which objective is the treatment of infections caused by *Mycobacterium avium paratuberculosis* (MAP). The increasing evidence of the involvement of this pathogen in the development of the disease, led to the evaluation of the effectiveness of a triple anti-mycobacterial therapy. Nevertheless, limited results were obtained with this approach, which can be associated with bioavailability issues derived from the reduced aqueous solubility of these drugs.

The development of Nanostructured Lipid Carriers (NLC) is an interesting strategy to increase the solubility of drugs, but their presence in the market is still limited, undoubtedly due to the difficulties encountered at different stages of their development and to reproducibility issues.

In this context, the aim of this work is focused on the rational design and development, through a robust and reproducible formulation procedure, of an NLC formulation that allows rifabutin (RFB) release, an anti-mycobacterial hydrophobic drug model, within intestinal macrophages, where MAP has been reported to establish a persistent infection.

On this purpose, the effect of different variables, such as the proportions of the different formulation components or the homogenization speed, over the characteristics of the resulting NLCs was analyzed, using Artificial Intelligence (AI) tools such as Neurofuzzy Logic. A two-step experimental design was carried out. The objective of the first step was to delimit the knowledge space of NLC, using a wide range of experimental variables. The second step was performed within a narrower range of experimental variables, in order to define the design space of the system.

An optimization process assisted by AI tools, such as Artificial Neural Networks and Genetic algorithms was also carried out, making possible the estimation of the optimal formulation parameters. This process allowed for the obtention an NLC formulation with a reduced size and size distribution, negative zeta potential, a suitable RFB payload, a spheroidal morphology, and a good stability.

The ability of the optimal NLC formulation to provide a selective drug release within the intestinal macrophages was evaluated. Results revealed that RFB-loaded NLC exhibit promising features in terms of permeability through Caco-2 cell monolayers, macrophage internalization, biocompatibility, and selective drug release in intracellular medium. Furthermore, the information gathered from these assays suggests that the administration of these nanosystems would allow for the achievement of an effective RFB dose inside the intestinal macrophages.

Finally, the transformation of NLC dispersions into solid dosage forms through a lyophilization process was performed in order to facilitate the oral administration of the developed nanocarriers. On this purpose, Neurofuzzy Logic was also employed to analyze the impact of different lyophilization conditions, such as freezing rate, cryoprotectants selected or their concentration and characteristics, over the properties exhibited by the achieved dried

products. The information gathered from this study enabled a better understanding of the physicochemical phenomena driving lyophilization process and cryoprotectants mechanism of action. On the other hand, this information also allowed for the obtention of lyophilized products exhibiting suitable characteristics, including a good maintenance of NLC formulations initial properties.

Overall, it is necessary to highlight that outcomes of this work revealed the great potential of the NLC formulations developed for the treatment of intracellular infections, such as those produced by MAP in Crohn´s disease. Furthermore, the usefulness of AI tools on the development of nanoparticulated systems, as NLC, from the initial stages of their design, to their conversion into a solid dosage form, has also been proven.

RESUMEN

Uno de los principales obstáculos en el desarrollo y empleo de un gran número de fármacos, es su reducida solubilidad acuosa, que limita en gran medida su biodisponibilidad y, por lo tanto, su aplicación clínica. Un ejemplo de ello es la terapia anti-micobacteriana de la enfermedad de Crohn, cuyo objetivo es el tratamiento de las infecciones causadas por *Mycobacterium avium paratuberculosis* (MAP). La creciente evidencia de la implicación de este patógeno en el desarrollo de la enfermedad, condujo a la evaluación de la efectividad de una triple terapia anti-micobacteriana. Esta aproximación terapéutica dio lugar a unos resultados limitados, lo que podría deberse a problemas de biodisponibilidad derivados de la reducida hidrosolubilidad de estos fármacos.

El desarrollo de Portadores de Lípidos Nanoestructurados (NLC) constituye una estrategia interesante para incrementar la solubilidad de los fármacos, pero su presencia en el mercado aún es limitada, sin duda por las dificultades encontradas en las diferentes etapas de su desarrollo y a problemas de reproducibilidad.

Por ello, el objetivo de este trabajo se centra en el diseño racional y en el desarrollo, a través de un procedimiento de formulación robusto y reproducible, de una formulación de NLC que permita la liberación de rifabutina (RFB), un fármaco anti micobacteriano hidrofóbico modelo, en el interior de los macrófagos intestinales, donde MAP establece infecciones persistentes.

Con este fin, se llevó a cabo un análisis del efecto de diferentes variables, como las proporciones de los diferentes componentes de las formulaciones o la velocidad de homogenización, sobre las características de los NLC resultantes, empleando herramientas de Inteligencia Artificial (AI), como la Lógica Neurodifusa. Se llevó a cabo un diseño experimental en dos etapas. El objetivo de la primera consistió en delimitar el espacio de conocimiento de los NLC, empleando un amplio rango de las variables. A continuación, en función de los resultados se llevó a cabo una segunda etapa, en la que se utilizaron rangos de las variables más reducidos, con el objetivo de definir el espacio de diseño de los NLC.

A continuación, se realizó un proceso de optimización, con ayuda de otras herramientas de AI, como las Redes Neuronales Artificiales y los Algoritmos genéticos, que posibilitaron la estimación de los parámetros óptimos de formulación. Esto permitió la obtención de una formulación de NLC con un tamaño y una dispersión de tamaños reducidos, potencial zeta negativo, una adecuada carga de RFB, una morfología esferoidal y una buena estabilidad.

Se evaluó la capacidad de las formulaciones de NLC optimizadas para proporcionar una liberación selectiva de fármaco en el interior de los macrófagos intestinales. Los resultados obtenidos mostraron que los NLC cargados con RFB presentan características prometedoras en términos de permeabilidad a través de monocapas de células Caco-2, internalización por parte de macrófagos, biocompatibilidad y liberación selectiva de fármaco en medio intracelular. La información adquirida a través de estos ensayos sugiere que la administración de estos nanosistemas conduciría a la obtención de una dosis efectiva de RFB en el interior de los macrófagos intestinales.

Por último, se llevó a cabo la transformación de las dispersiones de NLC en formas de dosificación sólidas, mediante un proceso de liofilización, con el propósito de facilitar su administración por vía oral. Con este fin, se empleó de nuevo la Lógica Neurodifusa para

analizar el impacto de diferentes condiciones de liofilización, como la velocidad de congelación, los crioprotectores empleados o su concentración y sus características, sobre las propiedades de los productos obtenidos. La información derivada de este estudio permitió una mayor comprensión de los fenómenos fisicoquímicos existentes tras el proceso de liofilización y el mecanismo de acción de los crioprotectores. Por otra parte, esta información permitió también la obtención de productos liofilizados con propiedades adecuadas, incluyendo un buen mantenimiento de las propiedades iniciales de las formulaciones de NLC.

Como conclusión, cabe destacar que los resultados obtenidos en este trabajo han demostrado el gran potencial de las formulaciones de NLC desarrolladas para el tratamiento de infecciones intracelulares, como las producidas por MAP en la enfermedad de Crohn. Asimismo, se ha comprobado la utilidad de las herramientas de AI en el desarrollo de sistemas nanoparticulados como los NLC, desde las etapas iniciales de su diseño, hasta su conversión en una forma de dosificación sólida.

RESUMO

Un dos principais obstáculos no desenvolvemento e emprego dun gran número de fármacos, é a súa reducida solubilidade acuosa, que limita en gran medida a súa biodispoñibilidade e, polo tanto, a súa aplicación clínica. Un exemplo disto é a terapia anti-micobacteriana da enfermidade de Crohn, cuxo obxectivo é o tratamento das infeccións causadas por *Mycobacterium avium paratuberculosis* (MAP). A crecente evidencia da implicación deste patóxeno no desenvolvemento da enfermidade, conduciu á avaliación da efectividade dunha triple terapia anti-micobacteriana. Esta aproximación terapéutica deu lugar a uns resultados limitados, o que podería deberse a problemas de biodispoñibilidade derivados da reducida hidrosolubilidade destes fármacos.

O desenvolvemento de Portadores de Lípidos Nanoestructurados (NLC) é unha estratexia interesante para incrementar a solubilidade dos fármacos, pero a súa presenza no mercado aínda é limitada, sen dúbida polas dificultades atopadas nas diferentes etapas do seu desenvolvemento e a problemas de reproducibilidade.

Por iso, o obxectivo deste traballo céntrase no deseño racional e no desenvolvemento, a través dun procedemento de formulación robusto e reproducible, dunha formulación de NLC que permita a liberación de rifabutina (RFB), un fármaco anti-micobacteriano hidrofóbico modelo, no interior dos macrófagos intestinais, onde MAP establece infeccións persistentes.

Con este fin, levouse a cabo unha análise do efecto de diferentes variables, como as proporcións dos diferentes compoñentes das formulacións ou da velocidade de homoxenización, sobre as características dos NLC resultantes, empregando ferramentas de Intelixencia Artificial (AI), como a Lóxica Neurodifusa. Levouse a cabo un deseño experimental en dúas etapas. O obxectivo da primeira consistiu en delimitar o espazo de coñecemento dos NLC, empregando un amplo rango das variables. A continuación, en función dos resultados levouse a cabo unha segunda etapa, na que se utilizaron rangos das variables máis reducidos, co obxectivo de definir o espazo de deseño dos NLC.

A continuación, realizouse un proceso de optimización, con axuda doutras ferramentas de AI, como as Redes Neuronais Artificiais e os Algoritmos xenéticos, que posibilitaron a estimación dos parámetros óptimos de formulación. Isto permitiu a obtención dunha formulación de NLC cun tamaño e unha dispersión de tamaños reducidos, potencial zeta negativo, unha adecuada carga de RFB, unha morfoloxía esferoidal e unha boa estabilidade.

Avaliouse a capacidade das formulacións de NLC optimizadas para proporcionar unha liberación selectiva de fármaco no interior dos macrófagos intestinais. Os resultados obtidos mostraron que os NLC cargados con RFB presentan características prometedoras en termos de permeabilidade a través de monocapas de células Caco-2, internalización por parte de macrófagos, biocompatibilidade e liberación selectiva de fármaco no medio intracelular. A información adquirida a través destes ensaios suxire que a administración destes nanosistemas conduciría á obtención dunha dose efectiva de RFB no interior dos macrófagos intestinais.

Por último, levouse a cabo a transformación das dispersións de NLC en formas de dosificación sólidas, mediante un proceso de liofilización, co propósito de facilitar a súa administración por vía oral. Con este fin, empregouse de novo a Lóxica Neurodifusa para analizar o impacto de diferentes condicións de liofilización, como a velocidade de conxelación,

os crioprotectores empregados, ou a súa concentración e as súas características, sobre as propiedades dos produtos obtidos. A información derivada deste estudo permitiu unha maior comprensión dos fenómenos fisicoquímicos existentes tras o proceso de liofilización e o mecanismo de acción dos crioprotectores. Por outra banda, esta información permitiu tamén a obtención de produtos liofilizados con propiedades adecuadas, incluíndo un bo mantemento das propiedades iniciais das formulacións de NLC.

Como conclusión, cabe destacar que os resultados obtidos neste traballo demostraron o gran potencial das formulacións de NLC desenvolvidas para o tratamento de infeccións intracelulares, como as producidas por MAP na enfermidade de Crohn. Así mesmo, comprobouse a utilidade das ferramentas de AI no desenvolvemento de sistemas nanoparticulados como os NLC, desde as etapas iniciais do seu deseño, até a súa conversión nunha forma de dosificación sólida.

RESUMO *IN EXTENSO*

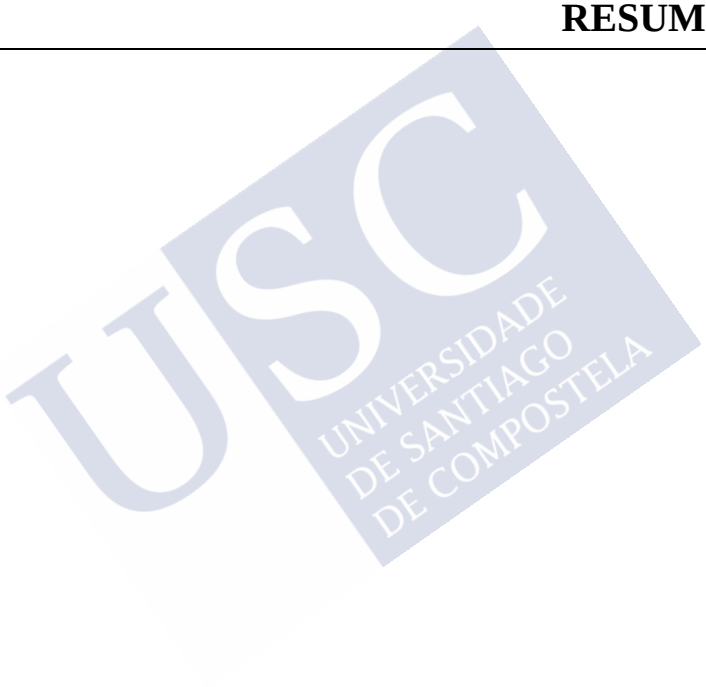

USC
UNIVERSIDADE
DE SANTIAGO
DE COMPOSTELA

1. INTRODUCIÓN

A reducida hidrosolubilidade de moitos fármacos e candidatos a fármaco limita, en gran medida, a súa absorción e biodispoñibilidade, condicionando o desenvolvemento e emprego en clínica de numerosos compostos potencialmente interesantes (1). A terapia anti-micobacteriana da enfermidade de Crohn (CD), unha coñecida enfermidade inflamatoria intestinal, constitúe un exemplo das limitacións asociadas a esta baixa hidrosolubilidade de determinados compostos activos. Este enfoque terapéutico está orientado á erradicación de *Mycobacterium avium paratuberculosis* (MAP), unha micobacteria cada vez máis relacionada co desenvolvemento desta doenza (2), que establece infeccións persistentes no interior dos macrófagos intestinais (3). Ata a data, obtivéronse resultados prometedores co emprego combinado de fármacos anti-micobacterianos, como a rifabutina, a claritromicina e a clofazimina, en termos de remisión da enfermidade a longo prazo ou cicatrización da mucosa intestinal (4). Con todo, estes datos non aportaron evidencia suficiente para a inclusión destes compostos en diversas guías de práctica clínica, coma a europea, a estadounidense ou a británica (5). Algúns autores sinalaron á reducida hidrosolubilidade, elevada lipofilia e, coma consecuencia, aos problemas de biodispoñibilidade destes compostos, coma potencial causa da limitación na súa utilidade clínica (6-8).

Na actualidade, existen diferentes alternativas para resolver os problemas asociados á limitada hidrosolubilidade dos fármacos, coma a elaboración de nanoemulsións, micelas poliméricas, nanocristais de fármaco ou nanopartículas (1). Estas estratexias están baseadas na redución do tamaño de partícula ao rango nanométrico, o que permite obter un aumento considerable da solubilidade e da velocidade de disolución debido ao incremento na área superficial (9). Ademais, o emprego de nanopartículas como vehículo dos compostos anti-MAP, podería reportar beneficios adicionais, coma unha menor incidencia de efectos adversos e fenómenos de resistencia a antibióticos (10, 11), debido á súa capacidade para dirixir os fármacos a determinados tipos celulares, coma os macrófagos intestinais (9, 10).

Entre a gran variedade existente de sistemas nanoparticulados, as nanopartículas lipídicas (LN) destacan por ser sistemas coloidais biodegradables, cunha boa capacidade para cargar fármacos hidrofóbicos e para levar a cabo unha liberación controlada destes a través de diversas vías de administración (12-14). Actualmente, poden distinguirse dúas xeracións de LN, a primeira, coñecida coma nanopartículas lipídicas sólidas (SLN), e a segunda, constituída polos transportadores lipídicos nanoestruturados (NLC) (15, 16). Ambos tipos de LN están compostos por lípidos estabilizados por unha capa de tensioactivos, pero diferéncianse na introdución dun lípido líquido na matriz dos NLC (16). Esta pequena innovación demostrou ser de gran utilidade para mellorar a capacidade de carga de fármacos e a estabilidade dos NLC, con respecto aos SLN (15, 16).

Ambos tipos de LN poden elaborarse a partir dunha gran variedade de procedementos, entre os que se distinguen os métodos de alta enerxía (como a homoxeneización a alta presión), métodos de baixa enerxía (como a inversión de fases) e procedementos que inclúen o emprego de disolventes orgánicos (coma o método de emulsificación-evaporación) (17, 18). Tamén, en función do procedemento de formulación e dos materiais de partida empregados, é posible modificar a localización do fármaco na matriz lipídica, o que posibilita a obtención de perfís de

liberación inmediata ou sostida (17, 19), en función das necesidades terapéuticas, convertendo ás LN en sistemas de administración de fármacos cunha gran versatilidade.

Non obstante, a pesar do gran potencial destes nanosistemas, a súa presenza no mercado redúcese ao campo da nutrición, os nutracéuticos e, especialmente, ao sector cosmético, no que se comercializaron máis de 25 formulacións de LN (20). Respecto ás LN elaboradas con fins terapéuticos, é necesario mencionar que, a pesar dos numerosos ensaios preclínicos levados a cabo ata a data con este tipo de sistemas, a súa presenza en ensaios clínicos é actualmente escasa e limítase a dúas únicas vías de administración, a oral e la tópica. Esta lenta tradución do traballo realizado no campo das LN, en ensaios clínicos e produtos comercializados coincide, en gran medida, coa condición actual da maioría dos sistemas nanoparticulados (21). Esta situación podería estar relacionada coa aparición de dificultades nas diferentes etapas do desenvolvemento destes complexos sistemas (21), facendo necesaria a aplicación de novas estratexias, como as baseadas na calidade por deseño (QbD). Estas aproximacións posibilitarían un deseño racional dos nanosistemas e a obtención de procedementos de manufactura reproducibles, o que axilizaría en gran medida a comercialización das formulacións.

Dentro das estratexias baseadas na QbD, a Intelixencia Artificial (AI) espertou un interese crecente nos últimos anos no sector farmacéutico. Ferramentas de AI como a lóxica neurodifusa (NFL), os algoritmos xenéticos ou as redes neuronais artificiais (ANN), foron aplicadas con éxito na optimización de diversos procesos farmacéuticos, coma o desenvolvemento de hidroxeles, formulacións de compresión directa ou micropartículas (22-24).

2. OBXECTIVOS

Partindo dos antecedentes anteriormente expostos, o presente traballo ten por obxectivo a obtención, a través dun procedemento simple e reproducible, dunha formulación de NLC que permita a liberación de RFB, un fármaco anti-micobacteriano hidrofóbico modelo, no interior dos macrófagos intestinais.

No marco deste obxectivo xeral, establecéronse os seguintes obxectivos específicos:

1. Avaliar a idoneidade de ferramentas de Intelixencia Artificial, coma a NFL, para analizar o efecto da composición e as condicións de formulación sobre as características dos NLC cargados con RFB (**Capítulo I**).
2. Analizar a aplicabilidade de ferramentas de Intelixencia Artificial (coma as ANN e os algoritmos xenéticos) para proporcionar unha estimación das condicións óptimas de formulación necesarias para a obtención de NLC cun tamaño nanométrico monodisperso e unha adecuada capacidade de carga de RFB (**Capítulo I**).
3. Verificar a robustez do proceso de optimización levado a cabo a través da caracterización fisicoquímica dos NLC obtidos (**Capítulos I e II**).
4. Analizar o perfil de liberación, o comportamento térmico e a morfoloxía dos NLC, así coma do comportamento *in vitro* en cultivos celulares das formulacións desenvolvidas en termos de biocompatibilidade, permeabilidade e captación celular (**Capítulo II**).

5. Valorar a aplicabilidade da NFL para adquirir unha mellor comprensión do impacto das condicións empregadas para a liofilización dos NLC sobre as propiedades finais dos pos liofilizados (LP) (**Capítulo III**).
6. Estudar os fenómenos fisicoquímicos existentes tras o proceso de liofilización e a eficacia crioprotectora dos azucres (**Capítulo III**).
7. Obter LP con propiedades adecuadas para a súa administración por vía oral, fácilmente re-dispersables e que mostren un elevado mantemento das propiedades iniciais dos NLC (**Capítulo III**).

3. MATERIAIS E MÉTODOS

3.1. FORMULACIÓN E CARACTERIZACIÓN DOS NLC

As formulacións de NLC leváronse a cabo mediante homoxeneización a alta cizalla en quente con axuda dun Ultra-Turrax T25 (IKA Labortechnik, Alemaña). Os materiais de partida empregados foron ácido oleico e Precirol® ATO 5, como lípidos líquido e sólido, respectivamente, xunto con Epikuron® 145 V (lecitina de soia) e Tween® 80, como tensioactivos.

A determinación do tamaño e do potencial zeta das formulacións levouse a cabo mediante dispersión dinámica de luz (DLS) e anemometría de dispersión láser, respectivamente, nun Zetasizer Nano ZS (Malvern Instruments, Reino Unido). As medidas foron realizadas a 25±1°C, tras a adecuada dilución das mostras en auga Milli-Q®.

A análise morfolóxica dos NLC levouse a cabo mediante dúas técnicas diferentes: microscopía electrónica de transmisión (TEM) e microscopía de forza atómica (AFM). No caso da análise TEM, as suspensións de NLC foron previamente tinxidas con acetato de uranilo, mentres que o estudo de AFM se realizou empregando un modo de non contacto, tras o secado das mostras con nitróxeno.

A eficiencia de encapsulamento (EE) e a capacidade de carga (DL) de RFB dos NLC foi determinada mediante cromatografía líquida de alta resolución (HPLC), tras a súa separación do fármaco non encapsulado empregando membranas de diálise (MWCO 3.5 KDa) ou columnas de cromatografía de exclusión de tamaño Sephadex G-25/PD-10 (GE Healthcare Life Sciences, EE. UU.). A extracción do fármaco encapsulado levouse a cabo mediante a rotura dos nanosistemas con acetonitrilo.

A análise do perfil de liberación *in vitro* do fármaco a partir dos NLC desenvolvidos realizouse en celas de Franz termostatizadas a 37°C, empregando dous medios simulados diferentes: fluído intestinal simulado (SIF) e fluído intracelular simulado. Mentres que o primeiro foi preparado segundo os estándares de la farmacopea americana (USP), o segundo obtívose mediante lise de macrófagos murinos (Raw 264.7, ATCC, EE. UU.). A tempos predeterminados, tomáronse mostras do compartimento receptor das celas, e a cuantificación do fármaco liberado levouse a cabo mediante HPLC.

A resistencia térmica dos NLC desenvolvidos avaliouse mediante DLS empregando o Zetasizer Nano ZS. Para isto, tras a adecuada dilución das partículas con auga Milli-Q®, a suspensión foi sometida a un ciclo de quentamento-arrefriamento (25-80°C, 80-25°C), durante o cal se realizaron medicións do tamaño de partícula cada 0.5°C.

3.2. MODELADO MEDIANTE FERRAMENTAS DE INTELIXENCIA ARTIFICIAL

No desenvolvemento deste traballo empregáronse tres programas de Intelixencia Artificial diferentes: Dataform® v3.1, FormRules® v4.03 e INForm® v5.01 (Intelligensys Ltd, Reino Unido). Dataform® v3.1 empregouse no establecemento de algún dos deseños experimentais do traballo. FormRules® v4.03, un programa que integra ANN e lóxica difusa (25), utilizouse para determinar o efecto de diferentes variables nos resultados dos procesos farmacéuticos analizados. Finalmente, INForm® v5.01, un programa que combina ANN e algoritmos xenéticos (23), foi empregado no proceso de optimización dos procedementos farmacéuticos estudados.

A calidade dos modelos obtidos mediante FormRules® e INForm® foi analizada mediante os coeficientes de determinación (R^2), que permitiron avaliar a capacidade de predición e as análises de varianza (ANOVA) que permitiron avaliar a exactitude (22).

3.3. ESTUDOS CELULARES *IN VITRO*

A biocompatibilidade das formulacións de NLC desenvolvidas determinouse en macrófagos derivados da liña monocítica humana THP-1 (ATCC, EE. UU.). Para isto, as células foron expostas durante 24 horas a diferentes concentracións de NLC no rango de 0.3-0.03 mg/ml de nanopartículas. Transcorrido este período de incubación, levouse a cabo o ensaio de proliferación celular WST-1 (Roche, Suíza) de acordo coas instrucións propostas polo fabricante, e determinouse a viabilidade celular como porcentaxe con respecto ao control correspondente.

A internalización dos nanosistemas avaliouse tamén en macrófagos humanos empregando NLC marcadas fluorescentemente con cumarina 6 (C6), seguindo aproximacións de tipo cualitativo e cuantitativo. No caso da aproximación cuantitativa, as formulacións de NLC foron incubadas cos macrófagos durante 2 horas, previa determinación da fluorescencia inicial a t_0 nun lector de placas (Fluostar Optima, BMG Labtech, Germany). Transcorrido este tempo, retiráronse as mostras, lisáronse as células e mediuse a fluorescencia post-lise. A internalización dos NLC determinouse a partir do cociente entre a fluorescencia post-lise e a fluorescencia inicial. A aproximación cualitativa levouse a cabo mediante microscopía confocal, tras a tinción do núcleo e o citoplasma dos macrófagos con ProLong® Gold Antifade con DAPI e Alexa Fluor™ 647 faloidina, respectivamente.

Avaliouse tamén a permeabilidade dos NLC a través de monocapas de células Caco-2 (ATCC, EE. UU.). Para isto, as células foron sementadas en insertos de cultivo celular Corning® Transwell® (Corning, EE. UU). Antes de proceder co experimento determinouse a resistencia eléctrica transepitelial para comprobar a correcta formación dunha monocapa intacta. O ensaio levouse a cabo mediante a adición de NLC cargadas con RFB e marcadas fluorescentemente con C6 no compartimento dador. A tempos predeterminados retiráronse mostras do compartimento aceptor, e a súa fluorescencia determinouse no lector de placas. Os resultados obtidos empregáronse para estimar a concentración de RFB incluída nos NLC presentes no compartimento aceptor a diferentes tempos, xunto coa súa permeabilidade aparente (P_{app}).

3.4. LIOFILIZACIÓN E RECONSTITUCIÓN DAS SUSPENSIÓNS DE NLC E DETERMINACIÓN DA OSMOLARIDADE

A liofilización das suspensións de NLC levouse a cabo nun liofilizador Telstar LyoQuest Plus -85°C/ECO (Telstar, España), durante 24 horas, mantendo a cámara nunhas condicións de temperatura e presión de, aproximadamente, -70°C e 0.01 milibares. A liofilización dos NLC levouse a cabo sen compostos engadidos, e tamén tras a adición de diferentes azucres crioprotectores (CPs) (trehalosa, glucosa, sacarosa, lactosa, sorbitol, manitol e fructosa). As concentracións de crioprotector empregadas oscilaron entre o 2.5 e o 20%, excepto no caso da lactosa e do manitol, para os que se avaliaron concentracións do 2.5 ao 10% e do 2.5 ao 15%, respectivamente.

Os produtos liofilizados obtidos foron reconstituidos en auga Milli-Q®. A súa redispersión realizouse mediante homoxeneización manual, seguida dunha sonicación de 30 segundos empregando un Sonicator 700W Sonic Dismembrator (Fisher Scientific, EE. UU.).

As determinacións de osmolaridade das dispersións de NLC, auga Milli-Q® e as solucións acuosas dos distintos crioprotectores estudados ás concentracións avaliadas realizáronse nun osmómetro de presión de vapor Vapro® (modelo 5600, Wescor ELITechGroup, EE. UU.).

4. RESULTADOS E DISCUSIÓN

4.1. CAPÍTULO I: DELIMITANDO O ESPAZO DE COÑECEMENTO E DESEÑO DOS TRANSPORTADORES LIPÍDICOS NANOESTRUTURADOS MEDIANTE FERRAMENTAS DE INTELIXENCIA ARTIFICIAL

O primeiro paso no desenvolvemento das formulacións de NLC cargadas con RFB consistiu na elección dos materiais e do procedemento de formulación máis axeitados. Para isto, seleccionáronse como compoñentes da matriz lipídica o ácido oleico (lípido líquido, LL) e o Precirol® ATO 5 (lípido sólido), debido á súa ampla utilización, e ao seu status GRAS (xeralmente recoñecido como seguro) (26, 27). Tamén, se seleccionaron o Tween® 80 e o Epikuron® 145 V (lecitina) como tensioactivos, co obxecto de combinar os efectos de estabilización por mecanismos non iónicos e iónicos exercidos, respectivamente, por estes dous compostos (28, 29). Por último, empregouse a RFB como fármaco anti-micobacteriano hidrofóbico modelo. Respecto ao procedemento de formulación, optouse pola homoxeneización a alta cizalla en quente, debido, principalmente, á súa simplicidade (18), que facilitará, previsiblemente, o seu escalado a nivel industrial.

Unha vez seleccionados os compoñentes e o método de formulación máis adecuados, empregouse FormRules®, un software de NFL (23), para estudar o efecto das diferentes variables do proceso de formulación sobre as propiedades dos NLC obtidos. Este estudo levouse a cabo mediante un deseño experimental en dúas etapas. A primeira delas destinouse a definir o "espazo de coñecemento" dos NLC cargados con RFB. Para isto, analizouse o efecto de 4 variables experimentais (velocidade de homoxeneización e porcentaxes de RFB, LL e Tween® 80 empregados), sobre o tamaño, a distribución de tamaños e o potencial zeta (ZP), utilizando un amplo rango de velocidades e concentracións (**Táboa 3.1**). Neste caso, o tamaño e a distribución de tamaños dos NLC resultantes expresáronse en función do diámetro medio e da porcentaxe do pico 1 (pico máis pequeno obtido, excluíndo os asociados a micelas de

tensioactivo), debido a que la elevada dispersión dos nanosistemas obtidos (**Táboa 3.4**) non permitiu o emprego dos parámetros habituais.

Os modelos de NFL obtidos para o tamaño e a porcentaxe do pico 1 mostraron valores de R^2 superiores ao 70% e valores de f calculados superiores aos críticos (**Táboa 3.3**), o que indica unha elevada capacidade preditiva e un bo funcionamento do modelo, respectivamente (23). Non obstante, o programa non permitiu a obtención dun modelo adecuado para o ZP, debido á similitude existente entre os resultados obtidos para este parámetro.

De acordo con estes modelos, o diámetro medio do pico 1 dos NLC, veríase afectado pola interacción entre a proporción de Tween® 80 e a velocidade de homoxeneización. Mentres que esta mesma interacción, xunto coa proporción de RFB empregada condicionaría as porcentaxes do pico 1 obtidos (**Táboa 3.3**). A influencia destes parámetros podería estar relacionada coa formación de escuma producida por un exceso de tensioactivo e axitación, así como pola adición dun exceso de fármaco, que dificultaría a correcta formación dos nanosistemas. Considerando a información proporcionada polas regras "SI-ENTÓN" extraídas a partir dos modelos (ver **Anexo I**), pode afirmarse que o "espazo de coñecemento" dos NLC cargados con RFB, se caracterizaría polo emprego dunha proporción baixa/media de Tween® 80 (ata 3% w/v), unha porcentaxe de RFB inferior ao 6% e unha velocidade de axitación media/alta (~12000-20000 rpm).

A partir da información obtida nesta primeira aproximación, levouse a cabo un segundo deseño, máis adaptado ás características dos nanosistemas. Con este fin, utilizáronse concentracións máis baixas de Tween® 80 e RFB e rangos más delimitados de LL e velocidade de axitación. Así mesmo, introduciuse a proporción do co-tensoactivo lecitina como quinta variable (**Táboa 3.2**). Neste caso, a monodispersión dos NLC obtidos (**Táboa 3.5**) permitiu o emprego de parámetros habituais, como o tamaño promedio Z ou o índice de polidispersión (PDI) para reflectir o tamaño e a distribución de tamaños dos nanosistemas. Nesta etapa, estudáronse tamén características adicionais dos NLC como a eficiencia de encapsulación (EE) e a carga de fármaco (DL).

Tras a modelización mediante FormRules® da base de datos xerada, obtivéronse modelos de NFL adecuados para todos os parámetros estudados. De acordo con estes, a interacción entre as proporcións de LL e RFB empregadas e a porcentaxe de Tween® 80 utilizado condicionan o tamaño dos NLC obtidos (**Figura 3.2**). Igualmente, as proporcións de LL e de Tween® 80 empregadas determinan tamén diversas características dos nanosistemas, como o PDI, o ZP, a EE e a DL (**Figuras 3.3, 3.4, 3.5 e 3.6**). Por último, a DL veríase tamén afectada pola velocidade de homoxeneización e a cantidade de RFB empregadas.

Considerando as regras "SI-ENTÓN" extraídas a partir destes modelos (ver **Anexo I**), pode afirmarse que proporcións elevadas de LL darían lugar a un tamaño e un PDI máis reducidos, un potencial zeta máis negativo e uns valores de EE e DL superiores. Sen embargo, cantidades maiores de Tween® 80, aínda que conducirían tamén a unha redución no tamaño e o PDI dos nanosistemas, actuarían de forma diferente sobre a carga do fármaco, dando lugar a valores baixos de EE e DL. A redución do tamaño e o PDI dos NLC co emprego de cantidades superiores de LL e Tween® 80, pode deberse a unha maior eficiencia de emulsificación asociada á elevada cantidade de tensioactivo. Mentres que a importante presenza de LL, facilitaría a

redución da tensión superficial por parte do emulsificante (30). Con respecto ao ZP, detectouse tamén unha lixeira influencia da porcentaxe de lecitina empregada sobre este parámetro. Deste xeito, o emprego de proporcións elevadas de LL e lecitina darían lugar a un potencial zeta máis negativo, o que estaría asociado á carga negativa destes compostos (29, 31). Non obstante, unha maior proporción de Tween® 80, produciría o efecto contrario, ao localizarse preto da interface das nanopartículas, contrarrestando a súa carga negativa (32).

Por outra parte, a redución dos parámetros asociados á carga de fármaco (EE e DL) ao incrementar o tensioactivo, podería deberse precisamente á redución no tamaño de partícula, que limitaría o espazo dispoñible para o fármaco na matriz dos NLC (33). Á súa vez, a redución da DL con velocidades de homoxeneización elevadas podería relacionarse tamén coa diminución do tamaño. Mentres que a mellora na capacidade de carga de RFB co emprego de cantidades maiores de LL estaría posiblemente relacionada cunha maior solubilidade do fármaco na matriz (34).

Finalmente, partindo da base do coñecemento xerado mediante NFL, estimáronse as condicións óptimas de formulación coa axuda de INForm®. Despois de asignar pesos ás diferentes variables para obter un equilibrio adecuado entre as características fisicoquímicas e a carga de RFB dos NLC, obtívose que o emprego dun 5% de LL, un 0.5% de lecitina, un 1.9% de Tween® 80, e unha velocidade de axitación de 14892 rpm, daría lugar á obtención de NLC cargados con RFB cun tamaño de 152 nm, un PDI de 0.23, un ZP de -19 mV e uns valores de EE e DL de 100% e 5%, respectivamente.

Co fin de validar os modelos de NFL obtidos e verificar os valores preditos por INForm®, preparáronse NLC utilizando os parámetros optimizados suxeridos polo programa e avaliouse a súa estabilidade despois dun mes de almacenamento a 5 ± 1°C. A posterior caracterización das formulacións validou os modelos ao revelar unha elevada concordancia coas predicións e confirmou a boa estabilidade dos sistemas (**Táboa 3.7**). En base a estes resultados, pode afirmarse que as regras "SI-ENTÓN" obtidas mediante NFL facilitaron a comprensión das interaccións fisicoquímicas existentes entre os diferentes compoñentes das formulacións. Á súa vez, os modelos de ANN e os algoritmos xenéticos posibilitaron a estimación das condicións óptimas de formulación para a obtención de NLC coas características desexadas.

4.2. CAPÍTULO II: OS TRANSPORTADORES LIPÍDICOS NANOESTRUTURADOS CARGADOS CON RIFABUTINA COMO FERRAMENTA NO TRATAMENTO ANTI-MICOBACTERIANO ORAL DA ENFERMIDADE DE CROHN

Co obxectivo de comprobar a reproducibilidade do procedemento de optimización levado a cabo na etapa previa do traballo, os NLC cargados con RFB elaboráronse por sextuplicado. Preparáronse tamén formulacións de NLC sen cargar (brancas) empregando os mesmos parámetros optimizados, a modo de control. Así mesmo, de forma previa á caracterización destes nanosistemas, introduciuse unha etapa de diálise empregando unha membrana molecular porosa, co fin de evitar interferencias producidas por compoñentes non incorporados nas formulacións. Tal e como se amosa na **Táboa 4.1**, existe unha elevada similitude entre as NLC brancas e cargadas. Ademais, os valores de tamaño, PDI, EE e DL dos NLC cargados, coinciden de forma precisa cos preditos por INForm®, demostrando a elevada reproducibilidade do

procedemento desenvolvido. A única discrepancia destacable correspóndese cos valores de ZP obtidos, que amosan valores máis negativos neste caso, o que podería relacionarse coa eliminación dun exceso de Tween® 80 durante a diálise (32).

Despois da comprobación da reproducibilidade dos nanosistemas optimizados, levouse a cabo unha caracterización adicional dos mesmos en termos de morfoloxía e resistencia térmica. A análise morfolóxica realizouse mediante TEM e AFM. As imaxes obtidas confirmaron os tamaños de partícula previamente descritos (**Figuras 4.2** e **4.3**) e revelaron que os NLC brancos e cargados presentan unha morfoloxía esferoidal, incluíndo unha serie de capas concéntricas cunha elevada densidade electrónica na parte central (**Figura 4.2B**). Esta particular morfoloxía está asociada ao polimorfo α dos lípidos (35), cuxo predominio se asocia cunha maior capacidade de carga e retención dos fármacos por parte da matriz lipídica (17). Con respecto á análise térmica das formulacións, levouse a cabo mediante DLS, sometendo aos nanosistemas a ramplas de quentamento-arrefriamento. Os resultados obtidos mostraron que os NLC presentaron variacións de tamaño mínimas durante o ensaio (**Figura 4.1**), o que indica unha adecuada estabilidade térmica (11). Esta estabilidade baixo condicións de temperatura elevada pode resultar de especial interese para a transformación destas nano-dispersións nun produto sólido, facilmente administrable por vía oral como cápsulas ou comprimidos.

Tras esta ampla caracterización dos nanosistemas, realizáronse unha serie de ensaios orientados a avaliar a seguridade das formulacións de NLC e a súa capacidade para cumprir co seu obxectivo de dirixir ao antibiótico RFB cara o interior dos macrófagos intestinais. Considerando que, tras a administración oral das formulacións, e de forma previa ao seu paso a través do epitelio intestinal, estas entrarían en contacto co medio intestinal, comezouse pola análise da capacidade dos NLC para controlar a liberación de RFB neste medio. Para isto, levouse a cabo un ensaio de cesión en medio intestinal simulado (SIF) con enzimas. Os resultados obtidos mostraron unha liberación de fármaco indetectable mediante HPLC, o que suxire que os nanosistemas desenvolvidos poderían controlar de forma eficiente a liberación de fármaco no intestino.

A continuación, estimouse a capacidade dos NLC para atravesar a barreira intestinal, mediante a realización dun ensaio de permeabilidade en monocapas de células Caco-2. Este estudo ofrece unha boa correlación cos resultados *in vivo* en humanos e foi amplamente utilizado para estimar a permeabilidade dos fármacos (36). Os resultados obtidos mostraron que, tras dúas horas de ensaio, a permeabilidade dos NLC incrementouse linealmente, permitindo o paso a través da monocapa de concentracións de RFB de 0.43±0.01 µg/mL e 0.9±0.1 µg/mL transcorridas 24 e 48 horas, respectivamente (**Figura 4.8**). Estes resultados suxiren que, tras 24 h, que é o tempo de tránsito intestinal en pacientes de Crohn (37), alcanzaríase unha concentración moi próxima á concentración mínima inhibitoria (MIC) descrita para o fármaco, que se atopa no rango de 0.5-4 µg/mL (38). Así mesmo, o coeficiente de permeabilidade aparente obtido foi lixeiramente superior a 2×10^{-6} cm/s, que é o valor límite por encima do cal sería previsible alcanzar unha absorción completa en humanos (39). Á vista dos resultados obtidos e considerando que a permeabilidade en doentes sería superior *in vivo* debido a factores como a disrupción do epitelio intestinal (37), pode garantirse que os NLC permitirían a administración dunha dose efectiva de RFB aos macrófagos intestinais.

Despois do paso a través do epitelio, os NLC entrarían en contacto cos macrófagos intestinais, e para caracterizar a súa interacción con estas células, leváronse a cabo ensaios de biocompatibilidade e internalización en macrófagos derivados da liña monocítica THP-1.

A biocompatibilidade dos NLC foi avaliada empregando diferentes concentracións de nanopartículas (0.3, 0.12, 0.06 e 0.03 mg/mL). As células foron tratadas tamén con concentracións equivalentes de RFB, como control. Tal e como se pode apreciar na **Figura 4.5A**, os valores de viabilidade celular obtidos cos NLC (brancos e cargados) presentaron uns valores ≥70% co emprego dunha concentración de NLC inferior a 0.3 mg/mL. Así mesmo, o IC50 obtido para os NLC cargados (**Figura 4.6**), coincide co rango descrito para este tipo de nanosistemas (40), demostrando a adecuada biocompatibilidade das formulacións desenvolvidas. Por outra parte, a análise estatística realizada (ANOVA de dúas vías, $p < 0.05$), mostrou un efecto significativo do tratamento (NLC brancas ou cargadas), da concentración avaliada e da interacción entre estes dous factores sobre a viabilidade celular. Ademais, a proba post-hoc de Tukey levada a cabo a continuación, indicou a existencia dun efecto citotóxico concentración-dependente no caso das dúas formulacións de NLC. Non obstante, non se atoparon diferencias significativas na viabilidade celular derivadas do emprego dos NLC cargados con RFB nunha concentración de 0.06 e 0.12 mg/mL, polo que se seleccionou esta última concentración para continuar cos seguintes ensaios. Curiosamente, tampouco se atoparon diferencias significativas na viabilidade celular obtida cos controis realizados co fármaco (**Figura 4.5B**). Isto suxire que a citotoxicidade derivada do emprego das formulación de NLC, podería estar asociada fundamentalmente co emprego de tensioactivos, ou á inclusión do ácido oleico na matriz lipídica, tal e como sinalaron investigacións previas (41, 42).

Respecto á avaliación da internalización dos NLC, realizouse empregando dúas aproximacións diferentes, unha cualitativa, mediante microscopía confocal, e outra cuantitativa, mediante fluorescencia. As imaxes obtidas mediante microscopía confocal revelaron que os nanosistemas son claramente internalizados polos macrófagos (**Figura 4.7**), o que constitúe un interesante punto de partida para o tratamento de infeccións intracelulares como as producidas por MAP. Pola súa parte, a aproximación cuantitativa demostrou a existencia de diferenzas significativas entre a internalización das NLC brancas (8.33±1.15%) e das cargadas (13.39±1.44%), que se asociaron ao tamaño lixeiramente superior descrito para os NLC cargados (43). Cabe destacar tamén, que a porcentaxe de captación obtida no caso dos NLC cargados, daría lugar a unha cantidade de RFB internalizada de 0.078 µg, nun volume celular de aproximadamente 1.2475×10-4 mL, o que resultaría nunha concentración intracelular de 625 µg/mL. Este valor excede amplamente a MIC previamente descrita para o fármaco, garantindo a presenza dunha dose efectiva de antibiótico no interior dos macrófagos intestinais.

Unha vez comprobada a adecuada captación dos NLC por los macrófagos, é necesario analizar a capacidade dos nanosistemas para ceder fármaco no entorno intracelular. Para isto, levouse a cabo un ensaio de cesión nun fluído intracelular simulado, elaborado mediante a lise de macrófagos murinos. Os resultados obtidos mostraron que o fármaco comezou a ser detectable no medio de liberación transcorrida unha hora, incrementándose progresivamente ata ser cuantificable ás 16 horas do inicio do ensaio, momento no que se acadou unha cantidade de RFB no medio de 1.46±0.47 µg (0.1±0.03% do total). A discreta liberación descrita pode

asociarse á elevada lipofilia do fármaco (44) e á súa gran solubilidade na matriz lipídica, o que dificulta a súa difusión cara o medio acuoso (45). Non obstante, é necesario considerar tamén a elevada dilución enzimática levada a cabo na preparación do medio, xa que a concentración das enzimas no interior dos macrófagos sería moi superior á do medio empregado nestes ensaios, dando lugar previsiblemente a una cesión máis significativa. Tendo en conta estes resultados, e os previamente obtidos no ensaio de liberación en SIF, pode afirmarse que os NLC posibilitarían unha liberación selectiva de RFB no interior dos macrófagos intestinais, unha característica de especial interese no tratamento de infeccións intracelulares, coma as producidas na enfermidade de Crohn.

4.3. CAPÍTULO III: EFECTIVIDADE CRIOPROTECTORA DOS AZUCRES NA LIOFILIZACIÓN DE TRANSPORTADORES LIPÍDICOS NANOESTRUTURADOS

A pesar do enorme potencial dos NLC desenvolvidos, é necesario considerar que as nano-dispersións lipídicas se ven sometidas a diversos fenómenos fisicoquímicos que favorecen a súa desestabilización (46). Ademais, a súa natureza lipídica condicionaría previsiblemente a estabilidade en medio gástrico destes sistemas (47), dificultando a súa administración oral, e facendo necesaria a súa transformación nunha forma de dosificación sólida, que permita a súa inclusión en comprimidos ou cápsulas gastroresistentes.

A liofilización é unha técnica de probada utilidade para mellorar a estabilidade dos nanosistemas que, malia á súa elevada complexidade, se leva a cabo seguindo aproximacións de tipo ensaio-erro (48). Así, esta etapa do traballo centrouse na análise (mediante ferramentas de AI coma a NFL) dos mecanismos fisicoquímicos responsables do proceso de liofilización e da acción dos CPs, para establecer un procedemento de liofilización adecuado para os NLC desenvolvidos.

Con este fin, levouse a cabo a preparación e liofilización de formulacións de NLC brancas. O proceso de liofilización foi precedido dunha etapa de conxelación, na que se empregou nitróxeno líquido (conxelación rápida) ou un conxelador de -80°C (conxelación lenta). Os resultados obtidos tras a reconstitución dos pos liofilizados (LP), (expresados como o Δ tamaño, Δ PDI e Δ ZP dos LP con respecto aos valores iniciais das suspensións de NLC), demostraron que estes nanosistemas presentan unha boa estabilidade durante o proceso de liofilización. Con todo, os LP resultantes mostraron diferentes signos de colapso, como aspecto gomoso e unha difícil redispersión (48), facendo necesario o emprego de CPs.

Desta maneira, avaliouse a eficacia da selección de CPs especificada na sección de materiais e métodos, ás diferentes concentracións descritas, para protexer aos NLC durante o proceso de liofilización. Así mesmo, co obxectivo de adquirir unha maior comprensión das propiedades destes compostos, os CPs foron clasificados en función do seu peso molecular (MW_{CP}), e a súa osmolaridade (Π) ás distintas concentracións estudadas (%CP) foi determinada experimentalmente. A caracterización completa dos CPs estudados pode atoparse na **Táboa 5.1**.

Unha vez completada a caracterización destes compostos, levouse a cabo a súa adición ás dispersións de NLC, que foron tamén liofilizadas. Tras a reconstitución dos LP, obtivéronse amplos rangos de Δ tamaño e Δ PDI (**Figuras 5.2** e **5.3**). Á súa vez, observáronse unha serie de

tendencias relacionadas co tipo de CP, a concentración e velocidade de conxelación. Deste xeito, obtívose que a efectividade dos CPs, en termos de Δ tamaño e Δ PDI, modifícase en función da concentración utilizada, observándose diferentes comportamentos en función do tipo de CP (monosacáridos, azucres alcohois e disacáridos). Observouse tamén que, en xeral, o emprego dunha velocidade de conxelación rápida favorece a obtención de LP con valores de Δ tamaño e Δ PDI reducidos. Porén os valores de Δ ZP dos LP presentaron rangos máis estreitos (**Figura 5.4**), con lixeiras neutralizacións derivadas da adsorción de algúns CPs á superficie dos nanosistemas (49).

Co fin de estudar os fenómenos existentes tras as tendencias reveladas polos resultados experimentais, realizouse unha análise en dúas etapas coa axuda de FormRules®, o programa de NFL previamente empregado no desenvolvemento das formulacións. Para isto, levouse a cabo unha primeira aproximación destinada a avaliar o efecto das distintas condicións de liofilización (velocidade de conxelación, CP seleccionado e % CP) sobre o Δ tamaño, Δ PDI e Δ ZP dos LP obtidos. Esta primeira análise foi seguida dunha segunda aproximación máis centrada no estudo do efecto de propiedades específicas dos CPs (MW_{CP} e Π) e da velocidade de conxelación seleccionada, sobre as propiedades dos LP.

FormRules® modelizou o Δ tamaño e o Δ PDI obtidos con éxito en ambas aproximacións, desenvolvendo modelos cunha adecuada capacidade de predición e un bo funcionamento (**Táboas 5.2** e **5.3**). Sen embargo, o programa non conseguiu atopar un modelo adecuado para o Δ ZP, debido ao estreito rango de valores experimentais descrito para este parámetro.

Cabe destacar que os resultados obtidos en ambos modelos de NFL coincidiron en gran medida. Desta maneira observouse que o Δ tamaño vese afectado pola interacción entre o CP seleccionado e a velocidade de conxelación (1° modelo, **Táboa 5.2**), e pola interacción entre o MW_{CP} e a velocidade de conxelación (2° modelo, **Táboa 5.3**). Mentres que a velocidade de conxelación condiciona, de forma individual, o Δ PDI en ambos modelos. Así mesmo, de acordo coas regras "SI-ENTÓN" extraídas do 1° modelo (datos mostrados no **Anexo III**), unha velocidade de conxelación rápida promove, en xeral, a obtención de LP con valores reducidos de Δ tamaño e Δ PDI. Esta tendencia coincide con teorías previas que suxiren que un arrefriamento rápido promove a xeración de cristais de xeo pequenos, reducindo o estrés mecánico sobre as nanopartículas (48). Con todo, actualmente aínda existe certa controversia relativa á velocidade óptima de conxelación previa á liofilización (50, 51).

Por outra parte, o 2° modelo proporcionou información máis específica, que pode contribuír a aclarar esta controversia. Os resultados obtidos nesta segunda aproximación indicaron que a velocidade de conxelación óptima depende do MW_{CP}, en liña con teorías previamente propostas por outros autores (50). De acordo con estas teorías, a medida que a fronte de conxelación avanza, xéranse cristais de xeo e unha solución crio-concentrada constituída polas nanopartículas e outros elementos da formulación (48, 50). Deste xeito, a cantidade de CP dispoñible para protexer aos nanosistemas nesta solución, depende da velocidade de conxelación utilizada e da velocidade de difusión dos compostos cara a fase crio-concentrada (50). Esta difusión verase afectada, como é lóxico, polo MW_{CP}, sendo máis rápida canto menor sexa este parámetro.

Neste sentido, observouse un mellor funcionamento dos CPs cun MW inferior a 200 g/mol, con velocidades de conxelación rápidas. Esta preferencia pode deberse á rápida migración destes compostos, que lles permite protexer aos NLC e beneficiarse simultaneamente das vantaxes asociadas ás velocidades de conxelación rápidas, como a formación de cristais de xeo máis pequenos (48, 50). O efecto contrario obtívose para CPs cun MW no rango de 220-300 g/mol, cunha maior preferencia por velocidades de conxelación lentas. Curiosamente, os CPs cun MW superior a 300 g/mol mostran unha maior independencia da velocidade de conxelación, o que pode asociarse cunha maior Tg descrita para estes compostos (52). Isto permitiríalles vitrificar antes durante o transcurso do proceso de liofilización, protexendo aos NLC na matriz vítrea xerada, minimizando así o dano ocasionado aos nanosistemas e o efecto da velocidade de conxelación.

Así mesmo, os modelos de NFL obtidos revelaron tamén a influencia da interacción entre o CP seleccionado e a súa %CP (1° modelo, **Táboa 5.2)** ou do MW_{CP} e Π (2° modelo, **Táboa 5.3**), sobre o Δ tamaño e Δ PDI dos LP obtidos. A información extraída do primeiro modelo suxire que o %CP necesario para a obtención de LP con valores reducidos de Δ tamaño e Δ PDI, varía en función do CP seleccionado. De acordo coas regras "SI-ENTÓN" (ver **Anexo III**), os azucres alcohois avaliados, manitol e sorbitol, dan lugar aos peores resultados en termos de Δ tamaño. Respecto á glucosa e á fructosa, obtívose que a súa eficacia crioprotectora é superior cando se empregan nunha proporción baixa-media (ata o 10%). Non obstante, a sacarosa require unha concentración media-alta, superior ao 2.5% no caso de empregar una velocidade de conxelación rápida, ou incluso maior ao 12.5%, se se selecciona unha velocidade lenta. Finalmente, as concentracións medias (3.75-12.5%) parecen ser as máis adecuadas para CPs como a trehalosa ou a lactosa. No caso do Δ PDI, as conclusións son bastante similares ás descritas para o Δ tamaño, acadándose, en xeral, uns valores de Δ PDI baixos.

Con relación ao segundo modelo de NFL desenvolvido, os resultados indican que a Π requirida para a obtención de LP con valores de Δ tamaño e Δ PDI reducidos, xeralmente incrementan progresivamente co MW_{CP}. Estes requirimentos graduais poderían estar asociados, tamén, cos fenómenos de difusión dos CPs cara la fase crio-concentrada onde se atopan os NLC, anteriormente comentados. Deste xeito, a adición dunha elevada proporción dun CP de difusión lenta, podería incrementar a súa presenza na solución crio-concentrada, permitindo a adecuada protección dos nanosistemas (50). Ademais, debido á natureza coligativa de la Π (53), os seus requirimentos estarían directamente relacionados co %CP, xustificando a elevada similitude entre ambos modelos.

Aínda que estes requirimentos graduais se cumpren á perfección para a maioría dos CPs estudados, como a glucosa, a fructosa (MW=180.16 g/mol) ou a sacarosa (MW=342.3 g/mol), a trehalosa e a lactosa (MW=342.3 g/mol) constitúen unha excepción. Porén, isto podería deberse á elevada eficacia crioprotectora da trehalosa (48), que daría lugar a unha redución da concentración requirida deste composto, e á tendencia da lactosa a cristalizar durante a conxelación (48). A posible agregación e fusión dos nanosistemas derivada da cristalización deste CP (48), xustificaría a redución no %CP óptimo neste último caso. Do mesmo modo, o manitol e o sorbitol son compostos que tamén cristalizan durante a conxelación (54), o que podería explicar a súa limitada efectividade crioprotectora.

A diferenza doutros traballos previos, nos cales se seleccionan unhas condicións concretas de liofilización, os resultados obtidos suxiren que a liofilización dos NLC pode ser levada a cabo empregando diferentes variables, sempre que se combinen de maneira adecuada. Proponse así un sistema de clasificación tipo semáforo, que pode consultarse na **Figura 5.4**, indicando en cor verde as condicións de liofilización máis adecuadas para cada CP en termos de velocidade de conxelación e %CP.

En síntese, cabe destacar que esta etapa do traballo pon de manifesto a importancia do QbD para optimizar os recursos dispoñibles, establecendo de forma racional un proceso de liofilización adecuado para os NLC. O coñecemento derivado deste estudio posibilitaría, á súa vez, a conversión dos NLC cargados con RFB desenvolvidos nunha forma de dosificación sólida, adecuada para a súa administración por vía oral. Finalmente, a inclusión destes produtos sólidos en cápsulas gastrorresistentes ou comprimidos, permitiría aos nanosistemas alcanzar de forma segura o medio intestinal, no cal as súas prometedoras características foron previamente demostradas.

5. CONCLUSIÓNS

Os resultados obtidos permiten extraer as seguintes conclusións:

1. Demostrouse a utilidade da NFL para proporcionar unha maior comprensión do efecto da composición e das condicións de formulación, xunto coas súas interaccións, sobre as características dos NLC cargados con RFB desenvolvidos, permitindo o establecemento dos espazos de coñecemento e deseño para estes nanosistemas.
2. As ANN e os Algoritmos xenéticos posibilitaron a estimación dos parámetros máis adecuados de formulación, para a obtención de formulacións de NLC monodisperas, cun tamaño nanométrico, carga negativa e unha elevada capacidade de carga de RFB.
3. O emprego de estatexias de QbD, coma os programas de AI anteriormente mencionados, permitiu o desenvolvemento dunha formulación de NLC cargados con RFB coas características desexadas, mediante un proceso de fabricación simple e reproducible. Os nanosistemas obtidos presentaron tamén unha morfoloxía esferoidal, xunto cunha elevada biocompatibilidade e estabilidade.
4. A avaliación *in vitro* dos NLC cargados con RFB demostrou que a permeabilidade a través das monocapas de células Caco-2, a captación por parte dos macrófagos e a liberación selectiva de RFB en medio intracelular obtidas para estes nanosistemas, asegurarían unha dose intracelular efectiva de RFB no interior das células fagocíticas. Convertendo así aos NLC desenvolvidos nunha estratexia prometedora para o tratamento de infeccións intracelulares, como as producidas na CD.
5. A NFL permitiu tamén analizar o impacto das condicións de liofilización sobre as propiedades dos pós liofilizados obtidos. Así como a adquisición dunha mellor comprensión do mecanismo de acción dos azucres empregados como CPs, e dos fenómenos fisicoquímicos responsables do proceso de liofilización.

6. As dispersións de NLC transformáronse con éxito en formas de dosificación sólidas aptas para a súa administración por vía oral, mediante un procedemento de liofilización establecido de forma racional. Os produtos liofilizados resultantes mostraron unha adecuada redispersibilidade, xunto cun alto mantemento das propiedades iniciais das formulacións, tras a súa reconstitución.

Como conclusión xeral, cabe destacar que este traballo pon de manifesto a importancia da nanotecnoloxía para sacar o máximo proveito ás terapias antibióticas actualmente dispoñibles, destinadas ao tratamento de infeccións intracelulares. Así mesmo, mostra a importancia do emprego de estratexias de QbD, como as ferramentas de AI, en procesos farmacéuticos, particularmente, no desenvolvemento de nanopartículas, co fin de acelerar o seu emprego en clínica.

6. EXPERIMENTOS EN CURSO E PERSPECTIVAS FUTURAS

Actualmente, desenvolveuse con éxito unha formulación de NLC cargados con RFB, con características prometedoras para o tratamento de infeccións ocasionadas por patóxenos intracelulares como *M. avium paratuberculosis* (MAP). Con todo, a efectividade destes nanosistemas atópase aínda pendente de confirmación. Así mesmo, a análise de estratexias de modificación superficial dos NLC, destinados a mellorar a súa captación por parte dos macrófagos, presentaría tamén un considerable interese.

Co obxectivo de incrementar a captación das formulacións por parte destas células fagocíticas, fixeronse estudos preliminares de desenvolvemento de diferentes estratexias baseadas no recubrimento dos NLC con distintos compostos, como a manosa ou os ácidos micólicos (MAs) (**Figura 8.1**). A primeira consistiu en explotar a elevada presenza de receptores de manosa nos macrófagos (10, 55) para promover a internalización dos NLC. Por outra parte, o emprego de MAs, uns lípidos da parede bacteriana cun importante papel biolóxico (56, 57), está orientado á estimulación da fagocitose mediante a imitación da superficie micobacteriana.

Levouse a cabo caracterización, en termos fisicoquímicos (tamaño, PDI, ZP) e de internalización por parte dos macrófagos, dos NLC recubertos, para avaliar posibles cambios con respecto ás formulacións de NLC iniciais. Deste xeito, a caracterización fisicoquímica dos NLC recubertos, revelou modificacións atribuíbles aos procedementos de recubrimento dos NLC empregados (**Táboa 8.1**). Os resultados de internalización obtidos mostraron unha captación significativamente superior á dos NLC orixinais soamente no caso das formulacións recubertas con MAs, chegando a alcanzarse valores de internalización unhas catro veces superiores (**Táboa 8.1**).

Por outra parte, a avaliación da eficacia anti-micobacteriana das formulacións de NLC desenvolvidas: NLC cargadas con RFB, NLC recubertas con manosa e NLC recubertas con MAs, foi levada a cabo mediante a súa incubación con macrófagos infectados con MAP. A determinación da carga bacteriana remanente tras a administración dos diferentes tratamentos levouse a cabo mediante un instrumento Bactec MGIT 960, seguindo o protocolo descrito na **sección 8**. Os resultados obtidos non mostraron diferencias significativas na carga bacteriana das células tratadas coas diferentes formulacións de NLC, con respecto ás células sen tratar

(**Táboa 8.2**). Non obstante, considerando que se observaron resultados moi similares para as células tratadas cunha solución de RFB empregada a modo de control, os datos obtidos poderían asociarse ao lento crecemento de MAP e á actividade bacteriostática da RFB.

En síntese, cabe destacar que a incorporación dos MAs constitúe unha estratexia prometedora para o desenvolvemento de nanosistemas de liberación de fármacos dirixidos a células fagocíticas, aínda que sería necesaria unha análise máis detallada dos NLC recubertos desenvolvidos. Respecto á avaliación da eficacia das formulacións en macrófagos infectados, unha mellor adaptación do deseño experimental á velocidade de crecemento deste microorganismo e á actividade do antibiótico, podería permitir a detección de diferenzas na inhibición do crecemento bacteriano para as distintas mostras analizadas.

REFERENCIAS

1. Chen H, Khemtong C, Yang X, Chang X, Gao J. Nanonization strategies for poorly water-soluble drugs. Drug Discov Today. 2011; 16 (7-8): 354-360.
2. Davis WC. On deaf ears, Mycobacterium avium paratuberculosis in pathogenesis Crohn's and other diseases. World J Gastroenterol. 2015; 21 (48): 13411-13417.
3. Hostetter J, Steadham E, Haynes J, Bailey T, Cheville N. Phagosomal maturation and intracellular survival of Mycobacterium avium subspecies paratuberculosis in J774 cells. Comp Immunol Microbiol Infect Dis. 2003; 26 (4): 269-283.
4. Kuenstner JT, Naser S, Chamberlin W, Borody T, Graham DY, McNees A, et al. The Consensus from the Mycobacterium avium ssp. paratuberculosis (MAP) Conference 2017. Front Public Health. 2017; 5: 208.
5. Honap S, Johnston E, Agrawal G, Al-Hakim B, Hermon-Taylor J, Sanderson J. Anti-Mycobacterium paratuberculosis (MAP) therapy for Crohn's disease: an overview and update. Frontline Gastroenterol. 2020; 0: 1–7.
6. Salem II, Steffan G, Düzgünes N. Efficacy of clofazimine–modified cyclodextrin against Mycobacterium avium complex in human macrophages. Int J Pharm. 2003; 260 (1): 105-114.
7. Inoue Y, Yoshimura S, Tozuka Y, Moribe K, Kumamoto T, Ishikawa T, et al. Application of ascorbic acid 2-glucoside as a solubilizing agent for clarithromycin: solubilization and nanoparticle formation. Int J Pharm. 2007; 331 (1): 38-45.
8. Nirbhavane P, Vemuri N, Kumar N, Khuller GK. Lipid Nanocarrier-Mediated Drug Delivery System to Enhance the Oral Bioavailability of Rifabutin. AAPS PharmSciTech. 2016; 18 (3): 829-837.
9. Wais U, Jackson AW, He T, Zhang H. Nanoformulation and encapsulation approaches for poorly water-soluble drug nanoparticles. Nanoscale. 2016; 8 (4): 1746-1769.
10. Vieira AC, Magalhães J, Rocha S, Cardoso MS, Santos SG, Borges M, et al. Targeted macrophages delivery of rifampicin-loaded lipid nanoparticles to improve tuberculosis treatment. Nanomedicine. 2017; 12 (24): 2721-2736.
11. Gaspar DP, Faria V, Goncalves LM, Taboada P, Remunan-Lopez C, Almeida AJ. Rifabutin-loaded solid lipid nanoparticles for inhaled antitubercular therapy: Physicochemical and in vitro studies. Int J Pharm. 2016; 497 (1-2): 199-209.
12. Taratula O, Kuzmov A, Shah M, Garbuzenko OB, Minko T. Nanostructured lipid carriers as multifunctional nanomedicine platform for pulmonary co-delivery of anticancer drugs and siRNA. J Control Release. 2013; 171 (3): 349-357.
13. Qi R, Li YZ, Chen C, Cao YN, Yu MM, Xu L, et al. G5-PEG PAMAM dendrimer incorporating nanostructured lipid carriers enhance oral bioavailability and plasma lipid-lowering effect of probucol. J Control Release. 2015; 210: 160-168.
14. Gainza G, Bonafonte DC, Moreno B, Aguirre JJ, Gutierrez FB, Villullas S, et al. The topical administration of rhEGF-loaded nanostructured lipid carriers (rhEGF-NLC) improves healing in a porcine full-thickness excisional wound model. J Control Release. 2015; 197: 41-47.
15. Müller RH, Shegokar R, Keck CM. 20 years of lipid nanoparticles (SLN and NLC): present state of development and industrial applications. Curr Drug Discov Technol. 2011; 8 (3): 207-227.

16. Martins S, Sarmento B, Ferreira DC, Souto EB. Lipid-based colloidal carriers for peptide and protein delivery-liposomes versus lipid nanoparticles. Int J Nanomedicine. 2007; 2 (4): 595-607.
17. Gordillo-Galeano A, Mora-Huertas CE. Solid lipid nanoparticles and nanostructured lipid carriers: A review emphasizing on particle structure and drug release. Eur J Pharm Biopharm. 2018; 133: 285-308.
18. Alvarez-Trabado J, Diebold Y, Sanchez A. Designing lipid nanoparticles for topical ocular drug delivery. Int J Pharm. 2017; 532 (1): 204-217.
19. Souto E, Almeida A, Müller R. Lipid nanoparticles (SLN®, NLC®) for cutaneous drug delivery: structure, protection and skin effects. J Biomed Nanotechnol. 2007; 3 (4): 317-331.
20. Danaei M, Dehghankhold M, Ataei S, Hasanzadeh Davarani F, Javanmard R, Dokhani A, et al. Impact of Particle Size and Polydispersity Index on the Clinical Applications of Lipidic Nanocarrier Systems. Biomacromolecules. 2018; 10 (2): 57.
21. Desai N. Challenges in development of nanoparticle-based therapeutics. AAPS J. 2012; 14 (2): 282-295.
22. Diaz-Rodriguez P, Landin M. Smart design of intratumoral thermosensitive beta-lapachone hydrogels by Artificial Neural Networks. Int J Pharm. 2012; 433 (1-2): 112-118.
23. Rodriguez-Dorado R, Landin M, Altai A, Russo P, Aquino RP, Del Gaudio P. A novel method for the production of core-shell microparticles by inverse gelation optimized with artificial intelligent tools. Int J Pharm. 2018; 538 (1-2): 97-104.
24. Landin M, Rowe RC, York P. Advantages of neurofuzzy logic against conventional experimental design and statistical analysis in studying and developing direct compression formulations. Eur J Pharm Sci. 2009; 38 (4): 325-331.
25. Colbourn EA, Rowe RC. Novel approaches to neural and evolutionary computing in pharmaceutical formulation: challenges and new possibilities. Future Med Chem. 2009; 1 (4): 713-726.
26. Khosa A, Reddi S, Saha RN. Nanostructured lipid carriers for site-specific drug delivery. Biomed Pharmacother. 2018; 103: 598-613.
27. Takalkar D, Desai N. Nanolipid Gel of an Antimycotic Drug for Treating Vulvovaginal Candidiasis-Development and Evaluation. AAPS PharmSciTech. 2018; 19 (3): 1297-1307.
28. Shah R, Eldridge D, Palombo E, Harding I. Composition and structure. In: Shah R, Eldridge D, Palombo E, Harding I (Eds). Lipid nanoparticles: production, characterization and stability. 1st edition. New York, USA: Springer International Publishing; 2015. p. 11-22.
29. Ogawa S, Decker EA, McClements DJ. Production and characterization of o/w emulsions containing droplets stabilized by lecithin−chitosan−pectin mutilayered membranes. J Agric Food Chem. 2004; 52 (11): 3595-3600.
30. Song A, Zhang X, Li Y, Mao X, Han F. Effect of liquid-to-solid lipid ratio on characterizations of flurbiprofen-loaded solid lipid nanoparticles (SLNs) and nanostructured lipid carriers (NLCs) for transdermal administration. Drug Dev Ind Pharm. 2016; 42 (8): 1308-1314.
31. Ham-Pichavant F, Sèbe G, Pardon P, Coma V. Fat resistance properties of chitosan-based paper packaging for food applications. Carbohydr Polym. 2005; 61 (3): 259-265.

32. Schubert MA, Müller-Goymann CC. Characterisation of surface-modified solid lipid nanoparticles (SLN): influence of lecithin and nonionic emulsifier. Eur J Pharm Biopharm. 2005; 61 (1-2): 77-86.
33. Gaba B, Fazil M, Khan S, Ali A, Baboota S, Ali J. Nanostructured lipid carrier system for topical delivery of terbinafine hydrochloride. Bull. Fac. Pharm. Cairo Univ. 2015; 53 (2): 147-159.
34. Müller RH, Radtke M, Wissing SA. Nanostructured lipid matrices for improved microencapsulation of drugs. Int J Pharm. 2002; 242 (1-2): 121-128.
35. Bunjes H, Steiniger F, Richter W. Visualizing the structure of triglyceride nanoparticles in different crystal modifications. Langmuir. 2007; 23 (7): 4005-4011.
36. Chaves LL, Costa Lima SA, Vieira ACC, Barreiros L, Segundo MA, Ferreira D, et al. Nanosystems as modulators of intestinal dapsone and clofazimine delivery. Biomed Pharmacother. 2018; 103: 1392-1396.
37. Mohan LJ, Daly JS, Ryan BM, Ramtoola Z. The future of nanomedicine in optimising the treatment of inflammatory bowel disease. Scand J Gastroenterol. 2019; 54 (1): 18-26.
38. Zanetti S, Molicotti P, Cannas S, Ortu S, Ahmed N, Sechi LA. "In vitro" activities of antimycobacterial agents against Mycobacterium avium subsp. paratuberculosis linked to Crohn's disease and paratuberculosis. Ann Clin Microbiol Antimicrob. 2006; 5: 27.
39. Grès M-C, Julian B, Bourrié M, Meunier V, Roques C, Berger M, et al. Correlation between oral drug absorption in humans, and apparent drug permeability in TC-7 cells, a human epithelial intestinal cell line: comparison with the parental Caco-2 cell line. Pharm Res. 1998; 15 (5): 726-733.
40. Doktorovova S, Souto EB, Silva AM. Nanotoxicology applied to solid lipid nanoparticles and nanostructured lipid carriers-a systematic review of in vitro data. Eur J Pharm Biopharm. 2014; 87 (1): 1-18.
41. Schöler N, Olbrich C, Tabatt K, Müller R, Hahn H, Liesenfeld O. Surfactant, but not the size of solid lipid nanoparticles (SLN) influences viability and cytokine production of macrophages. Int J Pharm. 2001; 221 (1-2): 57-67.
42. Yin H, Too HP, Chow GM. The effects of particle size and surface coating on the cytotoxicity of nickel ferrite. Biomaterials. 2005; 26 (29): 5818-5826.
43. Chono S, Tanino T, Seki T, Morimoto K. Influence of particle size on drug delivery to rat alveolar macrophages following pulmonary administration of ciprofloxacin incorporated into liposomes. J Drug Target. 2006; 14 (8): 557-566.
44. Global Alliance for TB drug development. Rifabutin. Tuberculosis (Edinburgh, Scotland). 2008; 88 (2): 145-147
45. Iqbal N, Vitorino C, Taylor KM. How can lipid nanocarriers improve transdermal delivery of olanzapine?. Pharm Dev Technol. 2017; 22 (4): 587-596.
46. Heurtault B, Saulnier P, Pech B, Proust JE, Benoit JP. Physico-chemical stability of colloidal lipid particles. Biomaterials. 2003; 24 (23): 4283-4300.
47. Ana R, Mendes M, Sousa J, Pais A, Falcao A, Fortuna A, et al. Rethinking carbamazepine oral delivery using polymer-lipid hybrid nanoparticles. Int J Pharm. 2019; 554: 352-365.

48. Abdelwahed W, Degobert G, Stainmesse S, Fessi H. Freeze-drying of nanoparticles: formulation, process and storage considerations. Adv Drug Deliv Rev. 2006; 58 (15): 1688-1713.
49. Caetano LA, Almeida AJ, Goncalves LM. Effect of Experimental Parameters on Alginate/Chitosan Microparticles for BCG Encapsulation. Mar Drugs. 2016; 14 (5): 90.
50. Lee MK, Kim MY, Kim S, Lee J. Cryoprotectants for freeze drying of drug nano-suspensions: effect of freezing rate. J Pharm Sci. 2009; 98 (12): 4808-4817.
51. Yue PF, Li G, Dan JX, Wu ZF, Wang CH, Zhu WF, et al. Study on formability of solid nanosuspensions during solidification: II novel roles of freezing stress and cryoprotectant property. Int J Pharm. 2014; 475 (1-2): 35-48.
52. Aksan A, Toner M. Isothermal Desiccation and Vitrification Kinetics of Trehalose−Dextran Solutions. Langmuir. 2004; 20 (13): 5521-5529.
53. Vujovic P, Chirillo M, Silverthorn DU. Learning (by) osmosis: an approach to teaching osmolarity and tonicity. Adv Physiol Educ. 2018; 42 (4): 626-635.
54. Andreani T, Kiill CP, de Souza ALR, Fangueiro JF, Doktorovová S, Garcia ML, et al. Effect of cryoprotectants on the reconstitution of silica nanoparticles produced by sol–gel technology. J Therm Anal Calorim. 2014; 120 (1): 1001-1007.
55. Irache JM, Salman HH, Gamazo C, Espuelas S. Mannose-targeted systems for the delivery of therapeutics. Expert Opin Drug Deliv. 2008; 5 (6): 703-724.
56. Marrakchi H, Laneelle MA, Daffe M. Mycolic acids: structures, biosynthesis, and beyond. Chem Biol. 2014; 21 (1): 67-85.
57. He Z, De Buck J. Localization of proteins in the cell wall of Mycobacterium avium subsp. paratuberculosis K10 by proteomic analysis. Proteome Sci. 2010; 8 (1): 21.

USC
UNIVERSIDADE
DE SANTIAGO
DE COMPOSTELA

1. INTRODUCTION

USC
UNIVERSIDADE
DE SANTIAGO
DE COMPOSTELA

SECTION A. CHROHN´S DISEASE: MYCOBACTERIAL HYPOTHESIS AND ANTIMICROBIAL MANAGEMENT

USC
UNIVERSIDADE
DE SANTIAGO
DE COMPOSTELA

1. 1. THE GENUS MYCOBACTERIUM AND MYCOBACTERIAL DISEASES

The genus Mycobacterium includes a heterogeneous group of microorganisms (1), among which two complexes can be distinguished, *Mycobacterium tuberculosis complex* and *Mycobacterium avium* complex (2). The first group is composed by species such as *M. tuberculosis*, *M. bovis*, *M. africanum*, *M canetii* and *M. microti* (2, 3). *Mycobacterium avium complex* includes *M. chimaera*, *M. avium* and *M. intracellulare* (2). Both groups exhibit high genetic similarity and lead to similar pathologies (3). Furthermore, in addition to these two complexes, the existence of several species such as *M. leprae*, *M. ulcerans*, *M. chelonae*, *M. kansasii*, *M. marinum*, *M. fortuitum*, *M. scrofulaceum* or *M. abscessus*, among others, has also been reported (2).

Mycobacterial diseases are still a major health problem today. Probably, the most famous mycobacterial disease is tuberculosis (TB), a pulmonary disorder caused by *M. tuberculosis* via aerosol inhalation, and subsequent bacilli colonization of alveolar macrophages (4). Moreover, it can also involve extrapulmonary manifestations, primarily, in the case of immunocompromised patients (2). This disease exhibits a huge global impact, with an annual estimated incidence of 8.6 million, and constitutes a burden in the developing world, where Human Immunodeficiency Virus (HIV)-TB combination has become a major issue (5). Another example of mycobacterial disease is leprosy, a widely known disorder produced by *Mycobacterium leprae*, which has been reported to produce bodily deformities that usually trigger social stigmatization. Nowadays, this disease is mainly present in developing countries, where it still constitutes a health concern (2).

Regarding members of MAC, *M. avium* and *M. intracellulare*, were reported to produce regional lymphadenitis, pulmonary disease or even disseminated disease (2). However, the diseases produced by these microorganisms are more frequently seen in immunocompromised VIH-coinfected patients, mostly in the case of disseminated manifestations (2). On the other hand, *M. avium subspecies paratuberculosis* (MAP), a sub-species of *M avium* (6), has been reported to be the causative agent of Johne´s disease, a chronic cattle enteritis (2, 6, 7), and has gained some relevance due to its association with Crohn´s disease (CD) development in humans. This relationship between MAP and CD will be discussed in detail below.

1.1.1. *Mycobacterium avium paratuberculosis* and CD

CD is a chronic inflammatory bowel condition, progressively leading to gut damage and poor patients quality of life (8). The disease might course with transmural involvement, and can affect any part of the gastrointestinal tract, from the mouth to the anus (6, 9). CD tends to course with outbreaks, alternating with remission periods (10, 11), and symptomatology usually includes abdominal pain, vomiting, nausea, weight loss or diarrhea (10). It is frequently diagnosed during adolescence and early adulthood (9), and despite being traditionally associated with developed and industrialized countries (10), a recent analysis of CD´ epidemiology revealed that nowadays, incidence in developing countries is rising, while a more stable pattern is observed for developed ones (9). Nevertheless, this tendency to stabilization in the developed world has been reported to occur mostly among adults, while a rising incidence among young children and adolescents has been found (12, 13).

CD´ etiology has constituted a controversial subject since its discovery (7). It was initially classified as an autoimmune disease, but today it is associated with a combination of environmental and genetic factors and to the presence of persisting agents (6). However, it remains to be elucidated if these agents are pathogenic or if an inappropriate inflammatory response to the normal microbiome has been occurring, or even if both of the hypothesis are correct (6). MAP and CD link has constituted a hot topic during the last century, with several articles investigating the potential implication of this microorganism in the disease included amongst the top cited articles in MAP research from 1911 to 2019 (14). This link was initially stablished based on the strong similarity amongst CD and Johne´s disease, in terms of lesions and symptomatology (6, 7). MAP is very widespread in the environment. It is also present in meat and dairy products. MAP has been shown to resist pasteurization, so humans are chronically exposed to this microorganism (6, 8).

Despite these evidences, difficulties associated with the isolation of MAP from CD patients, caused MAP to be discarded as a direct etiologic agent (7). Nowadays, due to advances in technology, MAP can be isolated in a variable percentage of 50-100% from biopsies and blood of CD patients, constituting a seven-fold proportion, approximately, regarding healthy individuals (6). This variability in MAP detection, has been associated with the technical process employed to isolate MAP´s deoxyribonucleic acid (DNA) (15). Since, these procedures tend to assume that DNA is found in the nucleus, discarding cytoplasm material, where MAP genetic material can be found due to its intracellular replication (15).

Furthermore, it has been described that genes linked with a higher incidence of CD, are often those involved in bacteria-immune interactions (8), leading to a higher susceptibility to MAP. This fact, along with the quite low pathogenic expression of this mycobacterium (8), might explain the existance of healthy individuals infected with MAP. Moreover, it is also important to notice that, despite the found difficulty, associated with the slow growth of MAP, the mycobacteria could be successfully grown *in vitro* by certain laboratories, after its isolation from some CD patients (15). In this way, these findings prove that the first and second of the Koch´s postulates, required to demonstrate MAP causative role in the disease, have been satisfied (15).

In addition, years ago, a report describing the oral inoculation of goats with mycobacteria recovered from the diseased ileum of a CD patient, showed that mycobacterium could be recovered from the intestine of all the inoculated animals, which also exhibited lesions highly similar to those observed in CD patients. However, the presence of acid-fast bacteria was only verifiable in half of the inoculated animals (16). In contrast, controls, which remained in all cases free of lesions and of acid-fast bacilli, were negative to bacteriologic culture (16). However, although this mycobacterium was initially reported to be an unclassified specie (16), it was later demonstrated to be actually MAP (6). Thus, these outcomes might be interpreted as the fulfillment of the third Koch´s postulate. Finally, it is also necessary to highlight that the re-isolation and re-culture of MAP from human and bovine origin has also been possible, ensuring the fulfillment of the fourth and last postulate (15).

Hence, it can be concluded that these evidences indicate that MAP could have been already fulfilled all the Koch´s postulates, as previously suggested by other authors (15), and that its implication in CD development therefore constitutes, at least, a worthy path to explore.

1.2. ANTI-MYCOBACTERIAL MANAGEMENT OF CD

Despite the existent links between MAP and CD development, CD´ management is currently focused on the inflammatory process control through corticosteroids, anti-tumor necrosis factor or anti-interleukin drugs, immunosuppressants or adhesion molecule inhibitors, while antibiotic use is restricted to perianal fistulas or suppurative complications (10). Those therapies are intended to maintain disease remission avoiding surgery (10). Although current treatments improve the quality of life of patients, to date, their ability to modify the long-term evolution of the disease has not been proven (11).

Antimycobacterial drugs constitute a diverse group of therapeutic agents, which are used alone, or in combination, to treat infections produced by microorganisms belonging to the genus *Mycobacterium* (17). Therefore, due to the previously discussed link, the evaluation of the efficacy of anti-mycobacterial agents in CD management undoubtedly constitutes an interesting approach. In this way, several studies and case reports described promising results, including long-term CD remissions or mucosal healing with the use of a combined anti-MAP therapy, which includes the use of clofazimine, clarithromycin and rifabutin (18, 19).

A phase III clinical trial sponsored by RedHill Biopharma, has recently been testing RHB-104, a combination of rifabutin (45 mg), clofazimine (10 mg) and clarithromycin (95 mg), in order to evaluate its efficacy and safety in adult CD patients (the MAP US study, MAPUS) (20). RHB-104 capsules were administered orally, following a dosage regimen of 5 capsules a day (20). Outcomes suggested that RHB-104 formulation exhibited a suitable safety profile, and a superior performance in comparison with the placebo, to achieve disease remissions at week 26, the primary study endpoint. CD remissions were considered to occur when a Crohn´s Disease Active Index (CDAI) value below 150 was achieved (21). In this way, it was found that a 37% and a 23% of patients of the treated and the placebo groups, respectively, achieved this objective. Moreover, treated patients have also been reported to experience some early benefits at week 16, and an improved remission maintenance at week 52 (secondary outcomes), when compared with the placebo group (21).

Currently, RedHill Biopharma continues with the MAP US 2 study that aims to test the safety and efficacy of RHB-104 in CD patients who remain with active disease after 26 weeks of treatment (21, 22). Additionally, they have included polymerase chain reaction (PCR) test for analyzing the evolution of the proportion of MAP blood positive patients from the baseline to week 52 (22). This approach is expected to provide relevant information regarding *in vivo* effectivity of RHB-104 formulation (23) and to demonstrate if MAP eradication triggers a significant clinical benefit (8).

Despite the notable interest of anti-MAP compounds in the therapy of CD suggested by the information previously discussed, other prospective clinical studies have not demonstrated the sustained benefit of the combined effects of triple therapy (24), therefore, to date, the evidence has not been considered sufficient to include anti-MAP compounds as a treatment for CD in the

clinical guidelines of the United Kingdom, United States, or Europe (8). Several authors claim that limitations associated with antibiotic dosing, trial design or the formulation employed in the previous study might be responsible for the poor results obtained (8, 18).

1.2.1. Properties of anti-mycobacterial drugs employed in the triple anti-MAP therapy of CD

Anti-MAP drugs are usually administered orally, as conventional formulations, such as capsules or tablets. Drug bioavailability through this route, is often conditioned by different properties such as solubility, intestinal permeability or drug dissolution rate (25). In this way, physicochemical properties that might be associated with the above-mentioned formulation-related issues, such as aqueous solubility or lipophilicity, along with other relevant information concerning the triple anti-MAP therapy will be discussed below.

Rifabutin is a spiro-piperidyl-rifamycin (**Figure 1A.1A)**, structurally related to rifampicin, which shares many of the properties exhibited by rifamycin´s family (23, 26). This compound exhibits a high lipophilicity and a reduced aqueous solubility of 0.19 mg/ml (27). Furthermore, its solubility is pH-dependent, as it is known to be an ionizable compound (28). Interestingly, at pH values reported in the intestinal mucosa, and within infected macrophages (pH = 5), the drug has been reported to stablish a strong interaction with biological membranes, which is responsible for its antibacterial activity, but also for its undesirable effects (28). Rifabutin has been reported to bind to the prokaryoyic β subunit of the DNA-dependent RNA polymerase, inhibiting transcription and protein synthesis (23, 26).

Clofazimine is an riminophenazine antibiotic (**Figure 1A.1B**.), exhibiting both anti-inflammatory and anti-mycobacterial activity (29, 30). It is also a highly hydrophobic drug, with an extremely reduced aqueous solubility (below 0.3 µg/mL) (29). Clofazimine acts, mainly, as a bacteriostatic agent, and bactericidal actions are considered minor pharmacodynamic properties (23). Although the mechanism of action of clofazimine has not yet been fully elucidated, its main site of action appears to be the outer membrane, while ion transporters and the bacterial respiratory chain have been described as possible targets (30). Moreover, the high permeability of this compound would predictably allow a suitable transmembrane penetration, accumulation in fatty tissue and, hence, a high uptake by phagocytes, where mycobacteria is known to stablish an infection (23). It is important to mention that although this antimicrobial compound displays an extensive tissue accumulation and a prolonged half-life, it was associated with a low risk of bacterial resistance, making it especially useful for the treatment of mycobacterial infections (23). Furthermore, its redox potential (20.18V at pH=7.25) is likely to favor intracellular redox cycling (23).

Clarithromycin is a macrolide antibiotic (**Figure 1A.1C)**, more specifically, a 6-methoxy derivative of erythromycin (31). This group of antibiotics exhibits a bacteriostatic effect at clinically relevant concentrations, and their mechanism of action consists on binding to the large 50s ribosomal subunit, inhibiting protein biosynthesis (23). Clarithromycin shows a high tissue affinity, particularly, for the lung (32), which could make it interesting to treat pulmonary infections. Furthermore, its high stability under acidic conditions contributes to increase its bioavailability through the oral route in comparison with other macrolides (32). However, its

low aqueous solubility (0.342 µg/mL) (33), and short half-life (3-4 hours) (34), limit its efficacy.

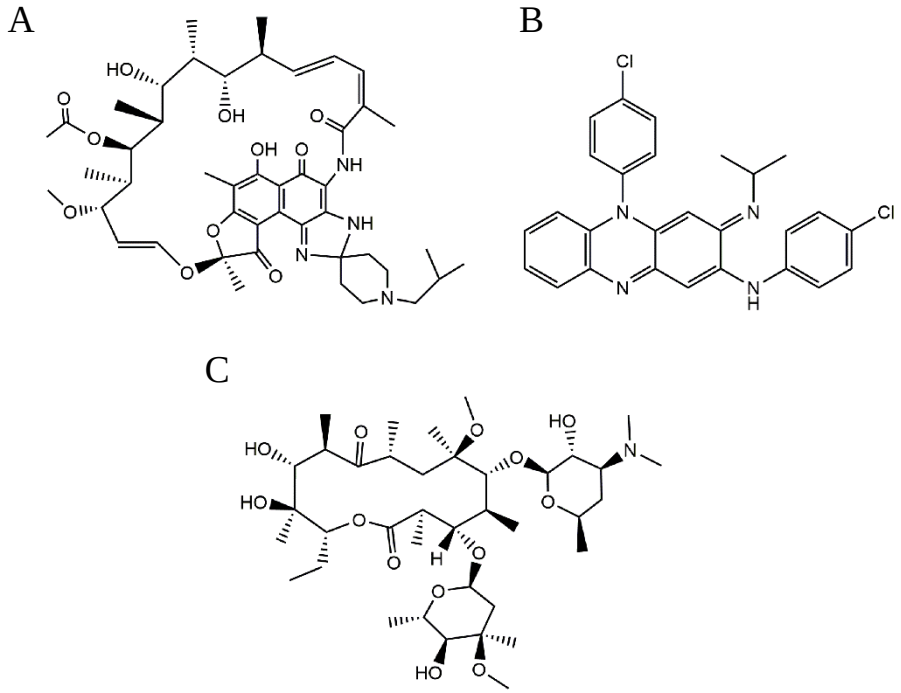

Figure 1A.1. Chemical structures of A) rifabutin, B) clofazimine and D) clarithromycin

1.2.2.Anti-mycobacterial spectrum of the drugs employed in the triple therapy of CD

Triple therapy has also been reported to be useful on the treatment of other mycobacterial diseases.

Rifabutin is active against different Mycobacterium species, including *Mycobacterium leprae*, *Mycobacterium africanum*, *Mycobacterium bovis* or Mycobacterium kansasii (27, 35). Its *in vitro* activity against *Mycobacterium tuberculosis*, even higher than rifampicin, makes it an interesting alternative to macrolides, (36). Rifabutin spectrum also includes different atypical microorganisms, such as *Mycobacterium avium* and *Mycobacterium avium complex* (MAC) (27, 35, 36), being employed in the prophylaxis of MAC infection in immunocompromised patients (36). According to a recent study, rifabutin shows a MIC ≤ 0.25-16 µg/ml in clinical isolates of *Mycobacterium avium* (23). Furthermore, rifabutin is usually associated with clarithromycin for the treatment of lung diseases produced by *Mycobacterium avium*, due to the protection conferred by rifabutin against development of clarithromycin resistance (23). Rifabutin has also reported to exert a considerable activity against MAP, showing a MIC in the range of 0.5-4 µg/ml in both human and animal isolated strains (37).

Clofazimine is part of the triple drug regimen proposed by the World Health Organization (WHO) for the management of leprosy (29, 38), caused by *Mycobacterium leprae* (39), due to its anti-inflammatory and antimicrobial properties (23). It is also employed in combination with

other compounds to treat disseminated MAC disease in immunocompromised patients, and it has been reported to be active against *Mycobacterium bovis*, *Mycobacterium avium* (MIC of 0.12 mg/ml) or *Mycobacterium tuberculosis* (MIC of 0.06-0.2 µg/ml) (23, 29). Despite its remarkable *in vitro* activity against *Mycobacterium tuberculosis* multidrug resistant strains, its efficacy in human tuberculosis has not been demonstrated (30). Early studies in higher primates and humans reported that clofazimine was ineffective when administered as monotherapy (23). This lack of efficacy together with its side effects considerably limit its clinical usefulness in tuberculosis treatment (23).

A retrospective study indicated that clofazimine concentration improves when administered together with a macrolide, suggesting that clofazimine and clarithromycin association constitute an interesting option for MAP treatment (23).

Clarithromycin has been reported to show a synergistic activity with standard anti-mycobacterial drugs, such as ethambutol, against *Mycobacterium tuberculosis* (31, 40, 41), which can be associated with its immune-modulating effects and due to its ability to promote bacterial permeability to other antimicrobial compounds, making it useful even in the case of multi-drug resistant strains (23). It is effective in MAC infections (3, 31, 35), exhibiting an activity 8 to 32-fold superior to erythromycin against *Mycobacterium avium* (23). Clarithromycin MIC against MAP *in vitro* is in the range of 0.25-0.5 µg/ml (23).

Therefore, these anti-mycobacterial compounds have a broad applicability, but limited by their physicochemical properties. Approaching and resolving those limitations with pharmaceutical technology tools should have impact, not only on anti-mycobacterial therapy of CD, but also, on the treatment other disorders such as tuberculosis and leprae, pathologies of great importance to public health.

1.3. FUTURE APPROACHES

Despite the enormous potential of anti-mycobacterium combined therapies in CD, the usage of these compounds is nowadays limited by their low aqueous solubility and low bioavailability, making necessary the administration of high antibiotic doses. In addition, the slow growth of many species of mycobacteria, such as *M. tuberculosis* or MAP (2), makes it necessary to establish prolonged treatment regimens that are often associated with lack of dose compliance, with phenomena of resistance to multiple drugs and failure of therapy (4). In addition, the administration of high doses causes the appearance of side effects of antibiotics and also triggers an imbalance in the intestinal microbiota, which can contribute to deteriorating the general health status of patients with CD (4).

Future work in the frame of anti-mycobacterial therapy of CD should focus on solving these issues, to take advantage of the full potential of anti-mycobacterial treatments. Furthermore, triple anti-MAP therapy optimization, could benefit the antimicrobial management of other important diseases, such as tuberculosis, leprae or pulmonary diseases.

Several strategies, such as the elaboration of nanoemulsions, polymeric micelles drug nanocrystals or nanoparticles (42-44) have been proposed to face drug solubility issues. All of them are based on drug particle size reduction to the nano range, which extraordinarily increases the surface area, producing a substantial improvement in water solubility and or the dissolution

rate and therefore, the bioavailability of drugs (45). The inclusion of the antimicrobial compounds in nanoparticles might offer additional advantages, which will be discussed below, in comparison with other drug delivery systems.

1.3.1. Nanoparticles as drug delivery systems for anti-mycobacterial drugs

Nanotechnology, an emerging technology in drug delivery (4), constitutes an interesting option to overcome issues related with oral administration of anti-MAP drugs. Nanoparticles have been defined as carriers, made from a wide variety of biocompatible substances, exhibiting dimensions below 1000 nm, and typically ranging from 5-350 nm of diameter (46). These particulate carriers exhibit several features, such as enhanced cellular uptake, ability to target certain cell types or the possibility to escape endo-lysosomal compartments allowing a sustained release inside the target cells (46), that make them ideal platforms for anti-mycobacterial compounds administration. In this way, their capacity to target specific cells, allows the achievement of a high antibiotic concentration within host mononuclear phagocytes, avoiding the administration of sub-therapeutic levels of drug, which often lead to worrying antibiotic resistance issues (36). The targeting ability of these carriers also reduces side effects, improving therapeutic index and patient compliance (4), which would also contribute to reduce antimicrobial resistance phenomena. Finally, nano-drug delivery systems also confer drug protection (4), which along with the increase in drug solubility, could lead to a notable improvement in drug bioavailability. This bioavailability increase along with the improved targeting ability of the nanocarriers, would allow for a dose reduction, further reducing side effects derived from anti-MAP therapy.

In order to improve oral anti-mycobacterial therapy of CD, these colloidal carriers, administered orally, accumulate in the intestinal inflamed sites, which are also densely infiltrated by immune cells, such as neutrophils or macrophages (47). This would facilitate the exposure of the microorganism to the drug within infected intestinal macrophages and would favor treatment in Crohn patients.

1.4. CONCLUSIONS

Evidence reported to date relating MAP and CD development makes mycobacterial hypothesis of CD a worthy path to explore. Despite the promising results obtained with the combined use of clofazimine, clarithromycin and rifabutin, novel technological approaches such as nanoparticles are required to improve the currently available anti-mycobacterial therapy of CD. Novel treatments would also be of interest for the management other life-threatening mycobacterial diseases, such as tuberculosis or leprae, due to the wide spectrum of anti-MAP compounds.

REFERENCES

1. Collins FM. Mycobacterial disease, immunosuppression, and acquired immunodeficiency syndrome. Clin Microbiol Rev. 1989; 2 (4): 360-377.
2. Saviola B, Bishai W. The genus Mycobacterium-medical. In: Dworkin M, Falkow S, Rosenberg E, Schleifer KH, Stackebrandt E (Ed).The prokaryotes: a handbook on the biology of bacteria. 3rd edition. New York, USA: Springer; 2006. p. 919-33.
3. Piersimoni C, Scarparo C. Pulmonary infections associated with non-tuberculous mycobacteria in immunocompetent patients. Lancet Infect Dis. 2008; 8 (5): 323-334.
4. Vieira AC, Magalhães J, Rocha S, Cardoso MS, Santos SG, Borges M, et al. Targeted macrophages delivery of rifampicin-loaded lipid nanoparticles to improve tuberculosis treatment. Nanomedicine. 2017; 12 (24): 2721-2736.
5. Lemmer Y, Kalombo L, Pietersen RD, Jones AT, Semete-Makokotlela B, Van Wyngaardt S, et al. Mycolic acids, a promising mycobacterial ligand for targeting of nanoencapsulated drugs in tuberculosis. J Control Release. 2015; 211: 94-104.
6. McNees AL, Markesich D, Zayyani NR, Graham DY. Mycobacterium paratuberculosis as a cause of Crohn's disease. Expert Rev Gastroenterol Hepatol. 2015; 9 (12): 1523-1534.
7. Davis WC. On deaf ears, Mycobacterium avium paratuberculosis in pathogenesis Crohn's and other diseases. World J Gastroenterol. 2015; 21 (48): 13411-13417.
8. Honap S, Johnston E, Agrawal G, Al-Hakim B, Hermon-Taylor J, Sanderson J. Anti-Mycobacterium paratuberculosis (MAP) therapy for Crohn's disease: an overview and update. Frontline Gastroenterol. 2020; 0: 1–7.
9. Sandberg K, Yarger E, Saeed S. Updates in diagnosis and management of inflammatory bowel disease. Curr Probl Pediatr Adolesc Health Care. 2020; 50 (5): 100785.
10. Feuerstein JD, Cheifetz AS. Crohn Disease: Epidemiology, Diagnosis, and Management. Mayo Clin Proc. 2017; 92 (7): 1088-1103.
11. Cosnes J, Gower-Rousseau C, Seksik P, Cortot A. Epidemiology and natural history of inflammatory bowel diseases. Gastroenterology. 2011; 140 (6): 1785-1794.
12. Bernstein C. Changes in the epidemiology of inflammatory bowel disease—clues for aetiology. Aliment Pharmacol Ther. 2017; 46 (10): 911-919.
13. Pasvol TJ, Horsfall L, Bloom S, Segal AW, Sabin C, Field N, et al. Incidence and prevalence of inflammatory bowel disease in UK primary care: a population-based cohort study. BMJ open. 2020; 10 (7): e036584.
14. Ekundayo TC, Okoh AI. Systematic Assessment of Mycobacterium avium Subspecies Paratuberculosis Infections from 1911–2019: A Growth Analysis of Association with Human Autoimmune Diseases. Microorganisms. 2020; 8 (8): 1212.
15. Greenstein RJ. Is Crohn's disease caused by a mycobacterium?. Comparisons with leprosy, tuberculosis, and Johne's disease. Lancet Infect Dis. 2003; 3 (8): 507-514.
16. Van Kruiningen H, Chiodini RJ, Thayer WR, Coutu JA, Merkal RS, Runnels PL. Experimental disease in infant goats induced by aMycobacterium isolated from a patient with Crohn's disease. Dig Dis Sci. 1986; 31 (12): 1351-1360.
17. Dasgupta A. Advances in antibiotic measurement. Adv Clin Chem. 2012; 56: 75-104.

18. Kuenstner JT, Naser S, Chamberlin W, Borody T, Graham DY, McNees A, et al. The Consensus from the Mycobacterium avium ssp. paratuberculosis (MAP) Conference 2017. Front Public Health. 2017; 5: 208.
19. Borody TJ, Bilkey S, Wettstein AR, Leis S, Pang G, Tye S. Anti-mycobacterial therapy in Crohn's disease heals mucosa with longitudinal scars. Dig Liver Dis. 2007; 39 (5): 438-444.
20. NIH. Efficacy and Safety of Anti-MAP Therapy in Adult Crohn's Disease (MAPUS). [ClinicalTrials.gov]. 2020. Available from: https://clinicaltrials.gov/ct2/show/results/NCT01951326. [Accessed on 14 July 2020].
21. RedHill Biopharma Announces Positive Top-Line Results from Phase III Study of RHB-104 in Crohns Disease [press release]. 2018. Available from: https://www.redhillbio.com/RedHill/Templates/showpage.asp?DBID=1&LNGID=1&TMID=178&FID=1384&PID=0&IID=8178. [Accessed on 14 July 2020].
22. NIH. Open Label Efficacy and Safety of Anti-MAP (Mycobacterium Avium Ssp. Paratuberculosis) Therapy in Adult Crohn's Disease (MAPUS2). [ClinicalTrials.gov]. 2020. Available from: https://clinicaltrials.gov/ct2/show/record/NCT03009396?view=record. [Accessed on 14 July 2020].
23. Savarino E, Bertani L, Ceccarelli L, Bodini G, Zingone F, Buda A, et al. Antimicrobial treatment with the fixed-dose antibiotic combination RHB-104 for Mycobacterium avium subspecies paratuberculosis in Crohn's disease: pharmacological and clinical implications. Expert Opin Biol Ther. 2019; 19 (2): 79-88.
24. Selby W, Pavli P, Crotty B, Florin T, Radford-Smith G, Gibson P, et al. Two-year combination antibiotic therapy with clarithromycin, rifabutin, and clofazimine for Crohn's disease. Gastroenterology. 2007; 132 (7): 2313-2319.
25. Jambhekar SS, Breen PJ. Drug dissolution: significance of physicochemical properties and physiological conditions. Drug Discov Today. 2013; 18 (23-24): 1173-1184.
26. Crabol Y, Catherinot E, Veziris N, Jullien V, Lortholary O. Rifabutin: where do we stand in 2016?. J Antimicrob Chemother. 2016; 71 (7): 1759-1771.
27. Global Alliance for TB drug development. Rifabutin. Tuberculosis (Edinburgh, Scotland). 2008; 88 (2): 145-147.
28. Pinheiro M, Silva AS, Reis S. Molecular interactions of rifabutin with membrane under acidic conditions. Int J Pharm. 2015; 479 (1): 63-69.
29. Salem II, Steffan G, Düzgünes N. Efficacy of clofazimine–modified cyclodextrin against Mycobacterium avium complex in human macrophages. Int J Pharm. 2003; 260 (1): 105-114.
30. Cholo MC, Steel HC, Fourie PB, Germishuizen WA, Anderson R. Clofazimine: current status and future prospects. J Antimicrob Chemother. 2012; 67 (2): 290-298.
31. Luo L, Chen Q, Gong H, Liu L, Zhou L, He H, et al. Capacity of cholesteryl hemisuccinate in ion pair/phospholipid complex to improve drug-loading, stability and antibacterial activity of clarithromycin intravenous lipid microsphere. Colloids Surf B Biointerfaces. 2018; 172: 262-271.
32. Kohno Y, Yoshida H, Suwa T, Suga T. Comparative pharmacokinetics of clarithromycin (TE-031), a new macrolide antibiotic, and erythromycin in rats. Antimicrob Agents Chemother. 1989; 33 (5): 751-756.

33. Inoue Y, Yoshimura S, Tozuka Y, Moribe K, Kumamoto T, Ishikawa T, et al. Application of ascorbic acid 2-glucoside as a solubilizing agent for clarithromycin: solubilization and nanoparticle formation. Int J Pharm. 2007; 331 (1): 38-45.
34. Sharma M, Gupta N, Gupta S. Implications of designing clarithromycin loaded solid lipid nanoparticles on their pharmacokinetics, antibacterial activity and safety. RSC Adv. 2016; 6 (80): 76621-76631.
35. Shulha JA, Escalante P, Wilson JW. Pharmacotherapy Approaches in Nontuberculous Mycobacteria Infections. Mayo Clin Proc. 2019; 94 (8): 1567-1581.
36. Gaspar DP, Faria V, Goncalves LM, Taboada P, Remunan-Lopez C, Almeida AJ. Rifabutin-loaded solid lipid nanoparticles for inhaled antitubercular therapy: Physicochemical and in vitro studies. Int J Pharm. 2016; 497 (1-2): 199-209.
37. Zanetti S, Molicotti P, Cannas S, Ortu S, Ahmed N, Sechi LA. "In vitro" activities of antimycobacterial agents against Mycobacterium avium subsp. paratuberculosis linked to Crohn's disease and paratuberculosis. Ann Clin Microbiol Antimicrob. 2006; 5: 27.
38. Thangaraju P, Venkatesan S. Current treatment guideline by the World Health Organization against leprosy: A positive focus. J Res Med Sci. 2019; 24 (1): 95.
39. Young RA, Mehra V, Sweetser D, Buchanan T, Clark-Curtiss J, Davis RW, et al. Genes for the major protein antigens of the leprosy parasite Mycobacterium leprae. Nature. 1985; 316 (6027):450-452.
40. Cavalieri SJ, Biehle JR, Sanders W. Synergistic activities of clarithromycin and antituberculous drugs against multidrug-resistant Mycobacterium tuberculosis. Antimicrob Agents Chemother. 1995; 39 (7): 1542-1545.
41. Van der Paardt A-F, Wilffert B, Akkerman OW, de Lange WC, van Soolingen D, Sinha B, et al. Evaluation of macrolides for possible use against multidrug-resistant Mycobacterium tuberculosis. Eur Respir J. 2015; 46 (2): 444-455.
42. Chen H, Khemtong C, Yang X, Chang X, Gao J. Nanonization strategies for poorly water-soluble drugs. Drug Discov Today. 2011; 16 (7-8): 354-360.
43. Hu L, Tang X, Cui F. Solid lipid nanoparticles (SLNs) to improve oral bioavailability of poorly soluble drugs. J Pharm Pharmacol. 2004; 56 (12): 1527-1535.
44. Thomas MJ, Slipper I, Walunj A, Jain A, Favretto ME, Kallinteri P, et al. Inclusion of poorly soluble drugs in highly ordered mesoporous silica nanoparticles. Int J Pharm. 2010; 387 (1-2): 272-277.
45. Wais U, Jackson AW, He T, Zhang H. Nanoformulation and encapsulation approaches for poorly water-soluble drug nanoparticles. Nanoscale. 2016; 8 (4): 1746-1769.
46. Maleki Dizaj S, Barzegar-Jalali M, Zarrintan MH, Adibkia K, Lotfipour F. Calcium carbonate nanoparticles as cancer drug delivery system. Expert Opin Drug Deliv. 2015; 12 (10): 1649-1660.
47. Mohan LJ, Daly JS, Ryan BM, Ramtoola Z. The future of nanomedicine in optimising the treatment of inflammatory bowel disease. Scand J Gastroenterol. 2019; 54 (1): 18-26.

SECTION B. LIPID NANOPARTICLES: FROM INITIAL DESIGN TO CLINICS*

*This introduction section has been extracted from a recently published book chapter: Rouco H[1], Diaz-Rodriguez P[1], Remuñán-López C[2], Landin M[1]. Recent advances in solid lipid nanoparticles formulation and clinical applications. In: Pippa N, Demetzos C. Nanomaterials for Clinical Applications. 1st edition: Elsevier; 2020. p. 213-47 (1).

Paperback ISBN: 9780128167052, eBook ISBN: 9780128168769.

[1] R+D Pharma Group (GI-1645), Department of Pharmacology, Pharmacy and Pharmaceutical Technology, Faculty of Pharmacy, University of Santiago de Compostela, Santiago de Compostela, Spain.

[2] NanoBiofar Group (GI-1643), Department of Pharmacology, Pharmacy and Pharmaceutical Technology, Faculty of Pharmacy, University of Santiago de Compostela, Santiago de Compostela, Spain.

USC
UNIVERSIDADE
DE SANTIAGO
DE COMPOSTELA

1.1. LIPID NANOPARTICLES

Lipid nanoparticles are colloidal systems composed by solid lipids and stabilized by a surfactant layer. This lipid-based nanocarriers group includes Solid Lipid Nanoparticles (SLN) and Nanostructured Lipid Carriers (NLC) (2).

1.1.1. Solid lipid nanoparticles

SLN are the first generation of lipid nanoparticles (3). SLN are constituted by a lipid core, solid at both room and body temperatures, surrounded by emulsifier molecules (4-6). The main advantages of SLN include excellent biocompatibility, ability to include a wide variety of bioactive molecules, rapid and effective formulation through different techniques without the need to include organic solvents and suitability for scaling up (7). The main limitations of SLN are associated with a reduced drug loading (DL) ability due to the lipid's crystalline nature and drug leakage during storage, related to gelation phenomena and lipids β-form that will be described in section 1.2.1.1. Gelation is the transformation of the colloidal suspension into a viscous gel, this process usually takes place after particle aggregation associated with lipid crystallization (8).

1.1.2. Nanostructured lipid carriers

NLC were designed to overcome the drawbacks of SLN and constitute the second generation of lipid nanoparticles (3). As for SLN, NLC matrix is solid at both room and body temperatures (6, 7). NLC show several advantages over the first generation of lipid nanoparticles, such as increased loading capacity, improved stability and higher flexibility in drug release modulation (7). Their improved characteristics are associated to the imperfect matrix structure created by mixing two spatially different molecules, a solid lipid and an oil (6).

1.2. FORMULATION COMPONENTS

SLN are composed of an oil phase and an aqueous phase in a ratio of 0.1 to 30% (w/w). Generally, the aqueous phase includes between 0.5 and 5% of surfactants. The oil phase can be constituted by a solid lipid or a mixture of different solid lipids. NLC are characterized by the combination of liquid (oil) and solid lipids in a ratio between 70:30 and 99.9:0.1 (solid lipid: oil), and total solid content of formulations can reach 95% (9).

1.2.1. Lipids

Lipids are a broad group of molecules that include triglycerides, partial glycerides, fatty acids, steroids, and waxes. Oils and fats are natural mixtures of mono, di and triglycerides containing fatty acids of different chain length and unsaturation degree (10). Most of them are approved as generally recognized as safe substances (11). Biocompatibility, biodegradability, capability of forming small particles (in the nanorange), DL capacity and stability in aqueous dispersion are the requirements of a lipid to be considered a suitable material to produce an optimal lipid nanoparticle formulation.

Several aspects must be carefully considered in the selection of the appropriate lipid variety to encapsulate a specific therapeutic agent: polymorphic state, type, amount used in the formulation process and liquid lipid combination possibility (12).

1.2.1.1. Lipids Polymorphic state

Four polymorphic forms have been described for lipids: α, β and β´ as the main forms and βi form (transitional form between β´and β) can also be observed, but in a lesser extent. Polymorphs are chemically identical but show different solubility, X-ray diffraction (XRD) pattern and melting point (12). After nanoparticles formation, lipids tend to partially recrystallize, in a highly disordered α form. During storage, polymorphic transitions from α form to a more stable β form via β´ can occur, which result in a reduction of the imperfections in the lipid matrix and the expulsion of the encapsulated drug. The extension of these phenomena depends on the storage conditions and the transition kinetics of the lipid(s) (12).

Recrystallization processes also affect particle size, size distribution, and shape of the resulting nanocarriers (12). During storage, nanoparticles may undergo directional crystal growth, altering their morphology from the spherical shape, characteristic of the α form, to a needle or plated–shape morphology, characteristic of the β form. If these needle-shaped structures with increased surface area are not stabilized by surfactants, flocculation occurs destabilizing the suspensions (12, 13). Flocculation phenomena may be responsible for the increase in particle size and size distribution reported in the literature for this type of systems (14). On the other hand, extremely slow transitions from β´ to the stable β form have been related to slight reductions in particle size during storage (15).

Proper knowledge and control about polymorphic behavior of the lipids in the formulation is necessary to develop stable nanocarriers.

1.2.1.2. Types of lipids

Different lipid types as fatty acids, glycerides, waxes, hard fats and steroids can be employed in lipid nanoparticle formulation (12). **Figure 1B.1** provides some examples of them.

Fatty acids are hydrocarbon chains that end in carboxylic acid groups with different chain lengths and unsaturation degrees that modulate their properties. Fatty acids of biological systems usually contain between 14 and 24 carbon atoms (C), being 16- and 18-C fatty acids the most common ones (16).

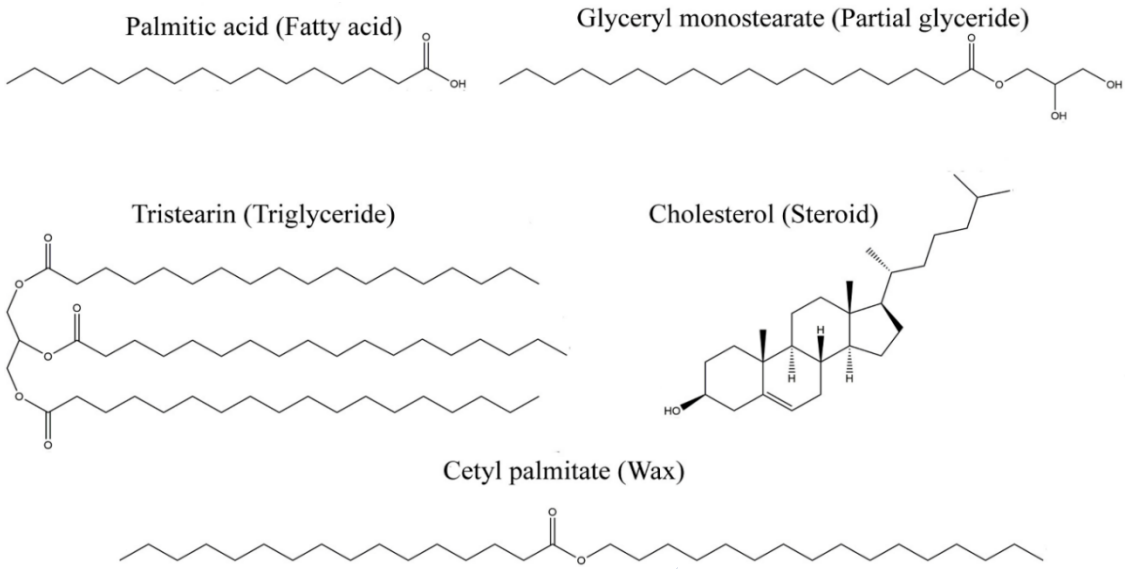

Figure 1B.1. Examples of chemical structures of different lipid types

Glyceride group includes ***triglycerides*** and ***partial glycerides*** (mono- and diglycerides), which differ in their degree of esterification with fatty acids (17).

Triglycerides are obtained by the esterification of glycerol with three fatty acids, which can be equal or not, usually showing a chain length of 16, 18 or 20 C. They can be classified according to their C chain length as short-chain (<5 C), medium-chain (6-12 C) and long-chain (>12 C), or according to their acyl substitution as mono-, di- and tri-acid (17). Medium-chain triglycerides present several advantages over long-chain triglycerides, such as higher solvent capacity and better stability towards oxidation (17).

Partial glycerides are esters of glycerol with fatty acids which contain unreacted hydroxyl groups. These substances named monoglycerides or diglycerides show interesting emulsifying properties, being considered as nonionic emulsifiers, since they do not produce ions in solution (18). Mixtures of mono, di and triglycerides (acylglycerol mixtures as e.g. Compritol® 888 ATO) are widely used for lipid nanoparticle formulation (19).

Waxes are defined as esters of fatty acids with alcohols, other than glycerol. They may contain free fatty acid functions, as is the case of beeswax, or free hydroxyl groups inside the molecule (20).

"**Hard fat**" includes (semi-) synthetic mixtures of mono, di and triglycerides of fatty acids C10-C18. These compounds show a low melting point, usually between 33 and 36°C (21).

Steroids include any synthetic or natural compound with a 1,2-cyclopentanophenanthrene backbone along with a side chain of variable length and two or more oxygen functions, such as carboxyl, carbonyl, aldehyde or alcohol (22).

The type of lipid selected strongly affects formulation properties as drug loading. As a general rule, the lesser lipid crystalline matrix order, the greater the DL capacity (12). Therefore lipids that produce highly crystalline particles with perfect lattices (such as monoacid triglycerides) often lead to the expulsion of the drug, whereas lipids that are composed of mixtures of mono, di and triglycerides (such as Precirol®) or lipids containing fatty acids of

different chain lengths, which form less-perfect crystals, offer more space for drug encapsulation (23). Other factors such as lipids hydrophobicity also determine the entrapment efficiency (EE) of lipophilic drugs. The high-lipid hydrophobicity derived from the long-chain fatty acids attached to the triglycerides (e.g., tripalmitin) results in an increase in the accommodation of lipophilic drugs and, therefore in a higher drug EE (24). In addition, emulsifying properties of mono and diglycerides, also contributes to improve DL capacity (25).

Lipid's structure seems to play a role on nanoparticles size. Lipids with smaller acyl chains have been reported to produce small-sized particles (26). The composition of the lipid matrix influences nanoparticle size and size distribution. Lipid polarity determines the surface charge of the nanoparticles and the zeta potential, conditioning their degree of agglomeration. Therefore, the use of lipids with a suitable polarity allows the production of nanoparticulate systems with a monodisperse particle size distribution and good stability (12). Other lipid excipients properties, such as speed of lipid crystallization and self-emulsifying capacity, are also known to affect the final size of lipid nanoparticles (23).

Drug release profile can fluctuate between nanoparticles prepared using different lipids. In physiological conditions, drug release from lipid nanoparticles occurs by simultaneous diffusion and erosion mechanisms. The lipid matrix degradation is mainly promoted by enzymes, and in a less extent, by hydrolytic processes (12). Prolonged release has been associated with slow drug diffusion from the lipid nanoparticles, which is highly related to some characteristics of the lipids such as hydrophobicity, hydrophilic-lipophilic balance (HLB) or melting point (12). Lipids of high hydrophobicity and low HLB are preferred to achieve controlled release drug delivery systems (12).

Nanoparticles stability during storage is an important factor that must be considered during lipid selection. Waxes, as cetyl palmitate and beeswax, exhibit superior stability in terms of particle size when compared to glycerides. However, its capacity for drug retention during storage depends, to a large extent, on the storage temperature and its tendency to form supercooled melts, as in the case for cetyl palmitate.

Within glycerides, the presence of high amounts of partial glycerides, such as monoglycerides, produces physical destabilization. On the other hand, the emulsifying properties of mono and diglycerides improve the surfactant layer around the nanoparticles avoiding agglomeration (20).

Acylglycerol mixtures such as glyceryl monostearate and glyceryl behenate are more efficient to prevent drug leakage and maintain DL during storage due to their less ordered lipid matrix (20). As noted earlier, highly ordered crystal packing of glycerides often leads to the drug expulsion in solidified state. Therefore, pure triglycerides, as in the case of tripalmitate, show the same behavior as waxes (20).

Finally, it is necessary to emphasize that, since most commercial lipid excipients are composed of mixtures of different chemical compounds, the inter- and intra-manufacturer variability is important and can have a great impact on the properties of the nanoparticles (27). Considering these aspects should help to avoid unexpected results after nanoparticle preparation.

1.2.1.3. Lipid proportion

The amount of lipids used during lipid nanoparticles formulation affects particle size and drug payload. Generally, an increase in lipid amount leads to an increase in particle size due to less efficient homogenization and greater tendency of lipids to agglomerate (12, 27). Some authors have reported this phenomenon when using increasing amounts of lipids during the formulation of nanoparticles by microemulsion or solvent injection techniques (28, 29).

Other authors have pointed out as a main factor the solvent: lipid ratio when using a modified solvent emulsification-evaporation technique for the nanoparticle formulation (30).

DL capacity is directly related to drug solubility in the lipid matrix. If drug solubility is high, a higher amount of lipid leads to an increase in drug payload. However, if drug solubility is low, the opposite effect occurs. In addition, the use of a high amount of lipid, increases the risk of crystallization, which can drastically reduce encapsulation efficiency (12).

1.2.1.4. Presence of a liquid lipid

The inclusion of a liquid lipid (oil) in the nanoparticle matrix is the main difference between SLN and NLC (31). It affects formulation parameters such as DL, size and drug release profile (12). NLC are highly heterogeneous structures with a large number of imperfections, which improves their DL capacity (12). In addition, the drugs solubility in liquid lipids is usually greater than in solid lipids (32). Several studies have described an increase in encapsulation efficiency and DL with the use of an increased amount of liquid lipid (33, 34). However, the opposite effect has also been described due to a loss in the drug immobilization capacity of the matrix by insufficient proportion of solid lipids (35).

Several authors have reported reductions in particle size as a consequence of the introduction of a liquid lipid into the nanoparticle matrix (33, 34), which may be related to differences in viscosity between both solid and liquid lipids. The inclusion of a large amount of oil in the lipid matrix reduces the surface tension, which leads to smaller nanoparticles with narrower size distributions (12). However, bigger particle sizes have also been described as a result of the increase in the amount of liquid lipid in the formulation (12, 35).

If the amount of oil further increases, there is an abrupt particle size reduction related to the solid lipids crystallization inhibition (12). Changes in particle size were also related to the reduced retention capacity of the lipid core described above, which leads to drug expulsion, producing changes in surface charge and leading to larger particle sizes and broader polydispersions (35).

The amount of liquid lipid in the nanoparticles also determines drug release profile. A high amount of oil in the matrix leads to an increase in the drug release rate due to the reduction in crystallinity and the increase of drug mobility into the NLC lipid core. The amount of liquid lipid must be carefully selected in order to optimize drug release profile (35).

1.2.2. Surfactants or emulsifiers

Surfactants are amphipathic molecules composed of a non-polar hydrophobic portion, consisting of a branched or linear hydrocarbon or fluorocarbon chain containing 8-18 carbon atoms, attached to a polar hydrophilic moiety. They are classified as ionic, non-ionic and

amphoteric (36). **Ionic** (anionic or cationic) **surfactants** confer electrostatic stability, while **non-ionic emulsifiers** provide stability by steric repulsion (17).

Most of **non-ionic emulsifiers** are too small to confer steric stability, but they are able to increase stability through the Gibbs-Marangoni effect (11), which consists on the rapid migration of the emulsifier towards the particle surface. This movement drags water, restoring its presence between particles and reducing surface concentration gradients (37).

Non-ionic surfactants are known to modulate the action of the lipase/co-lipase complex, which is responsible for "in vivo" lipid degradation. Pluronic® and Tween® are widely used non-ionic emulsifiers (11).

Amphoteric surfactants have several functional groups showing characteristics of anionic or cationic emulsifiers at high and low pH, respectively (17). Phospholipids and phosphatidylcholines, such as Lipoid® S75 and Lipoid® S100 are examples of amphoteric surfactants used in lipid nanoparticles formulation (4).

Sodium cholate and sodium dodecyl sulfate, among others, are **ionic surfactants**, which are commonly used for the preparation of lipid nanoparticles (11).

Surfactants can also be classified according to their hydrophilic-lipophilic balance (HLB), as hydrophilic (HLB > 11), intermediate (HLB 9 - 11) or lipophilic (HLB < 9). HLB values of emulsifiers are determined by the equilibrium between the strength and size of their hydrophilic and lipophilic groups (31).

Emulsifiers play two essential roles in lipid nanosystems: 1-facilitate the dispersion of the molten lipid in the aqueous phase during formulation process and 2-confer stability to the lipid nanoparticles after cooling (11). In addition, they modulate the crystallization process of lipid nanoparticles, since they interact with a large number of lipid molecules due to the small size of the nanoemulsions. The use of surfactants can improve the kinetic stability of the crystal structure generated even if it is thermodynamically less stable than other polymorphic forms (13).

Factors such as the administration route, the HLB of the emulsifier, the desired particle size or the preferred "*in vivo*" degradation pattern for the lipid matrix strongly condition the selection of the optimal surfactant (11). The best option for efficiently stabilize lipid nanosystems and preventing particle agglomeration is using combinations of emulsifiers (27).

A method of selecting emulsifiers based on HLB has been proposed. The HLB system consists of using a surfactant or combinations with an HLB as close as possible to the HLB of the lipids. This would ensure a good performance of the resulting nanosystem (31). The estimation of the required HLB can be carried out using the Grifinth equation or considering the values provided by manufacturers (38).

1.2.3. Other components

In addition to lipids and emulsifiers, other agents such as counterions, surface modifiers, cryoprotectants, antimicrobial agents and other preservatives may also be part of the lipid nanoparticles composition (5, 11). Counterions such as anionic polymers or organic ions can be incorporated into lipid nanoparticle formulations to encapsulate water-soluble cationic drugs (11). Cryoprotectants such as sorbitol, glucose and fructose are used in lyophilized

formulations. Parabens and thiomersal may also be included as antimicrobial agents and preservatives (5).

1.3. PRE-FORMULATION STUDIES

1.3.1. Solubility studies

Drug solubility in the lipid or combination of lipids should be properly characterized to know drug affinity for the nanoparticle matrix and establish the optimal drug: lipid ratio. For solid lipids, solubility studies are often performed by heating them 10 °C above their melting point and successively adding small amounts of drug until lipid saturation, which is considered to occur when the excess of solid drug remains for more than 8 hours (39). Alternatively, this study can be performed using a known amount of drug and increasing amounts of solid lipids. In this case, the end point of the experiment will be the amount of molten solid lipids that allows the formation of a clear solution. (40).

For liquid lipids, this analysis is usually accomplished by determining the highest amount of drug that can be dissolved in each candidate lipid. For this, an excess of drug is incorporated to a known amount of lipid in a vial, stirred at room temperature for 72 hours, centrifuged, and the amount of drug dissolved is quantified (40). A similar procedure can also be used for other formulation raw materials such as organic solvents and surfactants. Excess of drug is added to a known amount of the tested component (s). The blend is mixed, sonicated, and finally kept in an incubator shaker. After 8-12 hours, mixtures are centrifuged, and the drug is determined in the supernatant (41).

1.3.2. Partitioning analysis

Partitioning nature assay constitutes a different approach to investigate the affinity of a drug for the lipid matrix selected and is designed to predict, in an approximately way, the drug encapsulation in a certain lipid matrix. In this assay, drug is dispersed in a melted lipid along with hot phosphate buffer pH 7.4. The mixture is shaken for 30 minutes 10ºC above the melting point of the selected lipid. The aqueous phase is then separated from the lipid by centrifugation, and drug content is quantified in the supernatant. The partition coefficient is calculated by the subtraction of the amount of drug present in phosphate buffer to the total drug added, and the subsequent division by the amount of total drug (23).

1.3.3. Compatibility between solid lipids and liquid lipids

In the formulation of NLC, it is advisable to evaluate the compatibility between the selected lipids. This study can be carried out easily by mixing the solid lipid and the oil in different proportions at a temperature 5°C above the melting point of the solid lipid. Mixtures are analyzed visually after 1 and 24 hours of matrix solidification. Those that show a single phase are considered suitable for nanoparticles formulation (41).

An alternative method to evaluate the miscibility between solid and liquid lipids consists of mixing liquid and solid lipid in different proportions at 85ºC and cooling until solidification. Then hydrophilic filter paper is smeared with these mixtures and observed. The absence of oil droplets on the paper is indicative of a good miscibility between lipids (42).

1.4. FORMULATION PROCEDURES

Formulation procedures of SLN and NLC can be categorized into three groups. High-energy methods, low-energy methods, and approaches based on organic solvents (5). Moreover, several formulation techniques to produce lipid nanoparticles in solid state have also been reported (43), although they are not widespread.

1.4.1. High-energy methods

High-energy methods are based on the use of equipment, which produces particle size reduction through the generation of high shear forces or pressure distortions (5).

1.4.1.1. High-pressure homogenization

High-pressure homogenization can be performed at high or low temperature (5, 7, 44). First, lipids are heated 5°C /10°C above their melting point and the drug is dispersed in the melt. If the high-temperature process is used, the aqueous solution is also heated and added to the oil phase. The pre-emulsion is obtained using a high-shear mixer and homogenized in a high-pressure homogenizer at elevated temperature until the desired particle size is achieved. Finally, the nanoemulsion is cooled at room temperature (5, 44). If the cold technique is performed, the drug-lipid melt is cooled using liquid nitrogen or dry ice and ground by a ball-mill or a mortar. The powder obtained is dispersed in a cold aqueous-surfactant solution and homogenized using a high-pressure homogenizer at room temperature or even lower (5, 44).

High-pressure homogenization method is simple and cost-effective. Nevertheless, in the hot method, high temperature during homogenization is mandatory (7), being a limitation for thermolabile drugs. Cold homogenization helps to overcome this problem and constitutes a well-established advantageous procedure for large-scale manufacture avoiding organic solvents (7).

1.4.1.2. Emulsification-sonication technique

This technique is carried out by melting the drug-lipid mixture above the melting point of lipids and dispersing it in aqueous-surfactant solution kept at the same temperature by means of a high-shear mixer. The resulting emulsion is ultrasonicated to reduce particle size, and finally nanoparticles are obtained by cooling the nanoemulsion at room temperature. The main disadvantage is the possibility of dispersions contamination with metals during sonication (5, 44).

1.4.1.3. Supercritical fluid technology

A compound in the supercritical state, at temperature and pressure above the critical values behaves like gas and liquid simultaneously. The solubility of a substance in the supercritical fluid (SCF) can be regulated through small changes in pressure. CO_2 is the most commonly used SCF because of its low critical point, nontoxicity and low cost (43). Two main methods have been described for lipid nanoparticle production, gas-assisted melting atomization (GAMA) and supercritical fluid extraction of emulsions (SCFEE).

In GAMA, lipids are melted and exposed to supercritical CO_2 in a mixing chamber. The saturated lipid mixture is sprayed through a nozzle into a chamber. The rapid depressurization of the mixture generates a high supersaturation and precipitation of lipid microparticles. The microparticles are collected, dispersed in water, and using a vortex or ultrasound, fragmented to obtain nanoparticles (43).

In the SCFEE process, drug-loaded O/W (oil-in-water) emulsions are introduced into the upper part of an extraction column. The introduction of supercritical CO_2 countercurrent through the lower part leads to the extraction of solvents and the precipitation of drug-lipid particles. The main advantage of this technique is the high efficiency of elimination of solvents (43).

1.4.1.4. Hot high-shear homogenization

This technique is performed by heating separately an aqueous and an oil phase 10ºC above lipids' melting point. The aqueous phase is added onto the oil phase, and homogenization is performed by a high-shear laboratory mixer at constant temperature. The obtained nanodispersions are cooled down to allow lipid crystallization (39). This technique is extremely simple, but it has the limitation of the potential presence of microparticles in the final dispersion (45).

1.4.2. Low energy methods

This category includes methods that do not require a large amount of energy and/or those in which the reduction of the particle size can take place spontaneously (5).

1.4.2.1. Microemulsion technique

In this method, nanoparticles are obtained spontaneously due to the high surfactant-lipid ratio used (5). To generate nanoparticles, a preheated surfactant-containing aqueous solution is added onto a melted drug-lipid mixture and emulsified under mild agitation. Then the emulsion is dispersed in an excess of cold water maintaining the agitation to achieve a nanoemulsion, which results in the formation of nanoparticles after droplet crystallization (5, 44). The main advantage of this technique is its suitability for large-scale production (7, 44). Among its disadvantages, the high amount of emulsifying agents and the great dilution of the nanoparticles can be noted (5, 7).

1.4.2.2. Double emulsion

This method is used to produce lipid nanoparticles including hydrophilic drugs or peptides (5), which are usually known as lipospheres, because of their large particle size (44). A blend of melted lipids and an active ingredient aqueous solution is mixed to form a W/O (water-in-oil) microemulsion, which is dispersed in an aqueous solution containing a hydrophilic stabilizer to form a W/O/W (water-in-oil-in-water) double emulsion. Lipid nanoparticles are obtained after emulsion dilution in cold water (5).

1.4.2.3. Membrane contractor technique

In this procedure, a drug-lipid melt is pushed through a hydrophobic porous membrane toward an aqueous-surfactant solution which is circulating inside the membrane module dragging away the lipid droplets. Finally, these lipids droplets form the nanoparticles when the aqueous phase is cooled at room temperature (5, 7). Its main advantages are simplicity (7) and possibility to achieve a continuous production (5).

1.4.2.4. Phase inversion technique

Phase inversion induced by heat is performed by preparing a mixture of water, emulsifier, lipid, and drug under stirring, which is subsequently subjected to three heating and cooling cycles (85°-60°-85°) (7). These cycles produce the inversion of emulsion phases, progressively reducing droplet size (5). Nanoparticles are finally obtained by dilution in cold water (5, 7). Its principal advantages are the avoidance of organic solvents, while its main disadvantage is the tedious formulation process (7).

1.4.2.5. Coacervation

This formulation method is based on the fact that the presence of surfactants produces the precipitation of free fatty acids from their micelles. A salt of a fatty acid is dispersed in an emulsifier solution. The mixture is heated until the Kraft point of the salt of the fatty acid under agitation. When a clear solution is achieved, an ethanolic solution containing the drug is added gently under constant stirring to obtain a single phase. The addition of an acidifying solution or a coacervation agent promotes the formation of the nanoparticle suspension (5).

1.4.3. Organic solvent-based approaches

In this category, the particle size reduction is achieved by the addition of organic solvents (5) which is precisely its main drawback (44).

1.4.3.1. Solvent emulsification-evaporation method

In this technique, lipids dissolved in water-immiscible organic solvents (chloroform, cyclohexane) are emulsified with an aqueous phase containing surfactants by stirring. The evaporation of the solvent during the emulsification leads to lipids precipitation and nanoparticles formation (7, 44). The main advantage of this method is its suitability for thermosensitive drugs. However, the high dilution of the dispersions obtained constitute its major drawback (7, 44).

1.4.3.2. Solvent emulsification-diffusion method

Solvent-emulsification diffusion method involves the use of partially water-miscible organic solvents (ethyl formate, benzyl alcohol) which are saturated with water, to dissolve the lipids (44). The oil-in-water emulsion is dispersed into water under continuous stirring, producing the diffusion of the organic solvent and the lipids precipitation with the subsequent nanoparticle formation (5, 7, 44). The solvent can be removed by distillation or ultrafiltration

(5). The main disadvantage of this formulation procedure is the high dilution of the dispersions obtained (44).

1.4.3.3. Solvent injection method

Lipids and active ingredients are dissolved in a water-miscible organic solvent (methanol, acetone, isopropanol) or a water-miscible solvent mixture. After that the organic solution is injected through an injection needle in an aqueous solution of emulsifiers under stirring, producing the solvent migration and nanoparticle precipitation (5, 44). Among the advantages of this technique are equipment simplicity, easy handling, and agile production process (**Table 1B.1**) (44).

Table 1B.1. Methods of lipid Nanoparticle production. Advantages and disadvantages

High Energy methods				
Method	**Advantages**	**Disadvantages**	**Examples**	**References**
Hot High-pressure homogenization	Simple, cost-effective, no organic solvents, easy to scale up	High temperature, not suitable for thermolabile drugs, high energy input	Progesterone-loaded SLN and NLC, Dibucaine-loaded SLN	(7, 44, 46-49)
Cold High-pressure homogenization	Simple, cost-effective, easy to scale up, no organic solvents, suitable for thermosensitive drugs in some cases, suitable for hydrophilic drugs	More cycles and higher pressures required, high energy input, high temperature used in melting step	Lysozime-loaded SLN, Vinorelbine bitartrate-loaded SLN	(7, 44, 45, 48-51)
Emulsification-sonication technique	High shear mixing, no organic solvents, simplicity, low surfactant concentration	Potential metallic contamination, polydisperse suspensions, not suitable for thermolabile drugs	Vorinostat-loaded SLN, Raloxifene-loaded SLN	(5, 7, 44, 48, 52, 53)
Supercritical fluid technology	High efficiency of solvent elimination, nanoparticles in solid state, rapid, suitability for labile compounds	Use of organic solvents, use of complex equipment	Camptothecin-loaded SLN, Ketoprofen-loaded SLN and Indomethacin-loaded SLN	(43, 49, 54, 55)
Hot high shear homogenization	Simplicity, no organic solvents, low surfactant concentration, low cost	Microparticles in the final product, not suitable for thermolabile drugs	Rifabutin-loaded NLC and SLN, Resveratrol-loaded SLN and NLC	(34, 39, 45, 48, 49, 56)

Low Energy methods				
Microemulsion technique	Easy scale up, no organic solvents, reduced particle size and size distribution	High proportions of emulsifiers, high nanoparticle dilution	Ofloxacin-loaded NLC, Topotecan-loaded SLN and NLC	(5, 7, 44, 48, 57, 58)
Double emulsion	No complex equipment, suitable for hydrophilic drugs, suitable for thermolabile drugs	Large particle size, use of organic solvents, high nanoparticle dilution	Vancomycin-loaded SLN, Puerarin-loaded SLN	(5, 45, 48, 49, 59, 60)
Membrane contractor technique	Simplicity, possible continuous production	Membrane obstruction	Vitamin E-loaded SLN	(5, 7, 61)
Phase inversion technique	Easy to scale up, no organic solvent	Tedious process, emulsion instability	Idebenone-loaded SLN	(5, 7, 48, 62, 63)
Coacervation	Low cost, suitable for thermolabile drugs, shape and size can be modulated by reaction conditions	Possibility of components degradation due to acidic conditions	Didodecylmethotrexate-loaded SLN, Temozolomide-loaded SLN	(48, 64, 65)
Organic solvent-based approaches				
Solvent emulsification-evaporation	Suitable for thermosensitive drugs, simple equipment, small particle size and size distribution, reproducibility	Use of organic solvents, high nanoparticle dilution, emulsion instability	Diclofenac sodium-loaded SLN, Ritonavir-loaded SLN	(7, 44, 48, 49, 63, 66, 67)
Solvent emulsification-diffusion	Suitable for thermosensitive drugs, simple equipment, small particle size and size distribution, reproducibility	Use of organic solvents, high nanoparticle dilution, emulsion instability	Budesonide-loaded SLN, 5-fluorouracil-loaded	(5, 7, 44, 63, 68-70)
Solvent injection	Simplicity, fast production, suitable for thermosensitive drugs	Use of organic solvents	Ciprofloxacin hydrochloride-loaded SLN, Econazole nitrate-loaded NLC	(7, 44, 48, 63, 71, 72)

1.5. CHARACTERIZATION TECHNIQUES

1.5.1. Particle size and size distribution

The nanoparticles particle size and size distribution are evaluated by Laser Diffraction (LD) and Photon Correlation Spectroscopy, also known as Dynamic Light Scattering (DLS) (5, 44). The simultaneous use of both techniques is recommended because they complement each other in the range of particle sizes they determine (25). Particle size distribution is characterized by the polydispersity index, which ranges between 0 to 1. Values close to 0 correspond to monodisperse samples, while values close to 1 are indicative of highly polydisperse distributions (5). These techniques are based on projected surface light scattering effects of the particles, so not spherical shapes or broad particle size distributions can generate misunderstandings of the obtained values. It is recommended to confirm the results using imaging techniques (5, 25).

1.5.2. Surface charge

Zeta potential values are commonly used to express superficial charge magnitude in aqueous dispersions and can be estimated through the determination of the electrophoretic/electroacoustic mobility. Zeta potential can also be estimated by DLS and LD (5) being indicative of nanoparticles long-term physical stability. It has been reported that absolute values higher than 30 mV are required to assure stability in terms of pure electrostatic interactions. However, if surfactants providing steric stabilization are used, an absolute value of 20 mV is enough for nanoparticle stabilization (5, 7).

1.5.3. Morphology

Nanoparticle morphology can be evaluated by scanning electron microscopy (SEM), transmission electron microscopy (TEM), atomic force microscopy (AFM) and their cryogenic variations (5). These techniques also provide information about particle size, surface topography, aggregation, and internal structure (7). The most widely used technique is TEM, which usually requires negative staining, followed by SEM that involves drying the sample and coating it with a metallic layer (5), which can cause alterations of the nanoparticles (25). AFM allows sample observation in hydrated state, without coating or staining steps (5). Image techniques involving cryofixation, as CryoTEM or CryoFESEM (Cryo field emission SEM), can be suitable alternatives, since they allow particle observation in a frozen hydrated state (7).

1.5.4. Degree of crystallinity and polymorphism

Crystalline state and polymorphism should be carefully characterized since they can affect lipid nanoparticle encapsulation efficiency and release profile. It should be considered that thermodynamic stability increases and loading capacity decreases in the following order: supercooled melt > α-modification > β´-form > β-modification (7).

Differential Scanning Calorimetry (DSC) and XRD are two commonly used techniques to evaluate crystal structure and polymorphic behavior of SLN and NLC (5, 44).

DSC technique allows the detection of melting point modifications and melting enthalpies of lipids (25, 44), providing information about structure, physical state, phase transitions, and

interactions between components (5). XRD allows the characterization and the identification of lipid and drug structures and the prediction of lipid molecules arrangement and phase behavior (44).

1.5.5. Coexistence of different colloidal structures

When producing lipid nanoparticles, it is common to obtain dispersions of different coexisting colloidal structures (liposomes, nanoemulsions, micelles, mixed micelles and supercooled melts) with dynamic phenomena between them, affecting particle stability, DL and drug release behavior (7). Electron Spin Resonance and Nuclear Magnetic Resonance are useful noninvasive techniques to study these phenomena together with the existence of oily nanocompartments (multiple-type NLC) (7, 25, 44).

1.5.6. Entrapment efficiency and drug loading

DL capacity is defined as the percentage of drug incorporated in the particles regarding to the total nanoparticle weight. EE is defined as the percentage of drug incorporated into the particle with respect to the total amount of drug added (5, 6). It should be noticed that EE percentages can reach high values if a low amount of drug is added, so it is always advisable to pay attention to DL values (6). To determine both parameters, it is necessary to separate the drug from the formulation, for which techniques such as ultrafiltration, centrifugation or dialysis can be used (5). The quantification of the drug can be determined indirectly, by measuring the free drug in the aqueous phase (73) or directly, disrupting the lipid matrix with organic solvents (34).

1.6. DRUG INCORPORATION MODELS

1.6.1. Drug loading models of solid lipid nanoparticles

Two different structural models have been proposed for SLN. The first model corresponds to the α-polymorph form of lipids which maintains a spherical shape after cooling. The second model has been associated to the β or β´ forms of lipids that lead, after solidification, to a platelet-like layered structure with several creases and borders (5).

The affinity of the drug for the different formulation components determines its distribution within the SLN (5). Three models have been proposed for SLN of the spherical-shaped structure: homogeneous matrix or homogeneous matrix of solid solution (**Fig. 1B.2A**), drug-enriched shell (**Fig. 1B.2B**) and drug-enriched core (**Fig. 1B.2C**).

1.6.1.1. Homogeneous matrix

The active ingredient is molecularly and homogeneously dispersed into the lipid nanoparticle matrix or forming amorphous drug clusters (4, 6). Drug release occurs by diffusion and degradation of the lipid matrix (6) and a controlled drug release can be achieved (4). This type of drug incorporation can be obtained by avoiding heat during formulation process, optimizing the drug-lipid ratio in hot techniques (4), without using surfactants or alternatively

using emulsifiers that cannot solubilize the drug (25). Highly hydrophobic drugs with high-crystallization temperatures favors the generation of this model (5).

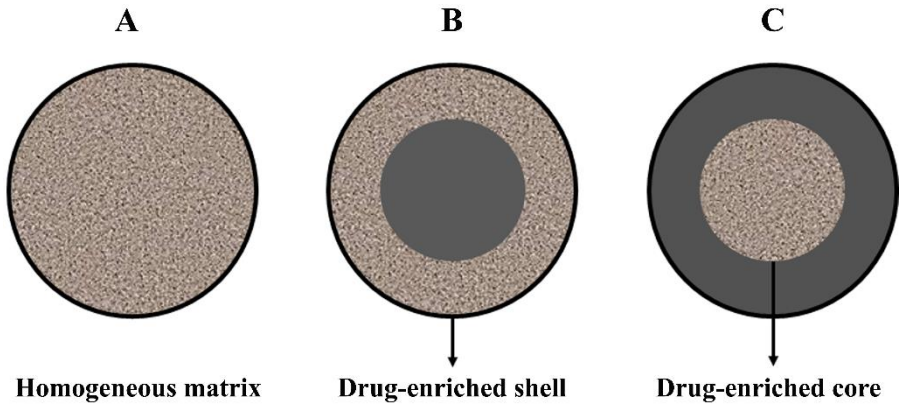

Figure 1B.2. SLN drug incorporation models. (A) Homogeneous matrix. (B) Drug-enriched shell. (C) Drug enriched core. SLN, Solid lipid nanoparticles

1.6.1.2. Drug-enriched shell

Nanoparticles present a core-shell structure where drug is located in the shell (6). If nanoparticle matrix started to solidify when the repartition process takes place, an accumulation of drug in the nanosystem shell occurs. Drug release profiles of this kind of nanoparticles are characterized by a burst release, due to the drug accumulation in the outer part of the particles (74). This type of drug incorporation is obtained when lipids of high-crystallization temperatures, high-surfactant concentration, low amount of drug, and hot techniques are selected (4-6).

1.6.1.3. Drug-enriched core

Nanoparticles present a core-shell structure where drug is accumulated in the core (6). Drug release profile is expected to follow a prolonged release pattern (4, 6). This structure is obtained when the recrystallization of the lipid occurs after the precipitation of the drug. This occurs when working at drug concentrations in the melted lipid near saturation so that the crystallization of the lipid occurs after the crystallization of the drug (4, 6, 25).

Besides these incorporation models, it is also necessary to consider that drug incorporation in the aqueous phase as well as in the nanoparticle interface is also possible, leading to a rapid release of the active ingredient. This phenomenon is associated with β polymorphic forms, which often lead to drug expulsion (5).

1.6.2. Nanostructured lipid carriers drug loading models

Three different structural models of NLC, depending mainly on the type of lipid used, have been described (4): imperfect (**Fig. 1B.3A**), amorphous (**Fig. 1B.3B**) and multiple oil-in-solid fat-in-water (O/F/W) (**Fig. 1B.3C**).

1.6.2.1. Imperfect type

In this type of NLC, DL capacity is improved by increasing imperfections in the crystal order (7). This can be performed by adding a sufficient amount of oil to the solid lipid to decrease the order of the lipid matrix due to the presence of mixtures of mono, di and triacylglycerols and fatty acids of different chain lengths (4). In this structure, the drug molecules can be included in the gaps between the fatty acid chains of triglycerides in the crystal (75).

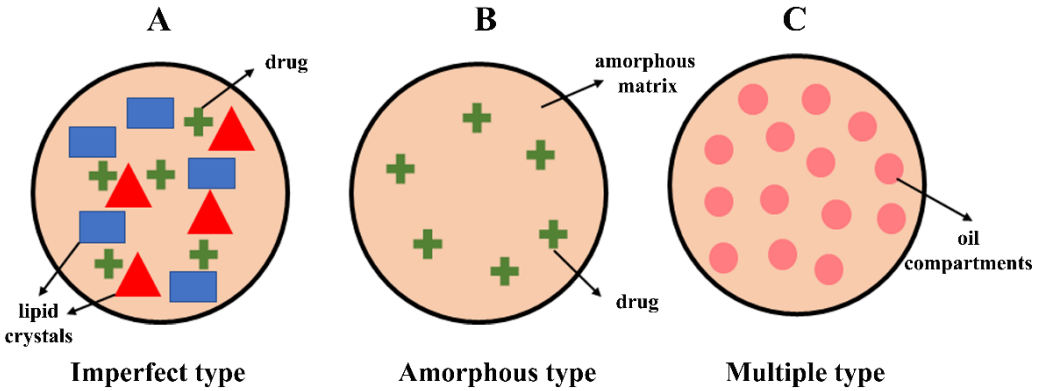

Figure 1B.3. NLC structural types. (A) Imperfect type. (B) Amorphous type. (C) Multiple type. NLC, Nanostructured lipid carriers

1.6.2.2. Amorphous type

In amorphous NLC, drug expulsion during storage due to β-modification is avoided by the generation of an unstructured amorphous lipid matrix (7). For this purpose, the solid lipid is mixed with special lipids such as isopropyl myristate, hydroxyoctacosanyl hydroxystearate, or dibutyl adipate (4, 7) that do not recrystallize during the cooling step, creating an amorphous structure (4).

1.6.2.3. Multiple oil-in-solid fat-in-water (O/F/W) type

Multiple-type NLC (**Fig. 1B.3C**) show several tiny oil compartments embedded in the nanoparticles structure that increase DL. The structure reminds the W/O/W emulsions (75). A prolonged release of drug controlled by the solid lipid matrix around the small compartments can be achieved with this model (7). This type of NLC can be obtained using amounts of oil greater than its solubility in the solid lipid (4). During the cooling step, the oil droplets reach the miscibility region, precipitate and remain fixed within the nanoparticles structure through the solidification of the solid lipid (4).

1.7. ADMINISTRATION ROUTES

Lipid nanoparticles offer a high potential as drug delivery systems through different administration routes such as topical, parenteral, oral, pulmonary, ocular or intranasal (7, 43).

1.7.1. Topical administration

Dermal and transdermal administration of drugs is an interesting approach for the management of dermatological pathologies, increasing the amount of drug in the site of action

for a local effect or even looking for a systemic therapy (76). The main barrier of the skin is the stratum corneum, which can be crossed via the cell, paracellular or follicular pathways. In addition to its barrier effect, the skin also has its own metabolism that hinders drug absorption by this route (76, 77).

Lipid nanoparticles have certain advantages for topical application: drug protection, modulation of drug release, improved bioavailability, increased skin penetration and adhesion to the stratum corneum. It is known that after its topical application, SLN and NLC form a hydrophobic film with occlusive properties. As a consequence of the strengthening of the lipid barrier, the loss of transepidermal water is prevented and the skin hydration increases (76, 77).

Large lipid nanoparticles (>100 nm) can remain on skin surface or accumulate in hair follicles, generating a drug reservoir and releasing active ingredients towards epidermis and dermis, so having a local effect (76).

Small lipid nanoparticles (<100 nm) can reach blood circulation, having a systemic effect. In addition, its composition gives them the ability to alter the structure of the stratum corneum. The lipids interact with those of the skin and the surfactants act as absorption promoters (76, 77).

During the last years, SLN and NLC have been tested *in vitro*, *ex vivo* or *in vivo* animal models as drug delivery systems to topically administer different drugs to treat skin disorders, chronic wounds or even rheumatoid arthritis (76, 77). Some selected drug used examples are tretinoin (78), acyclovir (79), methotrexate (80), recombinant human epidermal growth factor (81), astragaloside IV (82), minoxidil (83) or resveratrol (84). The use of lipid nanoparticle formulations has been linked to various therapeutic benefits such as improved efficacy, transdermal drug permeation, and penetration of the stratum corneum, or an increase in the local concentration of the drug, together with a reduction in systemic absorption and the irritation of the skin (77).

Lipid nanoparticle suspensions can be transformed in semi-solid formulations to facilitate topical application, for example, by dispersing the nanosystems in freshly prepared hydrogels or by adding gelling agents to the aqueous phase (nanoemulgels). Moreover, SLN and NLC have been widely studied for cosmetic purposes, as is the case of formulations with antiage, antioxidant, ultraviolet blocker and hydrating properties (77).

1.7.2. Parenteral administration

Among the advantages of parenteral lipid nanoparticles are their particulate nature, the protection of the drug, the suitability for the encapsulation of lipophilic and hydrophilic drugs, the potential controlled release of the drug, the cost of the raw materials, and the ease scaling up process (85). In addition, the biodegradability of lipids also makes this kind of nanoparticles a good alternative for this purpose (86).

The main limitation associated with the intravenous administration of these systems is their rapid clearance by the reticuloendothelial system, which can be avoided by modifying them superficially with compounds such as polyethylene glycol or Pluronic F68 (stealth nanoparticles) (86).

SLN and NLC have been widely studied to treat cardiovascular diseases, rheumatoid arthritis, parasites, inflammatory processes, liver diseases, pain or cancer, via parenteral route (85, 86). Several formulations have been developed and tested both *in vitro* and *in vivo*, as is the case of camptothecin- and paclitaxel-loaded SLN (87, 88) or docetaxel-loaded NLC (89), among others. Formulations show an improved efficacy together with an increased retention time after parenteral administration. SLN and NLC functionalization with several ligands allows targeting to specific organs, as brain, being useful for treating brain diseases by taking advantage of their ability to overcome the blood-brain barrier (85, 86). Bromocriptine- and apomorphine-loaded NLC or clozapine-loaded SLN are some examples of lipid nanoparticles designed for brain targeting using parenteral route (90, 91).

1.7.3. Oral administration

Oral route is regarded as the preferred administration route due to its many advantages, such as patient compliance, ease of self-administration, painlessness, cost-effectiveness and feasibility for outpatients (92, 93). The main challenges for drugs oral administration are related to the characteristics of the active molecules (low aqueous solubility, stability or permeability) and to the physiological barriers of the gastrointestinal tract: chemical and enzymatic environment, gastrointestinal epithelium (GI), mucosal barrier, presence of multidrug efflux proteins such as glycoprotein P (P-gp) in the membrane of epithelial cells, first-pass metabolism and variability due to the presence of food (92, 93).

The formulation of drugs in lipid nanoparticles for oral administration, confers various benefits such as increased drug solubilization capacity in the GI tract, the protection of labile drugs, the potential controlled release properties, the increase in the residence time, and the potential selective drug delivery (92, 93). In addition, nanoparticles undergo lymphatic absorption that increases the bioavailability and half-life of drugs that undergo hepatic first-pass effect and are also useful in the case of drugs with toxic metabolites. Drugs which interact with P-gp can also be efficiently delivered through the oral route when administered as lipid nanoparticles (92).

Lipid nanoparticles can be administered orally as aqueous dispersions or solid dosage forms (powders, capsules, pellets or tablets) (43). They can undergo a digestive process by enzymes, releasing the drug, which crosses the enterocytes and reaches the systemic circulation or alternatively the drugs released together with the products obtained from the digestion of lipids, can form micelles with the bile salts and reach the enterocytes, avoiding the first-pass metabolism by the formation of chylomicrons (92). If nanoparticles avoid digestion process, they could reach portal circulation via paracellular route or lymphatic system through M cells (92), although there is still no consensus about this possibility (92, 93).

Recently, the usefulness of SLN has been explored for the administration of different drugs and natural products through the oral route for the treatment of several pathologies, such as cancers, central nervous system diseases, cardiovascular diseases, infections, diabetes, and osteoporosis. They have shown promising results both *in vitro* and in animal models (93). NLC have also been employed to administer orally a wide variety of active molecules such as anticancer (94), antiinflammatory (95), antihypertensive (41) or antidiabetic drugs (96), among

others. Strategies such as surface modification to improve adhesion and diffusion across the mucus as well as peptide ligands have also been evaluated. Those lipid nanosystems have helped to overcome low solubility, stability, permeability problems or drugs' high toxicity and to improve pharmacokinetic parameters of NLC-loaded drugs. Various oils from plant and animal sources have been included in NLC (as liquid lipid) and drug delivery in the oral cavity using lipid nanoparticles included in hydrogels to treat infections has also been studied (92).

1.7.4. Pulmonary administration

Drug delivery through the inhalation offers a huge potential for both local and systemic therapy (97, 98). Lipid nanoparticles advantages for pulmonary drug delivery include good biocompatibility and biodegradability, deep lung deposition, prolonged mucoadhesion, lung retention and controlled release, improving therapeutic efficacy of drugs, reducing required dose, and increasing dose interval (97).

SLN and NLC for pulmonary administration should be biocompatible and fulfill aerodynamic requirements that vary depending on whether the therapy is systemic or local. For systemic treatments, lipid nanoparticles with 1-3 μm aerodynamic diameters are required to achieve deep lung deposition and drug absorption. For local delivery, the requirements depend on the lung area to be treated (97). Lipid nanoparticles can be administered as suspensions using nebulizers or as dry powders and their size can be modulated as a function of its composition and formulation method (97, 98).

Systemic treatments via inhalation can be interesting alternatives for peptide and protein delivery, which can be either incorporated into the lipid matrix or adsorbed onto the surface (97). In addition, lipid nanoparticles have also shown their potential to deliver other drugs, such as alendronate, to achieve a systemic effect, in this case, for osteoporosis treatment (99).

Regarding local pulmonary therapy, lipid nanoparticle formulations have been studied for the treatment of several diseases such as chronic obstructive pulmonary disease, asthma, lung cancer, cystic fibrosis or mycosis (97, 98). Some examples are epirubicin- and paclitaxel-loaded SLN (100, 101), or beclomethasone dipropionate- (102), tobramicin- (103) and itraconazole-loaded NLC (104).

Pulmonary tuberculosis treatment is another goal for lipid nanoparticles (97). It has been shown that lipid nanoparticles of size around 1μm provide an efficient alveolar macrophage targeting (105). As an example, SLN loaded with rifampicin, isoniazid and pyrazinamide have shown promising results (97). In addition, pulmonary administration of gene vectors, as plasmid-DNA and small interfering RNA (siRNA), using lipid nanoparticles has also been explored (97, 98).

1.7.5. Ocular administration

Topical ocular delivery is the most suitable route to treat superficial diseases and pathologies related to the anterior segment of the eye, due to its ease of administration, noninvasive nature, patient compliance, reduced systemic absorption, and avoidance of hepatic first-pass effect. However, the presence of barriers, metabolic (esterases and cytochrome P-450), static (corneal epithelium and stroma, and blood aqueous) or dynamic (lymphatic flow,

conjunctival flow and drainage of tears), hinders drugs administration. Therefore, treating the posterior segment of the eye by topical route still constitutes a challenge (106).

SLN and NLC offer certain advantages for the administration of drugs via the eye; they confer protection to drugs against lacrimal enzymes and binding proteins; they are able to overcome the eye's blood barriers; they allow controlled and prolonged release of drugs; they are biodegradable and biocompatible and they allow to decrease the dosage and therefore reduce side effects (106, 107).

During the last years, several SLN and NLC in eye drops or in semisolid hydrogels have been developed for the treatment of pathologies of the anterior and posterior segment of the eye as infections, ocular inflammation, glaucoma, cataracts or treatments of age related macular degeneration, which have produced higher bioavailability of the drugs (107). They have also been shown to be useful for administering genetic material, supplying it to the nucleus and favoring the transfection of the genes into the cells of the retina (108).

Research shows that lipid nanoparticles are ideal for efficiently administering therapeutic agents in the posterior segment of the eye (107).

1.7.6. Intranasal delivery

Intranasal delivery has been proposed as an alternative to parenteral route due to several advantages such as high surface area, rich blood supply in nasal mucosa, non-invasiveness and avoidance of hepatic and gastrointestinal metabolism, allowing a quick absorption and side effects and doses reduction (7). However, this route of administration is hampered by the presence of several enzymes, the adenosine triphosphate binding cassette of the nasal cavity and mucociliary clearance. In addition, it only allows the administration of high potency drugs in small volume formulations (109). The administration of lipid nanoparticles by this route helps to overcome some of those problems. Surface charge (cationic) modified SLN and NLC offer bioadhesion to nasal mucosa, biocompatibility and drug protection from degradation and P-gp efflux proteins activity. Moreover, the surfactants included in their composition are able to disrupt tight junctions in mucosal epithelium and improve absorption (109).

SLN have been successfully used as a release system for diclofenac, carvedilol, and flavonoids through intranasal route (109). In addition, the rich blood supply of respiratory epithelium makes this route adequate for systemic drug delivery, avoiding first-pass effect (109). During the last years intranasal route has been explored for targeting the central nervous system as it provides direct access from the nose to the brain and to the cerebrospinal fluid through the intra- and extra- neuronal pathways, overcoming blood-brain barrier (109, 110). This administration route has a great potential for the treatment of several neurodegenerative diseases such as Alzheimer, Parkinson, Amyotrophic Lateral Sclerosis, and Huntington's disease (109). Some examples of drug delivery systems based on lipid nanoparticles studied for neurodegenerative diseases management are rivastigmine-loaded SLN (111), rosmarinic acid-loaded SLN (112), astaxanthin-loaded SLN (113), tarenflurbil-loaded SLN (114) or chitosan-coated SLN complexed with siRNA and cell penetrating peptides (115). The administration of these drugs by means of lipid nanoparticles through the intranasal route provided different

benefits such as increased bioavailability, improved brain biodistribution profiles, higher mucoadhesiveness, and enhanced intracellular transport (109).

1.8. SOLID LIPID NANOPARTICLES AND NANOSTRUCTURED LIPID CARRIERS CASE STUDIES IN HUMANS FOR MEDICAL APPLICATIONS

The main commercial application of lipid nanoparticles is nowadays focused on the cosmetics, food/nutrition and nutraceuticals fields (116). The use of lipid nanoparticles is well stablished for cosmetic uses with more than 25 formulations already marketed (9). Despite the huge potential of SLN and NLC as drug delivery platforms, no current treatments based on this strategy are in the clinic (117). However, several preclinical and clinical studies have been performed using these nanoparticulated systems for medical applications. While the preclinical evaluation of these formulations was already described in the previous section, the clinical studies performed based on SLN and NLC are described in this section, categorized by the administration route selected.

1.8.1. Topical administration (Skin and mucosa)

SLN have been widely included in cosmetic and pharmaceutical industrial products for the skin care without the need of clinical trials for their commercialization approval (118, 119). Their ability to modulate skin penetration make them really useful for this purpose (120). Moreover, the treatment of numerous acute or chronic dermal and mucosal pathologies with lipid nanoparticles has also been explored. This administration route usually requires their combination with other pharmaceutical formulation forms such as gels or creams in where the nanoparticulate systems are incorporated to facilitate their administration.

The efficacy and safety of fluconazole-loaded SLN incorporated on a gel for the local therapy of skin fungal infections was assessed. Patients diagnosed with Pityriasis versicolor were topically treated twice daily for 4 weeks with one of the following groups: (1) 1% Carbopol 934 gel containing SLNs of 10% Compritol 888ATO+0.5% Cremophor RH40+1% Fluconazole; (2) 1% Carbopol 934 gel containing SLNs of 10% Precirol ATO5+0.5% Poloxamer 407+1% Fluconazole, or (3) commercially available product Candistan (Clotrimazole 1%). The final drug concentration used was 8–9 mg/1 per gram of gel. Treatments were applied twice a day for 4 weeks. The percentage of cure was significantly improved by the treatment with the gels containing SLN (groups 1 and 2) when compared to the commercially available product. Moreover, no adverse reactions were reported in any of the groups neither during treatment nor afterwards (121).

SLN have also been used for the topical treatment of recurrent condyloma acuminatum. For this purpose, SLN were loaded with podophyllotoxin and embedded on a gel. Patients with recurrent condyloma acuminatum were treated either with standard podophyllotoxin gel or with podophyllotoxin-SLN gel. The treatment with the nanoparticulated formulation reached similar wart clearance than the standard treatment but decreased recurrence rates and adverse effects (122).

Another approach used for topical treatment has been focused on the development of mucoadhesive dosage forms containing curcumin-loaded SLN for the treatment of

precancerous lesions in buccal mucosa. In this regard, SLN have shown an excellent loading capacity and a more controlled release when compared to the drug dispersed on the mucoadhesive gel. Moreover, curcumin-SLN also showed higher retention and penetration deep into the mucosal layers in an "*in vivo*" model. Patients diagnosed with erythroplakia were treated with either a conventional mucoadhesive gel or with the developed mucoadhesive formulation containing curcumin-loaded SLN at a dose of 6 mg curcumin per day for 6 weeks. Clinical evaluation consisted on pain index and lesion size. The incorporation of curmumin-loaded SLN into the formulation was able to significantly reduce the pain and size of the lesion. As a result, SLN were able to successfully deliver curcumin in a stable form enhancing its activity. The incorporation of curcumin-SLN into mucoadhesive gel provided an efficient approach for oral mucosal targeting (123).

Even though SLN are usually included into gels to facilitate topical administration, their nature also allows them to be incorporated into similar pharmaceutical formulation forms as creams (118). On this sense, clobetasol propionate was loaded in SLN and they were dispersed (amount equivalent of 0.05g of drug) on a topical cream. The loading capacity of the SLN reached 35% even though the formulation selected for the clinical assessment was the one incorporating 6% of drug based on the size of the SLN. Chronic eczema patients were treated with either clobetasol standard cream or clobetasol-SLN cream for 6 weeks. The therapeutic response was significantly improved on those patients treated with clobetasol-SLN cream in terms of degree of inflammation and itching when compared to the control group (124).

Similar approaches for local drugs administration have been also developed and clinically tested for the second generation of lipid nanoparticles. NLC have been used for the treatment of acne vulgaris by loading spironolactone on them. In this study, NLC were obtained by probe-ultrasonication and composed by stearic acid (solid lipid), oleic acid (liquid lipid), Span 80 (lipophilic surfactant) and spironolactone (SP). NLC were dispersed on a 1% Carbopol gel containing methyl paraben as preservative. This formulation was clinically tested for acne treatment in comparison to an alcoholic gel containing free spironolactone. With over 8 weeks of treatment, patients used 60g of either the gel containing 10 mg SP-NLC per gram of gel or alcoholic gel 50 mg SP per gram of gel. The treatment with SP-NLC promoted a reduction in the acne total lesion score together with a decrease in noninflammatory lesions when compared to the base line, similarly to the alcoholic gel after 8 weeks of treatment. Therefore, the use of SP-NLC has shown a good therapeutic effect on mild to moderate acne vulgaris and it was well tolerated (125).

On a similar study, acitretin-loaded nanostructured lipid carriers (Act-NLC) were obtained by the combination of the following components: oleic acid (liquid lipid), Precirol ATO 5 (solid lipid) and Tween® 80 (surfactant) containing 5% of drug. Lyophilized Act-NLC at an equivalent drug amount of 150 mg were incorporated to a Carbopol 934 P based gel. Psoriasis patients were then treated with either the standard acitretin gel twice daily or Act-NLC gel once a day for four weeks. Patients treated with the NLC-based formulation presented a reduction in erythema and a significant reduction in scaling, indicating moderate to excellent improvement in the disease symptoms when compared to the standard treatment (126).

1.8.2. Oral administration

Although several SLN and NLC formulations have been designed and tested *in vitro* or in preclinical studies for systemic administration, clinical studies for these systems are still limited. The high costs of the experiments together with their unexplored systemic side effects could be the reason of the lack of clinical trials on this route (93).

To clarify this point, the safety and tolerability of oral administered curcumin-loaded SLN has been assessed on healthy volunteers and cancer patients. Nanoparticles containing curcumin in the range of 20-30% of total formulation were administered orally as a single dose in a capsule of 2000 mg (containing 400-600 mg of curcumin), 3000 mg, or 4000 mg to late-stage osteosarcoma patients. The pharmacokinetic analysis showed high plasma curcumin concentrations and dose-related AUCs reaching the plasma concentration peak after 3.5 hours of administration. No adverse events were reported in either healthy volunteers or osteosarcoma patients (127).

Despite the promising clinical results of the above studies, it should be stated that all the clinical trials included presented a relatively small number of patients and these are treated for a short period of time, 8 weeks is the longest time point selected. Therefore, there is a long way to go for the establishment of SLN and NLC as a realistic clinical treatment alternative to conventional therapies. However, taking into account the improvement in their formulation technology over the last few years and the increased number of patented NLC-based formulations, these systems represent a promise for the pharmaceutical market which is expected to promote an increase in the number of clinical trials performed in the near future (128).

REFERENCES

1. Rouco H, Diaz-Rodriguez P, Remuñán-López C, Landin M. Recent advances in solid lipid nanoparticles formulation and clinical applications. In: Pippa N, Demetzos C. Nanomaterials for Clinical Applications. 1st edition: Elsevier; 2020. p. 213-47.
2. Martins S, Sarmento B, Ferreira DC, Souto EB. Lipid-based colloidal carriers for peptide and protein delivery-liposomes versus lipid nanoparticles. Int J Nanomedicine. 2007; 2 (4): 595-607.
3. Müller RH, Shegokar R, Keck CM. 20 years of lipid nanoparticles (SLN and NLC): present state of development and industrial applications. Curr Drug Discov Technol. 2011; 8 (3): 207-227.
4. Souto E, Almeida A, Müller R. Lipid nanoparticles (SLN®, NLC®) for cutaneous drug delivery: structure, protection and skin effects. J Biomed Nanotechnol. 2007; 3 (4): 317-331.
5. Gordillo-Galeano A, Mora-Huertas CE. Solid lipid nanoparticles and nanostructured lipid carriers: A review emphasizing on particle structure and drug release. Eur J Pharm Biopharm. 2018; 133: 285-308.
6. Muchow M, Maincent P, Müller RH. Lipid nanoparticles with a solid matrix (SLN, NLC, LDC) for oral drug delivery. Drug Dev Ind Pharm. 2008; 34 (12): 1394-1405.
7. Khosa A, Reddi S, Saha RN. Nanostructured lipid carriers for site-specific drug delivery. Biomed Pharmacother. 2018; 103: 598-613.
8. Heurtault B, Saulnier P, Pech B, Proust JE, Benoit JP. Physico-chemical stability of colloidal lipid particles. Biomaterials. 2003; 24 (23): 4283-4300.
9. Pardeike J, Hommoss A, Müller RH. Lipid nanoparticles (SLN, NLC) in cosmetic and pharmaceutical dermal products. Int J Pharm. 2009; 366 (1-2): 170-184.
10. Gaba B, Fazil M, Ali A, Baboota S, Sahni JK, Ali J. Nanostructured lipid (NLCs) carriers as a bioavailability enhancement tool for oral administration. Drug Deliv. 2015; 22 (6): 691-700.
11. Shah R, Eldridge D, Palombo E, Harding I. Composition and structure. In: Shah R, Eldridge D, Palombo E, Harding I (Eds). Lipid nanoparticles: production, characterization and stability. 1st edition. New York, USA: Springer International Publishing; 2015. p. 11-22.
12. Pathak K, Keshri L, Shah M. Lipid nanocarriers: Influence of lipids on product development and pharmacokinetics. Crit Rev Ther Drug Carrier Syst. 2011; 28 (4): 357-393.
13. Weiss J, Decker EA, McClements DJ, Kristbergsson K, Helgason T, Awad T. Solid Lipid Nanoparticles as Delivery Systems for Bioactive Food Components. Food Biophys. 2008; 3 (2): 146-154.
14. Suresh G, Manjunath K, Venkateswarlu V, Satyanarayana V. Preparation, characterization, and in vitro and in vivo evaluation of lovastatin solid lipid nanoparticles. AAPS PharmSciTech. 2007; 8 (1): 162-170.
15. Chen H, Chang X, Du D, Liu W, Liu J, Weng T, et al. Podophyllotoxin-loaded solid lipid nanoparticles for epidermal targeting. J Control Release. 2006; 110 (2): 296-306.
16. Berg JM, Tymoczko JL, Stryer L. Biochemistry. 5th edition. New York, USA: W.H. Freeman; 2002.

17. Khatak S, Dureja H. Structural Composition of Solid Lipid Nanoparticles for Invasive and Noninvasive Drug Delivery. Current Nanomaterials. 2018; 2 (3): 129-153.
18. Sharma KN, S.;Thakur, N.;Kishore,K. Partial Glycerides-An Important Nonionic Surfactant for Industrial Applications: An Overview. J Biol Chem Chron. 2017; 3 (1): 10-19.
19. Aburahma MH, Badr-Eldin SM. Compritol 888 ATO: a multifunctional lipid excipient in drug delivery systems and nanopharmaceuticals. Expert Opin Drug Deliv. 2014; 11 (12): 1865-1883.
20. Jenning V, Gohla S. Comparison of wax and glyceride solid lipid nanoparticles (SLN®). Int J Pharm. 2000; 196 (2): 219-222.
21. Bouwman-Boer Y. Practical Pharmaceutics. Pharmaceutisch Weekblad. 2015; 150 (14): 37.
22. Goad LJ, Akihisa T. Nomenclature and biosynthesis of sterols and related compounds. In: Goad LJ, Akihisa T (Eds.). Analysis of Sterols. 1st edition. Dordrecht, Netherlands: Springer; 1997. p. 1-42.
23. Vivek K, Reddy H, Murthy RSR. Investigations of the effect of the lipid matrix on drug entrapment, in vitro release, and physical stability of olanzapine-loaded solid lipid nanoparticles. AAPS PharmSciTech. 2007; 8 (4): 16-24.
24. Kumar VV, Chandrasekar D, Ramakrishna S, Kishan V, Rao YM, Diwan PV. Development and evaluation of nitrendipine loaded solid lipid nanoparticles: influence of wax and glyceride lipids on plasma pharmacokinetics. Int J Pharm. 2007; 335 (1-2): 167-175.
25. Müller RH, Mäder K, Gohla S. Solid lipid nanoparticles (SLN) for controlled drug delivery - a review of the state of the art. Eur J Pharm Biopharm. 2000; 50 (1): 161-177.
26. Triplett Ii MD, Rathman JF. Optimization of β-carotene loaded solid lipid nanoparticles preparation using a high shear homogenization technique. J Nanopart Res. 2009; 11 (3):601-614.
27. Mehnert W, Mäder K. Solid lipid nanoparticles: production, characterization and applications. Adv Drug Deliv Rev. 2001; 47 (2-3): 165-196.
28. Tiyaboonchai W, Tungpradit W, Plianbangchang P. Formulation and characterization of curcuminoids loaded solid lipid nanoparticles. Int J Pharm. 2007; 337 (1-2): 299-306.
29. Shah M, Pathak K. Development and statistical optimization of solid lipid nanoparticles of simvastatin by using 2(3) full-factorial design. AAPS PharmSciTech. 2010; 11 (2): 489-496.
30. Vitorino C, Carvalho FA, Almeida AJ, Sousa JJ, Pais AA. The size of solid lipid nanoparticles: an interpretation from experimental design. Colloids Surf B Biointerfaces. 2011; 84 (1):117-130.
31. Severino P, Andreani T, Macedo AS, Fangueiro JF, Santana MH, Silva AM, et al. Current State-of-Art and New Trends on Lipid Nanoparticles (SLN and NLC) for Oral Drug Delivery. J Drug Deliv. 2012; 2012: 750891.
32. Müller RH, Radtke M, Wissing SA. Nanostructured lipid matrices for improved microencapsulation of drugs. Int J Pharm. 2002; 242 (1-2):121-128.
33. Song A, Zhang X, Li Y, Mao X, Han F. Effect of liquid-to-solid lipid ratio on characterizations of flurbiprofen-loaded solid lipid nanoparticles (SLNs) and nanostructured lipid carriers (NLCs) for transdermal administration. Drug Dev Ind Pharm. 2016; 42 (8): 1308-1314.

34. Rouco H, Diaz-Rodriguez P, Rama-Molinos S, Remunan-Lopez C, Landin M. Delimiting the knowledge space and the design space of nanostructured lipid carriers through Artificial Intelligence tools. Int J Pharm. 2018; 553 (1-2): 522-530.
35. Kim JK, Park JS, Kim CK. Development of a binary lipid nanoparticles formulation of itraconazole for parenteral administration and controlled release. Int J Pharm. 2010; 383 (1-2): 209-215.
36. Som I, Bhatia K, Yasir M. Status of surfactants as penetration enhancers in transdermal drug delivery. J Pharm Bioallied Sci. 2012; 4 (1): 2-9.
37. Wilde P, Mackie A, Husband F, Gunning P, Morris V. Proteins and emulsifiers at liquid interfaces. Adv Colloid Interface Sci. 2004; 108-109: 63-71.
38. Kovacevic A, Savic S, Vuleta G, Müller RH, Keck CM. Polyhydroxy surfactants for the formulation of lipid nanoparticles (SLN and NLC): effects on size, physical stability and particle matrix structure. Int J Pharm. 2011; 406 (1-2): 163-172.
39. Gaspar DP, Faria V, Goncalves LM, Taboada P, Remunan-Lopez C, Almeida AJ. Rifabutin-loaded solid lipid nanoparticles for inhaled antitubercular therapy: Physicochemical and in vitro studies. Int J Pharm. 2016; 497 (1-2): 199-209.
40. Alam T, Khan S, Gaba B, Haider MF, Baboota S, Ali J. Adaptation of Quality by Design-Based Development of Isradipine Nanostructured-Lipid Carrier and Its Evaluation for In Vitro Gut Permeation and In Vivo Solubilization Fate. J Pharm Sci. 2018; 107 (11): 2914-2926.
41. Ranpise NS, Korabu SS, Ghodake VN. Second generation lipid nanoparticles (NLC) as an oral drug carrier for delivery of lercanidipine hydrochloride. Colloids Surf B Biointerfaces. 2014; 116: 81-87.
42. Kasongo KW, Pardeike J, Müller RH, Walker RB. Selection and characterization of suitable lipid excipients for use in the manufacture of didanosine-loaded solid lipid nanoparticles and nanostructured lipid carriers. J Pharm Sci. 2011; 100 (12): 5185-5196.
43. Battaglia L, Gallarate M. Lipid nanoparticles: state of the art, new preparation methods and challenges in drug delivery. Expert Opin Drug Deliv. 2012; 9 (5): 497-508.
44. Das S, Chaudhury A. Recent advances in lipid nanoparticle formulations with solid matrix for oral drug delivery. AAPS PharmSciTech. 2011; 12 (1): 62-76.
45. Alvarez-Trabado J, Diebold Y, Sanchez A. Designing lipid nanoparticles for topical ocular drug delivery. Int J Pharm. 2017; 532 (1): 204-217.
46. Esposito E, Sguizzato M, Drechsler M, Mariani P, Carducci F, Nastruzzi C, et al. Progesterone lipid nanoparticles: Scaling up and in vivo human study. Eur J Pharm Biopharm. 2017; 119: 437-446.
47. Barbosa DM, Ribeiro LN, Casadei BR, Da Silva CM, Queiróz VA, Duran N et al. Solid Lipid Nanoparticles for Dibucaine Sustained Release. Pharmaceutics. 2018; 10 (4): 231.
48. Lasa-Saracibar B, Estella-Hermoso de Mendoza A, Guada M, Dios-Vieitez C, Blanco-Prieto MJ. Lipid nanoparticles for cancer therapy: state of the art and future prospects. Expert Opin Drug Deliv. 2012; 9 (10): 1245-1261.
49. Wen J, Chen S, Chen G. Solid Lipid Nanoparticles. In: Roohinejad S, Greiner R, Oey I, Wen J (Eds.). Emulsion-based Systems for Delivery of Food Active Compounds: Formation,

Application, Health and Safety. 1st edition. Chichester, UK: John Wiley & Sons. 2018. p. 121-138.
50. Almeida AJ, Runge S, Müller RH. Peptide-loaded solid lipid nanoparticles (SLN): influence of production parameters. Int J Pharm. 1997; 149 (2): 255-265.
51. You J, Wan F, de Cui F, Sun Y, Du YZ, Hu FQ. Preparation and characteristic of vinorelbine bitartrate-loaded solid lipid nanoparticles. Int J Pharm. 2007; 343 (1-2): 270-276.
52. Tran TH, Ramasamy T, Truong DH, Shin BS, Choi HG, Yong CS, et al. Development of vorinostat-loaded solid lipid nanoparticles to enhance pharmacokinetics and efficacy against multidrug-resistant cancer cells. Pharm Res. 2014; 31 (8): 1978-1988.
53. Tran TH, Ramasamy T, Cho HJ, Kim Y, II, Poudel BK, Choi H-G, et al. Formulation and Optimization of Raloxifene-Loaded Solid Lipid Nanoparticles to Enhance Oral Bioavailability. J Nanosci Nanotechnol. 2014; 14 (7): 4820-4831.
54. Acevedo-Morantes CY, Acevedo-Morantes MT, Suleiman-Rosado D, Ramirez-Vick JE. Evaluation of the cytotoxic effect of camptothecin solid lipid nanoparticles on MCF7 cells. Drug Deliv. 2013; 20 (8):338-348.
55. Chattopadhyay P, Shekunov BY, Yim D, Cipolla D, Boyd B, Farr S. Production of solid lipid nanoparticle suspensions using supercritical fluid extraction of emulsions (SFEE) for pulmonary delivery using the AERx system. Adv Drug Deliv Rev. 2007; 59 (6): 444-453.
56. Gokce EH, Korkmaz E, Dellera E, Sandri G, Bonferoni MC, Ozer O. Resveratrol-loaded solid lipid nanoparticles versus nanostructured lipid carriers: evaluation of antioxidant potential for dermal applications. Int J Nanomedicine. 2012; 7: 1841-1850.
57. Ustundag-Okur N, Gokce EH, Bozbiyik DI, Egrilmez S, Ozer O, Ertan G. Preparation and in vitro-in vivo evaluation of ofloxacin loaded ophthalmic nano structured lipid carriers modified with chitosan oligosaccharide lactate for the treatment of bacterial keratitis. Eur J Pharm Sci. 2014; 63: 204-215.
58. Souza LG, Silva EJ, Martins AL, Mota MF, Braga RC, Lima EM, et al. Development of topotecan loaded lipid nanoparticles for chemical stabilization and prolonged release. Eur J Pharm Biopharm. 2011; 79 (1): 189-196.
59. Yousry C, Fahmy RH, Essam T, El-Laithy HM, Elkheshen SA. Nanoparticles as tool for enhanced ophthalmic delivery of vancomycin: a multidistrict-based microbiological study, solid lipid nanoparticles formulation and evaluation. Drug Dev Ind Pharm. 2016; 42 (11): 1752-1762.
60. Li Z, Yu L, Zheng L, Geng F. Studies on crystallinity state of puerarin loaded solid lipid nanoparticles prepared by double emulsion method. J Therm Anal Calorim. 2009; 99 (2): 689-693.
61. Charcosset C, El-Harati A, Fessi H. Preparation of solid lipid nanoparticles using a membrane contactor. J Control Release. 2005; 108 (1): 112-120.
62. Montenegro L, Trapani A, Latrofa A, Puglisi G. In vitro evaluation on a model of blood brain barrier of idebenone-loaded solid lipid nanoparticles. J Nanosci Nanotechnol. 2012; 12 (1): 330-337.
63. Yoon G, Park JW, Yoon I-S. Solid lipid nanoparticles (SLNs) and nanostructured lipid carriers (NLCs): recent advances in drug delivery. J Pharm Investig. 2013; 43 (5): 353-362.

64. Battaglia L, Muntoni E, Chirio D, Peira E, Annovazzi L, Schiffer D, et al. Solid lipid nanoparticles by coacervation loaded with a methotrexate prodrug: Preliminary study for glioma treatment. Nanomedicine. 2017; 12 (6): 639-656.
65. Clemente N, Ferrara B, Gigliotti CL, Boggio E, Capucchio MT, Biasibetti E, et al. Solid Lipid Nanoparticles Carrying Temozolomide for Melanoma Treatment. Preliminary In Vitro and In Vivo Studies. Int J Mol Sci. 2018; 19 (2): 255.
66. Liu D, Jiang S, Shen H, Qin S, Liu J, Zhang Q, et al. Diclofenac sodium-loaded solid lipid nanoparticles prepared by emulsion/solvent evaporation method. J Nanopart Res. 2010; 13 (6): 2375-2386.
67. Javan F, Vatanara A, Azadmanesh K, Nabi-Meibodi M, Shakouri M. Encapsulation of ritonavir in solid lipid nanoparticles: in-vitro anti-HIV-1 activity using lentiviral particles. J Pharm Pharmacol. 2017; 69 (8): 1002-1009.
68. Emami J, Mohiti H, Hamishehkar H, Varshosaz J. Formulation and optimization of solid lipid nanoparticle formulation for pulmonary delivery of budesonide using Taguchi and Box-Behnken design. Res Pharm Sci. 2015; 10 (1): 17-33.
69. Varshosaz J, Hassanzadeh F, Sadeghi H, Khadem M. Galactosylated nanostructured lipid carriers for delivery of 5-FU to hepatocellular carcinoma. J Liposome Res. 2012; 22 (3): 224-236.
70. Ganesan P, Narayanasamy D. Lipid nanoparticles: Different preparation techniques, characterization, hurdles, and strategies for the production of solid lipid nanoparticles and nanostructured lipid carriers for oral drug delivery. Sustain Chem Pharm. 2017; 6: 37-56.
71. Pignatello R, Leonardi A, Fuochi V, Petronio Petronio G, Greco AS, Furneri PM. A Method for Efficient Loading of Ciprofloxacin Hydrochloride in Cationic Solid Lipid Nanoparticles: Formulation and Microbiological Evaluation. Nanomaterials (Basel). 2018; 8 (5): 304.
72. Keshri L, Pathak K. Development of thermodynamically stable nanostructured lipid carrier system using central composite design for zero order permeation of econazole nitrate through epidermis. Pharm Dev Technol. 2013; 18 (3): 634-644.
73. Iqbal N, Vitorino C, Taylor KM. How can lipid nanocarriers improve transdermal delivery of olanzapine?. Pharm Dev Technol. 2017; 22 (4): 587-596.
74. zur Mühlen A, Schwarz C, Mehnert W. Solid lipid nanoparticles (SLN) for controlled drug delivery–drug release and release mechanism. Eur J Pharm Biopharm. 1998; 45 (2): 149-155.
75. Naseri N, Valizadeh H, Zakeri-Milani P. Solid Lipid Nanoparticles and Nanostructured Lipid Carriers: Structure, Preparation and Application. Adv Pharm Bull. 2015; 5 (3): 305-313.
76. Sala M, Diab R, Elaissari A, Fessi H. Lipid nanocarriers as skin drug delivery systems: Properties, mechanisms of skin interactions and medical applications. Int J Pharm. 2018; 535 (1-2): 1-17.
77. Garces A, Amaral MH, Sousa Lobo JM, Silva AC. Formulations based on solid lipid nanoparticles (SLN) and nanostructured lipid carriers (NLC) for cutaneous use: A review. Eur J Pharm Sci. 2018; 112: 159-167.
78. Nasrollahi SA, Abbasian AR, Farboud ES. In vitro comparison of simple tretinoin-cream and cream loaded with tretinoin-SLN. J Pharm Technol Drug Res. 2013; 2 (1): 13.

79. Cortesi R, Ravani L, Menegatti E, Drechsler M, Esposito E. Colloidal dispersions for the delivery of acyclovir: a comparative study. Indian J Pharm Sci. 2011; 73 (6): 687-693.
80. Lin YK, Huang ZR, Zhuo RZ, Fang JY. Combination of calcipotriol and methotrexate in nanostructured lipid carriers for topical delivery. Int J Nanomedicine. 2010; 5: 117-128.
81. Gainza G, Bonafonte DC, Moreno B, Aguirre JJ, Gutierrez FB, Villullas S, et al. The topical administration of rhEGF-loaded nanostructured lipid carriers (rhEGF-NLC) improves healing in a porcine full-thickness excisional wound model. J Control Release. 2015; 197: 41-47.
82. Chen X, Peng LH, Shan YH, Li N, Wei W, Yu L, et al. Astragaloside IV-loaded nanoparticle-enriched hydrogel induces wound healing and anti-scar activity through topical delivery. Int J Pharm. 2013; 447 (1-2): 171-181.
83. Wang W, Chen L, Huang X, Shao A. Preparation and Characterization of Minoxidil Loaded Nanostructured Lipid Carriers. AAPS PharmSciTech. 2017; 18 (2): 509-516.
84. Rigon RB, Fachinetti N, Severino P, Santana MH, Chorilli M. Skin Delivery and in Vitro Biological Evaluation of Trans-Resveratrol-Loaded Solid Lipid Nanoparticles for Skin Disorder Therapies. Molecules. 2016; 21 (1): 116.
85. Joshi MD, Müller RH. Lipid nanoparticles for parenteral delivery of actives. Eur J Pharm Biopharm. 2009; 71 (2): 161-172.
86. Fang CL, A Al-Suwayeh S, Fang JY. Nanostructured lipid carriers (NLCs) for drug delivery and targeting. Recent Pat Nanotechnol. 2013; 7 (1): 41-55.
87. Yang SC, Lu LF, Cai Y, Zhu JB, Liang BW, Yang CZ. Body distribution in mice of intravenously injected camptothecin solid lipid nanoparticles and targeting effect on brain. J Control Release. 1999; 59 (3): 299-307.
88. Chen DB, Yang TZ, Lu WL, Zhang Q. In vitro and in vivo study of two types of long-circulating solid lipid nanoparticles containing paclitaxel. Chem Pharm Bull. 2001; 49 (11): 1444-1447.
89. Liu D, Liu Z, Wang L, Zhang C, Zhang N. Nanostructured lipid carriers as novel carrier for parenteral delivery of docetaxel. Colloids Surf B Biointerfaces. 2011; 85 (2): 262-269.
90. Esposito E, Mariani P, Ravani L, Contado C, Volta M, Bido S, et al. Nanoparticulate lipid dispersions for bromocriptine delivery: characterization and in vivo study. Eur J Pharm Biopharm. 2012; 80 (2): 306-314.
91. Hsu SH, Wen CJ, Al-Suwayeh SA, Chang HW, Yen TC, Fang JY. Physicochemical characterization and in vivo bioluminescence imaging of nanostructured lipid carriers for targeting the brain: apomorphine as a model drug. Nanotechnology. 2010; 21 (40): 405101.
92. Poonia N, Kharb R, Lather V, Pandita D. Nanostructured lipid carriers: versatile oral delivery vehicle. Future Sci OA. 2016; 2 (3): FSO135.
93. Lin CH, Chen CH, Lin ZC, Fang JY. Recent advances in oral delivery of drugs and bioactive natural products using solid lipid nanoparticles as the carriers. J Food Drug Anal. 2017; 25 (2): 219-234.
94. Kumbhar DD, Pokharkar VB. Engineering of a nanostructured lipid carrier for the poorly water-soluble drug, bicalutamide: physicochemical investigations. Colloids Surf A Physicochem Eng Asp. 2013; 416: 32-42.

95. Wang Q, Cheng H, Zhou K, Wang L, Dong S, Wang D, et al. Nanostructured lipid carriers as a delivery system of biochanin A. Drug Deliv. 2013; 20 (8): 331-337.
96. Date AA, Vador N, Jagtap A, Nagarsenker MS. Lipid nanocarriers (GeluPearl) containing amphiphilic lipid Gelucire 50/13 as a novel stabilizer: fabrication, characterization and evaluation for oral drug delivery. Nanotechnology. 2011; 22 (27): 275102.
97. Weber S, Zimmer A, Pardeike J. Solid Lipid Nanoparticles (SLN) and Nanostructured Lipid Carriers (NLC) for pulmonary application: a review of the state of the art. Eur J Pharm Biopharm. 2014; 86 (1): 7-22.
98. Ngan CL, Asmawi AA. Lipid-based pulmonary delivery system: a review and future considerations of formulation strategies and limitations. Drug Deliv Transl Res. 2018; 8 (5): 1527-1544.
99. Ezzati Nazhad Dolatabadi J, Hamishehkar H, Valizadeh H. Development of dry powder inhaler formulation loaded with alendronate solid lipid nanoparticles: solid-state characterization and aerosol dispersion performance. Drug Dev Ind Pharm. 2015; 41 (9): 1431-1437.
100. Hu L, Jia Y, WenDing. Preparation and characterization of solid lipid nanoparticles loaded with epirubicin for pulmonary delivery. Pharmazie. 2010; 65 (8): 585-587.
101. Videira M, Almeida AJ, Fabra A. Preclinical evaluation of a pulmonary delivered paclitaxel-loaded lipid nanocarrier antitumor effect. Nanomedicine. 2012; 8 (7): 1208-1215.
102. Jaafar-Maalej C, Andrieu V, Elaissari A, Fessi H. Beclomethasone-loaded lipidic nanocarriers for pulmonary drug delivery: preparation, characterization and in vitro drug release. J Nanosci Nanotechnol. 2011;11(3):1841-1851.
103. Moreno-Sastre M, Pastor M, Esquisabel A, Sans E, Vinas M, Fleischer A, et al. Pulmonary delivery of tobramycin-loaded nanostructured lipid carriers for Pseudomonas aeruginosa infections associated with cystic fibrosis. Int J Pharm. 2016; 498 (1-2): 263-273.
104. Pardeike J, Weber S, Haber T, Wagner J, Zarfl HP, Plank H, et al. Development of an itraconazole-loaded nanostructured lipid carrier (NLC) formulation for pulmonary application. Int J Pharm. 2011; 419 (1-2): 329-338.
105. Mu H, Holm R. Solid lipid nanocarriers in drug delivery: characterization and design. Expert Opin Drug Deliv. 2018; 15 (8): 771-785.
106. Sanchez-Lopez E, Espina M, Doktorovova S, Souto EB, Garcia ML. Lipid nanoparticles (SLN, NLC): Overcoming the anatomical and physiological barriers of the eye - Part I - Barriers and determining factors in ocular delivery. Eur J Pharm Biopharm. 2017; 110: 70-75.
107. Sanchez-Lopez E, Espina M, Doktorovova S, Souto EB, Garcia ML. Lipid nanoparticles (SLN, NLC): Overcoming the anatomical and physiological barriers of the eye - Part II - Ocular drug-loaded lipid nanoparticles. Eur J Pharm Biopharm. 2017; 110: 58-69.
108. Apaolaza PS, Delgado D, del Pozo-Rodriguez A, Gascon AR, Solinis MA. A novel gene therapy vector based on hyaluronic acid and solid lipid nanoparticles for ocular diseases. Int J Pharm. 2014; 465 (1-2): 413-426.
109. Battaglia L, Panciani PP, Muntoni E, Capucchio MT, Biasibetti E, De Bonis P, et al. Lipid nanoparticles for intranasal administration: application to nose-to-brain delivery. Expert Opin Drug Deliv. 2018; 15 (4): 369-378.

110. Samaridou E, Alonso MJ. Nose-to-brain peptide delivery-The potential of nanotechnology. Bioorg Med Chem. 2018; 26 (10): 2888-2905.
111. Shah B, Khunt D, Bhatt H, Misra M, Padh H. Application of quality by design approach for intranasal delivery of rivastigmine loaded solid lipid nanoparticles: Effect on formulation and characterization parameters. Eur J Pharm Sci. 2015; 78: 54-66.
112. Bhatt R, Singh D, Prakash A, Mishra N. Development, characterization and nasal delivery of rosmarinic acid-loaded solid lipid nanoparticles for the effective management of Huntington's disease. Drug Deliv. 2015; 22 (7): 931-939.
113. Bhatt PC, Srivastava P, Pandey P, Khan W, Panda BP. Nose to brain delivery of astaxanthin-loaded solid lipid nanoparticles: fabrication, radio labeling, optimization and biological studies. RSC Adv. 2016; 6 (12): 10001-10010.
114. Muntimadugu E, Dhommati R, Jain A, Challa VG, Shaheen M, Khan W. Intranasal delivery of nanoparticle encapsulated tarenflurbil: A potential brain targeting strategy for Alzheimer's disease. Eur J Pharm Sci. 2016; 92: 224-234.
115. Rassu G, Soddu E, Posadino AM, Pintus G, Sarmento B, Giunchedi P, et al. Nose-to-brain delivery of BACE1 siRNA loaded in solid lipid nanoparticles for Alzheimer's therapy. Colloids Surf B Biointerfaces. 2017; 152: 296-301.
116. Danaei M, Dehghankhold M, Ataei S, Hasanzadeh Davarani F, Javanmard R, Dokhani A, et al. Impact of Particle Size and Polydispersity Index on the Clinical Applications of Lipidic Nanocarrier Systems. Biomacromolecules. 2018; 10 (2): 57.
117. Cipolla D, Shekunov B, Blanchard J, Hickey A. Lipid-based carriers for pulmonary products: preclinical development and case studies in humans. Adv Drug Deliv Rev. 2014; 75: 53-80.
118. Lakshminarayanan R, Ye E, Young DJ, Li Z, Loh XJ. Recent Advances in the Development of Antimicrobial Nanoparticles for Combating Resistant Pathogens. Adv Healthc Mater. 2018; 7 (13): 1701400.
119. Kaul S, Gulati N, Verma D, Mukherjee S, Nagaich U. Role of Nanotechnology in Cosmeceuticals: A Review of Recent Advances. Hindawi J. Pharm. 2018; 2018: 3420204.
120. Souto EB, Müller RH. Cosmetic features and applications of lipid nanoparticles (SLN, NLC). Int J Cosmet Sci. 2008; 30 (3): 157-165.
121. El-Housiny S, Shams Eldeen MA, El-Attar YA, Salem HA, Attia D, Bendas ER, et al. Fluconazole-loaded solid lipid nanoparticles topical gel for treatment of pityriasis versicolor: formulation and clinical study. Drug Deliv. 2017; 25 (1): 78-90.
122. Xie FM, Zeng K, Chen ZL, Li GF, Lin ZF, Zhu XL, et al. Treatment of recurrent condyloma acuminatum with solid lipid nanoparticle gel containing podophyllotoxin: a randomized double-blinded, controlled clinical trial. Nan Fang Yi Ke Da Xue Xue Bao. 2007; 27 (5): 657-659.
123. Hazzah HA, Farid RM, Nasra MM, Zakaria M, Gawish Y, El-Massik MA, et al. A new approach for treatment of precancerous lesions with curcumin solid-lipid nanoparticle-loaded gels: in vitro and clinical evaluation. Drug Deliv. 2016; 23 (4): 1409-1419.

124. Kalariya M, Padhi BK, Chougule M, Misra A. Clobetasol propionate solid lipid nanoparticles cream for effective treatment of eczema: formulation and clinical implications. Indian J Exp Biol. 2005; 43 (3): 233-240.
125. Kelidari HR, Saeedi M, Hajheydari Z, Akbari J, Morteza-Semnani K, Akhtari J, et al. Spironolactone loaded nanostructured lipid carrier gel for effective treatment of mild and moderate acne vulgaris: A randomized, double-blind, prospective trial. Colloids Surf B Biointerfaces. 2016; 146: 47-53.
126. Agrawal Y, Petkar KC, Sawant KK. Development, evaluation and clinical studies of Acitretin loaded nanostructured lipid carriers for topical treatment of psoriasis. Int J Pharm. 2010; 401 (1-2): 93-102.
127. Gota VS, Maru GB, Soni TG, Gandhi TR, Kochar N, Agarwal MG. Safety and pharmacokinetics of a solid lipid curcumin particle formulation in osteosarcoma patients and healthy volunteers. J Agric Food Chem. 2010; 58 (4): 2095-2099.
128. Beloqui A, Solinis MA, Rodriguez-Gascon A, Almeida AJ, Preat V. Nanostructured lipid carriers: Promising drug delivery systems for future clinics. Nanomedicine. 2016; 12 (1):143-161.

2. BACKGROUND, HYPOTHESIS AND OBJECTIVES

USC
UNIVERSIDADE
DE SANTIAGO
DE COMPOSTELA

2.1. BACKGROUND

Chapter I: "Delimiting the knowledge space and the design space of nanostructured lipid carriers through Artificial Intelligence tools"

Nanostructured lipid carriers (NLC) are biocompatible and biodegradable nanoscale systems, which have attracted increased attention in the controlled drug delivery field (1). However, despite its promising characteristics, obtaining optimized NLC remains a challenging task, mainly due to reproducibility problems, which requires careful design of the nanosystems and developed process engineering. This makes its clinical applicability difficult (2). In this sense, applying the concepts of quality by design (QbD) should result in robust formulations with possibilities of clinical application.

Artificial Intelligence tools such as Neurofuzzy Logic (NFL), Artificial Neural Networks (ANN) or Genetic algorithms have proven to be useful for the development of different drug delivery systems including micro- and nanoparticles (3, 4). To our knowledge, this technology has not been applied to date for the development and optimization of lipid nanoparticles.

Chapter II: "Rifabutin-loaded Nanostructured Lipid Carriers as a Tool in Oral Anti-mycobacterial Treatment of Crohn´s Disease"

Crohn´s disease is a chronic inflammatory bowel condition (5), whose etiology has constituted a controversial topic during the last years (6). Recently, increasing evidence supporting the involvement of *Mycobacterium avium paratuberculosis* (MAP) on the development of this pathology has been found (6). Although some case reports described promising remissions after anti-mycobacterial therapy (7), those treatments are limited by the low oral bioavailability of the anti-mycobacterial drugs (8) (e.g. rifabutin) and the altered gut conditions of patients (9).

NLC constitute an interesting alternative to solve these problems, because of their capacity to load lipophilic drugs, increasing their bioavailability (10). Furthermore, due to their nano-size, they are likely to accumulate in the inflamed bowel sites, where intestinal macrophages are known to be densely infiltrated (9). Furthermore, MAP has been reported to stablish a persisting infection inside these immune cells (11), making them an excellent target for anti-mycobacterial therapy.

Chapter III: "Cryoprotectant effectivity of sugars in Nanostructured Lipid Carriers lyophilization"

NLC, as lipid nano-dispersions, are subject of several physico-chemical phenomena leading to its destabilization (12). In order to improve stability and develop formulations (cachets, capsules, pellets or tablets) for the administration of the NLC by the oral route, it is necessary to find a method for water removal from NLC dispersions (13).

Lyophilization is considered a suitable technique to enhance long-term nanoparticles stability (14). Removing water from a frozen sample frequently requires the use of cryoprotectant molecules such as sugars, which protect the nanoparticles from the stresses generated during the process. Lyophilization is a complex procedure. Despite this, the development of the nanoparticle lyophilization stage is generally carried out by trial and error methods (14).

NFL, an Artificial Intelligence technology especially suitable to data mining (15), could constitute an interesting alternative to these arbitrary methodologies.

2.2. HYPOTHESIS

The main hypothesis of this thesis is that it is possible to develop, through simple and reproducible manufacturing processes, a robust nano-drug delivery system for an antimycobacterial drug, with a good safety profile and suitable for treating persisting intracellular infections in intestinal macrophages after oral administration. Furthermore, this main hypothesis can be subdivided into the following ones:

Hypothesis I: Artificial Intelligence tools can be used to rationally design a simple and reproducible manufacturing process for NLC loaded with rifabutin (RFB), a model anti-mycobacterial drug. The methodology of quality by design would allow establishing the design space within the knowledge space.

Hypothesis II: It is possible to obtain a biocompatible NLC formulation exhibiting a particle size within the nano-range, a narrow size distribution and a suitable RFB payload, able to guarantee the administration of an effective RFB dose administration inside macrophages after oral administration.

Hypothesis III: Artificial Intelligence can be employed to assist in the development of a lyophilization process suitable to convert NLC dispersions into dried powders with optimal properties.

2.3. OBJECTIVES

Objective I: Design of RFB-loaded NLC through Artificial Intelligence tools

- Evaluation of the suitability of Artificial Intelligence tools, such as NFL, to model small databases from reduced experimental designs, to gain insight into the effect of composition and operation conditions on the characteristics of RFB-loaded NLC.
- Assessment of the applicability of ANN and Genetic algorithms in the optimization process using a small database to obtain NLC exhibiting a nano-size, a narrow particle size distribution and a suitable RFB payload.

Results related to this objective will be displayed in Chapter I: "*Delimiting the knowledge space and the design space of nanostructured lipid carriers through Artificial Intelligence tools*" and have already been published (16).

Objective II: Evaluation of the in *vitro* performance of the developed RFB-loaded NLC

- Validation of the ANN model used for the NLC optimization process.
- Evaluation of release profile, thermal behavior and morphology displayed by NLC, as well as the *in vitro* performance in cell cultures of the developed formulations in terms of biocompatibility, permeability and cell uptake.

Results related to this objective will be displayed in Chapter II: "*Rifabutin-loaded Nanostructured lipid Carriers as a Tool in Oral Anti-mycobacterial Treatment of Crohn´s Disease*" and have already been published (17).

Objective III: Rational design of a lyophilization process suitable to convert NLC dispersions into a solid dosage form

- Evaluation of the applicability of Artificial Intelligence tools, such as NFL for a better understanding of lyophilization conditions impact over lyophilized powders (LP) final properties.
- Assessment of the existing physicochemical phenomena driving lyophilization process and cryoprotectant effectivity of sugars.
- Obtaining LP, easily redispersible and suitable for oral administration, which gives rise to NLC preserving their initial properties after reconstitution.

Results related to this objective will be displayed in Chapter III: "*Cryoprotectant effectivity of sugars in Nanostructured Lipid Carriers lyophilization*".

REFERENCES

1. Lasoń E, Sikora E, Ogonowski J. Influence of process parameters on properties of Nanostructured Lipid Carriers (NLC) formulation. Acta Biochim Pol. 2013; 60 (4): 773-777.
2. Desai N. Challenges in development of nanoparticle-based therapeutics. AAPS J. 2012; 14 (2): 282-295.
3. Jara MO, Catalan-Figueroa J, Landin M, Morales JO. Finding key nanoprecipitation variables for achieving uniform polymeric nanoparticles using neurofuzzy logic technology. Drug Deliv Transl Res. 2018; 8 (6): 1797-1806.
4. Rodriguez-Dorado R, Landin M, Altai A, Russo P, Aquino RP, Del Gaudio P. A novel method for the production of core-shell microparticles by inverse gelation optimized with artificial intelligent tools. Int J Pharm. 2018; 538 (1-2): 97-104.
5. Feuerstein JD, Cheifetz AS. Crohn Disease: Epidemiology, Diagnosis, and Management. Mayo Clin Proc. 2017; 92 (7): 1088-1103.
6. Davis WC. On deaf ears, Mycobacterium avium paratuberculosis in pathogenesis Crohn's and other diseases. World J Gastroenterol. 2015; 21 (48):13411-13417.
7. Kuenstner JT, Naser S, Chamberlin W, Borody T, Graham DY, McNees A, et al. The Consensus from the Mycobacterium avium ssp. paratuberculosis (MAP) Conference 2017. Front Public Health. 2017; 5: 208.
8. Blaschke TF, Skinner MH. The clinical pharmacokinetics of rifabutin. Clin Infect Dis. 1996; 22 (Suppl 1): 15-22.
9. Mohan LJ, Daly JS, Ryan BM, Ramtoola Z. The future of nanomedicine in optimising the treatment of inflammatory bowel disease. Scand J Gastroenterol. 2019; 54 (1): 18-26.
10. Khan S, Baboota S, Ali J, Khan S, Narang RS, Narang JK. Nanostructured lipid carriers: an emerging platform for improving oral bioavailability of lipophilic drugs. Int J Pharm Investig. 2015; 5 (4): 182-191.
11. Murphy JT, Sommer S, Kabara EA, Verman N, Kuelbs MA, Saama P, et al. Gene expression profiling of monocyte-derived macrophages following infection with Mycobacterium avium subspecies avium and Mycobacterium avium subspecies paratuberculosis. Physiol Genomics. 2006; 28 (1): 67-75.
12. Heurtault B, Saulnier P, Pech B, Proust JE, Benoit JP. Physico-chemical stability of colloidal lipid particles. Biomaterials. 2003; 24 (23): 4283-4300.
13. Battaglia L, Gallarate M. Lipid nanoparticles: state of the art, new preparation methods and challenges in drug delivery. Expert Opin Drug Deliv. 2012; 9 (5): 497-508.
14. Abdelwahed W, Degobert G, Stainmesse S, Fessi H. Freeze-drying of nanoparticles: formulation, process and storage considerations. Adv Drug Deliv Rev. 2006; 58 (15): 1688-1713.
15. Colbourn EA, Rowe RC. Novel approaches to neural and evolutionary computing in pharmaceutical formulation: challenges and new possibilities. Future Med Chem. 2009; 1 (4): 713-726.
16. Rouco H, Diaz-Rodriguez P, Rama-Molinos S, Remunan-Lopez C, Landin M. Delimiting the knowledge space and the design space of nanostructured lipid carriers through Artificial Intelligence tools. Int J Pharm. 2018; 553 (1-2): 522-530.

17. Rouco H, Diaz-Rodriguez P, Gaspar DP, Gonçalves L, Cuerva M, Remuñán-López C, et al. Rifabutin-Loaded Nanostructured Lipid Carriers as a Tool in Oral Anti-Mycobacterial Treatment of Crohn's Disease. Nanomaterials. 2020; 10 (11): 2138.

USC
UNIVERSIDADE
DE SANTIAGO
DE COMPOSTELA

3. CHAPTER I: DELIMITING THE KNOWLEDGE SPACE AND THE DESIGN SPACE OF NANOSTRUCTURED LIPID CARRIERS THROUGH ARTIFICIAL INTELLIGENCE TOOLS*

*The results from this chapter and its corresponding annex, have already been published as Rouco H[1], Diaz-Rodriguez P[1], Rama-Molinos S[1], Remuñán-Lopez C[2], Landin M[1]. Delimiting the knowledge space and the design space of nanostructured lipid carriers through Artificial Intelligence tools. Int J Pharm. 2018;553 (1-2):522-30 (1).
ISSN:0378-5173, e-ISSN:1873-3476.

[1] R+D Pharma Group (GI-1645), Department of Pharmacology, Pharmacy and Pharmaceutical Technology, Faculty of Pharmacy, University of Santiago de Compostela, Santiago de Compostela, Spain.
[2] NanoBiofar Group (GI-1643), Department of Pharmacology, Pharmacy and Pharmaceutical Technology, Faculty of Pharmacy, University of Santiago de Compostela, Santiago de Compostela, Spain

.

USC
UNIVERSIDADE
DE SANTIAGO
DE COMPOSTELA

ABSTRACT

Nanostructured lipid carriers (NLC) are biocompatible and biodegradable nanoscale systems with extensive application for controlled drug release. However, the development of optimal nanosystems along with a reproducible manufacturing process is still challenging. In this study, a two-step experimental design was performed, and databases were successfully modelled using Artificial Intelligence techniques as an innovative method to get optimal, reproducible, and stable NLC. The initial approach, including a wide range of values for the different variables, was followed by a second set of experiments with variable values in a narrower range, more suited to the characteristics of the system. NLC loaded with rifabutin, a hydrophobic drug model, were produced by hot homogenization and fully characterized in terms of particle size, size distribution, Zeta potential, encapsulation efficiency and drug loading. The use of artificial intelligence tools has allowed to elucidate the key parameters that modulate each formulation property. Stable nanoparticles with low sizes and polydispersions, negative zeta potentials and high drug loadings were obtained when the proportion of lipid components, drug, surfactants and stirring speed were optimized by FormRules® and INForm®. The successful application of Artificial intelligence tools on NLC formulation optimization constitutes a pioneer approach in the field of lipid nanoparticles.

USC
UNIVERSIDADE
DE SANTIAGO
DE COMPOSTELA

3.1. INTRODUCTION

Lipid nanoparticles (LN) constitute promising nanoscale systems that have recently raised high interest for drug and gene targeting and controlled delivery (2). They present as main advantages, small and controllable size, biocompatibility, biodegradability, physicochemical stability, cost-effectiveness and solvent-free production method suitable for high-scale manufacturing. Furthermore, derived from their structure, they confer chemical protection of incorporated drugs while their surface can be easily functionalized (3, 4).

Nanostructured Lipid Carriers (NLC) have been described as a smart second generation of lipid nanoparticles. The main difference with Solid Lipid Nanoparticles (SLN), first generation of LN, is based on the introduction of an oil component in the nanosystem matrix (5). The combination of two spatially different lipid molecules, solid and liquid, on the same system results in an imperfect nanoparticle matrix structure that enables an increase in drug loading capacity together with the minimization of drug expulsion during storage. Moreover, this blend allows the production of lipid particles that remain solid at both room and body temperatures (6).

NLC are well established drug carriers usually characterized by a biphasic pattern release profile, in which the drug is initially released by a burst effect followed by a sustained release at a constant rate (7). Many recent works have shown the potential of these nanoparticulated systems to achieve a specific controlled or sustained drug release for different administration routes such as topic (8), oral (9), pulmonary (10) or intravenous (11).

However, it is necessary to highlight that the development of optimized nanoparticle-based therapeutics is not an easy task. Nanoparticles are three dimensional structures formed by a complex superposition of several components, which may be affected by slight modifications in composition and manufacturing process, leading to unexpected consequences in the formulation characteristics (12). Due to their complexity, a deep understanding of the critical components of the systems and their interactions along with a reproducible manufacturing process is required to achieve the desired nanosystem (12).

Artificial Neural Networks (ANN) are computer programmes able to detect data trends and relationships and learn from experience, mimicking the learning process of the human brain (13). However, the interpretation of ANN may also not be a simple task (14). Neurofuzzy Logic (NFL) is a hybrid technology that combines the data learning capabilities of ANN with the ability of fuzzy logic to express concepts in a simplified way, as linguistic ¨IF-THEN¨ rules (15). The advantages derived from the use of this Artificial Intelligence tool in comparison with conventional experimental design and statistical analysis for the development of pharmaceutical formulations, have already been reported (16). Besides, the successful application of this technology on the development process of microparticles (17) and polymeric nanoparticles (18) has recently been described. However, to the best of our knowledge, NFL technology has never been applied in the field of LN. The use of this technology could be a useful tool on formulation optimization process of NLC. However, it is necessary to consider that changes in composition such as the use of different lipids, emulsifiers or even a different drug may alter the behavior of the nanosystems in terms of drug loading capacity, stability and physicochemical characteristics (19, 20). Despite the utility of the technology, models obtained

during the development of a specific formulation are experimental and must be specifically adapted to each preparation.

On this basis, the aim of this work is to show the potential of Artificial Intelligence tools to successfully model small databases from reduced experimental designs, in order to understand the effect of composition and operation conditions on the characteristics of loaded NLC. As a consequence, the knowledge space and the design space of the NLC can properly be defined and therefore, the optimization of the formulation can be carried out in order to achieve stable nanoparticles with sizes within the nano range, low polydispersity index, negative zeta potential and suitable drug payload.

3.2. Materials and methods

3.2.1. Materials

Rifabutin (RFB) was purchased from Carbosynth Limited (UK). Polysorbate 80 (Tween® 80) was purchased from Sigma Aldrich (Germany). Oleic acid was obtained from Merck (Portugal). Precirol® ATO 5 (glyceryl distearate) and Epikuron® 145V (deoiled phosphatidyl choline-enriched lecithin) were kind gifts from Gattefossé (France) and Cargill (Spain) respectively. Ultrapure water (MilliQ plus, Millipore Ibérica, Spain) was used throughout. The remaining solvents and reagents were analytical or HPLC grade.

3.2.2. Experimental design

To get a broader understanding of the formulation parameters effect on nanostructured lipid carriers (NLC) characteristics, this study was performed as a two-stage experiment. The initial approach included a wide range of experimental conditions while the second one used the knowledge derived from the initial model to narrow down the conditions suitable to get NLC. Both experimental designs were created by Dataform® v3.1 Software (Intelligensys Ltd, UK) using a Balanced Density Design with a minimum pattern of 7 for the first set of experiments, or 5 in the case of the second one. Four variables were considered for the initial experimental design (**Table 3.1**): amount of liquid lipid (Oleic acid, LL%), percentage of Tween® 80, stirring speed (rpm) and amount of the model drug rifabutin (RFB%). The drug and liquid lipid percentages were referred to the total lipid matrix (w/w) while the amount of Tween® 80 was referred to the aqueous phase (w/v). Based on the results obtained with this first model, a new experimental design more suited to obtain the desired characteristics of NLC was performed (**Table 3.2**). In this case, the amount of Epikuron® 145V (Lecithin%) used as co-emulsifier was included as a fifth variable in the design. The percentage of lecithin was referred to the total lipid matrix (w/w).

3.2.3. NLC formulation

Nanostructured lipid carriers (NLC) were prepared following a previously described hot high shear homogenization (HSH) method with slight modifications (21). Precirol® ATO 5 and oleic acid were used as the lipid components while Tween® 80 and Epikuron® 145V were used as surfactants. The lipid phase, formed by 300 mg of an oleic acid and Precirol® ATO 5 blend, with variable amounts of rifabutin, was melted at 80ºC. The aqueous phase (10 ml) was

prepared by dispersing Epikuron® 145V in a solution of Tween® 80 in ultrapure water and heated to the same temperature. Then, the hot aqueous phase was added to the lipid phase and homogenization was performed using an Ultra-Turrax T25 (IKA Labortechnik, Germany) for 10 min at 80ºC. NLC dispersions were finally obtained by cooling the hot nanoemulsion in an ice bath, with gentle agitation for 2 min. Each formulation was carried out at least by duplicate.

Table 3.1. Manufacturing conditions followed in NLC formulations (Experimental design 1)

Formulation	LL%	Tween®80%	Speed (rpm)	RFB%
1	25	6	20,400	10
2	38	2	9400	0
3	13	4	9400	15
4	75	3	13,400	5
5	50	7	13,400	12.5
6	63	5	13,400	2.5
7	0	1	20,400	7.5
8	38	4	20,400	2.5
9	13	2	13,400	12.5
10	50	6	13,400	0
11	63	3	20,400	15
12	75	7	9400	7.5
13	0	1	13,400	10
14	25	5	9400	5

Table 3.2. Manufacturing conditions followed in NLC formulations (Experimental design 2)

Formulation	LL%	Tween®80%	Lecithin%	Speed (rpm)	RFB%
15	40	1.5	0.5	13400	5
16	57.5	3	1	16800	3.75
17	75	1	0	20400	2.5
18	40	1	0	20400	5
19	75	3	0.5	13400	3.75
20	57.5	1.5	1	16800	2.5
21	40	1.5	0	13400	5
22	57.5	1	1	16800	2.5
23	75	3	0.5	20400	3.75
24	75	1.5	1	13400	5
25	40	3	0	20400	2.5
26	57.5	1	0.5	16800	3.75
27	57.5	1	0.5	13400	3.75
28	75	3	0	20400	2.5
29	40	1.5	1	16800	5

3.2.4. NLC characterization

3.2.4.1. Particle size, surface charge and physical stability

NLC particle sizes and surface charges were determined by Photon Correlation Spectroscopy (PCS) and laser Doppler anemometry, respectively, using a Zetasizer Nano-ZS (Malvern Instruments, UK). For size determination, samples were placed in polystyrene

cuvettes and properly diluted in ultrapure water. Measurements were performed at 25±1ºC. Results were expressed as size (Peak 1) and percentage (Peak 1%) of the most suitable peak for the first experimental design, or Z-average size (Size) and polydispersity index (PDI) for the second one. Surface charge was determined through particle mobility in an electric field to calculate nanoparticles zeta potential (ZP). To carry out this determination, samples were also diluted with ultrapure water and placed in a specific cuvette where a potential of ±150 mV was established. All the measurements were carried out in triplicate.

3.2.4.2. Encapsulation efficiency and drug loading

Encapsulation efficiency and drug loading determination was carried out as described in a previous work (22). After preparation, NLC dispersions were purified by size exclusion chromatography on Sephadex G-25/PD-10 columns (GE Healthcare Life Sciences, USA). This procedure allowed the separation of the free drug from the nanoparticle suspension. Purified NLC were dissolved with acetonitrile and centrifuged at 12000 rpm and 4ºC for 30 min, promoting the precipitation of the lipid phase. The encapsulated drug, which remains in the supernatant, was quantified by HPLC ($W_{loaded\ drug}$). The drug amount present in the supernatant of non-purified formulations subjected to the same protocol was used as 100% of drug content ($W_{total\ drug}$).

NLC RFB encapsulation efficiency (EE) and drug loading (DL) were calculated by the following equations:

$$EE\ (\%) = [W_{loaded\ drug}/W_{total\ drug}]\ x100 \qquad \textbf{Equation 3.1}$$

$$DL\ (\%) = [W_{loaded\ drug}/W_{lipid}]\ x100 \qquad \textbf{Equation 3.2}$$

Where $W_{total\ drug}$ is the weight of the drug in the formulation, $W_{loaded\ drug}$ is the incorporated drug and W_{lipid} is the weight of the lipid matrix.

3.2.5. High performance liquid chromatography with UV detection

Drug concentrations were assessed through high performance liquid chromatography (HPLC). The analysis was performed using an Agilent 1100 HPLC system (Agilent Technologies, USA) equipped with a C18 column (Waters symmetry C18 5 µm, 3.9×150 mm) following the method previously described by Gaspar et al (23). Briefly, twenty microliters of sample were injected and eluted with a mobile phase composed by a 53:47 v/v mixture of potassium dihydrogen phosphate 0.05 M/sodium acetate 0.05 M (pH adjusted to 4.0 with acetic acid) with acetonitrile (Scharlau, Spain). Drug quantification was performed in an isocratic mode with a 1 ml/min flow rate at 275 nm.

3.2.6. Modelling by Artificial Intelligence tools

Databases obtained from experimental designs 1 and 2 (**Table 3.1** and **Table 3.2**) were modelled using two different Artificial Intelligence software: FormRules® v4.03 (Intelligensys Ltd, UK) and INForm® v5.01 (Intelligensys Ltd., UK). FormRules® is a neurofuzzy logic (NFL)

technology that combines Artificial Neural Networks and Fuzzy Logic. NFL system allows answering "WHAT IF" questions, as the model is able to generate a complete set of "IF-THEN" rules that explain the effect of production process variables (composition and operation conditions) on the characteristics of NLC. In order to generate those rules, a fuzzification process is necessary. A complete explanation about the fuzzification process of inputs and outputs is available in the literature (24). In brief, every value of an input is categorized and described with a word (Low, Medium, High) together with a membership degree ranging from zero to one, as graphically shown in Supplementary **Figure A1 (Annex I)**. The outputs are always categorized as low or high together with the membership degree. In fuzzy-rule based systems as FormRules®, after modelling, the created knowledge is presented by IF-THEN rules or sentences that consist of two parts: an antecedent part stating conditions on the input variable(s), and a consequent part describing the corresponding values of the output variable(s).

On the other hand, INForm® brings together Artificial Neural Networks and Genetic Algorithms that allow the generated model to answer "HOW TO GET" questions and, therefore, optimize the nanoparticles by asking the models to find the conditions for NLC to have desirable properties.

For experimental design 1 and 2 outputs, the training parameters used for FormRules® v4.03 models were: ridge regression factor of $1\times e^{-6}$, structural risk minimization as model selection criteria (C_1 =0.60-0.83 and C_2 =4.80), two set densities, four maximum inputs per submodel and 15 maximum nodes per input.

The quality of the independent predictive model for each NLC parameter was evaluated using the determination coefficient of the Training or Test sets (R^2) expressed in percentage (predictability) and the analysis of variance (ANOVA) (accuracy) (25).

Train Set R^2 values are calculated by the following equation (26):

$$R^2 = [\,1 - \textstyle\sum_{i=1}^{n}(yi - yi')^2 \,/\, \sum_{i=1}^{n}(yi - yi'')^2] \times 100\% \qquad \textbf{Equation 3.3}$$

Where *y* is the experimental output in the data set, *y*' is the predicted output calculated by the model and *y*" is the mean of the output. Train set R^2 values between 70 and 99.9% are indicative of acceptable predictabilities (27).

The database from experimental design 2 was also modelled using INForm® v5.01 to select optimal NLC composition and manufacturing parameters able to fulfil all the formulation requirements in terms of size, surface potential, drug encapsulation and stability. On this purpose, results were randomly split in two sets of 15 and 3 formulation results, for model training and test respectively. The training parameters used for INForm® v5.01 models were: five inputs, one hidden layer, 2 nodes, transfer type (Asymmetric Sigmoid), output transfer type (Linear, Asymmetric sigmoid, Symmetric sigmoid or Tanh), momentum (0.8), learning rate (0.7), target interactions (1000), target mean squared error (0.0001) and random seed (10000). INForm® models were obtained with the following operation conditions for the genetic algorithms run: one population, population size (100), number of iterations (100), 50% of replacement, random seed (1), mutation standard deviation (0.1). For the optimization process, to get stable NLC, not only fresh formulation characteristics were taken into account but also

the storage effect on them. For this purpose, the formulations obtained in experimental design 2 were re-evaluated after 1 month of storage at 5±1°C in terms of size, PDI, zeta potential and drug loading. The obtained database was included for INForm® modelling to ensure the optimized formulation maintain its properties after storage. The optimal RFB loaded NLC formulation was then manufactured in quadruplicate and characterized as previously described. The results for the freshly prepared NLC and after 1 month of storage at 5±1ºC were used as validation dataset for the developed models.

3.2.7. Statistical analysis

Experimental results have been reported as mean ± standard deviation. Comparison of samples (n=4) was performed by one-way ANOVA (IBM SPSS 24 software); samples with a p-value < 0.01 were considered statistically significant different.

3.3. RESULTS AND DISCUSSION

3.3.1. Getting to know the experimental field

The main objective of the present work is to establish the use of Artificial Intelligence tools as a new methodology suitable for formulation optimization in the field of nanostructured lipid carriers (NLC). Towards this goal, as mentioned before, a two-step approach was used in which an initial experimental set up, with a wide range of each formulation parameter, was followed by a second experimental design, with variable values more appropriate for NLC development, using the insight from the previous step. In order to evaluate critical quality attributes of NLC drug carriers, such as encapsulation efficiency or drug loading, the antibiotic rifabutin was used as a model hydrophobic drug.

Furthermore, two widely used lipids in NLC formulations, oleic acid and Precirol® ATO 5 as liquid and solid lipids, respectively, were selected as the main lipid components for this study (28). The choice of these materials should allow to obtain models that could be applied to the development of a broad spectrum of lipid nanoparticles.

Four variables were originally selected in the production of NLC by hot shear homogenization (LL, Tween®80, stirring speed and RFB) and introduced as inputs in the model (**Table 3.3**). As result of their wide ranges, NLC formulations with very different sizes and polydispersities were obtained (**Table 3.4**). Although Z-average size is the most commonly used parameter to describe nanoparticulated systems size by dynamic light scattering, it can only be properly applied when samples are monodisperse and monomodal (29). Taking this into account, the outputs used to characterize NLC on the first set of experiments were the percentage and mean diameter of the lowest peak in size (peak 1; without considering peaks attributable to the surfactant micelles), together with their Zeta potential (**Table 3.3**). FormRules® succeeded in modelling those three outputs (**Table 3.3**) with R^2 values above 70%, indicative of reasonable model predictabilities (27). The computed f ratios presented values higher than critical f values for the degrees of freedom of the model, indicating no statistically significant differences between predicted and experimental results and therefore, good model performance (17). However, the variables included in the experimental design 1 only explain a

low percentage of the variability on zeta potential (R^2= 9.14), being this parameter similar for all the formulations.

From the obtained models (**Table 3.3**) we can gather that mean diameter and percentage of peak 1 were affected by interactions between Tween®80 proportion and stirring speed, easily attributable to the homogenization technique used in the formulation process. The use of a high amount of surfactant along with an intense mixing results in foam production, which hinders the correct NLC formation. In agreement with this, the use of the highest stirring speed and high Tween®80 (**Table 3.4**, Formulation 1) led to a peak 1 mean diameter of 3257.7 ± 567.3 nm with a 100% percentage of peak 1, the highest values of all the studied NLC. Moreover, percentage of peak 1 was, in less extent, also affected by the amount of rifabutin used in the formulation. High amounts of drug promoted the distortion of the particle formation process and the generation of NLC with bimodal and trimodal particle size distributions. The incorporation of 7.5% of rifabutin together with 75% of LL and 7% of Tween®80 at 9400 rpm promoted the production of NLC with the lowest percentage of peak 1 (17.9%) (**Table 3.4**, Formulation 12).

The use of NFL has allowed to obtain the combination of conditions in which a high percentage of peak 1 and particles below 285 nm would be obtained, highlighted in grey in **Figure 3.1**. Furthermore, as can be derived from the set of "IF-THEN" rules of the model (**Tables A1** and **A2, Annex I**), a low/medium proportion of Tween®80, a medium/high stirring speed along with an amount of drug lower than 6% should be used to successfully develop NLC with adequate physical properties (low mean size, high % of peak 1).

Table 3.3. Inputs selected by the NFL models for the experimental design 1, together with the predictability (R^2) and ANOVA parameter (indicative of accuracy). The most important submodel is bolded.

Output	Submodels	Inputs from Formrules®	R^2	Calculated f value	Degrees of freedom	f critical for p<0.01
Size peak 1	**Submodel 1**	**Tween®80 (%) × speed**	89.12	9.55	6 and 13	4.62
% peak 1	Submodel 1	RFB (%)	89.46	7.28	7 and 13	4.44
	Submodel 2	**Tween®80 (%) × speed**				
ZP	**Submodel 1**	**Speed**	9.14	0.55	2 and 13	6.7

Table 3.4. Formulations obtained in the first set of experiments (n=2)

Formulation	Size peak 1	% Peak 1	ZP
1	3257.7	100.0	-26.4
2	154.8	97.0	-26.2
3	137.2	20.2	-26.0
4	133.6	99.3	-28.2
5	1214.0	49.0	-29.0
6	210.2	95.9	-26.9
7	222.2	97.5	-27.8
8	209.6	96.7	-24.8
9	273.8	96.0	-29.1
10	211.1	96.5	-24.6
11	190.3	57.2	-27.4
12	101.0	17.9	-24.2
13	163.4	98.6	-20.7
14	188.9	74.9	-20.8

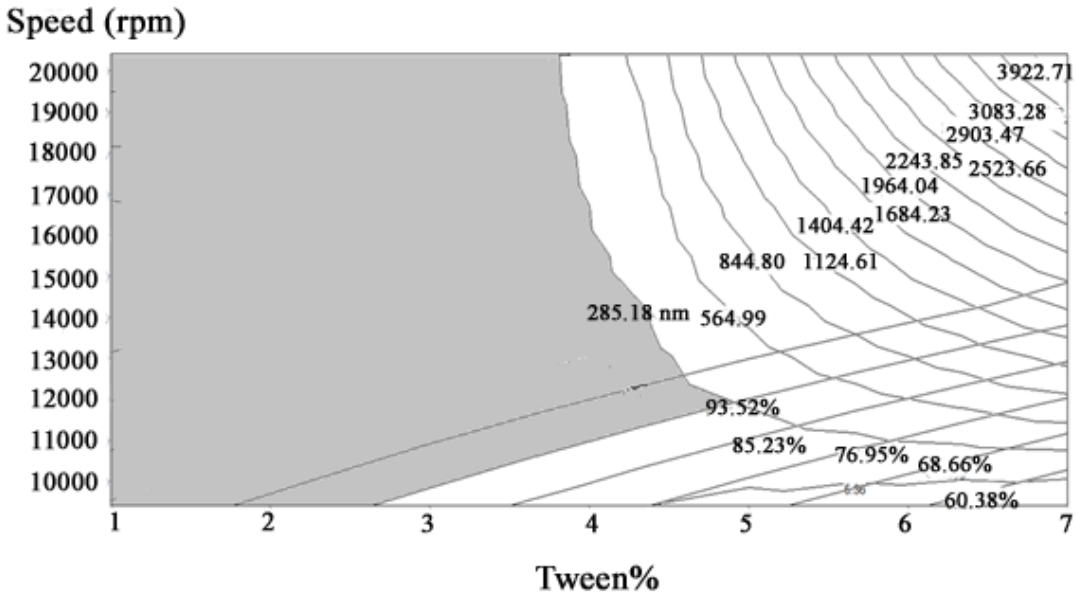

Figure 3.1. Effect of Tween® 80 (%) and speed (rpm) on mean size and percentage of peak 1

3.3.2. Defining the design space

Based on those results, experimental design 2, with a narrower range for stirring speed, concentration of Tween®80 and rifabutin was performed (**Table 3.2**). The use of co-emulsifiers is a common strategy to achieve nanoparticles with low particle size and high storage stability (30). For this reason, lecithin, a widely used emulsifier (28, 31, 32), was added in the range of 0-1% as co-surfactant, and therefore introduced as a new input in the experimental design. The selection of a more appropriate range of variables led to the obtaining of monodispersed nanosystems, which were characterized by the usual critical parameters of nanoparticles: Z-average size (size), polydispersity index (PDI) and zeta potential (ZP), together with encapsulation efficiency (EE) and drug loading (DL) (**Table 3.5**).

Table 3.5. Physicochemical characteristics, encapsulation efficiency and drug loading of formulations obtained in the second experimental design (n=2)

Formulation	Size (nm)		PDI		ZP (mV)		EE (%)		DL (%)	
	Mean	SD	Mean	SD	Mean	SD	Mean	SD	Mean	SD
15	370.5	8.6	0.33	0.00	-14.4	1.5	81.0	6.0	4.0	0.7
16	255.9	7.1	0.24	0.01	-13.2	0.6	67.0	4.8	2.7	0.1
17	227.6	0.8	0.33	0.02	-19.6	0.2	110.6	8.9	2.8	0.5
18	387.4	32.3	0.32	0.02	-16.8	0.4	78.4	0.4	3.6	0.1
19	154.9	11.4	0.16	0.03	-16.8	0.1	90.1	1.6	4.1	0.4
20	181.7	1.7	0.24	0.00	-19.8	0.7	90.4	4.0	2.3	0.2
21	292.1	3.6	0.25	0.01	-16.7	0.3	75.5	3.5	4.1	1.1
22	225.7	25.4	0.30	0.04	-20.0	1.3	95.4	21.0	2.1	0.4
23	222.4	38.2	0.19	0.02	-15.0	0.2	80.9	14.4	3.0	0.3
24	153.1	8.0	0.21	0.00	-19.7	0.0	104.3	4.6	5.3	0.0
25	201.4	6.7	0.26	0.02	-12.2	2.3	51.4	4.0	1.2	0.1
26	239.7	9.8	0.29	0.02	-18.4	0.3	81.6	6.7	3.1	0.2
27	231.0	6.4	0.27	0.07	-18.5	0.7	88.6	4.0	3.8	0.3
28	135.0	0.0	0.18	0.01	-16.6	0.2	103.3	0.0	2.4	0.3
29	242.6	22.3	0.30	0.02	-18.6	0.8	75.4	3.2	4.0	0.3

FormRules® was able to successfully model all the above-mentioned inputs, with R^2 values above 70%. Furthermore, computed f ratios showed values higher than critical f values, indicating a suitable prediction capacity and an adequate model performance. **Figures 3.2-3.6** show the influence of the different inputs (LL, Tween®80, lecithin, stirring speed and RFB) on the outputs (size, PDI, ZP, EE and DL) according to the NFL models obtained.

The variability in particle size is explained by two submodels, including the interaction between the amount of liquid lipid and percentage of drug together with the single effect of Tween®80 concentration (**Figure 3.2A**). An increase in size, attributable to the accommodation space required for the drug within the nanosystem, was produced when a high amount of drug was employed (33). However, increasing liquid lipid:solid lipid ratios (i.e. increase in LL) and Tween®80 percentages led to a decrease in size, counteracting the destabilizing effect of drug (**Table A3, Annex I**). As shown in the 3D plots obtained from the model (**Figure 3.2B**), when the Tween®80 concentration is fixed to 1.9%, the use of 75% of liquid lipid allows to obtain low size nanoparticles even when a high amount of rifabutin is added in the formulation process.

A

Submodels	Inputs from Formrules®	R^2	Calculated f value	Degrees of freedom	f critical for p<0.01
Submodel 1	**LL (%)× RFB (%)**	78.55	4.88	6 and 14	4.46
Submodel 2	Tween®80 (%)				

B

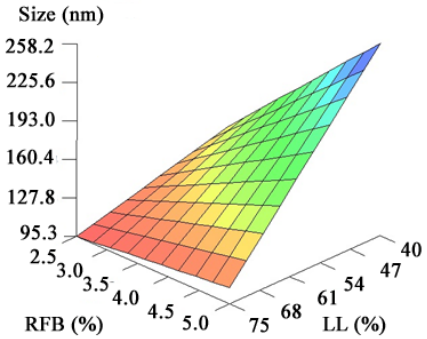

Figure 3.2. A) Inputs that explain the size variability and quality parameters of NFL model for size. The most important submodel is bolded, B) 3D plot of the influence of LL% and RFB% over the size when a 1.9% of Tween®80 is used

Single effects of liquid lipid and Tween®80 proportions also explain the variability of nanosystems PDI (**Figure 3.3A**). According to the set of "IF-THEN" rules (**Table A4, Annex I**), an increase in both variables led to a reduction on PDI. This effect might be due to an increase in the liquid lipid content that allows for a more efficient emulsification process. In agreement with the literature, the surface tension of the lipid droplets can be easily reduced by the emulsifying effect of Tween®80, leading to particles with lower and narrower size distributions (33, 34). As it can be observed in **Figure 3.3B**, when the amount of liquid lipid is fixed to 75% (the best condition in the size evaluation), only 1.2% of Tween®80 is required to maintain the PDI below 0.25, even when a high percentage of drug is used. In agreement with NFL predictions, the use of 75% of LL, 1.5% of Tween®80 and 5% of RFB led to NLC with a size of 153.1±8.0 nm and a PDI of 0.21±0.00 (**Table 3.5**, formulation 24).

A

Submodels	Inputs from Formrules®	R^2	Calculated f value	Degrees of freedom	f critical for p<0.01
Submodel 1	**Tween®80 (%)**	71.81	9.34	3 and 14	5.56
Submodel 2	LL (%)				

B

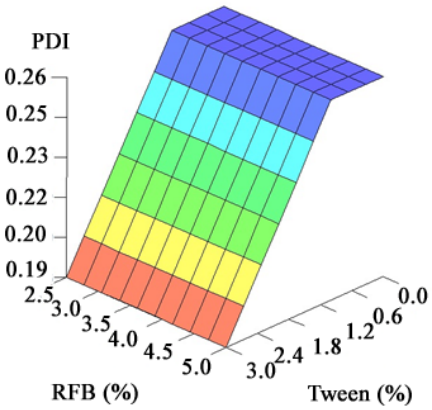

Figure 3.3. A) Inputs that explain the PDI variability and quality parameters of NFL model for PDI. The most important submodel is bolded, B) 3D plot of the influence of Tween®80 (%) and RFB (%) over the PDI when a 75% of LL is used.

The effect of the different inputs on zeta potential is shown in **Figure 3.4A**. This property was influenced by the percentage of liquid lipid and Tween® 80 employed. An increase in the LL on the nanosystem matrices led to a highly negative zeta potential, while Tween®80 produced the opposite effect (**Table A5, Annex I**). This reduction in zeta potential due to liquid lipid is easily attributable to the negative charge of the oleic acid (35). However, the increase

on the surface charge due to a higher amount of Tween®80, may be caused by the ability of non-ionic emulsifiers to localize close to the nanoparticle interface, counteracting the negative charge of the lipid matrix (36). As presented in **Figure 3.4B**, when the amount of liquid lipid is fixed to 75% (the best condition in the size evaluation), this effect begins to be noticeable from 1% of Tween®80. The experimental data support the ZP modifications predicted by NFL rules, when 3% of Tween®80 and 75% of LL are used, ZP value is -15.0± 0.2 (mV) (**Table 3.5**, formulation 23). Nevertheless, when 1% of Tween®80 and 75% of LL are employed ZP value reaches -19.6± 0.2 (mV) (**Table 3.5**, formulation 17). Interestingly, the setting of the LL on 75% using NFL models, allowed to distinguish a subtle effect of lecithin over the ZP of the formulations. The presence of lecithin, a negatively charged emulsifier (37), led to an increase in the negative values of ZP.

A

Submodels	Inputs from Formrules®	R^2	Calculated f value	Degrees of freedom	f critical for p<0.01
Submodel 1	**Tween®80 (%)**	77.77	12.83	3 and 14	5.56
Submodel 2	LL (%)				

B

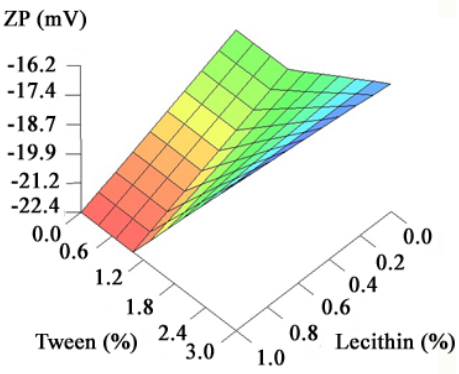

Figure 3.4. A) Inputs that explain the variability of ZP and quality parameters of NFL model for ZP. The most important submodel is bolded, B) 3D plot of the influence of Tween®80 (%) and lecithin (%) over the ZP when a 75% of LL is used.

On the other hand, variations in the encapsulation efficiency are explained by the amount of liquid lipid and Tween®80 in the formulations (**Figure 3.5A**) while the drug loading was conditioned, as is obvious, by the amount of drug added in the formulation process (**Figure 3.6A**). As shown in **Figure 3.6A**, liquid lipid, Tween®80 and stirring speed also shown an influence on drug loading. The use of a high amount of liquid lipid resulted in an increase in the EE and DL. In contrast, the selection of a high surfactant concentration led to a reduction on both parameters. The stirring speed used and the amount of drug added during formulation promoted the opposite effect over the drug loading, high amounts of rifabutin produced a high DL, while vigorous speeds resulted in a decrease on the drug content (**Tables A6 and A7**, **Annex I**).

The increase in the drug loading of the nanosystems detected by the NFL tools when a high liquid lipid:solid lipid ratio was used, is probably caused by the high solubility of the drug in the liquid lipid (5). The opposite effect, previously described for high Tween®80 proportions, might be related to the decrease in particle size associated to Tween®80, that results in a reduction of the available accommodation space for the drug (38). A similar effect was noticed for the stirring speed, which could be also related to the reduction in particle size. As it is shown in **Figure 3.5B**, Tween®80 concentration higher than 1.2%, promoted a more pronounced reduction in EE, while increasing amounts of LL resulted in the opposite effect. As an example,

NLC prepared using 3% of Tween®80 presented an EE of 51.4± 4.0% in the presence of 40% of LL, whereas values of 80.9± 14.4% for this output can be obtained when a 75% of LL was used (**Table 3.5**, formulations 25 and 23). As shown in **Figure 3.6B**, when LL and Tween®80 are set to 75% and 1.9% respectively, the DL of the formulations was strongly dependent on the stirring speed. Experimental data sustain the predictions of the NFL model. If the same amount of LL and Tween®80 are used, a stirring speed of 13400 rpm leads to a DL of 4.1±0.4% (**Table 3.5**, formulation 19). However, when a speed of 20400 rpm is applied, DL lows down to 2.4±0.3% (**Table 3.5**, formulation 28).

A

Submodels	Inputs from Formrules®	R^2	Calculated f value	Degrees of freedom	f critical for p<0.01
Submodel 1	**LL (%)**	81.42	16.07	3 and 14	5.56
Submodel 2	Tween®80 (%)				

B

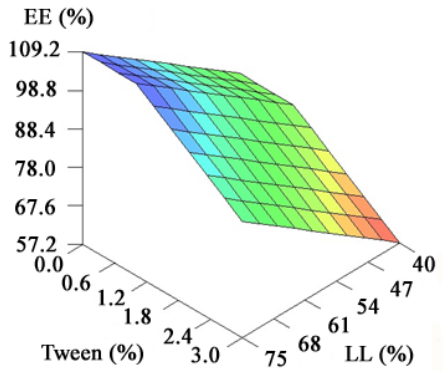

Figure 3.5. A) Inputs that explain the variability of EE and quality parameters of NFL model for EE. The most important submodel is bolded, B) 3D plot of the influence of Tween®80 (%) and LL (%) over EE (%).

A

Submodels	Inputs from Formrules®	R^2	Calculated f value	Degrees of freedom	f critical for p<0.01
Submodel 1	**RFB (%)**	98.3	76.93	6 and 14	4.46
Submodel 2	LL (%)				
Submodel 3	Speed (rpm)				
Submodel 4	Tween®80 (%)				

B

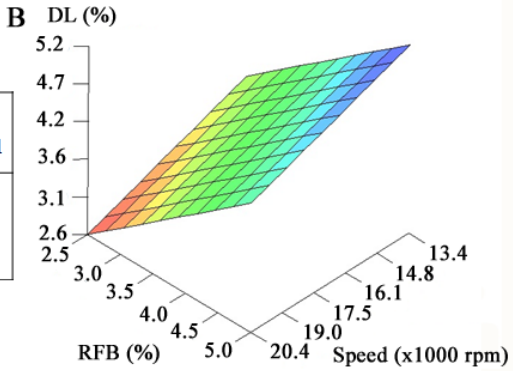

Figure 3.6. A) Inputs that explain the variability of DL and quality parameters of NFL model for DL. The most important submodel is bolded, B) 3D plot of the influence of RFB (%) and speed over DL (%) when a 75% of LL and a 1.9% Tween®80 is used.

Taking together, the set of "IF-THEN" rules (**Tables A3-A7**, **Annex I**), defines a RFB-loaded NLC design space characterized by a high liquid lipid content, a mild stirring speed along with a medium percentage of Tween®80. A nanosystem developed under these conditions is expected to successfully incorporate a 5% of drug maintaining a suitable size together with an adequate monodispersion.

3.3.3. Optimization of NLC by INForm®

High predictability ANN models were also generated by INForm®, being employed to select the best combination of variables (LL, Tween®80, lecithin, speed and RFB) to obtain

optimal rifabutin-loaded NLC, as a BCS class II drug model. The definition of optimal NLC requires the establishment of desirability functions for the five outputs analyzed. As an example, **Figure 3.7** shows the desirability function defined for the parameter size.

The requirements selected for the NLC freshly prepared and after 1 month of storage were: size lower than 250 nm, PDI lower than 0.19, negative ZP in the range -18.0 and -19.9 mV, EE of 100% and DL higher than 4%. Moreover, considering their priorities, weights were assigned to each input, being 10, 9, 8, 7 and 1 for DL, EE, size, PDI and ZP respectively.

Using Genetic Algorithms and the generated desirability functions, INForm® model selected the composition and operating conditions to develop the optimal formulation (**Table 3.6**). According to the ANN models, NLC produced using 75% of LL, 1.9% of Tween®80, 0.5% of lecithin, 5% of RFB and a speed of 14892 rpm would present a size of 152 nm, a PDI of 0.23, a zeta potential of -19 mV, an EE of 100% along with a DL of 5% that also maintain these properties after 1 month of storage.

To confirm the predicted values obtained by INForm® and to validate the ANN models, a formulation of NLC using the optimized parameters from **Table 3.6**, was carried out in quadruplicate. Results are presented in **Table 3.7**. As it can be observed, considering their corresponding standard deviations, the experimental values perfectly match the ones predicted by the model.

In addition, stability, which is a major concern in the development of nanosystems, proved to be adequate. The optimal formulation, stored in aqueous dispersion at 5±1ºC for 1 month (**Table 3.7**), does not show statistically significant differences in size, PDI and drug loading ($p \geq 0.01$) when compared to the fresh formulations. However, ZP was slightly influenced by the storage ($p = 0.001$) showing a decrease of 8.9± 2.2% that could promote a higher colloidal stability by electrostatic repulsion (39).

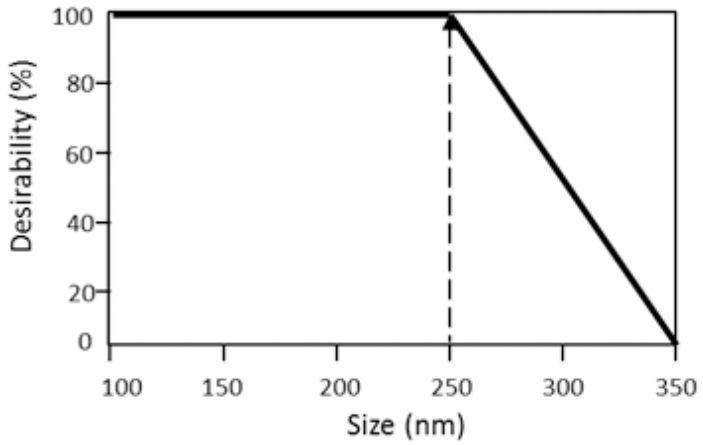

Figure 3.7. Example of desirability function for parameter size designed using the parameters from table 7.

Table 3.6. Selected inputs to obtain optimal rifabutin loaded NLC and predicted values of outputs obtained by INForm®.

Inputs	LL	Tween®80	Lecithin	Speed	RFB
	75%	1.9%	0.5%	14892.3 rpm	5%
	Outputs			**Predicted value**	
	Size (nm)			152	
	PDI			0.23	
	ZP (mV)			-19	
	EE (%)			100	
	DL (%)			5	

Table 3.7. Experimental values obtained for the optimal formulation selected by INForm® before and after the storage at 5ºC± 1ºC for a month.

	Size (nm)	PDI	ZP (mV)	EE (%)	DL (%)
t_0	176.0±16.5	0.22±0.03	-16.6±0.4	95.2±2.7	4.7±0.1
t_1	172.2±14.8	0.19±0.02	-18.2±0.3	-	4.2±0.2

3.4. CONCLUSIONS

The present work shows the usefulness of Artificial Intelligence tools to delimit the spaces of knowledge and design of NLC from results of experimental designs that include a small number of experiments (just 15 for 5 variables). The "IF-THEN" rules obtained through the neurofuzzy logic techniques allow to understand and explain the physical-chemical interactions that occur between the components of the nanoparticle systems. In addition, ANN model and genetic algorithms favor the estimation of the optimal conditions to formulate NLC of the desired characteristics and proper stability. Due to the known dependence of nanosystem properties on NLC composition, further studies should be carried out to ensure the ability of ANN and genetic algorithms to analyze the existing interactions between components and to predict formulation parameters, when using other compositions than the one employed on the current study.

REFERENCES

1. Rouco H, Diaz-Rodriguez P, Rama-Molinos S, Remunan-Lopez C, Landin M. Delimiting the knowledge space and the design space of nanostructured lipid carriers through Artificial Intelligence tools. Int J Pharm. 2018; 553 (1-2): 522-530.
2. Zhao Y, Huang L. Lipid nanoparticles for gene delivery. In: Huang L, Liu D, Wagner E (Eds.). Advances in Genetics. Cambridge, USA: Academic Press; 2014; 88: p 13-36.
3. Mendes M, Soares HT, Arnaut LG, Sousa JJ, Pais A, Vitorino C. Can lipid nanoparticles improve intestinal absorption?. Int J Pharm. 2016; 515 (1-2): 69-83.
4. Tapeinos C, Battaglini M, Ciofani G. Advances in the design of solid lipid nanoparticles and nanostructured lipid carriers for targeting brain diseases. J Control Release. 2017; 264: 306-332.
5. Müller RH, Radtke M, Wissing SA. Nanostructured lipid matrices for improved microencapsulation of drugs. Int J Pharm. 2002; 242 (1-2): 121-128.
6. Muchow M, Maincent P, Müller RH. Lipid nanoparticles with a solid matrix (SLN, NLC, LDC) for oral drug delivery. Drug Dev Ind Pharm. 2008; 34 (12): 1394-1405.
7. Kaul S, Gulati N, Verma D, Mukherjee S, Nagaich U. Role of Nanotechnology in Cosmeceuticals: A Review of Recent Advances. J Pharm (Cairo). 2018; 2018: 3420204.
8. Gainza G, Bonafonte DC, Moreno B, Aguirre JJ, Gutierrez FB, Villullas S, et al. The topical administration of rhEGF-loaded nanostructured lipid carriers (rhEGF-NLC) improves healing in a porcine full-thickness excisional wound model. J Control Release. 2015; 197: 41-47.
9. Qi R, Li YZ, Chen C, Cao YN, Yu MM, Xu L, et al. G5-PEG PAMAM dendrimer incorporating nanostructured lipid carriers enhance oral bioavailability and plasma lipid-lowering effect of probucol. J Control Release. 2015; 210: 160-168.
10. Taratula O, Kuzmov A, Shah M, Garbuzenko OB, Minko T. Nanostructured lipid carriers as multifunctional nanomedicine platform for pulmonary co-delivery of anticancer drugs and siRNA. J Control Release. 2013; 171 (3): 349-357.
11. Li H, Yang X, Zhou Z, Wang K, Li C, Qiao H, et al. Near-infrared light-triggered drug release from a multiple lipid carrier complex using an all-in-one strategy. J Control Release. 2017; 261: 126-137.
12. Desai N. Challenges in development of nanoparticle-based therapeutics. AAPS J. 2012; 14 (2): 282-295.
13. Agatonovic-Kustrin S, Beresford R. Basic concepts of artificial neural network (ANN) modeling and its application in pharmaceutical research. J Pharm Biomed Anal. 2000; 22 (5): 717-727.
14. Colbourn E, Rowe R. Neural computing boosts formulation productivity. Pharm Technol. 2003; 27: 22-25.
15. Colbourn EA, Rowe RC. Novel approaches to neural and evolutionary computing in pharmaceutical formulation: challenges and new possibilities. Future Med Chem. 2009; 1 (4): 713-726.
16. Landin M, Rowe RC, York P. Advantages of neurofuzzy logic against conventional experimental design and statistical analysis in studying and developing direct compression formulations. Eur J Pharm Sci. 2009; 38 (4): 325-331.

17. Rodriguez-Dorado R, Landin M, Altai A, Russo P, Aquino RP, Del Gaudio P. A novel method for the production of core-shell microparticles by inverse gelation optimized with artificial intelligent tools. Int J Pharm. 2018; 538 (1-2): 97-104.
18. Jara MO, Catalan-Figueroa J, Landin M, Morales JO. Finding key nanoprecipitation variables for achieving uniform polymeric nanoparticles using neurofuzzy logic technology. Drug Deliv Transl Res. 2018; 8 (6): 1797-1806.
19. Han F, Li S, Yin R, Liu H, Xu L. Effect of surfactants on the formation and characterization of a new type of colloidal drug delivery system: Nanostructured lipid carriers. Colloids Surf A Physicochem Eng Asp. 2008; 315 (1-3): 210-216.
20. Pathak K, Keshri L, Shah M. Lipid nanocarriers: influence of lipids on product development and pharmacokinetics. Crit Rev Ther Drug Carrier Syst. 2011; 28 (4): 357-393.
21. Estella-Hermoso de Mendoza A, Campanero MA, Lana H, Villa-Pulgarin JA, De La Iglesia-Vicente J, Mollinedo F, et al. Complete inhibition of extranodal dissemination of lymphoma by edelfosine-loaded lipid nanoparticles. Nanomedicine. 2012; 7 (5): 679-690.
22. Gaspar DP, Faria V, Goncalves LM, Taboada P, Remunan-Lopez C, Almeida AJ. Rifabutin-loaded solid lipid nanoparticles for inhaled antitubercular therapy: Physicochemical and in vitro studies. Int J Pharm. 2016; 497 (1-2): 199-209.
23. Gaspar MM, Cruz A, Penha AF, Reymao J, Sousa AC, Eleuterio CV, et al. Rifabutin encapsulated in liposomes exhibits increased therapeutic activity in a model of disseminated tuberculosis. Int J Antimicrob Agents. 2008; 31 (1): 37-45.
24. Landin M, Rowe RC. Artificial neural networks technology to model, understand, and optimize drug formulations. In: Aguilar JE (Ed). Formulation Tools for Pharmaceutical Development. 1st edition. Cambridge, UK: Woodhead publishing; 2013. p. 7-37.
25. Diaz-Rodriguez P, Landin M. Smart design of intratumoral thermosensitive beta-lapachone hydrogels by Artificial Neural Networks. Int J Pharm. 2012; 433 (1-2):112-118.
26. Shao Q, Rowe RC, York P. Comparison of neurofuzzy logic and neural networks in modelling experimental data of an immediate release tablet formulation. Eur J Pharm Sci. 2006; 28 (5): 394-404.
27. Colbourn E, Rowe R. Neural computing and pharmaceutical formulation. In: Swarbrick J, Boylan JC (Eds.). Encyclopedia of pharmaceutical technology. 3rd edition. New York, USA: Marcel Dekker; 2005. p. 145–157.
28. Khosa A, Reddi S, Saha RN. Nanostructured lipid carriers for site-specific drug delivery. Biomed Pharmacother. 2018; 103: 598-613.
29. Malvern Instruments Limited. Dynamic light scattering common terms defined [White paper]. Worcestershire, UK: 2011.
30. Mehnert W, Mader K. Solid lipid nanoparticles: production, characterization and applications. Adv Drug Deliv Rev. 2001; 47 (2-3): 165-196.
31. Kakkar V, Singh S, Singla D, Kaur IP. Exploring solid lipid nanoparticles to enhance the oral bioavailability of curcumin. Mol Nutr Food Res. 2011; 55 (3): 495-503.
32. Severino P, Andreani T, Macedo AS, Fangueiro JF, Santana MH, Silva AM, et al. Current State-of-Art and New Trends on Lipid Nanoparticles (SLN and NLC) for Oral Drug Delivery. J Drug Deliv. 2012; 2012: 750891.

33. Azhar Shekoufeh Bahari L, Hamishehkar H. The Impact of Variables on Particle Size of Solid Lipid Nanoparticles and Nanostructured Lipid Carriers; A Comparative Literature Review. Adv Pharm Bull. 2016; 6 (2): 143-151.
34. Song A, Zhang X, Li Y, Mao X, Han F. Effect of liquid-to-solid lipid ratio on characterizations of flurbiprofen-loaded solid lipid nanoparticles (SLNs) and nanostructured lipid carriers (NLCs) for transdermal administration. Drug Dev Ind Pharm. 2016; 42 (8): 1308-1314.
35. Ham-Pichavant F, Sèbe G, Pardon P, Coma V. Fat resistance properties of chitosan-based paper packaging for food applications. Carbohydr Polym. 2005; 61 (3): 259-265.
36. Schubert MA, Müller-Goymann CC. Characterisation of surface-modified solid lipid nanoparticles (SLN): influence of lecithin and nonionic emulsifier. Eur J Pharm Biopharm. 2005; 61 (1-2): 77-86.
37. Ogawa S, Decker EA, McClements DJ. Production and characterization of o/w emulsions containing droplets stabilized by lecithin−chitosan−pectin mutilayered membranes. J Agric Food Chem. 2004; 52 (11): 3595-3600.
38. Gaba B, Fazil M, Khan S, Ali A, Baboota S, Ali J. Nanostructured lipid carrier system for topical delivery of terbinafine hydrochloride. Bull. Fac. Pharm. Cairo Univ. 2015; 53 (2): 147-159.
39. Heurtault B, Saulnier P, Pech B, Proust JE, Benoit JP. Physico-chemical stability of colloidal lipid particles. Biomaterials. 2003; 24 (23): 4283-4300.

USC
UNIVERSIDADE
DE SANTIAGO
DE COMPOSTELA

4. CHAPTER II: RIFABUTIN-LOADED NANOSTRUCTURED LIPID CARRIERS AS A TOOL IN ORAL ANTI-MYCOBACTERIAL TREATMENT OF CROHN´S DISEASE*

*The results from this chapter and its corresponding annex, have already been published as Rouco H[1], Diaz-Rodriguez P[2], Gaspar DP[3], Gonçalves L[3], Cuerva M[4], Remuñán-López C[5], Almeida AJ[3] and Landin M[1]. Rifabutin-Loaded Nanostructured Lipid Carriers as a Tool in Oral Anti-Mycobacterial Treatment of Crohn's Disease. Nanomaterials. 2020;10 (11): 2138 (1). E-ISSN:2079-4991.

[1] R+D Pharma Group (GI-1645), Department of Pharmacology, Pharmacy and Pharmaceutical Technology, Faculty of Pharmacy, University of Santiago de Compostela, Santiago de Compostela, Spain.

[2] Drug Delivery Systems Group; Department of Chemical Engineering and Pharmaceutical Technology, School of Sciences, Universidad de La Laguna (ULL), Campus de Anchieta, 38200 La Laguna (Tenerife), Spain.

[3] Research Institute for Medicines (iMed.ULisboa), Faculty of Pharmacy, Universidade de Lisboa, 1649-003, Lisbon, Portugal.

[4] Department of Physical Chemistry, Nanomag laboratory, Universidade de Santiago de Compostela-Campus Vida; 15782 Santiago de Compostela; Spain.

[5] NanoBiofar Group (GI-1643), Department of Pharmacology, Pharmacy and Pharmaceutical Technology, Faculty of Pharmacy, University of Santiago de Compostela, Santiago de Compostela, Spain

USC
UNIVERSIDADE
DE SANTIAGO
DE COMPOSTELA

ABSTRACT

Oral anti-mycobacterial treatment of Crohn's disease (CD) is limited by the low aqueous solubility of drugs, along with the altered gut conditions of patients, making uncommon their clinical use. Hence, the aim of the present work is focused on the *in vitro* evaluation of rifabutin (RFB)-loaded Nanostructured lipid carriers (NLC), in order to solve limitations associated to this therapeutic approach. RFB-loaded NLC were prepared by hot homogenization and characterized in terms of size, polydispersity, surface charge, morphology, thermal stability, and drug payload and release. Permeability across Caco-2 cell monolayers and cytotoxicity and uptake in human macrophages was also determined. NLC obtained were nano-sized, monodisperse, negatively charged and spheroidal-shaped, showing a suitable drug payload and thermal stability. Furthermore, the permeability profile, macrophage uptake and selective intracellular release of RFB-loaded NLC, guarantee an effective drug dose administration to cells. Outcomes suggest that rifabutin-loaded NLC constitute a promising strategy to improve oral anti-mycobacterial therapy in Crohn´s disease.

USC
UNIVERSIDADE
DE SANTIAGO
DE COMPOSTELA

4.1. INTRODUCTION

Crohn's disease (CD) is a chronic inflammatory bowel condition with a higher predominance in industrialized countries, principally in Western Europe and North America (2). The disease is characterized by the presence of outbreaks followed by remission periods (2, 3), and although symptomatology is variable, diarrhea, abdominal pain, nausea, vomiting and weight loss are usually involved (2). The inflammatory process is usually transmural, involving any region of the digestive tract, affecting distal ileum and colon mainly (2, 3).

CD aetiology has been a controversial topic recently (4). Disease development is currently associated with genetic susceptibility and environmental factors, such as alterations in gut microbiome and treatment with antibiotics or non-steroidal anti-inflammatories (2, 3). Nevertheless, it is necessary to highlight the lately increment in scientific literature showing the contribution of the mycobacterial pathogen *Mycobacterium avium paratuberculosis* (MAP) in CD instauration (4, 5). Moreover, inflamed mucosal and submucosal layers in CD are infiltrated by immune cells such as macrophages (6). These cells constitute an interesting target for anti-mycobacterial therapy, since MAP is a facultative intracellular organism that resides in host macrophages, establishing a persistent infection (7).

Despite this information, CD's current treatment is still focused on the pharmacological control of the inflammatory process (using immunosuppressants, corticosteroids, anti-TNF or anti-interleukin drugs and adhesion molecule inhibitors) with the main objective of maintaining the disease remission stage without the need of surgery (2). However, although these treatments improve patients' quality of life, their ability to modify the long-term evolution of the disease has not been demonstrated yet (3).

Regarding the antibiotic use in CD, they are nowadays relegated to the treatment of perianal fistulas or disease suppurative complications (2). Still, some case reports describe long-term CD remissions after antibiotic therapy (5). Moreover, an open label extension phase III study sponsored by RedHill Biopharma is currently active testing orally administered capsules containing a combination of rifabutin, clofazimine and clarithromycin at fixed doses in CD patients (8). This study includes the introduction of a MAP PCR test at the baseline and the evaluation of changes of this blood status during the study (8), which would give insight into *in vivo* effectivity of this antibiotic combination (9) and into the clinical benefit derived from MAP eradication (10).

Although orally administered antimycobacterial drugs constitute a promising strategy in CD treatment, two aspects limit this approach. First, gut physiological parameters are altered in CD patients, which can reduce the possibilities to exploit pH, transit time or microbiome as targeting strategies for drug delivery (6). On the other hand, antimycobacterial drugs show high lipophilicity and low oral bioavailability (11-13).

In this context, particulate systems constitute an interesting approach, as they can accumulate in inflamed bowel sites (6). Additionally, nanoparticulated systems can be designed to load lipophilic drugs, improving its oral bioavailability (14, 15). Moreover, the drug particle reduction to nano size can lead to an enhanced water solubility and dissolution rate (16).

Among nanoparticulate systems, Nanostructured Lipid Carriers (NLC), the second generation of lipid nanoparticles (LN) (17), can be good candidates to formulate useful

antimycobacterial systems. NLC are solid matrices at both room and body temperatures (18). They are composed by a solid lipid and a liquid lipid (17) and present several advantages over the first generation of LN (known as Solid Lipid Nanoparticles or SLN), such as improved stability, higher suppleness in drug release modulation and increased drug loading capacity (18). NLC "in vitro" tolerability seems to be higher in comparison with other colloidal carriers, as polymeric nanoparticles (19), making them an interesting option for oral drug administration.

Therefore, the aim of this work is to investigate the performance of rifabutin (RFB)-loaded NLC (whose formulation procedure and composition were previously optimized by Artificial Intelligence tools), to demonstrate their safety and suitability to achieve an appropriate intestinal permeability and an efficient macrophages uptake. Our goal is to improve the current Crohn´s disease treatments intended to eradicate MAP housed within intestinal macrophages, an area in which, to the best of our knowledge, nanotechnology has never been applied. In this way, an extensive characterization of the nanosystems in terms of particle size, polydispersity, surface charge and drug payload, was performed. Thermal resistance, morphology, and drug release from NLC in different simulated media were also evaluated. Furthermore, an analysis of the in vitro performance of NLC in cell cultures including a permeability evaluation through Caco-2 monolayers, along with the assessment of cytotoxicity and uptake in human macrophages was carried out, in order to evaluate the targeting potential of the developed nanocarriers.

4.2. MATERIALS AND METHODS

4.2.1. Materials

Rifabutin (RFB) (98% purity) was purchased from Acros Organics™ (Fair Lawn, NJ, USA). Polysorbate 80 (Tween® 80), Coumarin 6, dialysis membrane (Spectrum™ Labs Spectra/Por, MWCO 3.5 KDa) and phorbol 12-myristate 13-acetate (PMA) were acquired from Sigma Aldrich (St Louis, MO, USA). Oleic acid was obtained from Merck (Darmstadt, Germany). Precirol® ATO 5 (glyceryl distearate) and Epikuron® 145V (deoiled phosphatidyl choline-enriched lecithin) were kind gifts from Gattefossé (Saint-Priest, France) and Cargill (Wayzata, MN, USA) respectively. THP-1, Caco-2 human colon carcinoma and RAW 264.7 cell lines were obtained from ATCC (Manassas, VA, USA). Alexa Fluor™ 647 phalloidin, ProLong® Gold Antifade reagent with DAPI, Gibco™ antibiotic-antimycotic (amphotericin B, penicillin, streptomycin), trypsin-EDTA, foetal bovine serum (FBS), Roswell Park Memorial Institute 1640 Medium (RPMI 1640), Minimum Essential Media (α-MEM) and phosphate buffered saline (PBS) were obtained from Thermo Fisher Scientific (Waltham, MA, USA). Dulbeco's Modified Eagle Medium (DMEM) was purchased from Corning (Corning, NY, USA). Antibiotic solution (10.000 units/mL penicillin, 10.000 µg/mL streptomycin) was acquired from GE Healthcare Life Sciences (Chicago, IL, USA). Cell proliferation kit (WST-1) was purchased from Roche (Basel, Switzerland). Ultrapure water (MilliQ plus, Millipore Ibérica, Madrid, Spain) was used throughout and the remaining solvents and reagents were analytical or HPLC grade.

4.2.2. NLC formulation

Several batches of NLC loaded with RFB were developed utilizing the composition and operating conditions of a previously optimized NLC system using Artificial Intelligence tools (20). Briefly, the components of the formulation were Precirol® ATO 5 and oleic acid as the lipid components (25:75 ratio), and Tween® 80 and Epikuron® 145V as surfactants. The drug (15 mg) was dissolved in the molten lipid phase at 80ºC (300 mg). The aqueous phase (10 ml), a dispersion of Epikuron® 145 V (0.5% w/w regarding the lipid phase weight) and Tween® 80 (1.9% w/v regarding aqueous phase) in Milli-Q® water, was heated at the same temperature, added to the lipid phase and hot shear homogenized (80ºC) using an Ultra-Turrax T25 (IKA Labortechnik, Staufen, Germany) at 14,800 rpm for 10 min, in a water bath. NLC dispersions were rapidly cooled by transferring them to an ice bath, with gentle stirring, for 2 min. Formulations were carried out in quintuplicate and subsequently dialyzed overnight (Molecular weight cut off, MWCO 3.5 KDa), in order to remove the non-incorporated components and obtain the purified NLC.

4.2.3. NLC characterization

4.2.3.1. Particle size, surface charge and physical stability

Particle size, polydispersity index and surface charge of NLC were determined using a Zetasizer Nano ZS (Malvern Instruments, Malvern, UK). For size and polydispersity index determinations, samples were placed in polystyrene cuvettes and diluted with Milli-Q® water (1:10). Surface charge was determined as zeta potential through particle mobility in an electric field. To carry out this determination, samples were also diluted with Milli-Q® water (1:10) and placed in a specific cuvette where a potential of ±150 mV was established. All the measurements were performed at 25±1ºC by quadruplicate.

4.2.3.2. Transmission electron microscopy (TEM)

Transmission electron microscopy was employed to evaluate morphology of blank (control NLC without drug) and RFB-loaded NLC and to confirm particle sizes previously obtained by DLS. Thus, NLC suspensions were placed on formvar/carbon coated grids (400 mesh) and stained with 2% (w/v) uranyl acetate. Finally, samples were analysed using a JEOL microscope (JEM 1010, Japan). Images were then obtained by using a CCD Orius-Digital Montage Plug-in camera (Gatan, Inc., Pleasanton, CA, USA) and analysed by means of a Gatan Digital Micrograph software (Gatan, Inc., USA). The number of particles considered for size determinations were 44 and 12 for blank and loaded NLC.

4.2.3.3. Atomic force microscopy (AFM)

NLC morphology, particle size and size distribution were also analysed by atomic force microscopy (AFM). This technique is based on the electrostatic interaction between the sample and the AFM tip, which allows for the determination of a sample topography. Measurements were conducted under normal ambient conditions using an XE-100 instrument (Park Systems, South Korea) in non-contact mode with the high-resonance non-contact AFM cantilever (ACTA probe, n=330 kHz). For AFM imaging, 20 µL of the sample were dropped

onto freshly exfoliated mica sheet (SPI Supplies, grade V-1 Muscovite) and after 5 min the mica was washed with Milli-Q® water and dried under nitrogen flow. All experiments were performed at room temperature. XEI® data processing tool (Park Systems, Suwon, South Korea) was used for the analysis of the obtained data, which were adjusted to a gaussian distribution.

4.2.3.4. Encapsulation efficiency and drug loading

Encapsulation efficiency and drug loading determinations were performed as previously described (20). Purified NLC and non-purified NLC (200 µL) were dissolved with acetonitrile (1.5 mL) and centrifuged at 16,099×g and 4ºC for 30 min. Centrifugation produces the precipitation of the lipid phase, while the drug remains in the supernatant. RFB quantification was performed by High Performance Liquid Chromatography (HPLC) as described in section 4.2.4. The amount of drug quantified in the supernatant of non-purified nanoparticles was used as total drug content.

Encapsulation efficiency (EE) and drug loading (DL) of NLC were calculated using the following equations:

$$EE\ (\%) = [W_{loaded\ drug}/W_{total\ drug}]\ x100 \qquad \textbf{Equation 4.1}$$

$$DL\ (\%) = [W_{loaded\ drug}/W_{lipid}]\ x100 \qquad \textbf{Equation 4.2}$$

Where $W_{loaded\ drug}$ is the amount of drug successfully incorporated in the formulation (remaining in the supernatant following acetonitrile addition), $W_{total\ drug}$ is the total amount of drug and W_{lipid} is the weight of the lipid vehicle.

4.2.3.5. Thermal analysis using Dynamic light scattering (DLS)

The influence of temperature on both, blank and RFB-loaded NLC suspensions stability was analysed by DLS in a Zetasizer Nano ZS. Three batches of each type of NLC (blank and loaded with RFB) were diluted as described above, and particle size measurements were made during heating and cooling cycles (25°C-90°C-25°C) at 0.5ºC/min in quartz cells. Particle size determinations were recorded every 0.5°C. Each batch was analysed in duplicate.

4.2.3.6. In vitro release studies

RFB release from loaded NLC was investigated in simulated intestinal fluid (SIF) and macrophage's lysate, in order to compare NLC behaviour in different environments, the intestinal tract and inside macrophages. SIF with pancreatin was prepared according to United States Pharmacopeia (USP).

In order to obtain macrophages cell lysate, Raw 264.7 cells (a murine macrophage cell line) were cultured in DMEM supplemented with 10% FBS and 1% penicillin/streptomycin and incubated at 37ºC and 5% CO_2. Cells were split when reaching 80% confluence by trypsinization and expanded until achieving enough number of cells. Cells were then trypsinized using standard conditions, washed with PBS, centrifuged, and resuspended in Milli-Q® water to achieve a concentration of 3.125 million cells/mL. Cell lysis was performed by

subjecting the cell suspension to three freeze-thaw cycles.

Drug release studies were performed by quadruplicate at 37ºC in horizontal Franz diffusion cells, where a 1:3 dilution of the nanoparticle suspension in release medium was put in the donor chamber. A dialysis membrane (MWCO 3.5 KDa) was placed between the two chambers to avoid the presence of NLC in the receptor chamber. At pre-set times, samples were taken from the receptor chamber and replaced with fresh medium. Drug quantification was performed by HPLC.

4.2.4. High Performance Liquid Chromatography method

RFB was quantified following a validated method previously described (21), using an Agilent 1100 HPLC system (Agilent Technologies, Santa Clara, CA, USA) equipped with a C18 column (Waters symmetry 5 µm, 3.9 × 150 mm). Throughout HPLC analysis, 20 microliters of each sample were injected and eluted with a mobile phase composed by a mixture of sodium acetate 0.05 M / potassium dihydrogen phosphate 0.05 M (pH adjusted to 4.0 with acetic acid) and acetonitrile (Scharlau, Barcelona, Spain) in a 53:47 (v/v) proportion. Drug quantification was performed at 275 nm, with a 1 mL/min flow rate in an isocratic mode.

4.2.5. *In vitro* cell studies

4.2.5.1. Cell viability studies

Cytotoxicity of NLC formulations was analysed using WST-1 (2-(4-iodophenyl)-3-(4-nitrophenyl)-5-(2,4-disulfophenyl)-2*H* tetrazolium, monosodium salt; Roche, Indianapolis, IN, USA), which produces a water-soluble formazan dye upon cellular reduction by the mitochondrial succinate-tetrazolium reductase (22, 23). Human monocytes (THP-1) were cultured in RPMI 1640 supplemented with 10% heat-inactivated FBS, 1% penicillin/streptomycin and 2-mercaptoethanol 0.05 mM at 37°C and 5% CO_2. Five days before the experiment, cells were differentiated to macrophages by stimulation with 200 nM of PMA for 3 days at a cell density of 2×10^5 cells/mL. Then, PMA-containing medium was replaced by fresh medium and cells were incubated for another two days with normal media. The day before the experiment, cells were seeded at a density of 2.5×10^4 cells/well in 96-well plates. Purified NLC samples were diluted to achieve a final concentration of 0.3, 0.12, 0.06 and 0.03 mg/mL of nanoparticles solid mass per volume. To evaluate cell viability, macrophages were incubated with blank and RFB-loaded NLC formulations, as well as with RFB solutions (concentration equivalent to those present in the previous NLC dilutions), for 24 hours (37°C, 5% CO_2). After the incubation period, samples were removed and 10 µL of WST-1 reagent along with 100 µL of culture medium were added to each well. After 2h of incubation with WST-1 reagent, absorbance was read at 450 nm in a microplate reader (Model 680, Bio-Rad, Hercules, CA, USA). Cell viability relative to negative control (Milli-Q® water or DMSO, as appropriate) was calculated according to the following equation:

$$\text{Cell viability (\%)} = \frac{Absorbance_{sample}}{Absorbance_{control}} \times 100 \qquad \textbf{Equation 4.3}$$

4.2.5.2. Confocal microscopy

Qualitative analysis of NLC internalization by THP-1 derived macrophages was performed by confocal microscopy. For this purpose, nanoparticles were fluorescently labelled with coumarin 6 by incorporating the fluorophore into the oil phase during the formulation process. Cells were seeded at a concentration of 5.3×10^4 cells/cm^2 in chambered cell culture slides (Nunc™ Lab-Tek II Chamber Slide™, Thermo Fisher Scientific, Waltham, MA, USA) the day before the experiment. Then, cells were incubated at 37°C and 5% CO_2 for five hours with the samples (blank and RFB-loaded NLC), which were added in a final concentration of 0.12 mg/mL. After this incubation period, culture medium was removed, and cells were washed twice with pre-warmed PBS. Cell fixation was performed using a 3.7% formaldehyde solution in PBS for 10 minutes at room temperature, followed by two washing steps with PBS. Then, a 0.1% Triton X-100 solution was added to permeabilize the cell membrane. Finally, cells were incubated with a 1:40 dilution of Alexa Fluor™ 647 phalloidin in PBS for 20 minutes in order to label the macrophages cytoskeleton, and after two extra washing steps, macrophages nucleus were stained with ProLong® Gold Antifade reagent with DAPI. Images were obtained using a confocal laser microscopy Leica SP5 (Leica Microsystems, Wetzlar, Germany).

4.2.5.3. Macrophage uptake quantification

To quantify NLC uptake by THP-1 derived macrophages, NLC were fluorescently labelled with coumarin 6 as previously described. Dialysis of the samples was also accomplished prior to perform the experiment. Macrophage uptake quantification was carried out according to a method previously described (24) with slight modifications. First, macrophages were seeded in 96-well plates at a cell density of 2.5×10^5 cells/mL and 100 µL per well, nanoparticle suspensions were added to them at a final concentration of 0.12 mg/mL, and fluorescence was determined in a microplate reader (Fluostar Optima, BMG Labtech, Offenburg, Germany) at an excitation and emission wavelength of 485 and 520 nm, respectively (Initial fluorescence). Cells were then incubated during two hours at 37°C and 5% CO_2. Samples were removed, and cells were subjected to three washing steps with 250 µL of a 20 mM glycine solution in PBS pH 7.4, in order to remove non-internalized nanoparticles and to quench their fluorescent signals. Finally, 100 µL of Triton X-100 1% were added to disrupt cellular membrane, and fluorescence was again measured (Fluorescence post-lysis). Macrophage uptake was calculated according to the following equation:

$$\text{Macrophage uptake (\%)} = \frac{Fluorescence_{post-lysis}}{Fluorescence_{initial}} \times 100 \qquad \textbf{Equation 4.4}$$

4.2.5.4. Nanoparticle permeation across Caco-2 cells monolayers

Permeation studies were performed in human colon carcinoma Caco-2 cell line according to a previously described protocol (25), with modifications. Cells were seeded at a concentration of 6.25×10^3 cells/cm^2 in Corning® Transwell® polycarbonate membrane cell culture inserts (Corning, Corning, NY, USA) and cultured in α-MEM supplemented with 20%

FBS, 1% penicillin/streptomycin and 1% antibiotic/antimycotic. Culture medium was replaced every 3-4 days and cells were incubated at 37°C and 5% CO_2 for 28 days, approximately, until the monolayer reached a suitable transepithelial electrical resistance (TEER). At the beginning of the experiment, TEER was higher than 400 Ω cm^2, which indicates the formation of an intact monolayer (25).

RFB-loaded NLC fluorescently labelled with coumarin 6 at a final concentration of 0.12 mg/mL or pure Milli-Q® water (control), were added in the donor compartment. After 2, 4, 6, 24 and 48 hours, samples were taken from the receptor compartment and replaced by fresh medium. Fluorescence was measured in a microplate reader (Fluostar Optima, BMG Labtech, Germany), as previously described, in order to evaluate NLC passage across the cell monolayer. Moreover, in order to correlate the amount of NLC present in the receptor compartment with the fluorescent signal obtained, a calibration curve was prepared in triplicate by measuring the fluorescence of known amounts of coumarin 6-labelled RFB-loaded NLC. Finally, permeability of NLC across Caco-2 cells was expressed either as the concentration of permeated RFB (µg/mL) regarding time elapsed, and as a function of the apparent permeability coefficient (P_{app}), which is employed to investigate the transport rate. P_{app} was determined according to the following equation:

$$P_{app}\ (cm/s) = \frac{dQ}{dt} \times \frac{1}{A \times C0} \qquad \textbf{Equation 4.5}$$

Where C_0 is the initial RFB concentration in the upper compartment (6 µg/mL), A is the growth area (0.33 cm^2) and dQ/dt is the appearance rate of the particles on the lower chamber based on its cumulative transport for 48 hours. This linear appearance rate was calculated as the slope resulting from the representation of the RFB amount present in the receptor compartment versus time.

4.2.6. Statistical analysis

All experiments were performed at least in triplicate. The data were expressed by mean ± SD and treated with IBM SPSS 24 software. The confidence interval was 95% ($p \leq 0.05$). The groups were compared by performing one-way (n=8) or two-way (n=6) analysis of variance (ANOVA), as appropriate, followed by post hoc Tukey's Multiple Comparison Test, and the significant differences between groups were determined.

4.3. RESULTS AND DISCUSSION

4.3.1. NLC characterization

NLC formulation procedure and composition were beforehand optimized by Artificial Intelligence (AI) tools in order to achieve optimal physicochemical properties along with a suitable drug payload (20). Stability of the developed nanocarriers has proven to be adequate after 1 month of storage at 5±1° C, in terms of particle size, polydispersity index and drug payload. Minor changes without impact over colloidal stability were found for zeta potential (20). Besides, an estimation of the characteristics of RFB-loaded NLC, prepared with these optimized parameters, was also provided (20). In this way, to verify the robustness of this

optimizations process, RFB-loaded NLC were prepared, and particle size, PDI, ZP and drug payload were again determined. Furthermore, this work includes further characterization of these nanocarriers in terms of morphology, thermal behaviour, release profile and *in vitro* performance in cell cultures.

4.3.1.1. Particle size, surface charge, physical stability, and drug payload

Blank and RFB-loaded NLC were prepared using hot high shear homogenization. Formulations were carried out in quintuplicate, dialyzed overnight and fully characterized in terms of particle size, size distribution, surface charge and drug load (**Table 4.1**).

Particle size and size distribution are known to affect NLC characteristics such as stability, release rate and biologic performance (18), and because of that, they should be carefully characterized. NLC formulations showed particle sizes within the nano range, with values of 111±3 nm and 151±34 nm, for blank and RFB-loaded nanocarriers, respectively. Differences in size observed between blank and loaded formulations could be associated with the required accommodation space for the drug (26). Regarding particle size distribution, blank NLC showed a polydispersity index (PDI) value of 0.23±0.00 whereas the loaded ones displayed an almost identical value of 0.22 ± 0.02. Therefore, the obtained PDI values were below 0.3 in both cases, that is an acceptable value for lipid nanocarriers and indicative of homogeneous particle size distribution (27). Remarkably, both size and PDI values obtained for RFB-loaded NLC are in close agreement with those previously predicted by Artificial Intelligence tools, which have been reported to be 152 nm and 0.23, for size and PDI, respectively (20).

Moreover, both blank and loaded nanocarriers showed zeta potential values close to -25 mV (-26 ± 2 and -24 ± 2 mV, for blank and RFB-loaded NLC, respectively), which guarantees a good colloidal stability if emulsifiers are included among formulation components (18, 28). These results differ slightly from those predicted by Artificial Intelligence tools, which showed slightly less negative values (-19 mV) (20). However, these differences in ZP could be easily associated with the dialysis step performed in this work after NLC formulation, which can favour the removal of NLC superficial components, such as Tween® 80, a non-ionic emulsifier. Since this type of emulsifiers has been reported to localize close to the nanoparticle interface, counteracting the negative charge of the lipid matrix (29), its partial removal is expected to lead to a more negative zeta potential. Furthermore, these small differences could only have a slight impact on colloidal stability and are not likely to influence the *in vivo* fate of the nanoformulations.

Concerning drug payload, RFB was incorporated to NLC at 5% (w/w) regarding lipid matrix weight showing a suitable drug payload, with an encapsulation efficiency (EE) of 92.83 ± 3.75% and a drug loading (DL) of 4.62 ± 0.33%. These values suggest almost all the added drug was successfully incorporated into the nanoparticle matrix. In the same way as in the case of particle size and PDI, EE and DL values obtained are almost identical to those predicted by Artificial intelligence tools, which have been reported to exhibit values of 100% and 5%, for EE and DL, respectively (20).

Hence, the NLC physicochemical characterization data show that they have a particle size within the nano-range, a monodisperse particle size distribution and a suitable drug payload.

Besides, the highly negative zeta potential exhibited by the formulations is expected to promote a good colloidal stability. Finally, the results of RFB-loaded NLC characterization closely agrees with those predicted by Artificial Intelligence, demonstrating the suitability of these tools to successfully optimize the design of nanoparticle-based drug delivery systems and develop robust and reproducible protocols of NLC preparation.

Table 4.1. Blank and RFB-loaded NLC characterization in terms of particle size, PDI, ZP, EE and DL (n=3±SD).

NLC	Size (nm)	PDI	ZP (mV)	EE (%)	DL (%)
Blank	111 ± 3	0.23 ± 0	-26 ± 2	-	-
RFB-loaded	151 ± 34	0.22 ± 0.02	-24 ± 2	92.83 ± 3.75	4.62 ± 0.33

4.3.1.2. Thermal analysis using Dynamic light scattering (DLS)

To assess NLC thermal stability, blank and RFB-loaded formulations were subjected to a heating stage from 25°C to 90°C, followed by a cooling step to the initial temperature. This approach was previously described to investigate the ability of lipid nanoparticle formulations to maintain their initial properties during high temperature-related procedures (24, 30).

In the case of blank NLC (**Figure 4.1.A**), particle size remains almost unchanged during the whole thermal analysis. A similar behaviour was observed for RFB-loaded NLC (**Figure 4.1.B**) but showing a slight reduction in nanoparticle size. Particle size maintenance along with the negligible size variations exhibited by both formulations throughout the assay indicate a good thermal stability. Therefore, results obtained suggest the developed NLC formulations are suitable for further temperature-requiring processes, as is the case of spray-drying (24), that could simplify the oral administration of NLC obtaining dried powders, which can be easily administered in capsules or tablets (31).

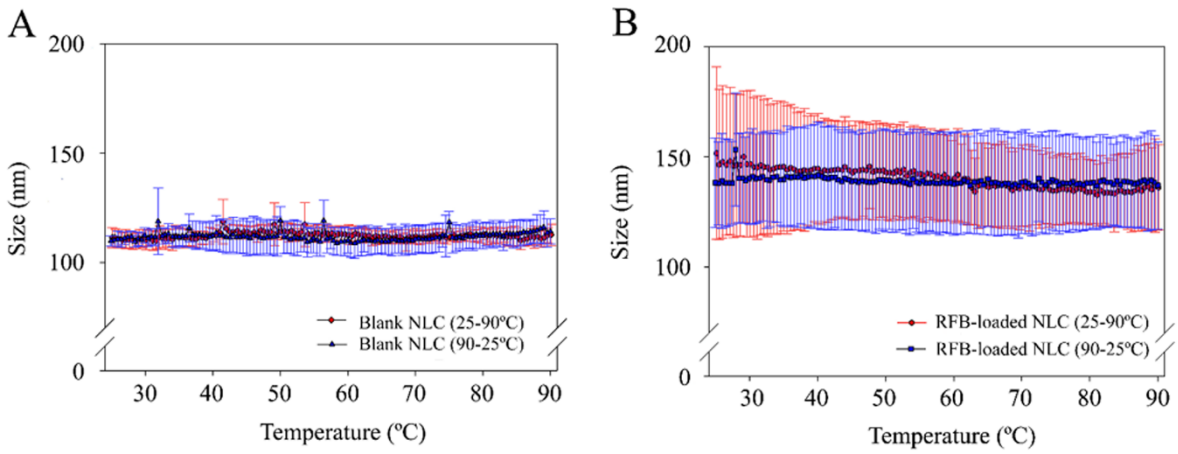

Figure 4.1. Dynamic light scattering thermograms of A) Blank nanostructured lipid carrier (NLC) formulations and B) Rifabutin (RFB)-loaded NLC formulations.

4.3.1.3. Transmission electron microscopy (TEM)

TEM technique was employed to evaluate both blank and RFB-loaded NLC morphology as well as to verify nanocarriers size, as recommended elsewhere (28). As shown in **Figure 4.2**, NLC exhibit a spheroidal morphology. Furthermore, in some images (such as **Figure 4.2.B**), a structure with concentric layers could be noticed, which is also disturbed towards the centre of the nanoparticle, exhibiting a high electron density. This lipid nanoparticle structure has been previously described, and associated with the polymorphic α-form of lipids (32). Moreover, a size of 119 ± 41 nm in the case of blank NLC and slightly higher (173 ± 85 nm) in the case of RFB-loaded ones was observed, confirming the results obtained by DLS.

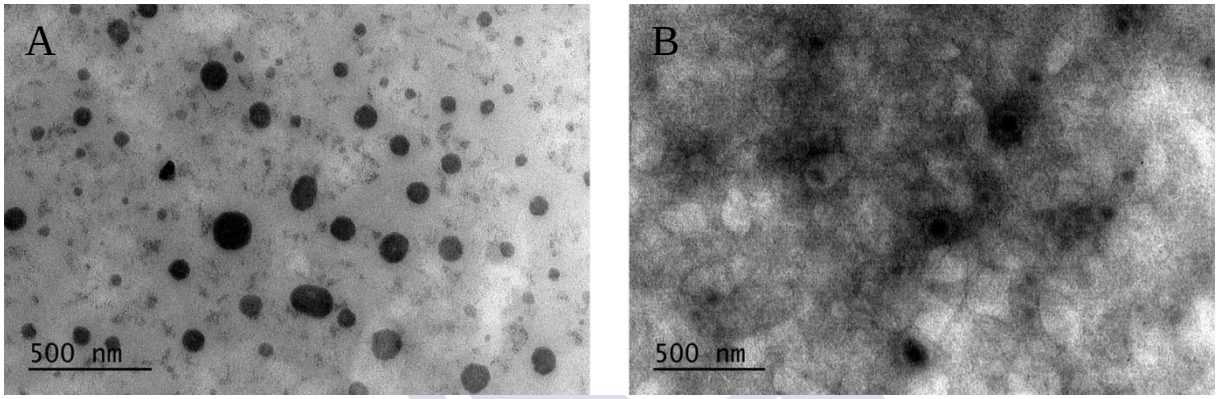

Figure 4.2. Transmission electron micrographs of A) Blank and B) RFB-loaded NLC.

4.3.1.4. Atomic force microscopy (AFM)

Blank and RFB-loaded NLC morphology, particle size and distribution were also assessed by Atomic force microscopy, a technique which gives insight of the sample z-dimension from the deflection of a fine leaf spring (known as the AFM cantilever) (33). Therefore, AFM is a useful tool to complete the information obtained by DLS and by the two-dimensional images provided by TEM.

In this way, the AFM images of blank and RFB-loaded nanoparticles depicted in **Figure 4.3**, confirm the spheroidal shape previously showed by TEM. Moreover, results derived from AFM analysis were expressed as the frequency (%) of nanoparticles exhibiting a specific height. Thus, blank, and RFB-loaded nanoparticles exhibited a similar size, as values of 43±3 nm and 33±1 nm, respectively, were obtained (**Figure 4.4**). The smaller nanoparticle height reported by AFM in comparison with the diameters obtained by DLS and TEM corroborates the existence of a spheroidal structure, closer to a disk than to a sphere. This structure further confirm the prevalence of the polymorphic α-form of lipids (28, 32), as previously mentioned, which has been associated with a high loading capacity and a low tendency to expulse the encapsulated drug from the lipid matrix (28).

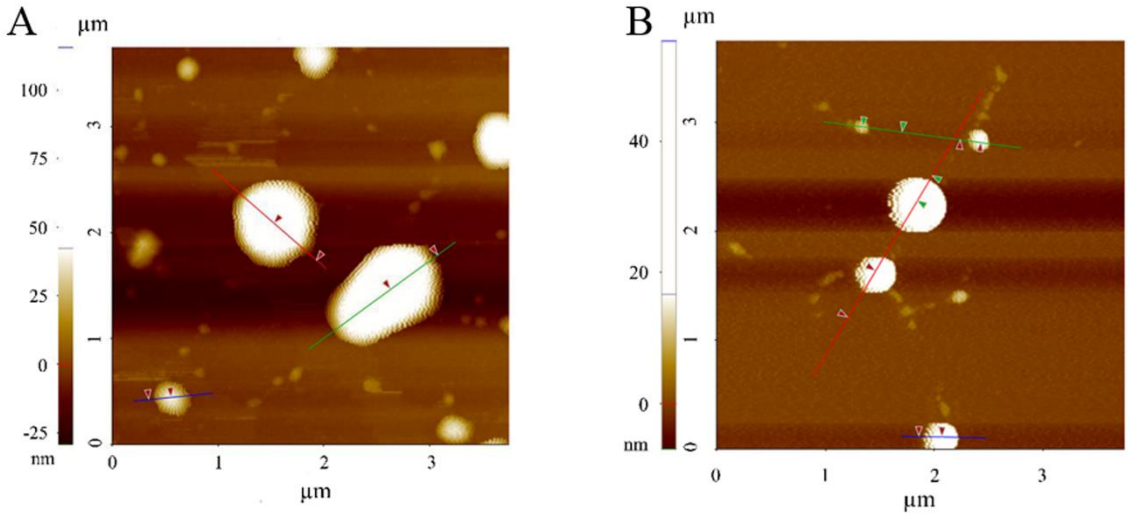

Figure 4.3. Atomic force microscopy images of A) Blank and B) RFB-loaded NLC.

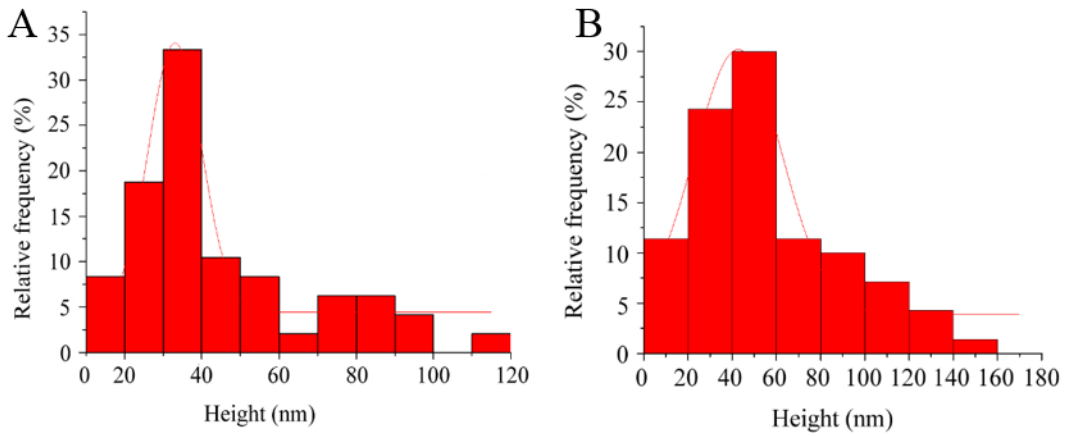

Figure 4.4. Particle size and size distribution according to AFM analysis of A) Blank and B) RFB-loaded NLC. Results were adjusted to a gaussian distribution.

4.3.1.5. *In vitro* release studies

Release studies were performed to investigate the ability of NLC to act as RFB reservoirs. This compound is an antimicrobial agent active against widely known *Mycobacterium* species, including *M. leprae*, *M. tuberculosis*, or MAP (9), an infectious agent increasingly related with CD development (4). Furthermore, RFB has been included in the triple oral anti-mycobacterial regimen currently under evaluation intended to eradicate MAP infection from CD patients (9). In this way, release from nanoparticles was performed in both simulated intestinal fluid (SIF) and macrophage's lysate, with the aim of analysing the expected drug release profile in the gut and intracellular environment, respectively. In the drug release study in SIF, the experimental results indicated the drug release from NLC in intestinal environment is negligible, since the amount of RFB released during the whole assay was not

detected by HPLC. Regarding RFB release assay in murine macrophage's lysate, the released drug started to be detectable at 1 hour, and increased progressively until 16 hours, when the amount of RFB in release medium was found to be quantifiable by HPLC. After 16 hours, 1.46 ± 0.47 µg of drug were detected in the receptor chamber of Franz diffusion cells, resulting in a release percentage of 0.1 ± 0.03% at the end of the experiment.

In physiological conditions, drug release from lipid nanocarriers has been reported to occur, simultaneously, through erosion and diffusion mechanisms (34). Poor RFB release from NLC obtained in the assays is likely to be related with the high lipophilicity of the drug (log P = 4.218) (35), as well as with the favourable conditions within the nanoparticle due to the high RFB solubility in the lipid matrix, which significantly reduces drug diffusion towards the aqueous release medium (36). Several authors employed different strategies to overcome these issues associated with the poor *in vitro* release profile of lipophilic drugs, such as the addition of ethanol (37) or surfactants (38) in the release medium. However, in most cases, these approaches are not representative of the *in vivo* environment.

Regarding drug release through lipid matrix degradation, it is necessary to consider it occurs primarily by enzymes, and also through hydrolytic processes, although in a lesser extent (34). Because of that, analysis of NLC matrix degradation by enzymes present in both intestine and macrophage intracellular environment constitutes an interesting approach. According to the results obtained, NLC matrix can efficiently endure pancreatin activity of SIF, however, it is more affected by enzymes present in macrophage intracellular environment. Despite the higher effectivity of these macrophage enzymes, the amount of drug released from nanoparticles is still low. This slight drug release can be associated with the low enzymatic concentration in macrophage lysate achieved after dilution of cell suspension with Milli-Q® water. Therefore, as this concentration would obviously be higher inside macrophages in physiological conditions, a greater drug release would also be expected in this case.

Hence, outcomes obtained constitute an interesting proof of concept of the controlled and selective drug release provided by NLC inside macrophages, where MAP has been reported to establish a persisting infection (7).

4.3.2. In vitro cellular studies

4.3.2.1. Cell viability studies

SLN and NLC are composed of biodegradable lipids with generally recognised as safe (GRAS) status (39). However, despite these promising features, further studies are required to support their therapeutic use (19). For this purpose, cell viability of THP-1 derived macrophages was analysed after NLC treatment.

Figure 4.5A shows cell viability after treatment with blank and RFB-loaded formulations at several concentrations (0.3, 0.12, 0.06 and 0.03 mg/mL). Besides, cells treated with equivalent RFB concentrations were used as control (**Figure 4.5B**). In general, formulations exhibited a good biocompatibility, leading to cell viabilities ≥70% for concentrations lower than 0.3 mg/mL. Two-way ANOVA ($p < 0.05$) points out a statistically significant effect of treatment (blank NLC or RFB-loaded NLC), NLC concentration, and their interaction on cell viability.

Post hoc Tukey's Multiple Comparison Test ($p < 0.05$) points out a NLC concentration-dependent cytotoxic effect. However, it shows no statistical differences in cell viability for the experiments carried out with RFB-loaded NLC at 0.12 mg/mL and 0.06 mg/mL, therefore the concentration 0.12mg/mL was selected for further assays.

On the other hand, no significant modifications in cell viability were observed for RFB solutions (**Figure 4.5B**) containing equivalent amounts of drug, which implies that the reduction in viability must be mainly attributed to the toxicity of NLC components (oleic acid or emulsifiers), as suggested by several authors (40, 41), and not to cytotoxic effects derived from RFB inclusion in the nanocarriers.

To allow the comparison of the cytotoxicity results obtained for RFB-loaded NLC with available data in literature, determination of IC_{50} was accomplished (**Figure 4.6**). The estimation of this value was performed from dose-response curves, where IC_{50} was defined as the concentration required to induce a 50% reduction in cell viability, resulting in a value of approximately 0.18 mg/mL. This finding is in line with previously published studies on lipid nanoparticle cytotoxicity, where IC_{50} was reported to be found mainly in the range of 0.1-1 mg/mL nanoparticles (19).

From the results obtained, NLC formulations present a suitable safety profile, similar to previously published works with lipid nanoparticles. Moreover, the highest NLC concentration, of all the tested ones, showing an adequate biocompatibility in THP-1 derived macrophages has been found to be 0.12 mg/mL. Considering that a cell viability ≥ 70% has been reported to be the threshold, according to ISO 10993-5 (42), below which a cytotoxic effect is considered to take place.

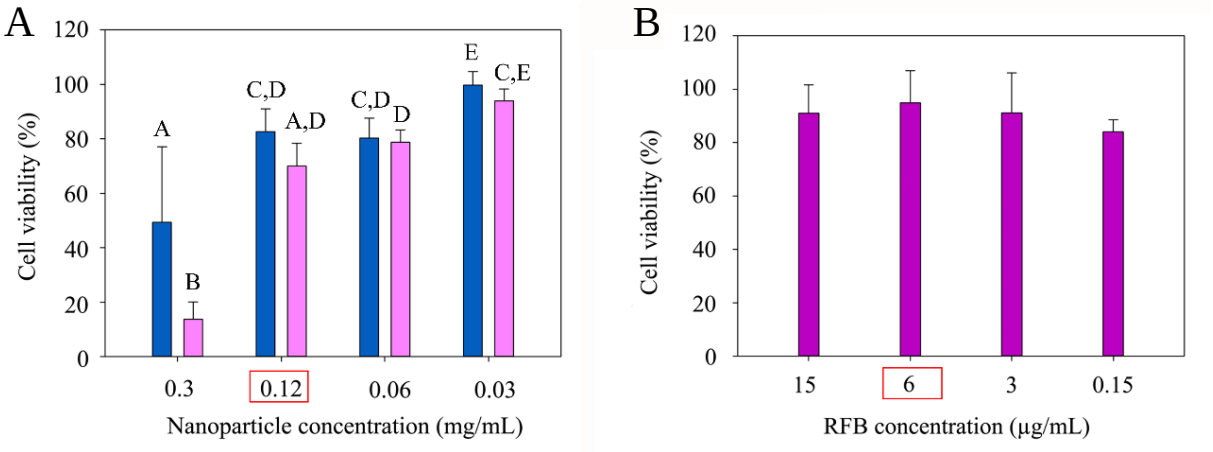

Figure 4.5. Cell viability (%) relative to control with Milli-Q® water of A) blank NLC formulations (dark blue colour) and RFB-loaded formulations (pink colour), using several nanoparticle concentrations (0.3, 0.12, 0.06 and 0.03mg/mL). B) Cell viability (%) relative to control with DMSO, of RFB solutions in DMSO prepared employing the same drug concentration as present in NLC formulations (purple colour). (A-E characters denote the homogeneous subsets pointed out by the post hoc Tukey's Multiple Comparison Test ($p < 0.05$).

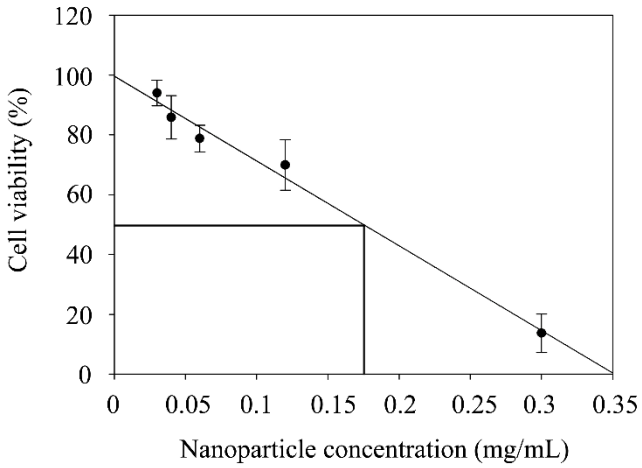

Figure 4.6. Dose response curve (R^2 = 0.9881) obtained from cell viability data at several RFB-loaded NLC concentrations. IC_{50} was calculated as the concentration of nanoparticles producing a 50% reduction in cell viability.

4.3.2.2. Confocal microscopy

Qualitative study of both blank and RFB-loaded NLC internalization by THP-1 derived macrophages was analysed employing a nanoparticle concentration of 0.12 mg/mL, in accordance with the results obtained in the cell viability experiment. Moreover, the selection of this value was based not only on the results obtained in the biocompatibility assay, but also on the drug concentration required to efficiently eradicate the mycobacterial infection.

Regarding this last point, a minimum inhibitory concentration (MIC) ranging from 0.5 to 4 µg/mL has been obtained *in vitro* for RFB in both human and animal isolated MAP strains. Interestingly, five of six MAP human isolates show a MIC of only 1 µg/ mL for this drug (43). Furthermore, RFB has been reported to slow the multiplication of three virulent strains of Mycobacterium avium complex (44), a group of which MAP is an important member (45), in a model of intracellular infection in human macrophages when a dose of 0.5 µg/mL is employed (44). Considering that RFB payload in NLC has been proven to reach almost a 5% of the solid content of the formulations, a dose of approximately 6 µg/mL of drug has been administered to macrophages. This drug concentration is clearly superior to the value required for RFB MIC, guaranteeing the administration of an effective dose to cells.

As observed in **Figure 4.7**, both blank (**Figure 4.7.A**) and RFB-loaded NLC (**Figure 4.7.B**) have been efficiently taken up by macrophages, which constitutes a promising start point for the treatment of infections produced by intracellular pathogens such as MAP. Images of separate channels of blank and loaded formulations are shown in **Figures A2.1** and **A2.2** (**Annex II**), respectively. Furthermore, images of NLC uptake by a macrophages group can be found in **Figure A2.3** (**Annex II**).

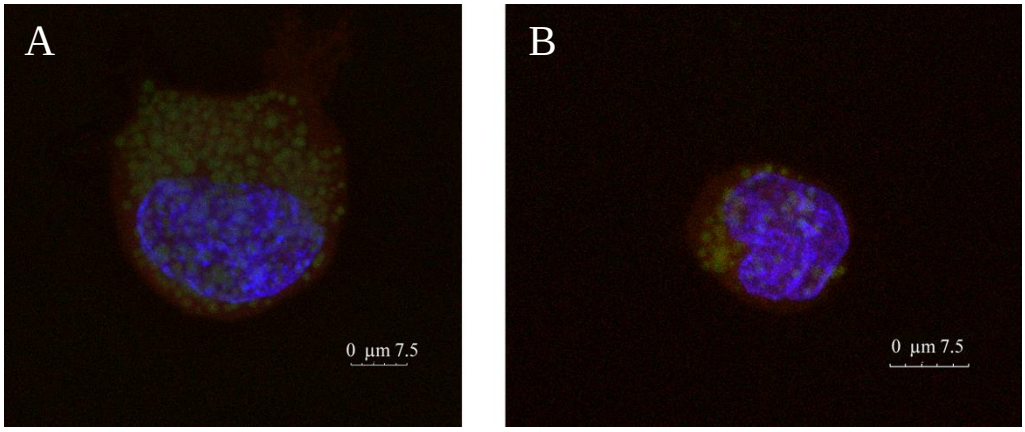

Figure 4.7. Confocal microscopy images of A) Blank and B) RFB-loaded NLC macrophages uptake. Red, blue and green colours represent cell cytoplasm (Alexa Fluor™ 647 phalloidin), cell nuclei (DAPI) and NLC formulations (Coumarin 6), respectively.

4.3.2.3. Macrophage uptake quantification

Nanoparticle internalization by macrophages was also investigated using a quantitative approach and NLC formulations at 0.12 mg/mL. In this method, blank formulations showed an internalization percentage of 8.33 ± 1.15% after two hours of exposure. Moreover, a higher internalization percentage, 13.39 ± 1.44 %, was obtained for RFB-loaded NLC. Statistical analysis (one-way ANOVA, $p < 0.05$) revealed significant differences between the uptake of blank and loaded formulations. This higher macrophages uptake reported for loaded formulations might be related to their size (151 ± 34 nm), larger than the blank ones (111 ± 3 nm), since the uptake of particulate systems by macrophages rises progressively with the particle size increase (46).

In addition, the uptake percentage obtained for RFB-loaded NLC reveals that the 13% of the administered dose (6 µg/mL or 0.6 µg each well) was efficiently taken up by macrophages, which constitutes a total RFB amount of 0.078 µg per well. Since each well contains 25.000 cells and human macrophages have a cell volume of approximately 4990 μm^3 (47), a total cell volume of 1.2475×10^{-4} mL is expected. Taking together the volumes of internalized drug and the total cell volume estimated, it is reasonable to think that an internalized concentration of 625 µg/mL could be achieved, which exceeds the range of the intracellular MIC previously reported. It is also important to note that colocalization phenomena amongst nanoparticles and mycobacteria have been suggested to occur by means of phagolysosomes fusion (48). In this way, RFB would not be free in the cytoplasm and hence, it would probably not be the substrate of efflux pumps which could modify the intracellular drug concentration indicated in this work.

4.3.2.4. Nanoparticle permeation across Caco-2 cells monolayers

Nanoparticle permeation across the intestinal barrier is required to reach intestinal macrophages. Despite some of them are able to extend dendrites into the intestinal lumen, the majority of the macrophages are located below the epithelial monolayer, in the lamina propria (49). The analysis of nanoparticles permeability across human colon carcinoma cell monolayers (Caco-2) has been reported to stablish a good correlation with human *in vivo* absorption and

has been broadly employed to predict drug permeability (25). The drug concentration in the receptor compartment was estimated from the NLC concentration in this compartment at different times. Results are shown in **Figure 4.8**. No NLC permeation across the Caco-2 monolayer occurred during the first two hours. After, RFB concentration in the receptor compartment increased linearly over time, achieving RFB concentrations of 3.29×10^{-4}, 0.06 ± 0.05, 0.43 ± 0.01 and 0.9 ± 0.1 µg/mL at 4, 6, 24 and 48 hours, respectively. In addition, a P_{app} value of 2.02×10^{-6} cm/s was obtained for RFB-NLC formulations. A P_{app} value of 2×10^{-6} cm/s has been reported as the threshold to achieve complete drug absorption in humans (50), therefore, the obtained value for RFB-NLC suggests that they exhibit good permeability across Caco-2 monolayers.

Besides, the achieved permeability allowed to obtain a drug concentration virtually in range with the previously mentioned MIC reported for RFB just after 24 hours of incubation with the nanocarriers, which is the accurate colonic transit time described for patients with CD (6). Moreover, the *in vivo* permeability exhibited by NLC across the intestinal membrane of CD patients is expected to be even higher than reflected by this assay. The disruption of the epithelial barrier shown by inflammatory bowel disease patients increases gut permeability and favours nanoparticle passage (6). In this way, nanoparticles are expected to accumulate preferentially in the intestinal inflamed sites, which are densely infiltrated with macrophages (6), ensuring the administration of an effective drug dose to the infected cells.

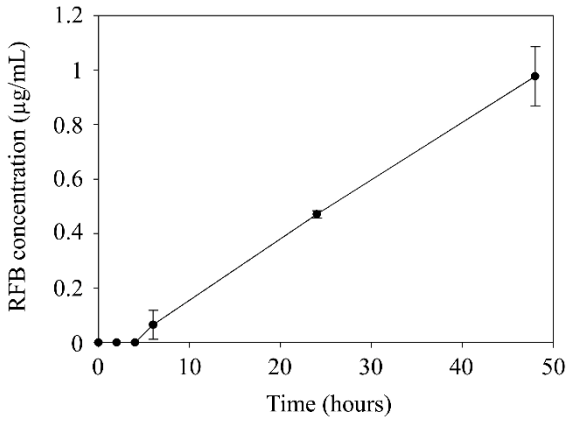

Figure 4.8. Permeation profile of rifabutin (RFB) loaded in NLC across Caco-2 cell monolayers expressed as a function of drug concentration in the lower compartment in a 48-hour time interval.

4.4. CONCLUSIONS

NLC showing a particle size within the nano-range (111±3-151±3 nm), a monodisperse size distribution (0.22±0.02-0.23±0.00), a negative zeta potential (-24±2- -26±2 mV) and a suitable rifabutin payload (4.62±0.33%) were successfully prepared using a formulation process previously optimized by Artificial Intelligence tools. Formulations exhibited a spheroidal appearance, a good ability to withstand high temperature-related processes and a good safety profile in cellular studies. Moreover, the efficient macrophage uptake of the developed NLC has been demonstrated allowing the obtention of a therapeutic rifabutin concentration after only two hours of incubation. This fact, along with the permeation exhibited by NLC across Caco-2

cell monolayers and their tendency to release the drug in the intracellular environment, guarantee the achievement of an effective rifabutin dose inside the phagocytic cells, where *mycobacterium avium paratuberculosis* is known to reside. Therefore, rifabutin-loaded NLC constitute a promising tool to improve anti-mycobacterial therapy in Crohn's disease.

REFERENCES

1. Rouco H, Diaz-Rodriguez P, Gaspar DP, Gonçalves L, Cuerva M, Remuñán-López C, et al. Rifabutin-Loaded Nanostructured Lipid Carriers as a Tool in Oral Anti-Mycobacterial Treatment of Crohn's Disease. Nanomaterials. 2020;10 (11): 2138.
2. Feuerstein JD, Cheifetz AS. Crohn Disease: Epidemiology, Diagnosis, and Management. Mayo Clin Proc. 2017; 92 (7): 1088-1103.
3. Cosnes J, Gower-Rousseau C, Seksik P, Cortot A. Epidemiology and natural history of inflammatory bowel diseases. Gastroenterology. 2011; 140 (6): 1785-1794.
4. Davis WC. On deaf ears, Mycobacterium avium paratuberculosis in pathogenesis Crohn's and other diseases. World J Gastroenterol. 2015; 21 (48): 13411-13417.
5. Kuenstner JT, Naser S, Chamberlin W, Borody T, Graham DY, McNees A, et al. The Consensus from the Mycobacterium avium ssp. paratuberculosis (MAP) Conference 2017. Front Public Health. 2017; 5: 208.
6. Mohan LJ, Daly JS, Ryan BM, Ramtoola Z. The future of nanomedicine in optimising the treatment of inflammatory bowel disease. Scand J Gastroenterol. 2019; 54 (1): 18-26.
7. Murphy JT, Sommer S, Kabara EA, Verman N, Kuelbs MA, Saama P, et al. Gene expression profiling of monocyte-derived macrophages following infection with Mycobacterium avium subspecies avium and Mycobacterium avium subspecies paratuberculosis. Physiol Genomics. 2006; 28 (1): 67-75.
8. NIH. Open Label Efficacy and Safety of Anti-MAP (Mycobacterium Avium Ssp. Paratuberculosis) Therapy in Adult Crohn's Disease (MAPUS2). [ClinicalTrials.gov]. 2020. Available from: https://clinicaltrials.gov/ct2/show/record/NCT03009396?view=record. [Accessed on 14 July 2020].
9. Savarino E, Bertani L, Ceccarelli L, Bodini G, Zingone F, Buda A, et al. Antimicrobial treatment with the fixed-dose antibiotic combination RHB-104 for Mycobacterium avium subspecies paratuberculosis in Crohn's disease: pharmacological and clinical implications. Expert Opin Biol Ther. 2019; 19 (2): 79-88.
10. Honap S, Johnston E, Agrawal G, Al-Hakim B, Hermon-Taylor J, Sanderson J. Anti-Mycobacterium paratuberculosis (MAP) therapy for Crohn's disease: an overview and update. Frontline Gastroenterol. 2020; 0: 1–7.
11. Blaschke TF, Skinner MH. The clinical pharmacokinetics of rifabutin. Clin Infect Dis. 1996; 22 (Suppl 1): 15-22.
12. Zhang Y, Feng J, McManus SA, Lu HD, Ristroph KD, Cho EJ, et al. Design and Solidification of Fast-Releasing Clofazimine Nanoparticles for Treatment of Cryptosporidiosis. Mol Pharm. 2017; 14 (10): 3480-3488.
13. Inoue Y, Yoshimura S, Tozuka Y, Moribe K, Kumamoto T, Ishikawa T, et al. Application of ascorbic acid 2-glucoside as a solubilizing agent for clarithromycin: solubilization and nanoparticle formation. Int J Pharm. 2007; 331 (1): 38-45.
14. Ceci C, Graziani G, Faraoni I, Cacciotti I. Strategies To Improve Ellagic Acid Bioavailability: From Natural Or Semisynthetic Derivatives To Nanotechnological Approaches Based On Innovative Carriers. Nanotechnology. 2020; 3 1(38): 382001.

15. Cacciotti I, Chronopoulou L, Palocci C, Amalfitano A, Cantiani M, Cordaro M, et al. Controlled release of 18-β-glycyrrhetic acid by nanodelivery systems increases cytotoxicity on oral carcinoma cell line. Nanotechnology. 2018; 29 (28): 285101.
16. Wais U, Jackson AW, He T, Zhang H. Nanoformulation and encapsulation approaches for poorly water-soluble drug nanoparticles. Nanoscale. 2016; 8 (4): 1746-1769.
17. Müller RH, Petersen RD, Hommoss A, Pardeike J. Nanostructured lipid carriers (NLC) in cosmetic dermal products. Adv Drug Deliv Rev. 2007; 59 (6): 522-530.
18. Khosa A, Reddi S, Saha RN. Nanostructured lipid carriers for site-specific drug delivery. Biomed Pharmacother. 2018; 103: 598-613.
19. Doktorovova S, Souto EB, Silva AM. Nanotoxicology applied to solid lipid nanoparticles and nanostructured lipid carriers - a systematic review of in vitro data. Eur J Pharm Biopharm. 2014; 87 (1):1-18.
20. Rouco H, Diaz-Rodriguez P, Rama-Molinos S, Remunan-Lopez C, Landin M. Delimiting the knowledge space and the design space of nanostructured lipid carriers through Artificial Intelligence tools. Int J Pharm. 2018; 553 (1-2): 522-530.
21. Gaspar MM, Cruz A, Penha AF, Reymao J, Sousa AC, Eleuterio CV, et al. Rifabutin encapsulated in liposomes exhibits increased therapeutic activity in a model of disseminated tuberculosis. Int J Antimicrob Agents. 2008; 31 (1): 37-45.
22. Tominaga H, Ishiyama M, Ohseto F, Sasamoto K, Hamamoto T, Suzuki K, et al. A water-soluble tetrazolium salt useful for colorimetric cell viability assay. Anal Comm. 1999; 36 (2): 47-50.
23. Ngamwongsatit P, Banada PP, Panbangred W, Bhunia AK. WST-1-based cell cytotoxicity assay as a substitute for MTT-based assay for rapid detection of toxigenic Bacillus species using CHO cell line. J Microbiol Methods. 2008; 73 (3):211-215.
24. Gaspar DP, Faria V, Goncalves LM, Taboada P, Remunan-Lopez C, Almeida AJ. Rifabutin-loaded solid lipid nanoparticles for inhaled antitubercular therapy: Physicochemical and in vitro studies. Int J Pharm. 2016; 497 (1-2): 199-209.
25. Chaves LL, Costa Lima SA, Vieira ACC, Barreiros L, Segundo MA, Ferreira D, et al. Nanosystems as modulators of intestinal dapsone and clofazimine delivery. Biomed Pharmacother. 2018; 103: 1392-1396.
26. Gaba B, Fazil M, Khan S, Ali A, Baboota S, Ali J. Nanostructured lipid carrier system for topical delivery of terbinafine hydrochloride. Bull. Fac. Pharm. Cairo Univ. 2015; 53 (2): 147-159.
27. Danaei M, Dehghankhold M, Ataei S, Hasanzadeh Davarani F, Javanmard R, Dokhani A, et al. Impact of Particle Size and Polydispersity Index on the Clinical Applications of Lipidic Nanocarrier Systems. Pharmaceutics. 2018; 10 (2): 57.
28. Gordillo-Galeano A, Mora-Huertas CE. Solid lipid nanoparticles and nanostructured lipid carriers: A review emphasizing on particle structure and drug release. Eur J Pharm Biopharm. 2018; 133: 285-308.
29. Schubert MA, Müller-Goymann CC. Characterisation of surface-modified solid lipid nanoparticles (SLN): influence of lecithin and nonionic emulsifier. Eur J Pharm Biopharm. 2005; 61 (1-2): 77-86.

30. Mancini G, Lopes RM, Clemente P, Raposo S, Gonçalves LMD, Bica A, et al. Lecithin and parabens play a crucial role in tripalmitin-based lipid nanoparticle stabilization throughout moist heat sterilization and freeze-drying. Eur J Lipid Sci Technol. 2015; 117 (12): 1947-1959.
31. Battaglia L, Gallarate M. Lipid nanoparticles: state of the art, new preparation methods and challenges in drug delivery. Expert Opin Drug Deliv. 2012; 9 (5): 497-508.
32. Bunjes H, Steiniger F, Richter W. Visualizing the structure of triglyceride nanoparticles in different crystal modifications. Langmuir. 2007; 23 (7): 4005-4011.
33. Sitterberg J, Ozcetin A, Ehrhardt C, Bakowsky U. Utilising atomic force microscopy for the characterisation of nanoscale drug delivery systems. Eur J Pharm Biopharm. 2010; 74 (1): 2-13.
34. Pathak K, Keshri L, Shah M. Lipid nanocarriers: influence of lipids on product development and pharmacokinetics. Crit Rev Ther Drug Carrier Syst. 2011; 28 (4): 357-393.
35. Global Alliance for TB drug development. Rifabutin. Tuberculosis (Edinburgh, Scotland). 2008; 88 (2): 145-147.
36. Iqbal N, Vitorino C, Taylor KM. How can lipid nanocarriers improve transdermal delivery of olanzapine?. Pharm Dev Technol. 2017; 22 (4): 587-596.
37. Li H, Zhao X, Ma Y, Zhai G, Li L, Lou H. Enhancement of gastrointestinal absorption of quercetin by solid lipid nanoparticles. J Control Release. 2009; 133 (3): 238-244.
38. Das S, Ng WK, Kanaujia P, Kim S, Tan RB. Formulation design, preparation and physicochemical characterizations of solid lipid nanoparticles containing a hydrophobic drug: effects of process variables. Colloids Surf B Biointerfaces. 2011; 88 (1): 483-489.
39. Lasa-Saracibar B, Estella-Hermoso de Mendoza A, Guada M, Dios-Vieitez C, Blanco-Prieto MJ. Lipid nanoparticles for cancer therapy: state of the art and future prospects. Expert Opin Drug Deliv. 2012; 9 (10): 1245-1261.
40. Schöler N, Olbrich C, Tabatt K, Müller R, Hahn H, Liesenfeld O. Surfactant, but not the size of solid lipid nanoparticles (SLN) influences viability and cytokine production of macrophages. Int J Pharm. 2001; 221 (1-2): 57-67.
41. Yin H, Too HP, Chow GM. The effects of particle size and surface coating on the cytotoxicity of nickel ferrite. Biomaterials. 2005; 26 (29): 5818-5826.
42. ISO. Biological Evaluation of Medical Devices Part 5: Tests for Cytotoxicity: In vitro Methods. In: ISO10993-5. 3rd edition. Brussels, Belgium: 2009.
43. Zanetti S, Molicotti P, Cannas S, Ortu S, Ahmed N, Sechi LA. "In vitro" activities of antimycobacterial agents against Mycobacterium avium subsp. paratuberculosis linked to Crohn's disease and paratuberculosis. Ann Clin Microbiol Antimicrob. 2006; 5: 27.
44. Perronne C, Gikas A, Truffot-Pernot C, Grosset J, Pocidalo J, Vilde J. Activities of clarithromycin, sulfisoxazole, and rifabutin against Mycobacterium avium complex multiplication within human macrophages. Antimicrob Agents Chemother. 1990; 34 (8): 1508-1511.
45. Bull TJ, Sidi-Boumedine K, McMinn EJ, Stevenson K, Pickup R, Hermon-Taylor J. Mycobacterial interspersed repetitive units (MIRU) differentiate Mycobacterium avium subspecies paratuberculosis from other species of the Mycobacterium avium complex. Mol Cell Probes. 2003; 17 (4): 157-164.

46. Chono S, Tanino T, Seki T, Morimoto K. Influence of particle size on drug delivery to rat alveolar macrophages following pulmonary administration of ciprofloxacin incorporated into liposomes. J Drug Target. 2006; 14 (8): 557-566.
47. Krombach F, Münzing S, Allmeling A-M, Gerlach JT, Behr J, Dörger M. Cell size of alveolar macrophages: an interspecies comparison. Environ Health Perspect. 1997; 105 (Suppl 5):1261-1263.
48. Lemmer Y, Kalombo L, Pietersen RD, Jones AT, Semete-Makokotlela B, Van Wyngaardt S, et al. Mycolic acids, a promising mycobacterial ligand for targeting of nanoencapsulated drugs in tuberculosis. J Control Release. 2015; 211: 94-104.
49. Bain CC, Mowat AM. Intestinal macrophages–specialised adaptation to a unique environment. Eur J Immunol. 2011; 41 (9): 2494-2498.
50. Grès M-C, Julian B, Bourrié M, Meunier V, Roques C, Berger M, et al. Correlation between oral drug absorption in humans, and apparent drug permeability in TC-7 cells, a human epithelial intestinal cell line: comparison with the parental Caco-2 cell line. Pharm Res. 1998; 15 (5): 726-733.

USC
UNIVERSIDADE
DE SANTIAGO
DE COMPOSTELA

5. CHAPTER III: CRYOPROTECTANT EFFECTIVITY OF SUGARS IN NANOSTRUCTURED LIPID CARRIERS LYOPHILIZATION

USC
UNIVERSIDADE
DE SANTIAGO
DE COMPOSTELA

ABSTRACT

Lyophilization is often employed to convert nanoparticle suspensions to solid dosage forms. This work proposes the use of Neurofuzzy Logic (NFL) to allow a better understanding of the lyophilization process and cryoprotectants (CPs) performance on Nanostructured Lipid Carriers (NLC) dispersions. NLC were produced by hot high shear homogenization, frozen at different freezing speeds and lyophilized using several sugars at variable concentrations. NLC were characterized before and after lyophilization and results were expressed as increase in particle size (Δ size), polydispersity index (Δ PDI) and zeta potential (Δ ZP) of lyophilized powders (LP) regarding initial dispersions. CPs were characterized in terms of molecular weight (MW). Osmolarity (Π) of the CPs solutions at the different concentrations under study was also determined. Databases obtained were then modelled through FormRules®, an NFL software. The use of NFL revealed that CPs MW usually determines the most suitable freezing conditions and CPs proportions required. This generated knowledge would allow a rational selection of the lyophilization process variables to obtain NLC LP with suitable properties.

USC
UNIVERSIDADE
DE SANTIAGO
DE COMPOSTELA

5.1. INTRODUCTION

Nanostructured Lipid Carriers (NLC) are drug delivery systems experiencing increased attention in the pharmaceutical field (1). They exhibit a core matrix composed of solid and liquid lipids, showing several advantages over conventional carriers, such as improved solubility capacity and drug half-life, greater permeability and better stability during storage (1). Furthermore, in recent years, scientific literature has evidenced the utility of these nanocarriers to achieve controlled release in various administration routes such as intravenous (2), pulmonary (3), oral (4) or topic (5).

Despite these promising features, lipid nano-dispersions are susceptible to hydrolysis, gelation, flocculation, creaming and sedimentation or coalescence triggering system destabilization (6). Stability issues, together with the need to produce easy to transport and store dosage forms (7), makes necessary their drying to obtain a powder that, once reconstituted, generates the original NLC. With this regard, lyophilization using cryoprotectants (CPs) is considered an appropriate approach to enhance long-term nanoparticles stability avoiding freezing stress (8). The most commonly used CPs are sugars such as trehalose, mannitol, sucrose and glucose, which are known to vitrify at a certain temperature, generating a glassy matrix capable of protecting nanoparticles from the ice mechanical stress (9).

The lyophilization performance involves a significant number of variables related to the characteristics of the formulation, the addition or not of cryoprotectants and the operating conditions. In general, the lyophilization operating conditions are established by trial and error procedures, without considering the interactions between these variables, and not analysing in depth the mechanisms involved (8).

In the last decade, Artificial Intelligence (AI) tools, such as Artificial Neural Networks (ANN) or Neurofuzzy Logic (NFL) systems, have gained increasing attention for pharmaceutical applications (10), being used to study and optimize various processes such as wet granulation (11), the formulation of micro- and nanoparticles (12, 13) or the preparation of hydrogels (14, 15).

ANN are biologically inspired artificial intelligence tools, designed to mimic the information processing of the human brain, allowing to stablish relationships between the process variables (inputs) and experimental results (outputs) (14). NFL systems are hybrid technologies remarkably suitable for data mining, as they integrate the ability of ANNs to learn from data and the capacity of fuzzy logic to express concepts in a simple way through linguistic "IF-THEN" rules (10).

On this basis, the aim of the present work is to rationally stablish suitable lyophilization procedures for NLC through the knowledge generated by AI tools. This analysis also aims to allow a better understanding of the lyophilization conditions (CP type and concentration or freezing speed) impact on lyophilized NLC properties, and to assess the physicochemical phenomena driving the lyophilization process and sugars effectivity as CP.

5.2. MATERIALS AND METHODS

5.2.1. Materials

Precirol® ATO 5 (glyceryl distearate) and Epikuron® 145V (deoiled phosphatidyl choline-enriched lecithin) were kindly donated by Gattefossé (France) and Cargill (USA) respectively. Polysorbate 80 (Tween® 80), Oleic acid, D- (+)-trehalose dihydrate, D-mannitol (≥98%), D-(-)-fructose, D-sorbitol and dialysis membrane (Spectrum™ Labs Spectra/Por, MWCO 3.5 KDa) were acquired from Sigma Aldrich (USA). D-glucose anhydrous and lactose were obtained from Fisher Scientific (USA) and Merck (Spain), respectively. D- (+)-sucrose was acquired from Acros Organics, Fisher Scientific (USA). Ultrapure water (MilliQ plus, Millipore Ibérica, Spain) was used throughout.

5.2.2. NLC formulation

NLC formulations were prepared by hot high shear homogenization, following a procedure previously optimized in our laboratory through Artificial Intelligence tools (13). Oleic acid and Precirol® ATO 5 were used as liquid and solid lipid, respectively, while Epikuron® 145V and Tween® 80 were employed as emulsifiers. Briefly, an oil phase (300 mg), composed by a 75:25 ratio of liquid:solid lipid was melted at 80°C. Then, an aqueous phase (10 ml), comprising Epikuron® 145V (0.5% w/w regarding oil phase) and Tween® 80 (1.9% w/v regarding aqueous phase) was also heated at 80ºC and added to the oil phase. The mixture was hot high shear homogenized at 14,800 rpm for 10 min using an Ultra-Turrax T25 (IKA Labortechnik, Germany), leading to a NLC dispersion which was cooled in an ice bath, for 2 min with gentle stirring.

Furthermore, to remove the non-incorporated components, nanoparticle dispersions were overnight dialyzed using a porous membrane (Spectrum™ Labs Spectra/Por, MWCO 3.5 KDa). The particle size and surface charge of the NLC were characterized as indicated below.

5.2.3. NLC lyophilization and reconstitution

A selection of cryoprotectants (trehalose, lactose, sucrose, sorbitol, glucose, fructose, and mannitol) at different concentrations (2.5, 5, 10, 15 and 20% w/v) were used for the lyophilization of NLC. In addition, the effect of two freezing procedures was also evaluated (fast by immersion in liquid nitrogen or slow in a freezer at -80ºC).

Briefly, 2 ml of dialyzed NLC suspensions (n=2) were mixed with accurate amounts of the CPs in 5 ml tubes. Then, mixtures were manually homogenized (by tubes inversion) until complete dissolution and subsequently frozen. Lyophilization was carried out by duplicate in a freeze dryer Telstar LyoQuest Plus -85°C/ECO (Telstar, Spain) for 24 hours. During the process, the chamber temperature was maintained at -70°C, under a high vacuum of 0.01 mbar, approximately.

Lyophilized NLCs (50 mg) were resuspended in 10 ml of Milli-Q® water. The dispersions were shaken manually and then sonicated for 30 seconds with a Sonicator 700W Sonic Dismembrator (Fisher Scientific, USA) to ensure complete resuspension. Then, the particle size and surface charge of the NLC were characterized again.

5.2.4.Particle size and surface charge characterization

NLC particle size, polydispersity index (PDI) and surface charge, before and after lyophilization process, were determined using a Zetasizer Nano ZS (Malvern Instruments, UK). Particle size and PDI measurements were performed in polystyrene cuvettes, after proper dilution with Milli-Q® water. Surface charge was determined through particle mobility in an electric field as zeta potential (ZP). For this purpose, a specific cuvette was employed where a potential of ±150 mV was established. All measurements were conducted by triplicate at 25±1°C. Results were expressed as the increase in particle size (Δ size), polydispersity index (Δ PDI) and zeta potential (Δ ZP).

5.2.5. Osmolarity determination

Samples of Milli-Q® water, NLC dispersions, and aqueous solutions of the CPs under evaluation were experimentally evaluated using a Vapro® vapor pressure osmometer (model 5600, Wescor, ELITechGroup, USA). Osmolarity values of CPs solutions were determined using concentrations ranging between 2.5-20%, except for lactose and mannitol, where the studied concentrations were 2.5-10% or 2.5-15%, respectively, due to their low aqueous solubility.

5.2.6. Modelling through Artificial Intelligence tools

The variables studied followed an experimental design for three variables (CP, CP concentration and freezing speed) at 7, 5 and 2 levels, respectively. Additionally, the database was completed with the CPs molecular weight (MW_{CP}) and the osmolarity at the specific concentration (**Table 5.1**). Moreover, the parameters derived from the NLC analysis regarding particle size and surface charge expressed as Δ Size, Δ PDI and Δ ZP were also added to the database (depicted in **Figures 5.2-5.4**).

Complete database was modelled using FormRules® v4.03 (Intelligensys Ltd, UK), which is a Neurofuzzy Logic (NFL) software that enables answering "WHAT IF" questions through the generation of "IF-THEN" rules (13). "IF-THEN" rules consist of an antecedent and a consequent part, indicating the relationship between the variables or inputs and the resulting values or outputs (13). These rules were obtained after a fuzzification process, where each value of an input is classified and described by a word (low, medium, or high) and an associated membership degree (MD) ranging from 0 to 1. Values of MD close to 1 indicate that a certain hypothesis is true (e.g. Δ Size is low), while values of MD close to 0 imply it is false (e.g. Δ Size is not low) (10).

Two Neurofuzzy logic models were carried out. Model 1 studies the effect of freezing speed, the CP and CP percentage (included as inputs), on the Δ Size, Δ PDI and Δ ZP of the LP (included as outputs). The training parameters selected for model 1 were: ridge regression factor of $1\times e^{-6}$, two set densities, Structural Risk Minimization as model selection criteria (C_1 =0.70 and C_2 = 4.80), 2 maximum inputs per submodel and 15 maximum nodes per input.

Model 2 explores the effect of specific CP characteristics (CP type, MW_{CP}, osmolarity) and the freezing speed on the three outputs. For model 2, training parameters similar to model 1

were used, with two exceptions: C_1 values needed adjustment (C_1 = 0.60-0.70) and also the maximum number of inputs per submodel (2-4).

The quality of the models for each output was assessed using the calculated f ratio from the analysis of variance (ANOVA) and the determination coefficient of train set (R^2), which estimate their accuracy and predictability, respectively. The train set R^2 values were calculated as follows (16):

$$R^2 = [\,1 - \sum_{i=1}^{n}(yi - yi')^2 / \sum_{i=1}^{n}(yi - yi'')^2] \times 100\% \qquad \textbf{Equation 5.1}$$

Where yi is the experimental value obtained for a given output, yi' is the predicted value for the output calculated by the model and yi'' is the mean of the experimental value. Values of R^2 ranging from 70 and 99.9% indicate satisfactory model predictabilities (17).

A calculated f ratio higher than critical f value for the same degrees of freedom indicates there are not statistically significant differences between predicted and experimental data, therefore the model is accurate.

5.3. RESULTS

5.3.1. Cryoprotectants characterization

The cryoprotectants (CPs) selected for this work include disaccharides, such as lactose, sucrose and trehalose, sugar alcohols, as mannitol and sorbitol, and monosaccharides, as fructose and glucose (**Figure 5.1)**. To better understand the CPs properties effect on the lyophilization procedure, these compounds were classified by their MW_{CP} and characterized in terms of osmolarity (Π) (**Table 5.1)**. Fructose and glucose have a MW_{CP} of ≈ 180.16 g/mol, while lactose, sucrose and trehalose have a MW_{CP} of ≈ 342.3 g/mol, and mannitol and sorbitol have a MW_{CP} of ≈ 182.17 g/mol (18).

On the other hand, Π led to values ranging from 154-1141, 135-1127, 72-248, 142-945, 131-1146, 73-602 and 70-538 mmol/kg for fructose, glucose, lactose, mannitol, sorbitol, sucrose and trehalose, respectively. Π values are in agreement with those expected by multiplying CPs molar concentration by their dissociation factor, which is known to be 1 for molecules that do not dissociate in solution, as it is the case of sugars. As an example, a 5% (w/v) solution of trehalose and glucose would exhibit a molarity of approximately 140 and 278 mmol/L, respectively, which closely agrees with the experimental Π values obtained.

Table 5.1. Variables included as inputs for modelling: CP type, CP concentration, MW_{CP} and osmolarity in aqueous solution.

CP	CP concentration (%)	Mw_{CP} (g/mol)	Π (mmol/kg)
Fructose	2.5	180.16	154
Fructose	5	180.16	279
Fructose	10	180.16	551
Fructose	15	180.16	894
Fructose	20	180.16	1141
Glucose	2.5	180.16	135
Glucose	5	180.16	257
Glucose	10	180.16	547
Glucose	15	180.16	820
Glucose	20	180.16	1127
Mannitol	2.5	182.17	142
Mannitol	5	182.17	270
Mannitol	10	182.17	593
Mannitol	15	182.17	945
Sorbitol	2.5	182.17	131
Sorbitol	5	182.17	253
Sorbitol	10	182.17	615
Sorbitol	15	182.17	864
Sorbitol	20	182.17	1146
Sucrose	2.5	342.3	73
Sucrose	5	342.3	140
Sucrose	10	342.3	300
Sucrose	15	342.3	434
Sucrose	20	342.3	602
Trehalose	2.5	342.3	70
Trehalose	5	342.3	134
Trehalose	10	342.3	281
Trehalose	15	342.3	381
Trehalose	20	342.3	538
Lactose	2.5	342.3	72
Lactose	5	342.3	142
Lactose	10	342.3	248

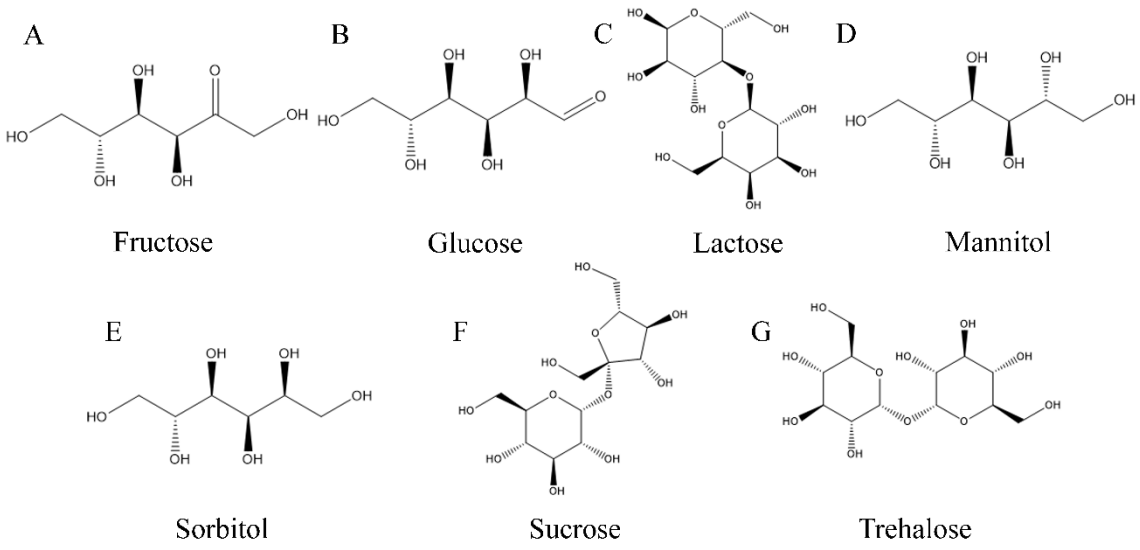

Figure 5.1. Chemical structure of A) Fructose, B) Glucose, C) Lactose, D) Mannitol, E) Sorbitol, F) Sucrose and G) Trehalose.

5.3.2. Physicochemical characterization of NLC and lyophilized powders

Both, size and PDI, are key parameters determining nanoparticles stability, and therefore, it is of utmost importance to control Δ Size and Δ PDI of NLC, which should be maintained as low as possible. NLC formulations (n=5), showed initially a particle size of 126±19 nm, a PDI of 0.28±0.05 and a ZP of -26±3 mV. The values of Δ Size, Δ PDI and Δ ZP were 62±9 nm, 0.10±0.06 and -2±1 mV for reconstituted NLC when fast freezing was carried out, and 61±7 nm, 0.14±0.07 and -1±2 mV when slow freezing was performed. The nanocarriers exhibited a suitable ability to endure lyophilization without CPs. However, NLC showed gummy-like appearance, and some difficulties were found during the re-constitution step, which justifies the need of CPs. The use of CPs allowed to obtain nanoparticles with a dry appearance, and easy and quick reconstitution. Moreover, after CPs incorporation, Δ Size values were in the range of 23±1-94±6 nm and 31±16-157±4 nm for fast and slow freezing, respectively. As it can be observed in **Figure 5.2**, CPs effectivity widely varies over the range of concentrations tested. Furthermore, a different behaviour pattern can be noticed as a function of the type of CP (monosaccharides, sugar alcohols or disaccharides), the concentration used and the freezing process. As an example, sucrose (a disaccharide) appears to perform better at high concentrations (**Figures 5.2.A** and **5.2.E**). At 2.5%, and with fast freezing, sucrose leads a Δ Size of 80±16 nm, while 20% sucrose promotes a smaller Δ Size of 40±21 nm. In contrast, a monosaccharide such as fructose appears to behave better at low proportions, exhibiting Δ Size values of 58 ± 2 nm and 87 ± 14 nm for concentrations of 2.5 and 20%, respectively, when fast freezing is employed. Besides, as a general trend, the use of fast freezing seems to favour low Δ Size values.

Δ PDI values ranged from 0.06±0.01-0.37±0.01 and 0.09±0.07-0.51±0.05 for fast and slow freezing, respectively. Similar trends to those described for Δ Size in terms of CP type, concentration and freezing speed were observed (**Figure 5.3**).

Finally, values of -5±3-+5±1 mV and -4±5-+7±6 mV were reported for Δ ZP using fast or slow freezing, respectively (**Figure 5.4)**. Interestingly, some CPs, such as lactose, fructose, or trehalose, promote ZP neutralization. Those increases are likely to trigger the destabilization of NLC formulations, due to reduced electrostatic repulsions, and therefore, variables involved in Δ ZP require further study using AI tools.

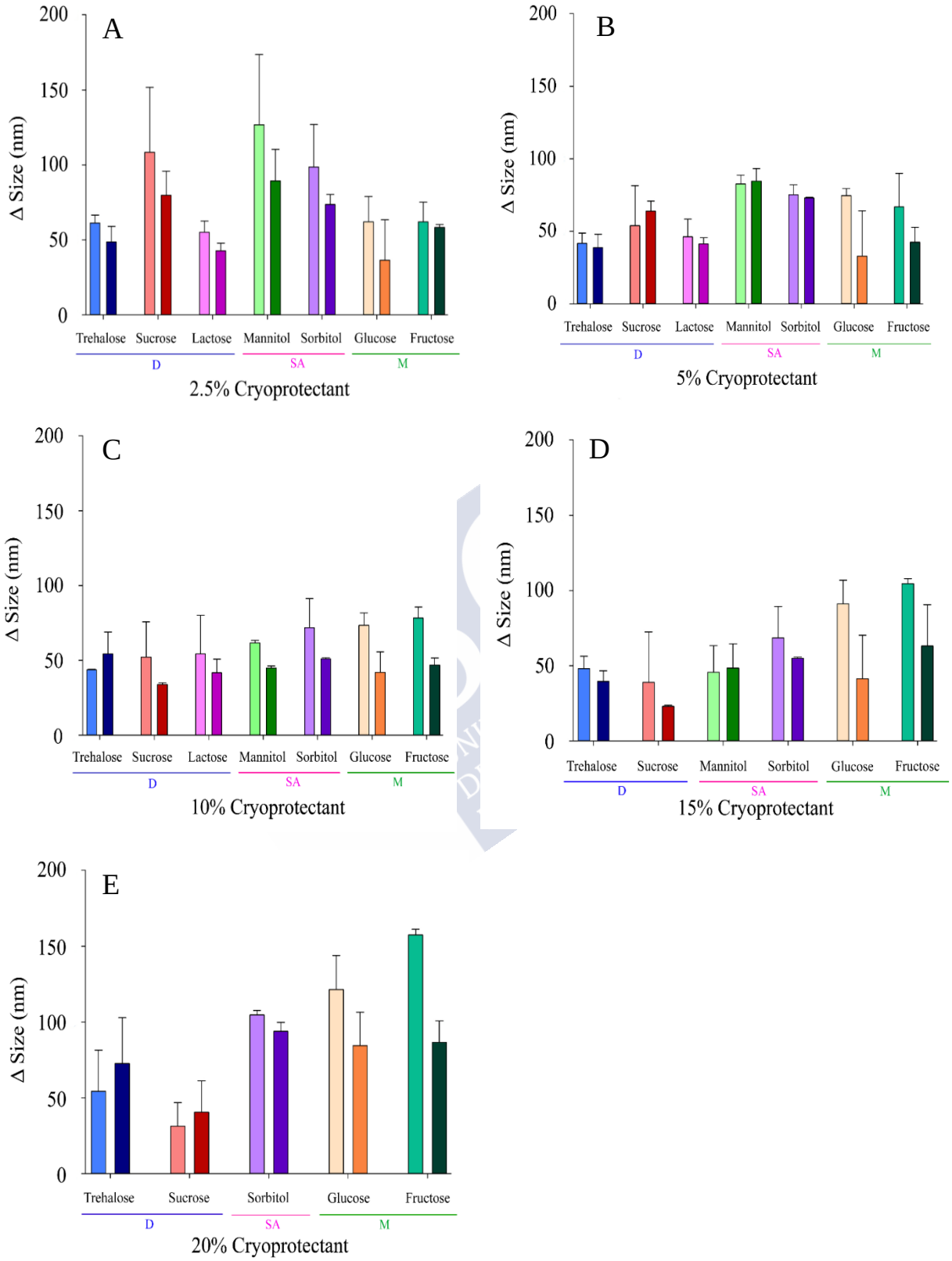

Figure 5.2. Increase in the size of the NLC (Δ Size), after lyophilization with different CPs at variable concentrations (2.5-20% w/v). Light colours correspond to slow freezing processes and dark colours to fast freezing processes. The CPs are grouped according to their type into disaccharides (D), sugar alcohols (SA) and monosaccharides (M).

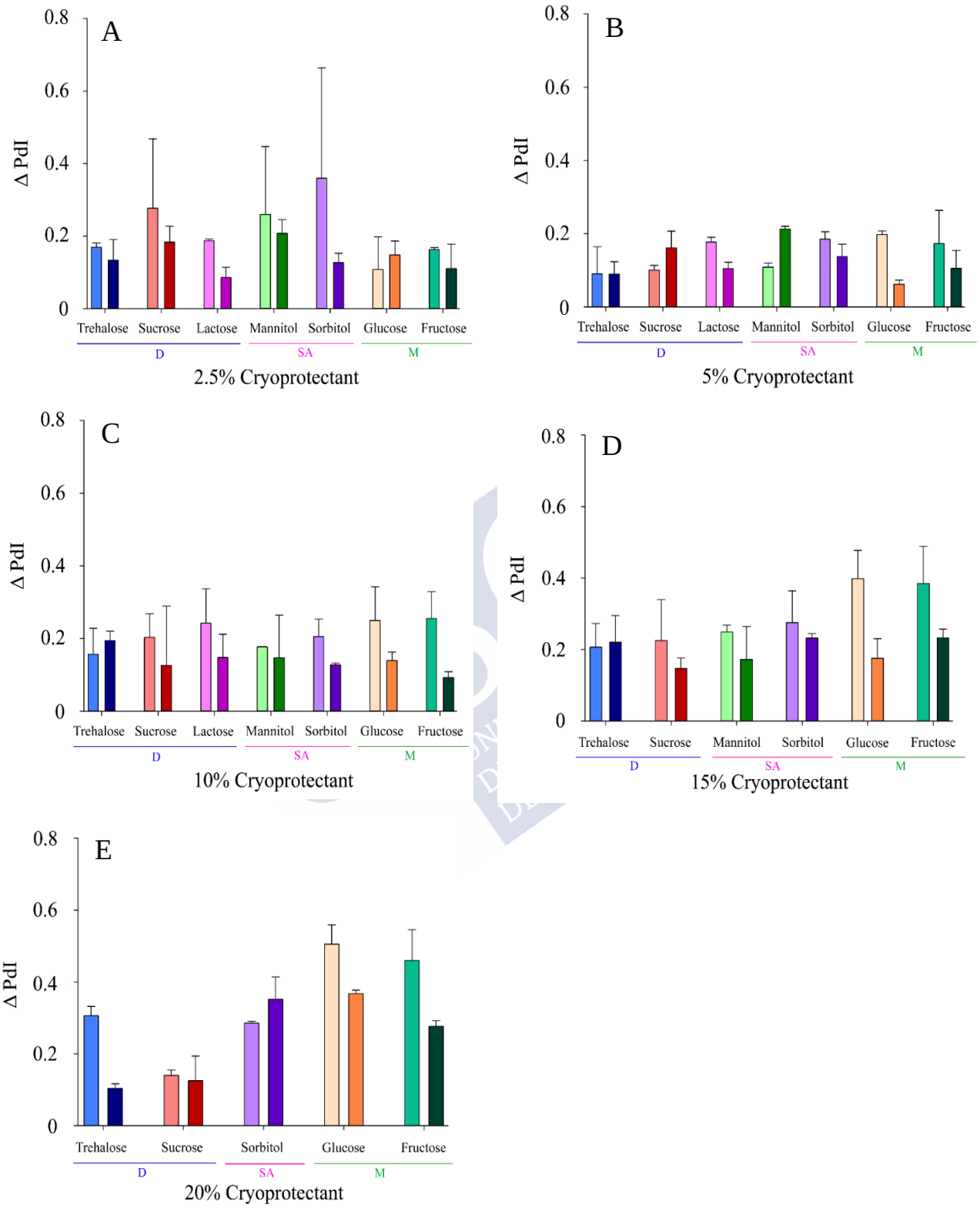

Figure 5.3. Increase in the polydispersity index of the NLC (Δ PDI), after lyophilisation with different CPs at variable concentrations (2.5-20% w/v). Light colours correspond to slow freezing processes and dark colours to fast freezing processes. The CPs are grouped according to their type into disaccharides (D), sugar alcohols (SA) and monosaccharides (M).

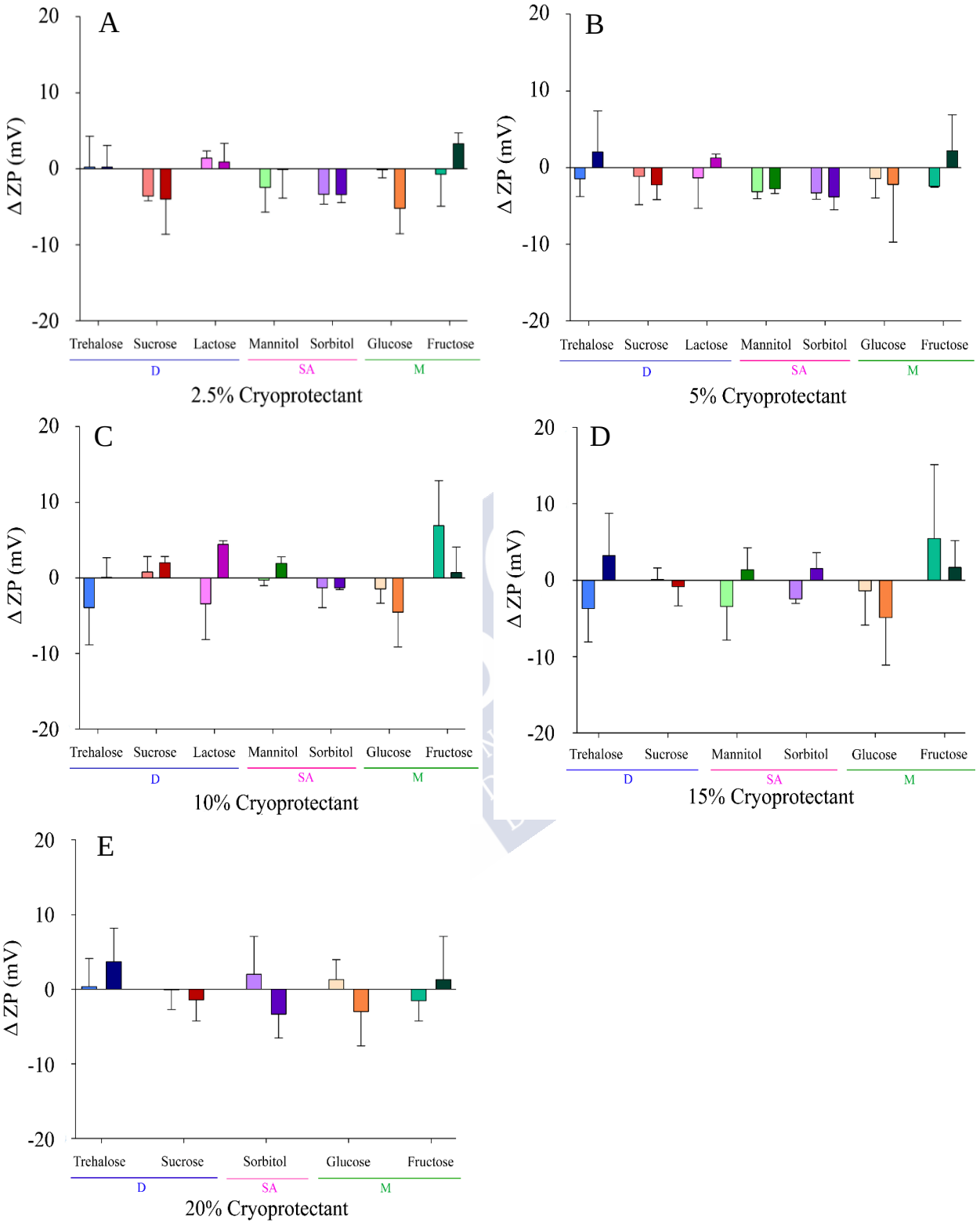

Figure 5.4. Increase in zeta potential of the NLC (Δ ZP), after lyophilisation with different CPs at variable concentrations (2.5-20% w/v). Light colours correspond to slow freezing processes and dark colours to fast freezing processes. The CPs are grouped according to their type into disaccharides (D), sugar alcohols (SA) and monosaccharides (M).

5.3.3. Influence of lyophilization variables over NLC characteristics (Model 1)

FormRules® succeeded in modelling Δ Size and Δ PDI parameters, as both R^2 values were above 70% (**Table 5.2**), indicating suitable predictabilities (17). Moreover, computed f values were higher than the critical ones for the degrees of freedom of the model, indicative of no statistically significant differences among predicted and experimental results and, therefore, accuracy (12). However, limited predictability (R^2= 51.35%) was achieved for the Δ ZP model, probably due to the similarity of the values obtained, indicating ZP variations cannot be completely explained by the variables studied.

Both Δ Size and Δ PDI are affected by the three variables studied: freezing speed, CP and concentration (%CP), having the interaction between the CP and the CP concentration, the strongest effect on both outputs (highlighted submodels in **Table 5.2**).

Table 5.2. Inputs selected by NFL models that explain Δ Size, Δ PDI and Δ ZP in lyophilized NLC formulations, along with predictability (R^2) and ANOVA parameter. The most relevant submodel is bolded, while models not meeting quality criteria are highlighted in red.

Output	Submodels	Inputs from FormRules®	R^2	Calculated f value	Degrees of freedom	f critical for p<0.01
Δ size	Submodel 1	CP × Speed	91.77	10.17	34 and 31	2.32
	Submodel 2	**CP × %CP**				
Δ PDI	**Submodel 1**	**CP × %CP**	76.04	8.29	18 and 47	2.34
	Submodel 2	Speed				
	Submodel 3	%CP				
Δ ZP	**Submodel 1**	**CP × Speed**	51.35	3.52	15 and 50	2.42
	Submodel 2	%CP				

According to the "IF-THEN" rules generated by FormRules® for Δ Size and Δ PDI (**Tables A1-A2**, **Annex III**), every CP requires a specific range of concentration for its best performance. As a general trend, a fast freezing speed favour the obtention of formulations exhibiting a low Δ Size. The sugar alcohols, mannitol and sorbitol, led the worst results for Δ Size in the whole range of concentrations, using either fast or slow freezing speeds (Rules 19-30, **Table A1**, **Annex III**). Fructose and glucose require low-medium concentrations (up to 12.5%), along with a fast freezing speed (Rules 1-12, **Table A1**, **Annex III**). On the other hand, sucrose should be employed at a medium-high concentration (over 2.5%) if a fast freezing speed is employed. Furthermore, an even higher sucrose proportion (above 12.5%) would be required if a slow freezing is selected. Fructose, glucose and sucrose perform slightly better if a fast freezing speed is employed (Rules 31-36, **Table A1**, **Annex III**). Finally, an optimum cryoprotective performance could be obtained with medium concentrations (2.5-12.5%) of trehalose and lactose. Furthermore, these disaccharides exhibit a similar behavior with both fast and slow freezing speeds (Rules 13-18 and 37-42, **Table A1**, **Annex III**).

Similar conclusions can be obtained from the Δ PDI model set of rules. Although in general, a low Δ PDI has been achieved, some differences amongst CPs have been found. In the same way as reported for Δ Size, mannitol and sorbitol also exhibited a poor performance

in terms of Δ PDI. However, the use of specific conditions such as CP proportions ranging from 7.5-12.5% and a fast freezing speed, would allow to obtain a low Δ PDI (Rules 31-50, **Table A2**, **Annex III**). Glucose, lactose, and fructose should be ideally employed in a low-medium concentration (up to 10%) to achieve a low Δ PDI. Regarding freezing step, no relevant differences have been found between freezing speeds for these three compounds (Rules 1-30, **Table A2, Annex III**). On the other hand, it has been found that sucrose exhibits a different behavior since it works better at medium-high concentrations and its concentration requirements vary depending on the freezing speed (above 3.75 and 12.5% for fast and slow freezing, respectively) (Rules 51-61, **Table A2**, **Annex III**). Lastly, rules for trehalose indicate that its use at low-mid proportions (up to 12.5% and in the range of 3.75-12.5% for fast and slow freezing speeds, respectively) leads to a small Δ PDI (Rules 62-71, **Table A2**, **Annex III**).

5.3.4. Influence of cryoprotectant properties and operation conditions over NLC characteristics (Model 2)

In a second and more detailed approach, the role of CP specific characteristics (such as MW_{CP} and Π) and freezing speed on Δ Size, Δ PDI and Δ ZP was modelled. FormRules® also succeeded in modelling Δ size and Δ PDI leading to R^2 higher than 70% and computed f values above the critical ones in both cases. A suitable model for Δ ZP was neither found in this case. The information provided by the NFL software shows that, both Δ Size and Δ PDI are explained by the interaction between MW_{CP} and Π. Moreover, Δ Size variations were also associated with the interaction of MW_{CP} and freezing speed, while changes in Δ PDI have been attributed to the freezing speed (**Table 5.3**).

Table 5.3. Inputs selected by NFL models that explain Δ Size, Δ PDI and Δ ZP in lyophilized NLC formulations, along with predictability (R^2) and ANOVA parameter. The most relevant submodel is bolded, while models not meeting quality criteria are highlighted in red.

Output	Submodels	Inputs from FormRules®	R^2	Calculated f value	Degrees of freedom	f critical for p<0.01
Δ size	**Submodel 1**	**MW_{CP} × Π**	74.38	10.14	14 and 49	2.47
	Submodel 2	MW_{CP} × Speed				
Δ PDI	**Submodel 1**	**MW_{CP} × Π**	70.50	12.65	10 and 53	2.68
	Submodel 2	Speed				
Δ ZP	**Submodel 1**	**Π**	1.58	0.49	2 and 61	4.97

The rules for Δ Size model indicate that CPs of low molecular weight, below 220 g/mol, perform better at low Π values. Those exhibiting a MW ranging from 220-300 g/mol need a medium–high Π values for obtaining low Δ Size. Interestingly, CPs with a MW above 300 g/mol showed a higher independence of Π values, as a low Δ Size would be obtained in all cases (Rules 1-9, **Table A4**, **Annex III**). Furthermore, similar results were obtained for Δ PDI although, in this case, Π requirements have been reported to increase progressively with the increase in MW_{CP} in all cases (Rules 1-9, **Table A5**, **Annex III**).

The interaction among MW_{CP} and freezing speed also plays a role on Δ Size. In this way, CPs of MW below 220 g/mol perform better when fast freezing is employed. Slower freezing is advisable for CPs of MW ranging from 220 to 300 g/mol, while a higher independence of freezing speed was found for CPs showing a MW above 300 g/mol (Rules 10-15, **Table A4**, **Annex III**). As an example, fructose (MW_{CP}=180.16 g/mol) at 10% (w/v) leads to values of Δ Size of 47±5 and 78±7 nm when fast and slow freezing, respectively, is carried out.

Furthermore, fast freezing speed promotes lower Δ PDI as indicated by a lower membership degree for rule 11 (Rules 10-11 **Table A5**, **Annex III**).

5.4. DISCUSSION

NLC formulations demonstrated a good ability to endure lyophilization process. This phenomenon might be related to the freezing speeds selected in this work (-80°C and -196°C), which are likely to limit nanoparticle movement, reducing aggregation (19). However, LP exhibited a gummy-like nature and a challenging re-dispersion, probably due to the presence of a high residual water content along with the absence of a porous structure. These features are associated with formulation collapse (8), and justify the use of cryoprotectants.

CPs are usually employed during lyophilization to protect nanoparticles from freezing stress (20), reduce aggregation and improve re-dispersion (19). Several CPs mechanisms of action have been proposed. Some authors have suggested the generation of a glassy matrix, where nanoparticles can be immobilized and protected, takes place when the glass transition temperature of the maximum cryo-concentrated solution is reached (Tg´) (8). Tg´ corresponds to the glass transition temperature (Tg) of the highly concentrated solution generated after the formation of ice crystals during freezing (8). Other authors have suggested that, during freezing, nanoparticles could be isolated by sugars in the unfrozen fraction, increased in volume by the addition of CPs, without requiring sugar vitrification (21). CPs can also act as lyoprotectants, conferring protection from drying stress (22), by generating hydrogen bonds with the polar groups of the nanoparticle surface, thus replacing water molecules (8).

In order to get insight into the use of cryoprotectants for NLC lyophilization, a group of widely employed sugars of different types, including sugar alcohols, monosaccharides, and disaccharides, were selected, and used at different concentrations. After nanoparticle lyophilization and reconstitution, particle size, PDI and ZP were determined and compared. Highly heterogeneous values for both Δ Size and Δ PDI were obtained, with several patterns for the different lyophilization conditions tested (freezing speed, CP type and concentration). Conversely, despite the Δ ZP increases observed for some LP with the use of certain CPs (as lactose, fructose or trehalose), in general, a narrow range of values was obtained for this parameter. This phenomenon is more likely to be associated with CP molecules adsorption to the nanoparticle surface (23), driven by the interaction among nanoparticles and the OH groups of CPs (8), rather than with an actual modification of the nanoparticle surface during the lyophilization process.

A traffic light classification system has been proposed from results obtained in model 1, generated by NFL, to analyze the effect of the CP selected, its concentration (%CP) and the freezing speed employed, over LP characteristics (Δ size, Δ PDI and Δ ZP) (**Table 5.4**). Not

advisable conditions to obtain low Δ size or Δ PDI are indicated in red while highly advisable conditions are denoted in green. This classification system has been set up from the obtained "IF-THEN" rules and their membership degrees (MD). Green and red colours represent lyophilization conditions which, according to "IF-THEN" rules exhibiting MD values higher than 0.75 to obtain low or high Δ size/Δ PDI values. Yellow colours represent conditions leading to either low or high Δ size/Δ PDI values, obtained from rules showing a MD ranging from 0.5-0.74.

Interestingly, the optimal ranges of %CP proposed by the NFL software for sugars such as sucrose, fructose, glucose or trehalose are in agreement with those selected by other authors as having the best protective effect (24) (**Table 5.4**).

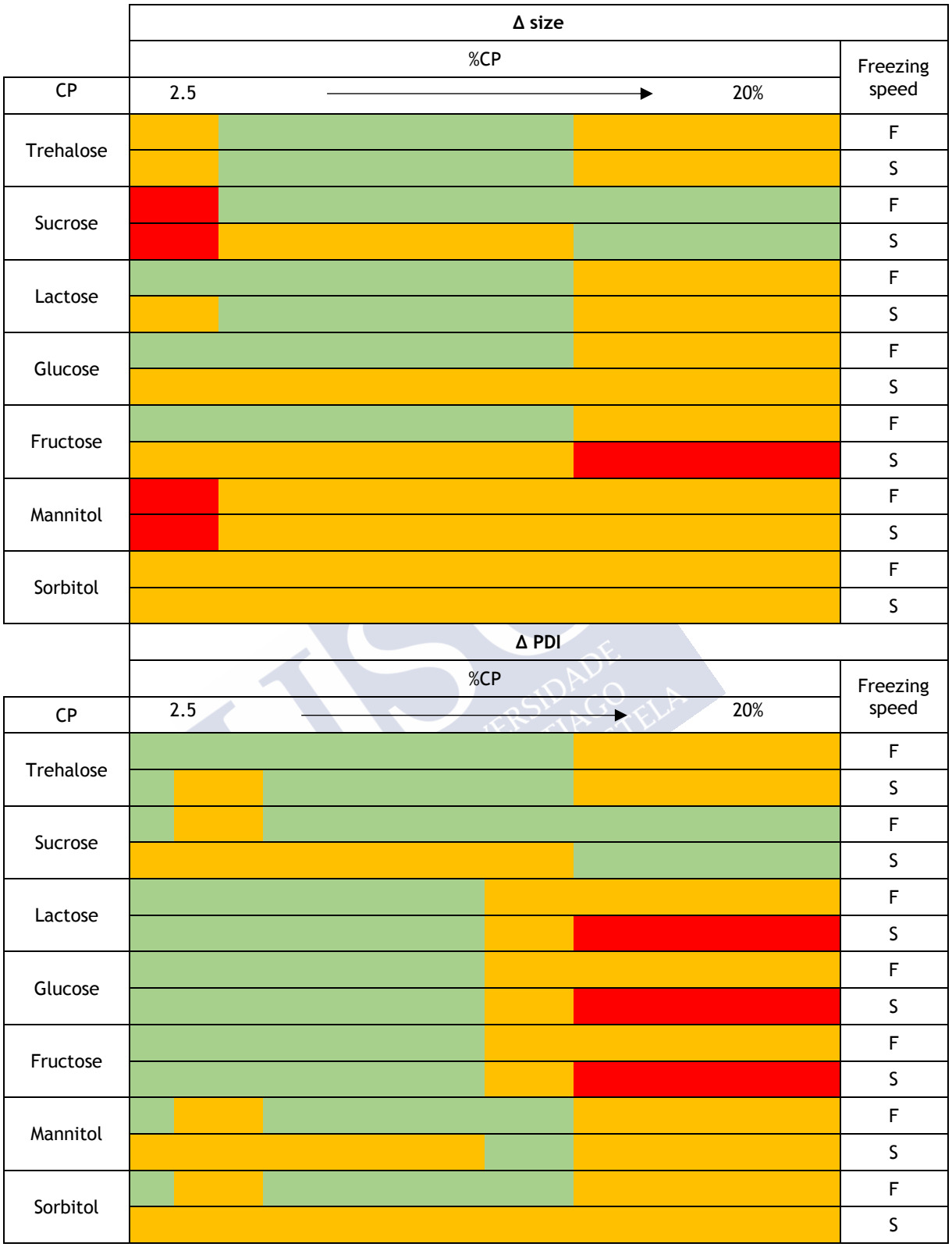

Figure 5.4. Summary of the information obtained from NFL models. Color scale indicates the most suitable lyophilization conditions to obtain LP with optimal properties (low Δ Size and Δ PDI). This suitability increases in the following order, from red (not advisable) to green (highly advisable):

Second NFL model, focused on understanding the role of certain CP parameters (such as MW_{CP} and Π, along with freezing speed) on LP properties, is in agreement with model 1 with a slightly lower predictive capacity.

Results from model 2 indicate that the MW_{CP} determines the optimal freezing speed and Π to obtain a product with easy redispersion and adequate characteristics (low Δ Size and Δ PDI). Thus, for CPs of MW below 220 g/mol (monosaccharides and sugar alcohols), low Π values and a fast freezing speed are preferred. CPs with a MW above 300 g/mol (disaccharides) work better at high Π values, and in these cases, the process is barely influenced by the freezing speed.

The scientific literature shows some controversy regarding the most suitable freezing speed for nanocarriers lyophilization (9, 25). Model 1 shows a general preference for fast freezing using liquid nitrogen, in agreement with previous theories, which indicate that fast supercooling leads to the generation of small ice crystals, reducing mechanical stress over nanocarriers (8). Results from model 2 help to explain the controversy as indicate that freezing speed requirements vary depending on the MW_{CP}, in agreement with data reported by other authors (9). As the freezing front progresses, ice crystals and a cryo-concentrated solution, consisting of nanoparticles and other formulation elements, are formed (8, 9). The amount of CP available to protect the nanoparticles varies as a function of the freezing speed and the diffusion rate of the CP molecules towards the cryo-concentrated phase (9), which in turn depends on the MW_{CP}. Low MW CPs must migrate faster than high molecular weight ones.

In this way, the preference for a rapid freezing observed for CPs with a MW below 220 g/mol can be explained by their expected fast migration capacity. This feature could allow to efficiently protect NLC, and also to take advantage from the fast freezing benefits, as smaller ice crystals generation (8, 9). Meanwhile, NLC dispersions stabilized with CPs exhibiting a MW ranging from 220 to 300 g/mol, would exhibit better properties in terms of Δ Size if a slower freezing rate is employed.

On the other hand, the higher independence from freezing speed observed for molecules exhibiting the highest MW (300 g/mol) can be related to their superior Tg (26). Disaccharides have higher Tg than monosaccharides (27), which explains why they vitrify earlier during the freezing process, immobilizing the NLC in a vitreous matrix and thus, minimizing particle damage and the effects of freezing. This effect is likely to be responsible for the lower prediction capacity of the second NFL model, due to the involvement of other CP characteristics different than MW in LP properties.

Furthermore, the variations in Π requirements as a function of the MW_{CP} described in the second model, could also be explained by the afore-mentioned diffusion phenomenon. Hence, the addition of a high amount of poorly diffusive CPs to the nanoparticles, could increase the presence of these compounds in the cryo-concentrated liquid phase and counteract their slow diffusion (9). Besides, considering Π is a colligative property, its requirements would be directly related with %CP, which explains the high similarity between the two NFL models.

As an example, fructose and glucose (MW_{CP}=180.16 g/mol) were found to be more effective when employed up to a certain concentration, while the use of higher CP proportions is more advisable for sucrose (MW_{CP}=342.3 g/mol). Nevertheless, trehalose and lactose

(MW_{CP}=342.3 g/mol) seemed to exhibit a different behaviour than that described for sucrose, as they were found to perform better when employed at medium concentrations (**Table 5.4**). These contradictory findings could be associated, on the one hand, with the remarkable protective activity of trehalose, triggered by features such as low hygroscopicity or absence of internal hydrogen bonding (8). On the other hand, lactose crystallization during freezing (28), could lead to the low %CP requirements observed. In this way, the formation of a eutectic with ice and the generation of CP crystals, could favour nanoparticle aggregation and fusion (8). Furthermore, mannitol and sorbitol have also been reported to crystallize during lyophilization process (29), which could explain the poor cryoprotective effectivity achieved with both CPs.

Therefore, in the same way as described for freezing speed, crystalline behaviour could also be associated with the lower prediction capacity shown by the second model, in comparison with the first one. Nevertheless, despite the existing discrepancies between the two models, the great similarity among them suggests that CPs osmotic properties do not seem to play a role on the cryoprotective activity of these compounds while CP concentration is crucial. Although sugars are known to be non-penetrating osmotic CPs, it is also necessary to consider these properties would be more relevant for cell cryopreservation, where osmotic activity of CPs leads to cell dehydration minimizing the generation of ice crystals inside cells (30). On the other hand, nanoparticle dehydration is less likely to occur, minimizing the effect produced by Π itself.

5.5. CONCLUSIONS

The neurofuzzy logic analysis allowed a better understanding of the role of lyophilization conditions, such as freezing speed or certain characteristics of the cryoprotectants used, on the properties of the nanoparticles obtained and to provide some insights into the physicochemical phenomena involved. The knowledge generated would allow a rational selection (avoiding trial and error approaches) of the variables used for lyophilization, to obtain easily redispersible NLCs, with similar characteristics to those initially produced. NLC lyophilization could be performed using a considerable variety of variables (CP choice, proportion employed or freezing speed) as long as they are properly combined. In this way, the use of monosaccharides such as glucose or fructose in a concentration up to 10% and a fast freezing speed is highly advisable. Besides, the addition of disaccharides, such as sucrose and trehalose, at concentrations from 12.5% and in the range of 3.75-12.5%, respectively, can also constitute interesting options to obtain NLC with suitable properties with any of the freezing speeds evaluated. Nonetheless, the usage of sugar alcohols, as mannitol or sorbitol, would not be advisable.

REFERENCES

1. Fang CL, Al-Suwayeh SA, Fang JY. Nanostructured lipid carriers (NLCs) for drug delivery and targeting. Recent Pat Nanotechnol. 2013; 7 (1): 41-55.
2. Beloqui A, Solinis MA, Delgado A, Evora C, del Pozo-Rodriguez A, Rodriguez-Gascon A. Biodistribution of Nanostructured Lipid Carriers (NLCs) after intravenous administration to rats: influence of technological factors. Eur J Pharm Biopharm. 2013; 84 (2): 309-314.
3. Taratula O, Kuzmov A, Shah M, Garbuzenko OB, Minko T. Nanostructured lipid carriers as multifunctional nanomedicine platform for pulmonary co-delivery of anticancer drugs and siRNA. J Control Release. 2013; 171 (3): 349-357.
4. Qi R, Li YZ, Chen C, Cao YN, Yu MM, Xu L, et al. G5-PEG PAMAM dendrimer incorporating nanostructured lipid carriers enhance oral bioavailability and plasma lipid-lowering effect of probucol. J Control Release. 2015; 210:160-168.
5. Gainza G, Bonafonte DC, Moreno B, Aguirre JJ, Gutierrez FB, Villullas S, et al. The topical administration of rhEGF-loaded nanostructured lipid carriers (rhEGF-NLC) improves healing in a porcine full-thickness excisional wound model. J Control Release. 2015; 197: 41-47.
6. Heurtault B, Saulnier P, Pech B, Proust JE, Benoit JP. Physico-chemical stability of colloidal lipid particles. Biomaterials. 2003; 24 (23): 4283-4300.
7. Qi J, Lu YI, Wu W. Manufacturing Solid Dosage Forms from Bulk Liquids Using the Fluid-bed Drying Technology. Curr Pharm Des. 2015; 21 (19): 2668-2676.
8. Abdelwahed W, Degobert G, Stainmesse S, Fessi H. Freeze-drying of nanoparticles: formulation, process and storage considerations. Adv Drug Deliv Rev. 2006; 58 (15): 1688-1713.
9. Lee MK, Kim MY, Kim S, Lee J. Cryoprotectants for freeze drying of drug nano-suspensions: effect of freezing rate. J Pharm Sci. 2009; 98 (12): 4808-4817.
10. Colbourn EA, Rowe RC. Novel approaches to neural and evolutionary computing in pharmaceutical formulation: challenges and new possibilities. Future Med Chem. 2009; 1 (4): 713-726.
11. Landin M. Artificial Intelligence Tools for Scaling Up of High Shear Wet Granulation Process. J Pharm Sci. 2017; 106 (1): 273-277.
12. Rodriguez-Dorado R, Landin M, Altai A, Russo P, Aquino RP, Del Gaudio P. A novel method for the production of core-shell microparticles by inverse gelation optimized with artificial intelligent tools. Int J Pharm. 2018; 538 (1-2): 97-104.
13. Rouco H, Diaz-Rodriguez P, Rama-Molinos S, Remunan-Lopez C, Landin M. Delimiting the knowledge space and the design space of nanostructured lipid carriers through Artificial Intelligence tools. Int J Pharm. 2018; 553 (1-2): 522-530.
14. Diaz-Rodriguez P, Landin M. Smart design of intratumoral thermosensitive beta-lapachone hydrogels by Artificial Neural Networks. Int J Pharm. 2012; 433 (1-2): 112-118.
15. Garcia-Del Rio L, Diaz-Rodriguez P, Landin M. New tools to design smart thermosensitive hydrogels for protein rectal delivery in IBD. Mater Sci Eng C Mater Biol Appl. 2020; 106: 110252.

16. Shao Q, Rowe RC, York P. Comparison of neurofuzzy logic and neural networks in modelling experimental data of an immediate release tablet formulation. Eur J Pharm Sci. 2006; 28 (5): 394-404.
17. Colbourn E, Rowe R. Neural computing and pharmaceutical formulation. In: Swarbrick J, Boylan JC (Eds.). Encyclopedia of pharmaceutical technology. 3rd edition. New York, USA: Marcel Dekker; 2005. p. 145–157.
18. National Center for Biotechnology Information (NCBI). PubChem [Internet]. 2020. Available from: http://pubchem.ncbi.nlm.nih.gov. [Accessed on 28 March 2020].
19. Varshosaz J, Eskandari S, Tabbakhian M. Freeze-drying of nanostructure lipid carriers by different carbohydrate polymers used as cryoprotectants. Carbohydr Polym. 2012; 88 (4): 1157-1163.
20. Fonte P, Andrade F, Azevedo C, Pinto J, Seabra V, van de Weert M, et al. Effect of the Freezing Step in the Stability and Bioactivity of Protein-Loaded PLGA Nanoparticles Upon Lyophilization. Pharm Res. 2016; 33 (11): 2777-2793.
21. Allison SD, dC Molina M, Anchordoquy TJ. Stabilization of lipid/DNA complexes during the freezing step of the lyophilization process: the particle isolation hypothesis. Biochim Biophys Acta Biomembr. 2000; 1468 (1-2): 127-138.
22. Fonte P, Reis S, Sarmento B. Facts and evidences on the lyophilization of polymeric nanoparticles for drug delivery. J Control Release. 2016; 225: 75-86.
23. Caetano LA, Almeida AJ, Goncalves LM. Effect of Experimental Parameters on Alginate/Chitosan Microparticles for BCG Encapsulation. Mar Drugs. 2016; 14 (5): 90.
24. Hua ZZ, Li BG, Liu ZJ, Sun DW. Freeze-Drying of Liposomes with Cryoprotectants and Its Effect on Retention Rate of Encapsulated Ftorafur and Vitamin A. Dry Technol. 2003; 21 (8): 1491-1505.
25. Yue PF, Li G, Dan JX, Wu ZF, Wang CH, Zhu WF, et al. Study on formability of solid nanosuspensions during solidification: II novel roles of freezing stress and cryoprotectant property. Int J Pharm. 2014; 475 (1-2): 35-48.
26. Aksan A, Toner M. Isothermal Desiccation and Vitrification Kinetics of Trehalose−Dextran Solutions. Langmuir. 2004; 20 (13): 5521-5529.
27. Kalichevsky-Dong M. The glass transition and microbial stability. In: Kilkast D, Subramaniam P. The Stability and Shelf-Life of Food. 1st edition. Cambridge, UK: Woodhead pubishing; 2000. p. 25-54.
28. Patil VV, Dandekar PP, Patravale VB, Thorat BN. Freeze Drying: Potential for Powdered Nanoparticulate Product. Dry Technol. 2010; 28 (5): 624-635.
29. Andreani T, Kiill CP, de Souza ALR, Fangueiro JF, Doktorovová S, Garcia ML, et al. Effect of cryoprotectants on the reconstitution of silica nanoparticles produced by sol–gel technology. J Therm Anal Calorim. 2014; 120 (1):1001-1007.
30. Barfield JP, McCue PM, Squires EL, Seidel GE, Jr. Effect of dehydration prior to cryopreservation of large equine embryos. Cryobiology. 2009; 59 (1): 36-41.

USC
UNIVERSIDADE
DE SANTIAGO
DE COMPOSTELA

6. GENERAL DISCUSSION

USC
UNIVERSIDADE
DE SANTIAGO
DE COMPOSTELA

One of the main hurdles for the development and usage of numerous drug and drug candidates, relies on their poor water solubility, which limits the bioavailability and absorption of these compounds, significantly hindering their clinical applicability (1). This is the case of anti-mycobacterial therapy of Crohn´s disease, which is focused on the eradication of *Mycobacterium avium paratuberculosis* (MAP) housed within intestinal macrophages. Despite the promising results described by several case reports with the use of anti-mycobacterial compounds such as rifabutin, clofazimine and clarithromycin (2), the low aqueous solubility of the drugs employed (3-5), significantly reduces their effectivity.

In order to overcome drug solubility issues, several strategies were described, including the use of nanotechnology-based drug delivery systems (1). Among the wide variety of existing nanoparticulated carriers, Lipid nanoparticles (LN) are in the spotlight for being biodegradable colloidal systems displaying a good ability to load hydrophobic drugs, as well as to achieve a controlled release through several administration routes (6-8). The main differences between the two existing generations of LN, Solid lipid nanoparticles (SLN) and Nanostructured lipid carriers (NLC), is the introduction of an oil in the lipid matrix of NLC, allowing them to exhibit a superior stability and drug loading capacity (9).

Despite the enormous potential of these nano-drug delivery systems, their commercial application is currently reduced to cosmetic, nutrition and nutraceutical fields, with more than 25 formulations already marketed (10). Furthermore, as previously discussed in the introduction section, regardless of the huge presence of preclinical studies relative to both SLN and NLC in the scientific literature, clinical trials performed up to date are scarce and related to oral and topic administration routes. This slow translation of lipid nanoparticle-based therapeutics into clinical studies and marketed products is in line with the present condition of most nano-drug delivery systems, and can be associated with problems found at different stages of the development of these highly complex systems (11). Therefore, quality-by-design (QbD) approaches, allowing a rational nanocarrier design and a reproducible manufacturing process are mandatory to accelerate their commercialization.

QbD approaches have gained increased attention during the last years in the pharmaceutical field. On this purpose, AI tools such as Neurofuzzy logic (NFL), Genetic algorithms or Artificial Neural Networks (ANN) have been successfully employed to optimize diverse pharmaceutical processes as hydrogels, direct compression formulations or microparticles development (12-14).

The aim of this thesis project was focused on the development of an NLC-based formulation intended to deliver rifabutin (RFB), a model hydrophobic anti-mycobacterial drug, to intestinal macrophages, through of a simple, robust, and reproducible method. The work has been structured in four main steps. First, NFL was used to evaluate the effect of composition and formulation conditions over RFB-loaded NLC properties (Chapter 1). Secondly, a combination of ANN and genetic algorithms was used to optimize RFB-loaded NLC formulations. Reproducibility of the formulations was assessed to verify the robustness of the optimization process, and further characterization of the developed nanocarriers was also performed (Chapter 1-2). Thereafter, the suitability of the optimized RFB-loaded NLC to provide a targeted drug delivery within intestinal macrophages, was evaluated (Chapter 2).

Finally, the last step was focused on the transformation of NLC dispersions into a solid dosage form through lyophilization. AI tools were also employed to analyze the impact of lyophilization conditions on NLC dried powders properties, as well as to give insight into cryoprotectants mechanisms of action and lyophilization procedure (Chapter 3).

Rational design of RFB-loaded NLC assisted by Artificial Intelligence tools

Based on their extensive use in LN formulation (15), oleic acid and Precirol® ATO 5 (glyceryl distearate) were selected as liquid and solid lipid, respectively. Both are GRAS substances (16), which reduces the probability of occurrence of remarkable cytotoxic effects. Tween® 80 and Epikuron™ 145V (phosphatidylcholine enriched soybean lecithin) selection combines the ionic stabilization provided by the negatively charged emulsifier lecithin (17), with the protection against aggregation, through the Gibbs-Marangoni effect, conferred by the non-ionic emulsifier Tween® 80 (18).

RFB, a spiro-piperidyl-rifamycin indicated to treat mycobacterial infections (19), was incorporated in NLC formulations as a model hydrophobic anti-mycobacterial drug.

Simplicity was the main criterion behind the selection of the formulation process (20). Therefore, hot high shear homogenization was selected for the NLC production, a simple procedure which is outlined in **Figure 6.1**.

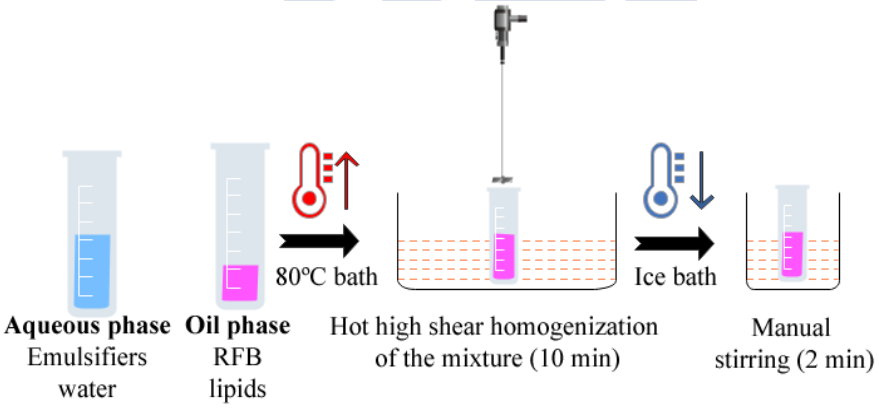

Figure 6.1. Schematic illustration of the main steps followed in NLC preparation by hot high shear homogenization. Created with biorender.com.

NFL models of high predictability and accuracy were obtained from the two experimental designs stablished. The first one **(Table 3.3)**, involved a wide range of experimental conditions (Table 3.1) which allowed to explore and establish the "knowledge space" of RFB-loaded NLC **(Figure 6.2)**. The size distribution profiles obtained for the formulations within the limits of this experimental design were not monodisperse and monomodal, which did not allow them to be characterized by the usual parameters of mean size and polydispersity index (PDI) (21). Most of the formulations have bimodal or even trimodal particle size distributions, as in the example of **Figure 6.3**. Therefore, zeta potential (ZP), and mean diameter and percentage of peak 1 (lowest peak in size, excepting peaks related with surfactant micelles) were modelled as a function of four variables: amount of oleic acid (liquid lipid, LL), percentage of Tween® 80, amount of RFB and stirring speed.

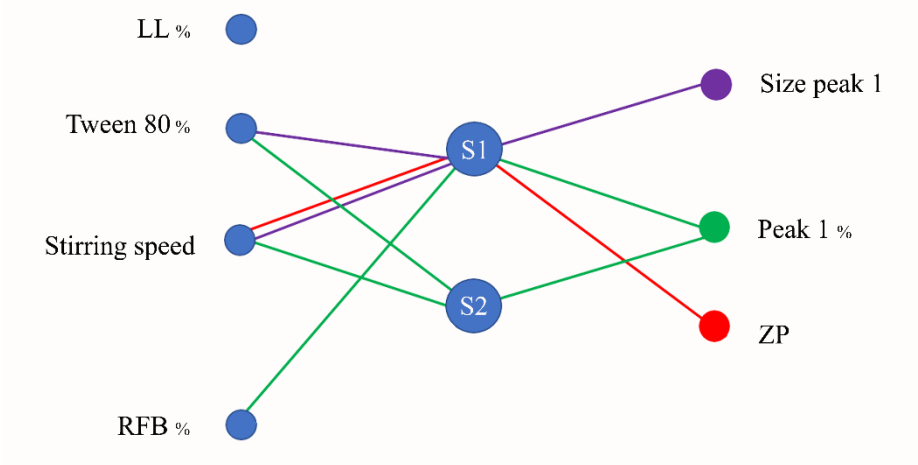

Figure 6.2. Formulation process parameters (inputs, left) afecting RFB-loaded NLC characteristics (outputs, right), according to the different submodels (S) gathered from NFL model 1.

NFL models (**Figure 6.2**) indicate that mean diameter and percentage of peak 1 are mainly determined by the interaction between Tween® 80 proportion and the stirring speed, which is likely to be related with the disturbance of NLC formation (22). Additionally, RFB increases the distortion during the particle formation process leading to the generation of particles of different sizes, as shown in **Figure 6.3**. Information derived from model 1 ("IF-THEN" rules shown in **Annex I**) allows to delimit the "knowledge space" and serves as a start point for the development of a monodisperse and monomodal formulations.

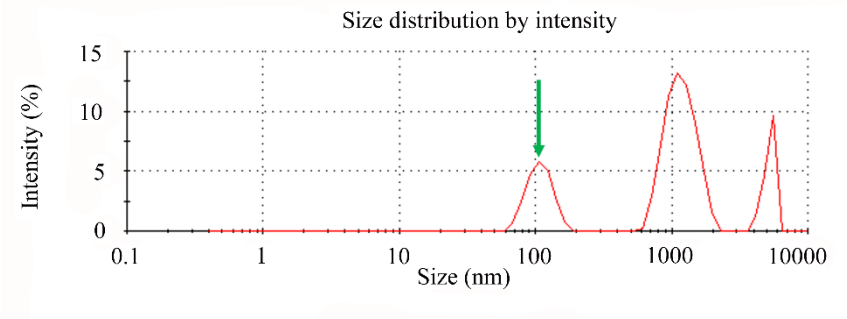

Figure 6.3. Example of trimodal particle size distribution. The peak considered as 1 is signaled by means of an arrow.

The limits for Tween® 80 proportion (up to 3% w/v) and stirring speed (~12000-20000 rpm), are shown by the area in grey of **Figure 3.1**. Additionally, a drug amount below 6% is also required to obtain RFB-loaded NLC of suitable properties.

On this basis, the second experimental design with narrower ranges of variables (stirring speed and proportions of RFB, Tween® 80 and liquid lipid), together with an additional one (lecithin proportion), was stablished (**Table 3.2**). Within the narrower limits, all NLC formulations were monodisperse (**Table 3.5**). NLC present negative ZP and variable encapsulation efficiency (EE) and drug loading (DL).

Modeling results by NFL **(Figure 6.4)** shows that the variability in NLC particle size is mainly explained (78.55%) by the interaction among liquid lipid and RFB percentages, together with the proportion of Tween® 80 (**Figure 3.2**). Similar results were obtained for PDI, which was also affected by Tween® 80 and liquid lipid proportions (**Figure 3.3**). The "IF-THEN" rules of the NFL models (data shown in **Annex I**), indicated that the increase in the proportion of liquid lipids and Tween® 80 lead to a reduction in both size and PDI. This fact can be attributed to the improvement in the efficiency of the emulsification process caused by the high proportion of emulsifier, and the reduction in surface tension due to the high presence of liquid lipids (23). On the other hand, high amounts of RFB led to an increase in NLC size, which could be easily associated with its accommodation space within the nanoparticle matrix (24).

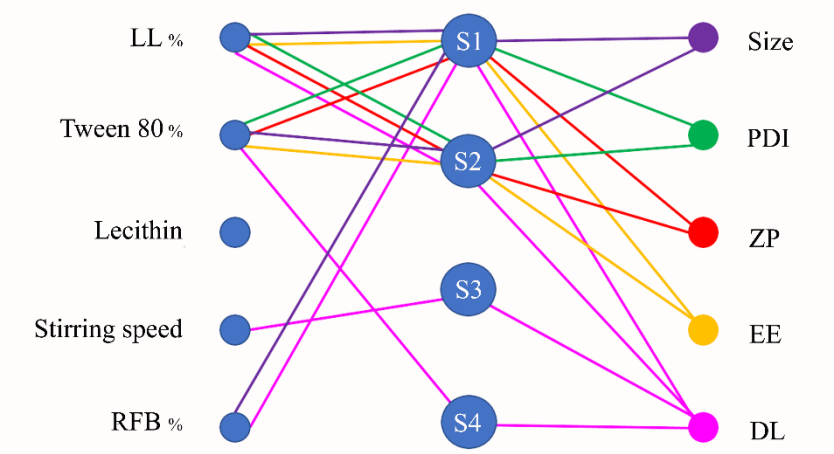

Figure 6.4. Formulation process parameters (inputs, left) afecting RFB-loaded NLC characteristics (outputs, right), according to the different submodels (S) gathered from NFL model 2.

Liquid lipid and Tween® 80 percentages also determine ZP of RFB-loaded NLC (**Figure 3.4**). Increasing proportions of liquid lipid and lecithin, both negatively charged products, lead to highly negative zeta potential values (17, 25). Tween® 80 counteracts this effect as this non-ionic emulsifier is located close to the NLC interface (26).

Variations in the parameters defining drug payload, EE and DL, were also mainly explained by the amount of liquid lipid and Tween® 80. In addition, DL was also affected by stirring speed and, obviously, by RFB percentage (**Figures 3.5**-**3.6**). High proportions of liquid lipid in which the drug is highly soluble, improve EE and DL, in agreement with other authors (27).

Large proportions of Tween® 80 lead to a reduction in EE and DL. Furthermore, a vigorous stirring speed also compromises the drug loading of the formulations. These effects may be related to the reduction in particle size when using high proportions of emulsifier and high stirring speeds, since it leads to a reduction in the space available to host the drug within NLC matrix.

It is important to highlight the different compositional and operating conditions requirements to achieve the best results for the different parameters studied. As an example, increasing the proportion of Tween® 80 reduces PDI, which is good, but it also reduces DL and EE, which is a major deficiency (**Figure 3.3**, **Figure 3.5** **and** **Figure 3.6**).

As is common in the formulation development field, it is necessary to reach a compromise solution to achieve the best values for all parameters simultaneously, that is, to carry out an **optimization process**. The NFL models offer the possibility of establishing the **design space** for these formulations, that would be characterized by a high liquid lipid content (~60-75%), an intermediate percentage of Tween® 80 (~2%) and a gentle stirring speed (~13000-16000 rpm). The formulation within these limits would foreseeably allow the incorporation of RFB at 5%, maintaining all the adequate physical properties NLC.

This demonstrates the usefulness of the NFL technique in providing a deep understanding of the influence of process variables on critical attributes of NLC and also in the development of the QbD concept.

Optimization and physicochemical characterization of RFB-loaded NLC

The use of AI tools allows to go a step further in the development of the QbD concept. The AI software, INForm®, which integrates ANN and genetic algorithms, allows obtaining models capable of answering "HOW TO GET" questions with direct application in the above-mentioned optimization processes (28), on the basis of the desirability values for the different parameters and their importance (weights) for the process.

Thus, INForm® was asked about how to obtain the minimum size (<250 nm) and PDI (<0.19), together with the maximum EE (100%) and DL (above 5%), and a ZP ranging from -18 and -19.9 mV for the NLC systems. Priority was given to drug loading in NLC (weights 10 and 9 for EE and DL, respectively), closely followed by size (weight 8) and size distribution (weight 7) parameters, and the lowest was given to ZP values (weight 1) as the combination of surfactants does not anticipate problems of colloidal instability (29).

Genetic algorithms simulate natural selection in biological environments (28). Thus, the ANN models generate a high number of predictions of the results of variables combination. Then the genetic algorithm selects the most suitable ones considering the desirability previously established for NLC properties. Based on the selection, a new generation of solutions is created, and a new selection of the best ones is carried out, as shown in **Figure 6.5**. After several of these processes, the compromise solution is reached for those variables that give rise to the NLC desirable parameters, that is, to the optimal formulation.

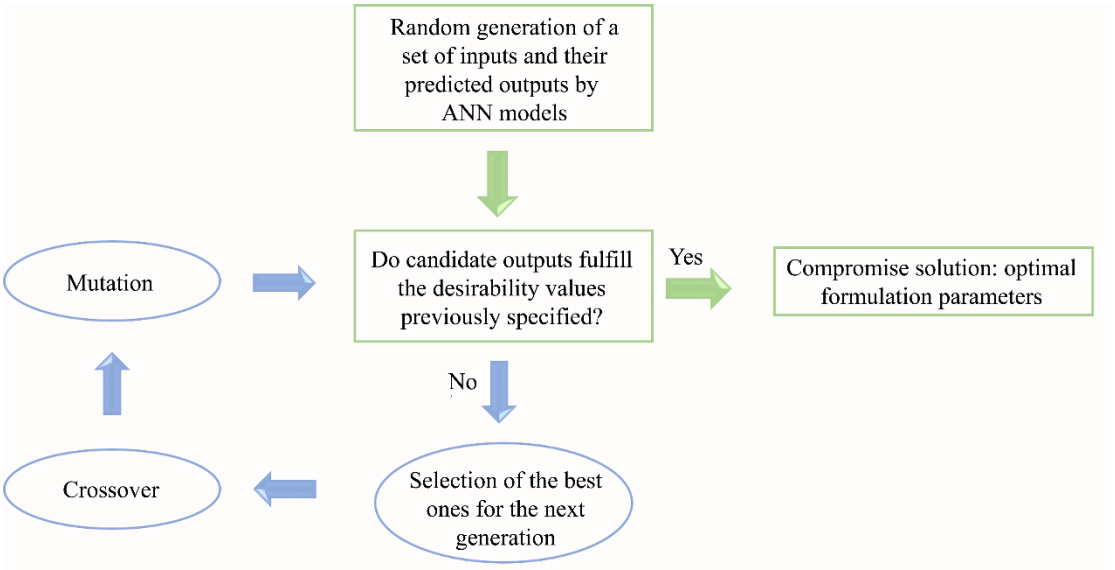

Figure 6.5.Steps followed in the formulation optimization process of RFB-loaded NLC using ANN and Genetic algoriths (INForm®).

According to INForm®, optimal RFB-loaded NLC selected by INForm® can be achieved using 75% of liquid lipid, 0.5% of lecithin, 1.9% of Tween® 80 and a stirring speed of 14892 rpm. Presumably, nanoparticle formulations should exhibit a mean size of 152 nm, a PDI of 0.23 and a ZP of -19 mV, along with an EE and DL of 100% and 5%, respectively (**Table 6.1**).

Table 6.1. Physicochemical characterization of optimized RFB-loaded NLC.

RFB-loaded NLC	Predicted values	Experimental values	Experimental values (purified NLC)
Size (nm)	152	176±17	151 ± 34
PDI	0.23	0.22±0.03	0.22 ± 0.02
ZP (mV)	-19	-17±0	-24 ± 2
EE%	100	95.2±2.7	92.83 ± 3.75
DL%	5	4.7±0.1	4.62 ± 0.33

The experimental production of NLC under these conditions allowed the validation of the optimization process. As shown in **Table 6.1**, experimental results are completely in agreement with predictions. Even after a dialysis purification process intended to avoid interferences from unincorporated components (purified NLC), NLC maintain acceptable values for all parameters. Little increments in negative charge of ZP after purification can be attributed to the removal of Tween® 80 (26). The strong agreement between the predicted and the experimental values highlights the applicability of AI tools in optimizing NLC formulations.

A full characterization of the developed NLC formulations was also carried out. First, optimal formulation has proven to be stable after 1 month of storage at 5 ± 1°C, since no statistically significant differences have been found among stored and fresh formulations ($p \geq 0.01$), except for ZP, experiencing a slight decline. This decrease could even improve colloidal stability by electrostatic repulsion (29).

Blank and RFB-loaded optimal NLC were produced and characterized by the following assays. The only relevant difference among formulations was the slightly lower particle size reported for blank NLC (111±3 nm), which was associated with the accommodation space required for the drug within the nanoparticles (24).

NLC formulations were characterized in terms of morphology and thermal stability. Both blank and RFB-loaded NLC exhibit a spheroidal morphology, closer to a disk than to a sphere as confirmed by transmission electron microscopy (TEM) and Atomic force microscopy (AFM) (**Figure 4.2 and 4.3**). Morphological analysis also allows us to withdraw some hypothesis about the polymorphic state of the lipids in the nanoparticles. As previously mentioned, lipids exist, mainly, in three different polymorphic forms (α, β and β´), and LN can suffer from polymorphic transitions after formulation, which are known to affect their stability and drug loading capacity (30). In this way, the spheroidal morphology of NLC formulations revealed by AFM, along with the structure with concentric layers showing a high electron density in the nanoparticle center, that could be observed in some TEM micrographs (**Figure 4.2B**), suggest the presence of the polymorphic α-form of lipids (31). The predominance of this polymorphic form has been related with positive features, such as high loading capacity and low drug leakage (32).

DLS analysis consisting of subjecting NLC to heating and cooling steps (25 °C - 90 °C- 25 °C), has previously been used to investigate the ability of lipid colloidal carriers to withstand high-temperature related procedures (33, 34), and can be useful for the transformation of NLC dispersions into dry powders. Negligible variations found in particle size of NLC with temperature (**Figure 4.1**) indicate suitability of these nanosystems for further temperature-related processing.

Applicability of RFB-loaded NLC to target intestinal macrophages

The suitability of the developed NLC formulations to provide a targeted drug delivery inside intestinal macrophages, where MAP is known to stablish a persisting infection (35) was also evaluated. RFB-loaded NLC are intended to pass across the epithelial barrier, towards the intestinal lumen, where they could be internalized by intestinal macrophages, releasing RFB content within these phagocytic cells (**Figure 6.6**).

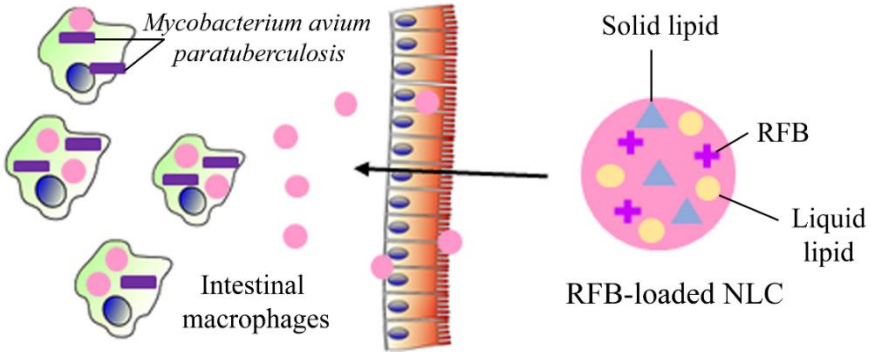

Figure 6.6. Schematic representation of RFB-loaded NLC passage across intestinal barrier and subsequent internalization by intestinal macrophages infected with MAP. Image extracted from Rouco et al (36).

Nanocarriers are expected to reach the intestinal epithelium unaltered. The ability of NLC to control RFB release in simulated intestinal fluid (SIF) was demonstrated by an *in vitro* dissolution test. Results revealed that NLC do not release RFB through the whole assay, suggesting that they could be able to efficiently control drug release in the intestinal environment.

NLC ability to cross the intestinal barrier was estimated through a permeability study performed in Caco-2 monolayers, generally accepted to study drug permeability, since its results correlate well with human *in vivo* absorption (37). After a two-hour lag period, RFB-loaded nanocarriers permeability increased linearly with time, reaching a RFB permeated concentration of 0.43 ± 0.01 µg/mL at 24 hours, and 0.9 ± 0.1 µg/mL after 48 hours (**Figure 4.8**). The apparent permeability coefficient was slightly higher than 2×10^{-6} cm/s, a threshold above which the absorption of the drug in humans is considered complete (38), indicating that RFB-loading NLC exhibit a suitable permeability across Caco-2 cell monolayers.

Considering that the *in vitro* minimum inhibitory concentrations (MIC) of RFB in strains isolated from humans and animals are in the range of 0.5-4 µg/mL (39), it could be deduced that after 24 hours, which is the colonic transit time reported for Crohn´s disease patients (40), NLC allowed RFB permeation at a concentration close to MIC. Certain pathological factors such as disruption of the epithelial barrier or the preferential accumulation of nanoparticles in inflamed intestinal areas with a remarkable infiltration of macrophages, would trigger an *in vivo* permeability of the nanosystems even higher than that reported by this assay (40). This would ensure the administration of an effective dose of drug to infected macrophages.

Once RFB-loaded NLC overcome the intestinal barrier, they are expected to get in contact with intestinal macrophages, as they are mainly located in the lamina propria, below the epithelial monolayer (41). Therefore, in order to analyze NLC interaction with those cells, biocompatibility and internalization studies were performed in THP-1 derived macrophages.

NLC biocompatibility was tested at several nanoparticle concentrations (0.3, 0.12, 0.06 and 0.06 mg/mL). Cells were also treated with equivalent RFB concentrations, as control. Blank and RFB-loaded NLC displayed good biocompatibility **(Figure 4.5A)**, leading to cell viabilities ≥ 70% for concentrations lower than 0.3 mg/mL. The statistical analysis performed (two-way ANOVA, $p < 0.05$) showed a significant effect of the treatment (blank or RFB-loaded NLC), the concentration of NLC and their interaction on cell viability. Furthermore, Tukey´s post hoc test performed, revealed the existence of a concentration dependent cytotoxic effect for both NLC formulations. No significant differences in cell viability were found between RFB-loaded NLC at 0.06 mg/mL and 0.12 mg/mL, and hence, the last one was selected for further assays. The NLC cytotoxicity could be associated with the incorporation of emulsifiers or oleic acid in the formulations, as proposed by other authors (42, 43), since as shown in **Figure 4.5B** no significant differences were found in cell viability for equivalent RFB concentrations.

IC_{50} for RFB-loaded NLC was 0.18 mg/mL (**Figure 4.6**), which is in line with previously published works, where IC_{50} values were mostly in the range of 0.1-1 mg/mL of lipid nanoparticles (44). Outcomes demonstrated that NLC exhibit a good biocompatibility and safety at 0.12 mg/mL.

Confocal microscopy revealed that both, blank and RFB-loaded NLC formulations were efficiently internalized by macrophages (**Figure 4.7**), which constitutes a promising start point for the treatment of intracellular MAP infections.

Quantitatively, the percentage of internalization was higher for RFB-loaded NLC (13.39 ± 1.44%) than for blank ones (8.33 ± 1.15%) with statistically significant differences ($p < 0.05$) between them. This must be related to the larger size of loaded NLC, as particulate systems uptake tends to increase progressively with particle size (45). Considering that the uptake reported for RFB-loaded NLC would lead to an internalized RFB amount of 0.078 µg in cell volume of 1.2475×10^{-4} mL, approximately, an internalized concentration of 625 µg/mL could be achieved, which largely exceeds the MIC range, guaranteeing effective intracellular RFB concentrations.

After intestinal macrophages internalization, NLC should be able to release RFB content in the intracellular environment. On the purpose of testing the release profile of NLC inside phagocytic cells, a simulated intracellular medium obtained from a murine macrophage cell line lysate was employed, intending to reproduce, as much as possible, *in vivo* conditions. It is necessary to consider that in physiological conditions, drug release from lipid nanoparticles is expected to occur by both, diffusion and erosion mechanisms (46). Favorable conditions within the nanoparticle triggered by the high solubility of RFB in the lipid matrix, would hinder drug diffusion to aqueous release medium (47), making lipid matrix degradation a worthy path to explore, which usually involves enzymatic activity (46).

Results obtained in the release studies show that after one hour lag period, drug started to be detectable in the simulated intracellular medium, increasing progressively to reach 1.46 ± 0.47 µg of RFB after 16 hours (0.1 ± 0.03%). The slight drug release could be easily associated to the dilution of macrophage enzymes required to prepare the simulated intracellular medium, but results represent an interesting proof of concept of the controlled and selective drug release within macrophages. The enzyme concentration is expected to be higher inside phagocytic cells in physiological conditions, therefore a higher drug release is envisaged *in vivo*, which allow the treatment of intracellular infections, such as that occurring in Crohn´s disease.

Transformation of NLC dispersions into a solid dosage form

Lipid nano-dispersions are subjected to several physicochemical phenomena, favoring nanocarriers destabilization (29). NLC formulations are likely to destabilize in the gastric environment due to lipid processing under acidic conditions (48), which hinders their oral administration. Therefore, it is necessary the transformation of NLC dispersions into solid dosage forms, easy to administer as enteric-coated pellets, tablets or capsules.

Lyophilization is a suitable and widely employed technique to improve long-term nanoparticles stability (49). Despite its reported complexity, most lyophilization studies lack an in–depth analysis of the interactions between the process variables or the mechanisms involved (49), and their possible impact on reproducibility and final properties of the lyophilized powders (LP).

Optimal NLC exhibited a good ability to withstand lyophilization process without CPs. However, LP exhibited signs of formulation collapse such as a gummy-like appearance and a challenging re-dispersibility (49), making necessary CPs use.

NFL was employed to give insight into the physicochemical phenomena triggering lyophilization process and cryoprotectant mechanism of sugars, in order to stablish a rational lyophilization procedure for NLC. The effect of speed of freezing, type and proportion of cryoprotectant on the characteristics of LP products (expressed as Δ size, Δ PDI and Δ ZP of LP, regarding initial NLC dispersions) in blank NLC formulations was studied (**Figure 6.7**).

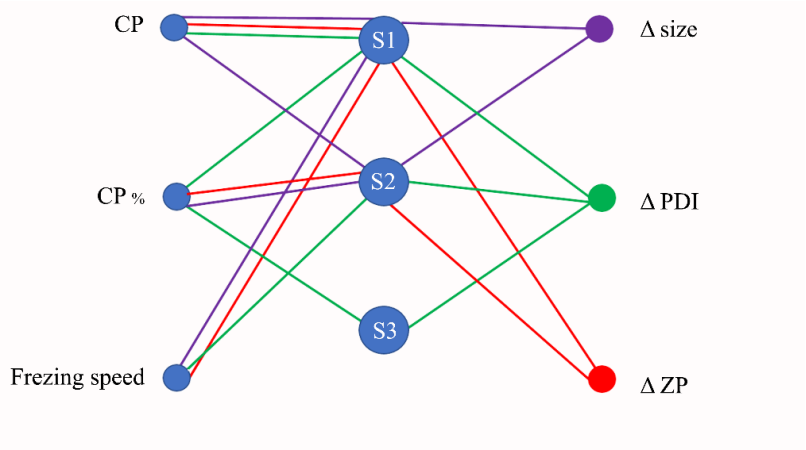

Figure 6.7. Lyophilization parameters (inputs, left) affecting LP properties under study (outputs, right), according to the different submodels (S) gathered from NFL model 1.

Furthermore, the effect of specific features of CPs, such as molecular weight (MW) and osmolarity (Π), along with their interaction with freezing speed, have also been investigated (**Figure 6.8**). Suitable NFL models were obtained for all the outputs under evaluation, except in the case of Δ ZP (**Tables 5.2** and **5.3**), probably because of the high similarity between the experimental values obtained for this parameter (**Figure 5.4**).

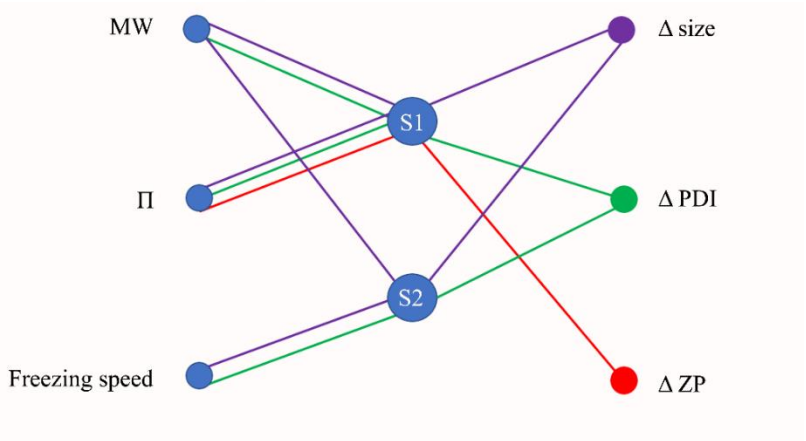

Figure 6.8. Lyophilization parameters (inputs, left) affecting LP properties under study (outputs, right), according to the different submodels (S) gathered from NFL model 2.

NFL allowed to establish general rules to carry out a rational lyophilization procedure for these NLC. A traffic light classification system has been generated from IF-THEN rules obtained by NFL to stablish the effect of the CP selected, its concentration (%CP) and the freezing speed employed, on LP characteristics (Δ size and Δ PDI) (**Figure 5.4**). Red, yellow and green colours indicate not advisable, medium and advisable conditions, respectively to obtain low Δ size or Δ PDI.

According to the classification system proposed, monosaccharides such as glucose and fructose should be employed at low-medium concentrations (up to 10%, preferably). On the other hand, disaccharides such as sucrose should be employed at medium-high concentrations (above 12.5%, preferably), while lactose and trehalose can be successfully employed at medium concentrations (2.5-10% and 3.75-12.5%, respectively). However, the addition of sugar alcohols, as mannitol and sorbitol, would not be advisable in NLC lyophilization. The limited effectivity observed for this compounds is in agreement with previous works, in which their poor ability to preserve nanoparticles or biomolecules, such as proteins, was associated with crystallization phenomena (50, 51), which could contribute to NLCs destabilization (50).

It is also interesting to mention that %CP requirements proposed by NFL software for several CPs, such as sucrose, fructose, glucose and trehalose, agree with sugar concentrations previously defined as of best protective effect in several works (52, 53). Besides, it is important to notice that these %CP requirements were reported to be higher for disaccharides than for monosaccharides, according to the "IF-THEN" rules derived from both NFL models (data shown in **Annex III**).

This fact might be associated with diffusion phenomena of CPs during freezing, towards the cryo-concentrated solution, in which nanoparticles are included (49, 54). The amount of CP available to protect the nanocarriers in the solution would depend on the diffusion rate of CP towards the cryo-concentrated phase (54), which would vary as a function of the MW_{CP}, being faster for low MW CPs (monosacharides) than for high MW ones (disaccharides). Hence, the fact that the addition of a high amount of a poorly diffusive compound, could increase its presence in the cryo-concentrated phase, counteracting its slow diffusion and allowing nanoparticles protection (54), explains the optimal %CP proposed in this work.

Concerning freezing speed, it was observed that, as a general trend, and specially, in the case of monosaccharides, a fast speed seems to favour the obtention of NLC of low Δ size and Δ PDI values (NFL model 1, **Annex III**). This is in agreement with previous theories suggesting that a fast supercooling leads to the generation of small ice crystals, reducing mechanical stress over nanoparticles (49). Nevertheless, for higher MW CPs, as is the case of disaccharides, a higher independence of freezing speed employed was observed (NFL model 2, **Annex III**).

This phenomenon might be associated with with the superior Tg of these compounds (55), that would allow them to vitrify earlier during freezing, protecting NLC within a vitreous matrix and minimizing the effects of freezing. Furthermore, it could also contribute to explain the controversy currently reflected by the scientific literature related to the most appropriate freezing speed for nanocarriers lyophilization (54, 56).

In view of the results obtained, it can be concluded that this step of the work highlights the importance of QbD to take the full potential of available resources by rationally stablishing a

lyophilization process suitable for NLC. Furthermore, the knowledge derived from this study would allow for the conversion of the developed RFB-loaded NLC formulations into a solid dosage form, suitable for oral administration. The inclusion of this solid products into gastro-resistant capsules or tablets, would allow the nanocarriers to safely reach the intestinal environment, in which their promising characteristics have already been demonstrated.

REFERENCES

1. Chen H, Khemtong C, Yang X, Chang X, Gao J. Nanonization strategies for poorly water-soluble drugs. Drug Discov Today. 2011; 16 (7-8):354-360.
2. Kuenstner JT, Naser S, Chamberlin W, Borody T, Graham DY, McNees A, et al. The Consensus from the Mycobacterium avium ssp. paratuberculosis (MAP) Conference 2017. Front Public Health. 2017; 5: 208.
3. Inoue Y, Yoshimura S, Tozuka Y, Moribe K, Kumamoto T, Ishikawa T, et al. Application of ascorbic acid 2-glucoside as a solubilizing agent for clarithromycin: solubilization and nanoparticle formation. Int J Pharm. 2007; 331 (1): 38-45.
4. Zhang Y, Feng J, McManus SA, Lu HD, Ristroph KD, Cho EJ, et al. Design and Solidification of Fast-Releasing Clofazimine Nanoparticles for Treatment of Cryptosporidiosis. Mol Pharm. 2017; 14 (10): 3480-3488.
5. Shanmuga Priya A, Sivakamavalli J, Vaseeharan B, Stalin T. Improvement on dissolution rate of inclusion complex of Rifabutin drug with beta-cyclodextrin. Int J Biol Macromol. 2013; 62: 472-80.
6. Taratula O, Kuzmov A, Shah M, Garbuzenko OB, Minko T. Nanostructured lipid carriers as multifunctional nanomedicine platform for pulmonary co-delivery of anticancer drugs and siRNA. J Control Release. 2013;171 (3): 349-357.
7. Qi R, Li YZ, Chen C, Cao YN, Yu MM, Xu L, et al. G5-PEG PAMAM dendrimer incorporating nanostructured lipid carriers enhance oral bioavailability and plasma lipid-lowering effect of probucol. J Control Release. 2015; 210: 160-168.
8. Gainza G, Bonafonte DC, Moreno B, Aguirre JJ, Gutierrez FB, Villullas S, et al. The topical administration of rhEGF-loaded nanostructured lipid carriers (rhEGF-NLC) improves healing in a porcine full-thickness excisional wound model. J Control Release. 2015; 197: 41-47.
9. Muchow M, Maincent P, Müller RH. Lipid nanoparticles with a solid matrix (SLN, NLC, LDC) for oral drug delivery. Drug Dev Ind Pharm. 2008; 34 (12): 1394-1405.
10. Danaei M, Dehghankhold M, Ataei S, Hasanzadeh Davarani F, Javanmard R, Dokhani A, et al. Impact of Particle Size and Polydispersity Index on the Clinical Applications of Lipidic Nanocarrier Systems. Biomacromolecules. 2018;10 (2): 57.
11. Desai N. Challenges in development of nanoparticle-based therapeutics. AAPS J. 2012; 14 (2): 282-295.
12. Diaz-Rodriguez P, Landin M. Smart design of intratumoral thermosensitive beta-lapachone hydrogels by Artificial Neural Networks. Int J Pharm. 2012; 433 (1-2):112-118.
13. Rodriguez-Dorado R, Landin M, Altai A, Russo P, Aquino RP, Del Gaudio P. A novel method for the production of core-shell microparticles by inverse gelation optimized with artificial intelligent tools. Int J Pharm. 2018; 538 (1-2): 97-104.
14. Landin M, Rowe RC, York P. Advantages of neurofuzzy logic against conventional experimental design and statistical analysis in studying and developing direct compression formulations. Eur J Pharm Sci. 2009; 38 (4): 325-331.
15. Khosa A, Reddi S, Saha RN. Nanostructured lipid carriers for site-specific drug delivery. Biomed Pharmacother. 2018; 103: 598-613.

16. Takalkar D, Desai N. Nanolipid Gel of an Antimycotic Drug for Treating Vulvovaginal Candidiasis-Development and Evaluation. AAPS PharmSciTech. 2018; 19 (3): 1297-1307.
17. Ogawa S, Decker EA, McClements DJ. Production and characterization of o/w emulsions containing droplets stabilized by lecithin−chitosan−pectin mutilayered membranes. J Agric Food Chem. 2004; 52 (11): 3595-3600.
18. Shah R, Eldridge D, Palombo E, Harding I. Composition and structure. In: Shah R, Eldridge D, Palombo E, Harding I (Eds). Lipid nanoparticles: production, characterization and stability. 1st edition. New York, USA: Springer International Publishing; 2015. p. 11-22.
19. Crabol Y, Catherinot E, Veziris N, Jullien V, Lortholary O. Rifabutin: where do we stand in 2016?. J Antimicrob Chemother. 2016; 71 (7): 1759-1771.
20. Alvarez-Trabado J, Diebold Y, Sanchez A. Designing lipid nanoparticles for topical ocular drug delivery. Int J Pharm. 2017; 532 (1): 204-217.
21. Malvern Instruments Limited. Dynamic light scattering common terms defined [White paper]. Worcestershire, UK: 2011.
22. Rouco H, Diaz-Rodriguez P, Rama-Molinos S, Remunan-Lopez C, Landin M. Delimiting the knowledge space and the design space of nanostructured lipid carriers through Artificial Intelligence tools. Int J Pharm. 2018; 553 (1-2): 522-530.
23. Song A, Zhang X, Li Y, Mao X, Han F. Effect of liquid-to-solid lipid ratio on characterizations of flurbiprofen-loaded solid lipid nanoparticles (SLNs) and nanostructured lipid carriers (NLCs) for transdermal administration. Drug Dev Ind Pharm. 2016; 42 (8): 1308-1314.
24. Gaba B, Fazil M, Khan S, Ali A, Baboota S, Ali J. Nanostructured lipid carrier system for topical delivery of terbinafine hydrochloride. Bull Fac Pharm Cairo Univ. 2015; 53 (2): 147-159.
25. Ham-Pichavant F, Sèbe G, Pardon P, Coma V. Fat resistance properties of chitosan-based paper packaging for food applications. Carbohydr Polym. 2005; 61 (3): 259-265.
26. Schubert MA, Muller-Goymann CC. Characterisation of surface-modified solid lipid nanoparticles (SLN): influence of lecithin and nonionic emulsifier. Eur J Pharm Biopharm. 2005; 61 (1-2): 77-86.
27. Müller RH, Radtke M, Wissing SA. Nanostructured lipid matrices for improved microencapsulation of drugs. Int J Pharm. 2002; 242 (1-2): 121-128.
28. Landin M, Rowe RC. Artificial neural networks technology to model, understand, and optimize drug formulations. In: Aguilar JE (Ed). Formulation Tools for Pharmaceutical Development. 1st edition. Cambridge, UK: Woodhead publishing; 2013. p. 7-37.
29. Heurtault B. Physico-chemical stability of colloidal lipid particles. Biomaterials. 2003; 24 (23): 4283-4300.
30. Shah M, Pathak K. Development and statistical optimization of solid lipid nanoparticles of simvastatin by using 2(3) full-factorial design. AAPS PharmSciTech. 2010; 11 (2): 489-496.
31. Bunjes H, Steiniger F, Richter W. Visualizing the structure of triglyceride nanoparticles in different crystal modifications. Langmuir. 2007; 23 (7): 4005-4011.

32. Gordillo-Galeano A, Mora-Huertas CE. Solid lipid nanoparticles and nanostructured lipid carriers: A review emphasizing on particle structure and drug release. Eur J Pharm Biopharm. 2018; 133: 285-308.
33. Gaspar DP, Faria V, Goncalves LM, Taboada P, Remunan-Lopez C, Almeida AJ. Rifabutin-loaded solid lipid nanoparticles for inhaled antitubercular therapy: Physicochemical and in vitro studies. Int J Pharm. 2016; 497 (1-2): 199-209.
34. Mancini G, Lopes RM, Clemente P, Raposo S, Gonçalves LMD, Bica A, et al. Lecithin and parabens play a crucial role in tripalmitin-based lipid nanoparticle stabilization throughout moist heat sterilization and freeze-drying. Eur J Lipid Sci Technol. 2015; 117 (12): 1947-1959.
35. Murphy JT, Sommer S, Kabara EA, Verman N, Kuelbs MA, Saama P, et al. Gene expression profiling of monocyte-derived macrophages following infection with Mycobacterium avium subspecies avium and Mycobacterium avium subspecies paratuberculosis. Physiol Genomics. 2006; 28 (1): 67-75.
36. Rouco H, Diaz-Rodriguez P, Gaspar DP, Gonçalves L, Cuerva M, Remuñán-López C, et al. Rifabutin-Loaded Nanostructured Lipid Carriers as a Tool in Oral Anti-Mycobacterial Treatment of Crohn's Disease. Nanomaterials. 2020;10(11):2138.
37. Chaves LL, Costa Lima SA, Vieira ACC, Barreiros L, Segundo MA, Ferreira D, et al. Nanosystems as modulators of intestinal dapsone and clofazimine delivery. Biomed Pharmacother. 2018; 103: 1392-1396.
38. Grès MC, Julian B, Bourrié M, Meunier V, Roques C, Berger M, et al. Correlation between oral drug absorption in humans, and apparent drug permeability in TC-7 cells, a human epithelial intestinal cell line: comparison with the parental Caco-2 cell line. Pharm Res. 1998; 15 (5): 726-733.
39. Zanetti S, Molicotti P, Cannas S, Ortu S, Ahmed N, Sechi LA. "In vitro" activities of antimycobacterial agents against Mycobacterium avium subsp. paratuberculosis linked to Crohn's disease and paratuberculosis. Ann Clin Microbiol Antimicrob. 2006; 5:27.
40. Mohan LJ, Daly JS, Ryan BM, Ramtoola Z. The future of nanomedicine in optimising the treatment of inflammatory bowel disease. Scand J Gastroenterol. 2019; 54 (1): 18-26.
41. Bain CC, Mowat AM. Intestinal macrophages-specialised adaptation to a unique environment. Eur J Immunol. 2011; 41 (9): 2494-2498.
42. Schöler N, Olbrich C, Tabatt K, Müller R, Hahn H, Liesenfeld O. Surfactant, but not the size of solid lipid nanoparticles (SLN) influences viability and cytokine production of macrophages. Int J Pharm. 2001; 221 (1-2): 57-67.
43. Yin H, Too HP, Chow GM. The effects of particle size and surface coating on the cytotoxicity of nickel ferrite. Biomaterials. 2005; 26 (29): 5818-5826.
44. Doktorovova S, Souto EB, Silva AM. Nanotoxicology applied to solid lipid nanoparticles and nanostructured lipid carriers - a systematic review of in vitro data. Eur J Pharm Biopharm. 2014; 87 (1): 1-18.
45. Chono S, Tanino T, Seki T, Morimoto K. Influence of particle size on drug delivery to rat alveolar macrophages following pulmonary administration of ciprofloxacin incorporated into liposomes. J Drug Target. 2006; 14 (8): 557-566.

46. Pathak K, Keshri L, Shah M. Lipid nanocarriers: Influence of lipids on product development and pharmacokinetics. Crit Rev Ther Drug Carrier Syst. 2011; 28 (4): 357-393.
47. Iqbal N, Vitorino C, Taylor KM. How can lipid nanocarriers improve transdermal delivery of olanzapine? Pharm Dev Technol. 2017; 22 (4): 587-596.
48. Ana R, Mendes M, Sousa J, Pais A, Falcao A, Fortuna A, et al. Rethinking carbamazepine oral delivery using polymer-lipid hybrid nanoparticles. Int J Pharm. 2019; 554: 352-365.
49. Abdelwahed W, Degobert G, Stainmesse S, Fessi H. Freeze-drying of nanoparticles: formulation, process and storage considerations. Adv Drug Deliv Rev. 2006; 58 (15):1688-1713.
50. Andreani T, Kiill CP, de Souza ALR, Fangueiro JF, Doktorovová S, Garcia ML, et al. Effect of cryoprotectants on the reconstitution of silica nanoparticles produced by sol–gel technology. J Therm Anal Calorim. 2014; 120 (1):1001-1007.
51. Piedmonte DM, Summers C, McAuley A, Karamujic L, Ratnaswamy G. Sorbitol Crystallization Can Lead to Protein Aggregation in Frozen Protein Formulations. Pharm Res. 2006; 24 (1): 136-146.
52. Hua ZZ, Li BG, Liu ZJ, Sun DW. Freeze-Drying of Liposomes with Cryoprotectants and Its Effect on Retention Rate of Encapsulated Ftorafur and Vitamin A. Dry Technol. 2003; 21 (8): 1491-1505.
53. Varshosaz J, Ghaffari S, Khoshayand MR, Atyabi F, Dehkordi AJ, Kobarfard F. Optimization of freeze-drying condition of amikacin solid lipid nanoparticles using D-optimal experimental design. Pharm Dev Technol. 2010; 17 (2): 187-194.
54. Lee MK, Kim MY, Kim S, Lee J. Cryoprotectants for freeze drying of drug nano-suspensions: effect of freezing rate. J Pharm Sci. 2009; 98 (12):4808-4817.
55. Aksan A, Toner M. Isothermal Desiccation and Vitrification Kinetics of Trehalose−Dextran Solutions. Langmuir. 2004; 20 (13): 5521-5529.
56. Yue PF, Li G, Dan JX, Wu ZF, Wang CH, Zhu WF, et al. Study on formability of solid nanosuspensions during solidification: II novel roles of freezing stress and cryoprotectant property. Int J Pharm. 2014; 475 (1-2): 35-48.

7. CONCLUSIONS

USC
UNIVERSIDADE
DE SANTIAGO
DE COMPOSTELA

This thesis focused on the development of a robust and reproducible Nanostructured lipid carrier (NLC) formulation, for the oral administration of hydrophobic anti-mycobacterial drugs, potentially useful for treating persistent intracellular infections, such as those that occur in intestinal macrophages of Crohn´s disease (CD) patients.
Results obtained allowed us to withdraw the following conclusions:

1. We have developed a nanostructured lipid carrier formulation (NLC), loaded with the model hydrophobic anti-mycobacterial drug rifabutin (RFB) up to 5%, through a simple and reproducible manufacturing process. The developed nanosystems exhibited spheroidal morphology and suitable physicochemical properties in terms of particle size, size distribution and surface charge, along with an adequate drug payload and a good safety and stability profile.

2. Artificial Intelligence tools such as Neurofuzzy logic (NFL), Artificial Neural Networks (ANN) and Genetic algorithms have proven to be useful to assist formulation development of NLC. NFL provided information regarding physicochemical interactions occurring among nanoparticle components, while ANN and Genetic algorithms allowed to predict the composition and operation conditions to obtain an optimal formulation, experimentally validated.

3. It was found that permeability across Caco-2 cell monolayers, macrophage uptake and selective RFB release in intracellular medium provided by NLC would ensure the achievement of an intracellular effective RFB dose inside phagocytic cells, making RFB-loaded NLC a promising strategy for the treatment of intracellular infections, such as those occurring in Crohn´s disease.

4. A rationally designed lyophilization procedure using NFL was successfully developed to convert NLC dispersions into solid dosage forms. NFL allowed a better understanding of carbohydrate cryoprotectants mechanism of action along with the physicochemical phenomena behind lyophilization process. NLC lyophilized powders were easily re-dispersible while maintaining initial NLC properties.

This work highlights the role of nanotechnology, and specially of NLC, to overcome solubility and permeability problems of antibiotic drugs and to improve intracellular infections. Furthermore, it also emphasizes the utility of Artificial Intelligence tools for developing nanoparticles within the Quality by Design concept giving robust and reproducible manufacturing processes, which undoubtedly should accelerate the transition of nanoparticulate administration systems towards their clinical use.

USC
UNIVERSIDADE
DE SANTIAGO
DE COMPOSTELA

8. ONGOING EXPERIMENTS AND FUTURE PERSPECTIVES

USC
UNIVERSIDADE
DE SANTIAGO
DE COMPOSTELA

Engineered NLC formulations could be improved by employing targeting strategies that increase their uptake by macrophages (1, 2).

On this purpose, preliminary work focused on the development and analysis of different targeting strategies and on the *in vitro* evaluation of the anti-mycobacterial efficacy of the developed nanocarriers have been carried out. This section includes a summary of the work carried out to date in this framework, together with the most relevant findings obtained. Finally, future prospects will be discussed.

8.1. ONGOING EXPERIMENTS

8.1.1. Targeting strategies

With the aim of increasing the targeting potential of the developed RFB-loaded NLC, two strategies were followed, including nanoparticle formulations coating with mannose or Mycolic acids.

8.1.1.1. Development of mannose-coated NLC

Mannose receptors are highly expressed in macrophages (1, 3), therefore, coating the nanoparticle formulations with mannose can be an approach to target macrophages and increase the NLC uptake. Mannose coating of NLC was carried out following two different procedures. The first one was based on a previously published protocol (1), with slight modifications (which we will refer to as mannose coating 1). In brief, a 2% w/w of stearylamine (Sigma Aldrich, USA) was included in the lipid phase during NLC formulation process, in order expose amine groups on the nanoparticle surface. Then, a 50 mM mannose (Sigma Aldrich, USA) solution was prepared in a pH=4 acetate buffer and incubated with NLC suspensions in a 1:1 proportion, under gentle stirring for 48 hours. The low pH employed in this process was intended to promote the ring opening of mannose molecules, favoring the reaction of the aldehyde group with free amine exposed onto the nanoparticle surface, leading to the generation of a Schiff´s base (-NCH-) (1). An overnight dialysis step, intended to remove non-incorporated mannose and residual formulation components, was performed.

The second procedure for coating RFB-loaded NLC with mannose (mannose coating 2) is simple and based on the tendency of nanoparticles to adsorb molecules due to their high surface energy (4), and on the reported ability of carbohydrates to stablish hydrogen bonds among their OH groups and the nanoparticle surface (5). It consisted on only a 24/48-hour nanoparticle incubation step with a 4% (w/v) mannose aqueous solution, using a 1:1 NLC/mannose solution ratio. The dialysis stage was also carried out overnight. A graphical representation of the mannose-coated nanoparticles obtained using the two coating procedures, was included in **Figure 8.1.**

8.1.1.2. Development of Mycolic acid-coated NLC

NLC coating was also carried out with Mycolic acids (MAs). This strategy was intended to increase nanoparticle uptake by macrophages by mimicking the mycolic acid envelope exhibited by pathogenic mycobacteria. These 2-alkyl, 3-hydroxy long-chain fatty acids are main and distinctive components of the mycobacterial cell envelope of several human

pathogens such as *Mycobacterium tuberculosis* and *Mycobacterium avium paratuberculosis* (6, 7). These components were reported to play an essential role on mycobacterial growth and survival (6, 7), and are responsible for important features exhibited by mycobacteria such as resistance to dehydration and chemical injury, virulence, reduced permeability to lipophilic antibiotics or ability to stablish persisting infections within the host, among others (8). Furthermore, in a recently published work (9), these compounds were encapsulated into isoniazid-loaded Poly (lactic-co-glycolic acid) (PLGA) nanoparticles, and results described by the authors suggested that after encapsulation, MAs are able to express onto the nanoparticle surface, leading to an increased uptake by murine macrophages (9).

For this purpose, MAs adhered directly to the nanoparticle surface with the aim of achieving its higher exposure. However, due to the high hydrophobicity of this compounds, incubation strategies involving aqueous solutions, such as those used for mannose, were not possible. As an alternative, a 1 mg/mL solution of MAs (Mycolic acids from *Mycobacterium tuberculosis*, Sigma Aldrich, USA), in oleic acid was performed (OA-MA solution), which was then homogenized with the RFB-loaded NLC dispersion through a pipette tip. This gentle homogenization step was intended to allow a direct contact between NLC and the OA-MA solution, which is expected to cover the nanoparticle surface, as shown in **Figure 8.1**.

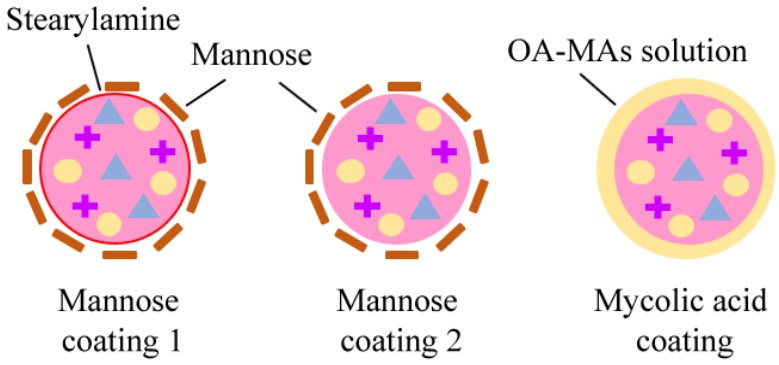

Figure 8.1. Graphical representation of A) Mannose-coated RFB-loaded NLC obtained by means of the first protocol described, B) Mannose-coated RFB-loaded NLC obtained by means of the second procedure, and C) MA-coated RFB-loaded NLC.

8.1.1.3. Physicochemical characterization and *in vitro* uptake analysis of coated NLC

After nanoparticle coating, particle size, PDI and ZP were determined in a Zetasizer Nano ZS, and compared with values reported for uncoated NLC, in order to evaluate changes in nanoparticles properties that could indicate the successful surface modification of NLC formulations. Particle size and size distribution for mannose-coated NLC remained almost unchanged (**Table 8.1)** confirming that mannosylation does not induce significant changes in NLC parameters, as reported in previous works (1, 10). However, mannose coating 1 procedure modifies the ZP towards positive values (4 ± 0 mV). This NLC positive surface charge is associated with the presence of amine groups in the nanoparticle surface due to stearylamine addition, confirming the successful coating of the nanosystems (1). Conversely, the mannose coating 2 procedure did not induce significant changes in ZP values (-24 ± 0.3 mV).

The negative ZP obtained for MA-coated NLC (-26 ± 0.1 mV) can be associated with the negative charge of the carboxyl groups of fatty acids, such as oleic and mycolic acids (11). Since oleic acid (OA) is a main component of NLC matrix, ZP modification due to nanoparticle coating with OA-MA is subtle. Furthermore, after coating with MAs a significant increase in the particle size of NLC (219 ± 31 nm) is observed, which may be associated with the generation of an OA layer on the surface of the NLC, as shown in **Figure 8.1**. Changes in particle size and zeta potential are indicative of a successful MA coating of RFB loaded NLC. However, excess OA-MA solution may involve the risk of instability, due to the coalescence of lipid droplets.

Table 8.1. Physicochemical characteristics and uptake (%) by human macrophages of naked RFB-loaded NLC, mannose-coated RFB-loaded NLC and mycolic acid-coated RFB-loaded NLC.

Formulation	Naked RFB-loaded NLC	RFB-loaded NLC + Mannose coating 1	RFB-loaded NLC + Mannose coating 2	RFB-loaded NLC + Mycolic acid coating
Size (nm)	151 ± 34	153 ± 2	148 ± 1	219 ± 31
PDI	0.22 ±0.02	0.16 ± 0.01	0.18 ± 0.02	0.61 ± 0.15
Zeta potential (mV)	-24 ± 2	4 ± 0	-24 ± 0.3	-26 ± 0.1
Macrophage Uptake (%)	14.66 ± 0.55	11.80 ± 1.74	14.66 ± 2.40	55.94 ± 5.62

Furthermore, nanoparticle uptake of naked and coated nanocarriers was also studied, in order to assess the targeting ability of the modified NLC formulations developed. Uptake studies were performed following the quantitative approach described in Chapter II. In this way, as can be seen in **Table 8.1**, no improvement in cell uptake was achieved with any of the mannose coatings. Uptake values of 11.80 ± 1.74% and 14.66 ± 2.40% were obtained for mannose coatings 1 and 2, respectively, which are close to that reported for uncoated RFB-loaded NLC (14.66 ± 0.55%). Interestingly, statistical analysis performed (ANOVA one-way) revealed significant differences among uncoated NLC, and those coated with mannose using the first experimental procedure, which showed a slightly lower cell uptake. This finding might be associated with stearylamine addition during the coating process, which results in positively charged NLC, less efficiently internalized. The higher macrophage uptake of negatively charged NLC has been associated with their potential to bind cationic sites on macrophage surface, and be recognized by the scavenger receptors, which were reported to facilitate anionic particles uptake by immune cells (12). On the other hand, no statistically significant differences were found for mannose-coated NLC obtained by means of the second mannose-coating procedure, in comparison with the uncoated formulations.

MAs-coated NLC present promising results. MA coating produces a statistically significant increase in the NLC uptake by human macrophages (55.94 ± 5.62%) (**Table 8.1**), in agreement with previous works with MAs and PLGA nanoparticles, where a 3 to 4-fold increase in nanoparticle uptake by phagocytic cells was reported (9).

8.1.2. *In vitro* evaluation of the anti-mycobacterial activity of naked and coated NLC

Assessment of the anti-mycobacterial activity is crucial to determine the effectivity of both coated and naked NLC-based therapeutics. This part of the work was performed in collaboration with the Department of Animal Health of Neiker-Tecnalia Basque Institute for Agricultural Research and Development.

8.1.2.1. *In vitro* infection of macrophages with *M. avium paratuberculosis*

In order to evaluate *in vitro* antimicrobial effectivity of the developed lipid nano-formulations, THP-1 derived macrophages were infected with *M. avium paratuberculosis* (MAP). On this purpose, THP-1 cells were differentiated to macrophages, as previously described in chapter II. Then, a mycobacterial inoculum of the MAP strain K10 (ATCC, USA), a laboratory-adapted isolate recovered from a bovine paratuberculosis clinical case, which was selected due to their reported similarity with human isolates, was prepared following a previously described procedure (13). The strain was cultured at 37±1°C, in tissue culture flasks containing Middlebrook 7H9 medium (Difco laboratories, USA), supplemented with Tween® 80 0.05% (w/v) (Sigma Aldrich, USA), glycerin 0.2%, 2 mg/L of mycobactin J (Allied Monitor Inc, USA) and oleic acid-albumin-dextrose-catalase 10% (BD MGIT OADC enrichment, Becton, Dickinson and company, USA).

Mycobacterial cells were isolated by centrifugation (3000 rpm, 20 min, 22°C) using a Beckman Coulter Allegra X-12 centrifuge (Beckman Coulter, USA). Then, the resulting pellets were washed three times with Hanks balanced salt solution (HBSS) and resuspended in 2 ml of the previous medium. The solution was forced to pass through a 27-gauge needle in order to disrupt the remaining bacterial aggregates and finally, the homogeneous suspension obtained, was kept in a falcon from 5 to 10 min. Then, 1 ml of HBSS was transferred to a McFarland tube and small volumes from the top fraction of the previous bacterial suspension were added progressively, until the turbidity of the suspension, determined by means of a Densimat (bioMérieux, France), corresponds to a of McFarland standard of 1 (3×10^8 colony forming units or CFUs/ml). Subsequently, macrophage infection was stablished following a previously described protocol (14). In brief, cells were washed with HBSS and incubated with MAP for 2 hours at 37°C and 5% CO_2, using a 1:10 cell:bacteria ratio (100 µl of McFarland 1 per well). Finally, after the 2-hours incubation step, the medium was replaced, and cells were washed twice with HBSS in order to remove the non-internalized mycobacteria.

8.1.2.2. Treatment of *M. avium paratuberculosis*-infected macrophages

Then, 0.12 mg/ml of RFB-loaded NLC, either coated or naked, were added to the infected macrophages, along with the culture media (RPMI 1640, supplemented as described in Chapter II), and incubated for 4 hours. Furthermore, blank NLC and infected cells without treatment were employed as positive controls of infection. A RFB solution at the same drug concentration as in the nanoparticles, was employed as negative control, in order to verify the anti-mycobacterial effect of RFB. After this second incubation phase, samples were removed, cells were washed with HBSS and fresh medium was added. Then they were kept in an incubator at 37°C and 5% CO_2 for 6 days, after which cells were lysed with 0.1% Triton X-

100. The lysate obtained was inoculated into Mycobacteria growth indicator (MGIT) tubes (Becton, Dickinson and company, USA) containing Middlebrook 7H9 broth modified with casein peptone and tris-4,7-diphenyl-1,10-phenathroline ruthenium chloride pentahydrate, which is an oxygen-sensitive fluorescent compound embedded in silicone in the base of the tube (13). Additionally, these tubes were supplemented with 800 µl of OADC, the reconstituted lyophilized antibiotic mixture BBL MGIT PANTA (Becton, Dickinson and company, USA) and 2 µg/ml of mycobactin J (13).

8.1.2.3. Preparation of standard curves

In order to allow MAP quantification, a standard curve for the MAP K10 strain employed was performed by duplicate. On this purpose, 10 fold serial dilutions in HBSS were prepared from the previous bacterial solution adjusted to McFarland standard of 1 (3×10^8 CFUs/ml), until a bacterial concentration of 3×10^2 CFUs was achieved. Then, 100 µl of each dilution were inoculated in the previously-described MGIT tubes (13).

8.1.2.4. Sample incubation in MGIT instrument and data analysis

Tubes including both lysate samples and standard curves points were introduced in a Bactec MGIT 960 instrument (Becton, Dickinson and company, USA), where they were incubated at 37±2°C and automatically monitored hourly, during 42 days in order to detect bacterial growth (positive tube) through an increase in fluorescence (13).

Time to detection (TTD), which is the time in which a tube was found to be positive, was recorded, and the tube was removed from the apparatus. Tubes without fluorescent positive signal after 42 days, were classified as negative (no bacterial growth) and also removed from the instrument (13).

TTD values obtained are shown in **Table 8.2**. The quantitative capacity of Bactec MGIT systems is based on the fact that generation time is proportional to the inoculum size (13). Therefore, TTDs were used to estimate the $\log_{10}$ CFU in each tube. TTDs for the standard tubes were plotted against the inoculum size of each calibration point and curves obtained were fitted to a one-phase exponential decay model, through the following equation (13):

$$\log 10\ Inoculum\ size = span \times e\,(-K \times TTD) + plateau \qquad \textbf{Equation 8.1}$$

Where span is the difference amongst TTD at t_0 and the plateau, plateau is the value for $\log_{10}$ CFU curve flattening and K is the extent of decay of $\log_{10}$ CFU (13). This equation was then employed to estimate $\log_{10}$ CFU of the samples, from the TTD obtained in the MGIT instrument. Values exhibited by all of the previously-mentioned parameters along with the estimated inoculum size can be found in **Table 8.2**. However, results obtained for surface-modified nanocarriers were not included in the table, due to cytotoxicity and contamination issues derived, respectively, from the addition of MA-coated and mannose-coated NLC to cell cultures. These issues suggest that further study of the biocompatibility of this surface-modified nanosystems should be performed, in order to adjust the administered nanoparticle dose.

Table 8.2. Time to detection, equation parameters and resulting MAP log_{10} CFU obtained for each analyzed sample.

Sample	TTD (days)	(-K X TTD)	e (-K X TTD)	span x e (-K X TTD)	span x e (-K X TTD) +plateau/ Log_{10} CFU	Log_{10} CFU Average	Log_{10} CFU SD
4 hours incubation							
Blk NLC 1	22.4	-0.69	0.50	7.47	2.67	2.58	0.13
Blk NLC 2	23.3	-0.72	0.49	7.28	2.48		
RFB- NLC 1	22.9	-0.71	0.49	7.37	2.57	2.60	0.04
RFB- NLC 2	22.6	-0.70	0.50	7.43	2.62		
RFB sol 1	22.5	-0.70	0.50	7.44	2.64	2.60	0.05
RFB sol 2	22.9	-0.71	0.49	7.37	2.57		
Untreated 1	22.7	-0.70	0.50	7.41	2.60	2.61	0.01
Untreated 2	22.6	-0.70	0.50	7.43	2.62		

In order to simplify the understanding of the results, data were also expressed as increase in log_{10} CFU achieved in treated cells (either with blank and loaded formulations, or with the drug solution), regarding untreated cells (**Figure 8.2**). These values were calculated by dividing log_{10} CFU average values achieved with the different treatments by those reported for untreated ones. The values highly close to one obtained, suggested that RFB-loaded NLC formulations were not able to reduce MAP load within macrophages after 6 days of infection. Moreover, statistical analysis (one-way ANOVA, $p > 0.05$, n=2) did not revealed significant differences between log CFU average values obtained with blank NLC, RFB-loaded NLC or RFB solution regarding those reported for untreated controls.

Results found for blank NLC formulations agree with those expected, as nanocarriers are not likely to restrict MAP growth. However, drug-loaded formulations and drug solution outcomes were unexpected. Since, RFB exhibits a minimum inhibitory concentration ranging from 0.5-4 µg/ml (15), RFB dose administered in the experiment was clearly superior (6 µg/ml). However, the results suggest that neither loaded NLC nor RFB reduce bacterial load (**Figure 8.2)**. The origin of inconclusive results may be due to limitations associated with the experimental design parameters. MAP exhibits an extremely slow growth rate (16) and RFB has bacteriostatic activity (17), which can make the experiment design incorrect.

An example of these limitations was previously described during the evaluation of the antimicrobial activity of both isoniazid-loaded PLGA nanoparticles and drug solution in *M. tuberculosis*-infected macrophages (18). In that work, the infected cells were incubated with the treatments for 5 hours, 1 or 2 days, followed by a second incubation step of 2 days after the extraction of the sample (18). The variable results obtained after the 5-hour incubation did not allow to draw conclusions about the efficacy of the treatment. Longer periods (1 and 2 days) produced significant improvements in mycobacterial growth inhibition.

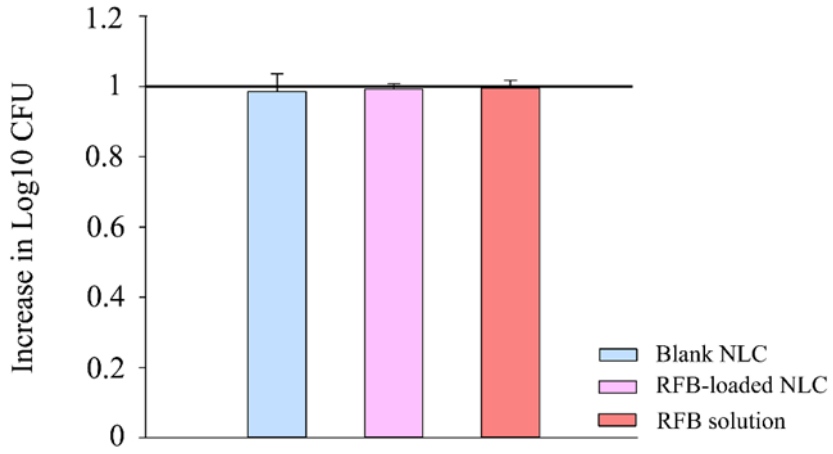

Figure 8.2. Increase in Log_{10} CFU, regarding untreated controls, obtained after a 4-hour treatment of MAP-infected macrophages with blank NLC (blue color), RFB-loaded NLC (pink color) and RFB solution (red color).

Also, during the evaluation of the *in vitro* efficacy of mannosylated rifampicin-loaded NLC, in macrophages infected with *M. avium*, it was observed that a 24-hour treatment of the infected cells with the nanocarriers or the drug solution, did not achieve significant effects in reducing mycobacterial load. A 24-hour re-incubation treatment at 3 days was necessary to restrict bacterial growth (1). These facts might explain the unsatisfying results obtained to date, with the administration of a single RFB-loaded NLC dose to MAP-infected macrophages.

8.2. FUTURE PERSPECTIVES

The use of coated-NLC formulations constitute a promising tool for the treatment of intracellular persisting infections, such as those produced by *Mycobacterium avium paratuberculosis*. The unsatisfactory results obtained with these preliminary studies require further development to optimize the coating protocol (ratio MA-OA/NLC) and the activity assay protocol of the coated formulations on infected macrophages.

Furthermore, it can also be interesting that basic characterization performed in terms of particle size and surface charge, are improved using other techniques such as static time-of-flight secondary ion mass spectrometry (TOF SIMS) or X-ray photoelectron spectroscopy (XPS), which have been previously employed for characterization of surface chemical composition of other particulate systems (19). Techniques such as Fourier-transform infrared spectroscopy (FTIR) or Differential scanning calorimetry (DSC) can also give insight into the efficacy of nanoparticle coating process. FTIR has been employed to allow the detection of the Schiff´s base generated during mannose coating 1 procedure, while DSC has been used detect differences between onset and melting temperatures or melting enthalpies of coated and uncoated nanocarriers that could indicate an efficient coating formation (1).

A detailed analysis of the cytotoxicity of the surface-modified NLC as well as the study of techniques suitable for their sterilization, are also required before proceeding with further assays.

Finally, regarding the efficacy evaluation of NLC formulations in MAP-infected macrophages, an improvement of the experimental design for the study of the growth rate of the mycobacteria is necessary, which allow for the detection of differences between the mycobacterial growth inhibition produced by the different samples. The administration of a refreshing treatment before cell lysis constitutes a worthy path to explore.

REFERENCES

1. Vieira AC, Magalhães J, Rocha S, Cardoso MS, Santos SG, Borges M, et al. Targeted macrophages delivery of rifampicin-loaded lipid nanoparticles to improve tuberculosis treatment. Nanomedicine. 2017; 12 (24): 2721-2736.
2. Pinheiro M, Ribeiro R, Vieira A, Andrade F, Reis S. Design of a nanostructured lipid carrier intended to improve the treatment of tuberculosis. Drug Des Devel Ther. 2016; 10: 2467-2475.
3. Irache JM, Salman HH, Gamazo C, Espuelas S. Mannose-targeted systems for the delivery of therapeutics. Expert Opin Drug Deliv. 2008; 5 (6): 703-724.
4. Xia XR, Monteiro-Riviere NA, Riviere JE. An index for characterization of nanomaterials in biological systems. Nat Nanotechnol. 2010; 5 (9): 671-675.
5. Abdelwahed W, Degobert G, Stainmesse S, Fessi H. Freeze-drying of nanoparticles: formulation, process and storage considerations. Adv Drug Deliv Rev. 2006; 58 (15): 1688-1713.
6. Marrakchi H, Laneelle MA, Daffe M. Mycolic acids: structures, biosynthesis, and beyond. Chem Biol. 2014; 21 (1): 67-85.
7. He Z, De Buck J. Localization of proteins in the cell wall of Mycobacterium avium subsp. paratuberculosis K10 by proteomic analysis. Proteome Sci. 2010; 8 (1): 21.
8. Bhatt A, Molle V, Besra GS, Jacobs WR, Jr., Kremer L. The Mycobacterium tuberculosis FAS-II condensing enzymes: their role in mycolic acid biosynthesis, acid-fastness, pathogenesis and in future drug development. Mol Microbiol. 2007; 64 (6): 1442-1454.
9. Lemmer Y, Kalombo L, Pietersen RD, Jones AT, Semete-Makokotlela B, Van Wyngaardt S, et al. Mycolic acids, a promising mycobacterial ligand for targeting of nanoencapsulated drugs in tuberculosis. J Control Release. 2015; 211: 94-104.
10. Mahajan S, Prashant C, Koul V, Choudhary V, K Dinda A. Receptor specific macrophage targeting by mannose-conjugated gelatin nanoparticles-an in vitro and in vivo study. Curr Nanosci. 2010; 6 (4): 413-421.
11. Guo Y, Liu X, Sun X, Zhang Q, Gong T, Zhang Z. Mannosylated lipid nano-emulsions loaded with lycorine-oleic acid ionic complex for tumor cell-specific delivery. Theranostics. 2012; 2 (11): 1104-1114.
12. Arnida, Janat-Amsbury MM, Ray A, Peterson CM, Ghandehari H. Geometry and surface characteristics of gold nanoparticles influence their biodistribution and uptake by macrophages. Eur J Pharm Biopharm. 2011; 77 (3): 417-423.
13. Abendaño N, Sevilla I, Prieto JM, Garrido JM, Juste RA, Alonso-Hearn M. Quantification of Mycobacterium avium subsp. paratuberculosis strains representing distinct genotypes and isolated from domestic and wildlife animal species by use of an automatic liquid culture system. J Clin Microbiol. 2012; 50 (8): 2609-2617.
14. Alonso-Hearn M, Abendano N, Ruvira MA, Aznar R, Landin M, Juste RA. Mycobacterium avium subsp. paratuberculosis (Map) Fatty Acids Profile Is Strain-Dependent and Changes Upon Host Macrophages Infection. Front Cell Infect Microbiol. 2017;7: 89.
15. Zanetti S, Molicotti P, Cannas S, Ortu S, Ahmed N, Sechi LA. "In vitro" activities of antimycobacterial agents against Mycobacterium avium subsp. paratuberculosis linked to Crohn's disease and paratuberculosis. Ann Clin Microbiol Antimicrob. 2006; 5: 27.

16. Saviola B, Bishai W. The genus Mycobacterium-medical. In: Dworkin M, Falkow S, Rosenberg E, Schleifer KH, Stackebrandt E (Ed).The prokaryotes: a handbook on the biology of bacteria. 3rd edition. New York, USA: Springer; 2006. p. 919-33.
17. Perronne C, Gikas A, Truffot-Pernot C, Grosset J, Pocidalo J, Vilde J. Activities of clarithromycin, sulfisoxazole, and rifabutin against Mycobacterium avium complex multiplication within human macrophages. Antimicrob Agents Chemother. 1990; 34 (8): 1508-1511.
18. Lemmer Y. Assessment of mycolic acids as ligand for nanoencapsulated anti-tuberculosis drug targeting [Doctoral dissertation]: University of Pretoria; 2011.
19. Grenha A, Seijo B, Serra C, Remunán-López C. Chitosan nanoparticle-loaded mannitol microspheres: structure and surface characterization. Biomacromolecules. 2007; 8 (7): 2072-2079.

ANNEX I

USC
UNIVERSIDADE
DE SANTIAGO
DE COMPOSTELA

Table A1.1. Set of IF-THEN rules for size peak 1 of experimental design 1. Degree of membership in parentheses.

Rules for Size peak 1		
Submodel 1		
IF Speed (rpm) is LOW AND % Tween is LOW	THEN M Size peak 1 (nm) is	LOW (0.96)
IF Speed (rpm) is LOW AND % Tween is MID	THEN M Size peak 1 (nm) is	LOW (1.00)
IF Speed (rpm) is LOW AND % Tween is HIGH	THEN M Size peak 1 (nm) is	LOW (1.00)
IF Speed (rpm) is HIGH AND % Tween is LOW	THEN M Size peak 1 (nm) is	LOW (0.96)
IF Speed (rpm) is HIGH AND % Tween is MID	THEN M Size peak 1 (nm) is	LOW (0.97)
IF Speed (rpm) is HIGH AND % Tween is HIGH	THEN M Size peak 1 (nm) is	HIGH (1.00)

Table A1.2. Set of IF-THEN rules for % peak 1 of experimental design 1. Degree of membership in parentheses.

Rules for % peak 1		
Submodel 1		
IF %RFB is LOW	THEN M % peak 1 is	HIGH (1.00)
IF %RFB is HIGH	THEN M % peak 1 is	HIGH (0.56)
Submodel 2		
IF Speed (rpm) is LOW AND %Tween is LOW	THEN M % peak 1 is	LOW (0.58)
IF Speed (rpm) is LOW AND %Tween is HIGH	THEN M % peak 1 is	LOW (1.00)
IF Speed (rpm) is MID AND %Tween is LOW	THEN M % peak 1 is	HIGH (1.00)
IF Speed (rpm) is MID AND %Tween is HIGH	THEN M % peak 1 is	LOW (0.71)
IF Speed (rpm) is HIGH AND %Tween is LOW	THEN M % peak 1 is	HIGH (0.50)
IF Speed (rpm) is HIGH AND %Tween is HIGH	THEN M % peak 1 is	HIGH (0.79)

Table A1.3. Set of IF-THEN rules for Z-average size of experimental design 2. Degree of membership in parentheses.

Rules for Z-average size		
Submodel 1		
IF %LL is LOW AND %RFB (T) is LOW	THEN Size (nm) is	LOW (0.89)
IF %LL is LOW AND %RFB (T) is HIGH	THEN Size (nm) is	HIGH (1.00)
IF %LL is HIGH AND % RFB (T) is LOW	THEN Size (nm) is	LOW (1.00)
IF %LL is HIGH AND %RFB (T) is HIGH	THEN Size (nm) is	LOW (1.00)
Submodel 2		
IF %Tween is LOW	THEN Size (nm) is	HIGH (0.73)
IF %Tween is MID	THEN Size (nm) is	LOW (1.00)
IF %Tween is HIGH	THEN Size (nm) is	LOW (0.52)

Table A1.4. Set of IF-THEN rules for PDI of experimental design 2. Degree of membership in parentheses.

Rules for PDI		
Submodel 1		
IF %Tween is LOW	THEN PDI is	HIGH (0.98)
IF %Tween is HIGH	THEN PDI is	LOW (0.94)
Submodel 2		
IF %LL is LOW	THEN PDI is	HIGH (0.85)
IF %LL is HIGH	THEN PDI is	LOW (0.80)

Table A1.5. Set of IF-THEN rules for zeta potential of experimental design 2. Degree of membership in parentheses.

Rules for Zeta potential		
Submodel 1		
IF % Tween is LOW	THEN ZP is	LOW (1.00)
IF % Tween is HIGH	THEN ZP is	HIGH (1.00)
Submodel 2		
IF %LL is LOW	THEN ZP is	HIGH (0.84)
IF %LL is HIGH	THEN ZP is	LOW (0.99)

Table A1.6. Set of IF-THEN rules for EE% of experimental design 2. Degree of membership in parentheses.

Rules for EE%		
Submodel 1		
IF %LL is LOW	THEN M EE (%) is	LOW (1.00)
IF %LL is HIGH	THEN M EE (%) is	HIGH (1.00)
Submodel 2		
IF %Tween is LOW	THEN M EE (%) is	HIGH (0.88)
IF %Tween is HIGH	THEN M EE (%) is	LOW (0.81)

Table A1.7. Set of IF-THEN rules for DL% of experimental design 2. Degree of membership in parentheses.

Rules for DL%		
Submodel 1		
IF %RFB (T) is LOW	THEN M DL (%) is	LOW (1.00)
IF %RFB (T) is HIGH	THEN M DL (%) is	HIGH (1.00)
Submodel 2		
IF %LL is LOW	THEN M DL (%) is	LOW (1.00)
IF %LL is MID	THEN M DL (%) is	LOW (0.89)
IF %LL is HIGH	THEN M DL (%) is	HIGH (1.00)
Submodel 3		
IF Speed (rpm) is LOW	THEN M DL (%) is	HIGH (0.93)
IF Speed (rpm) is HIGH	THEN M DL (%) is	LOW (0.88)
Submodel 4		
IF %Tween is LOW	THEN M DL (%) is	HIGH (0.77)
IF %Tween is HIGH	THEN M DL (%) is	LOW (0.72)

It must be considered that blue colour indicates the combination of inputs that led to the highest value of the output, while red colour shows the combination of inputs giving the lowest value.

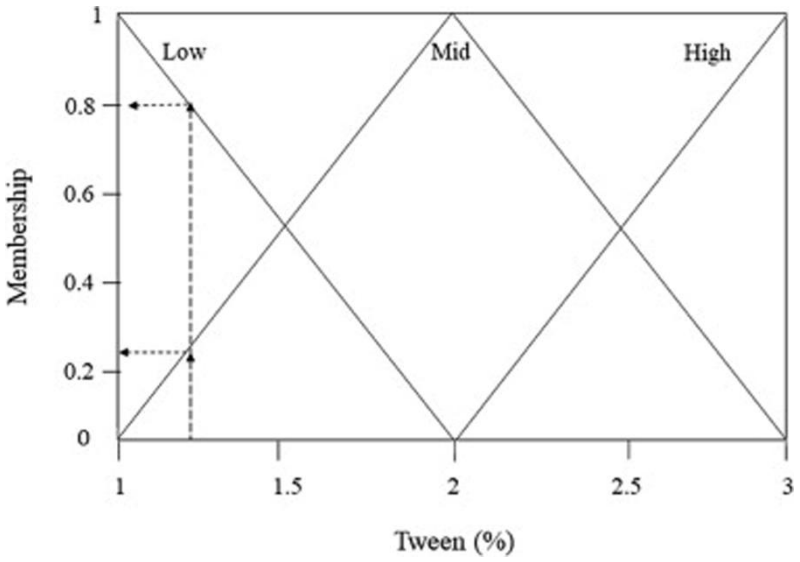

Figure A1.1. Fuzzyfication of the variable "Percentage of Tween" in the formulation which ranges between 1 and 3% in the study. The figure presents the categories low, medium and high with a triangular membership function. Every value of the variable (x) can be described by a word and a membership number ranging from zero to one. E.g. X value of Tween percentage can be described as low with a membership of 0.8 [LOW (0.8)] or medium with a membership of 0.25 [MID (0.25)].

USC
UNIVERSIDADE
DE SANTIAGO
DE COMPOSTELA

ANNEX II

USC
UNIVERSIDADE
DE SANTIAGO
DE COMPOSTELA

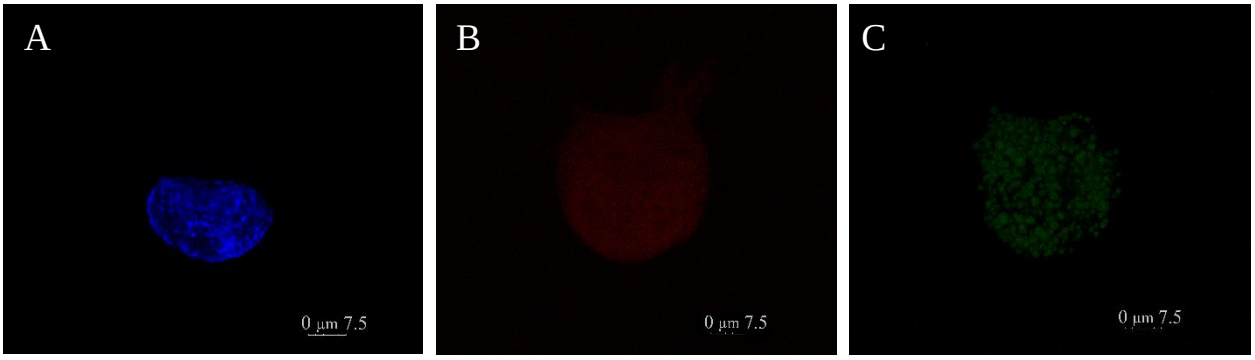

Figure A2.1. Confocal imaging of blank NLC macrophages uptake. Red, blue, and green colours represent cell cytoplasm (Alexa Fluor™ 647 phalloidin), cell nuclei (DAPI) and NLC formulations (Coumarin 6), respectively: (a) blue channel (b) red channel and (c) green channel.

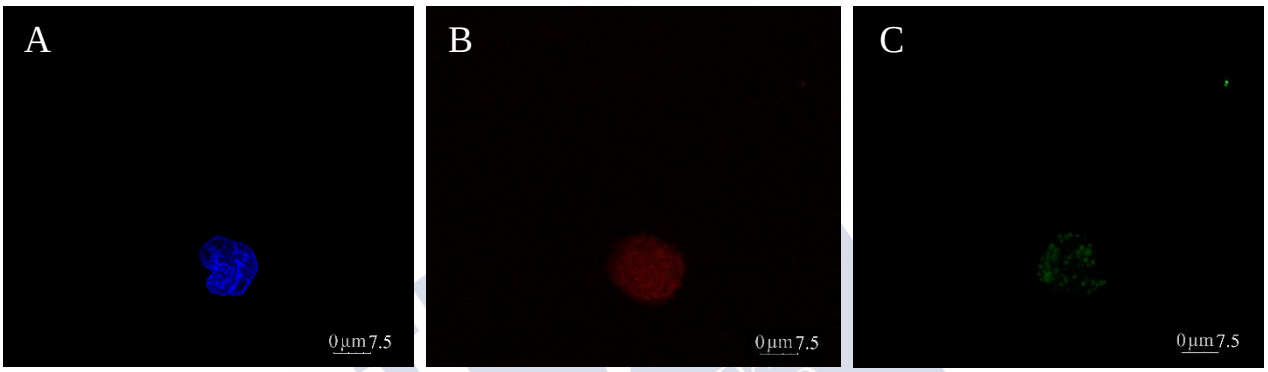

Figure A2.2. Confocal imaging of RFB-loaded NLC macrophages uptake. Red, blue, and green colours represent cell cytoplasm (Alexa Fluor™ 647 phalloidin), cell nuclei (DAPI) and NLC formulations (Coumarin 6), respectively: (a) blue channel (b) red channel and (c) green channel.

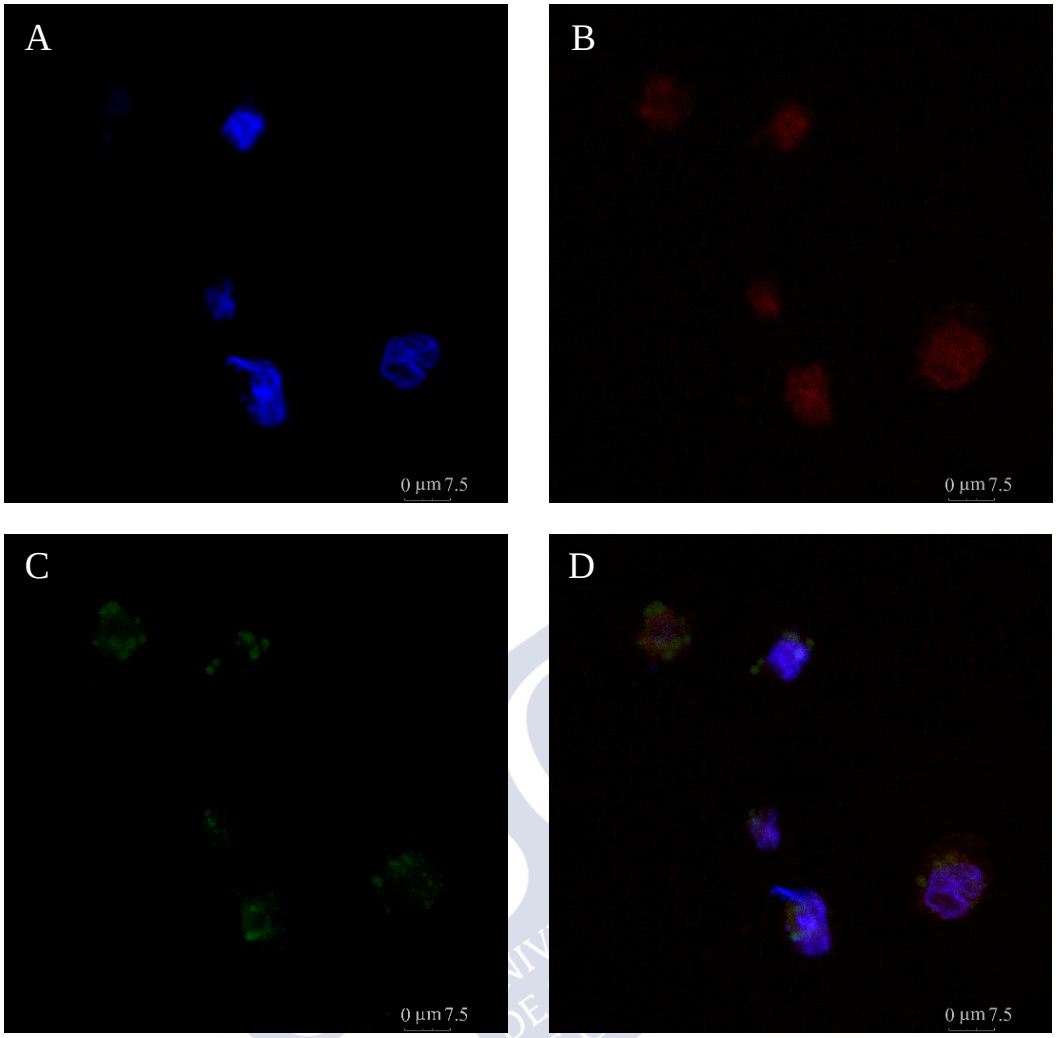

Figure A2.3. Confocal imaging of blank NLC uptake by a group of macrophages. Red, blue, and green colours represent cell cytoplasm (Alexa Fluor™ 647 phalloidin), cell nuclei (DAPI) and NLC formulations (Coumarin 6), respectively: (a) blue channel (b) red channel, (c) green channel and (d) overlay of the three channels.

ANNEX III

USC
UNIVERSIDADE
DE SANTIAGO
DE COMPOSTELA

Table A2.1. Set of combined IF-THEN rules for Δ size of the first NFL model. Degree of membership in parentheses.

Rules for Δ size		
1. IF Velocity is Fast AND CP is Fructose AND IF %CP is HIGH AND CP is Fructose	THEN Δ size (nm) is	HIGH (0.60)
2. IF Velocity is Fast AND CP is Fructose AND IF %CP is LOW AND CP is Fructose	THEN Δ size (nm) is	LOW (0.82)
3. IF Velocity is Fast AND CP is Fructose AND IF %CP is MID AND CP is Fructose	THEN Δ size (nm) is	LOW (0.89)
4. IF Velocity is Slow AND CP is Fructose AND IF %CP is HIGH AND CP is Fructose	THEN Δ size (nm) is	HIGH (0.86)
5. IF Velocity is Slow AND CP is Fructose AND IF %CP is LOW AND CP is Fructose	THEN Δ size (nm) is	LOW (0.56)
6. IF Velocity is Slow AND CP is Fructose AND IF %CP is MID AND CP is Fructose	THEN Δ size (nm) is	LOW (0.63)
7. IF Velocity is Fast AND CP is Glucose AND IF %CP is HIGH AND CP is Glucose	THEN Δ size (nm) is	LOW (0.56)
8. IF Velocity is Fast AND CP is Glucose AND IF %CP is LOW AND CP is Glucose	THEN Δ size (nm) is	LOW (0.99)
9. IF Velocity is Fast AND CP is Glucose AND IF %CP is MID AND CP is Glucose	THEN Δ size (nm) is	LOW (0.90)
10. IF Velocity is Slow AND CP is Glucose AND IF %CP is HIGH AND CP is Glucose	THEN Δ size (nm) is	HIGH (0.72)
11. IF Velocity is Slow AND CP is Glucose AND IF %CP is LOW AND CP is Glucose	THEN Δ size (nm) is	LOW (0.72)
12. IF Velocity is Slow AND CP is Glucose AND IF %CP is MID AND CP is Glucose	THEN Δ size (nm) is	LOW (0.62)
13. IF Velocity is Fast AND CP is Lactose AND IF %CP is HIGH AND CP is Lactose	THEN Δ size (nm) is	LOW (0.74)
14. IF Velocity is Fast AND CP is Lactose AND IF %CP is LOW AND CP is Lactose	THEN Δ size (nm) is	LOW (0.81)
15. IF Velocity is Fast AND CP is Lactose AND IF %CP is MID AND CP is Lactose	THEN Δ size (nm) is	LOW (0.88)
16. IF Velocity is Slow AND CP is Lactose AND IF %CP is HIGH AND CP is Lactose	THEN Δ size (nm) is	LOW (0.66)
17. IF Velocity is Slow AND CP is Lactose AND IF %CP is LOW AND CP is Lactose	THEN Δ size (nm) is	LOW (0.73)
18. IF Velocity is Slow AND CP is Lactose AND IF %CP is MID AND CP is Lactose	THEN Δ size (nm) is	LOW (0.81)
19. IF Velocity is Fast AND CP is Mannitol AND IF %CP is HIGH AND CP is Mannitol	THEN Δ size (nm) is	LOW (0.71)
20. IF Velocity is Fast AND CP is Mannitol AND IF %CP is LOW AND CP is Mannitol	THEN Δ size (nm) is	HIGH (0.77)
21. IF Velocity is Fast AND CP is Mannitol AND IF %CP is MID AND CP is Mannitol	THEN Δ size (nm) is	LOW (0.60)
22. IF Velocity is Slow AND CP is Mannitol AND IF %CP is HIGH AND CP is Mannitol	THEN Δ size (nm) is	LOW (0.62)
23. IF Velocity is Slow AND CP is Mannitol AND IF %CP is LOW AND CP is Mannitol	THEN Δ size (nm) is	HIGH (0.86)
24. IF Velocity is Slow AND CP is Mannitol AND IF %CP is MID AND CP is Mannitol	THEN Δ size (nm) is	LOW (0.50)
25. IF Velocity is Fast AND CP is Sorbitol AND IF %CP is HIGH AND CP is Sorbitol	THEN Δ size (nm) is	HIGH (0.50)
26. IF Velocity is Fast AND CP is Sorbitol AND IF %CP is LOW AND CP is Sorbitol	THEN Δ size (nm) is	LOW (0.51)

27. **IF Velocity is Fast AND CP is Sorbitol AND IF %CP is MID AND CP is Sorbitol**	THEN Δ size (nm) is	LOW (0.66)
28. **IF Velocity is Slow AND CP is Sorbitol AND IF %CP is HIGH AND CP is Sorbitol**	THEN Δ size (nm) is	HIGH (0.61)
29. **IF Velocity is Slow AND CP is Sorbitol AND IF %CP is LOW AND CP is Sorbitol**	THEN Δ size (nm) is	HIGH (0.60)
30. **IF Velocity is Slow AND CP is Sorbitol AND IF %CP is MID AND CP is Sorbitol THEN**	THEN Δ size (nm) is	LOW (0.55)
31. **IF Velocity is Fast AND CP is Sucrose AND IF %CP is HIGH AND CP is Sucrose**	THEN Δ size (nm) is	LOW (0.94)
32. **IF Velocity is Fast AND CP is Sucrose AND IF %CP is LOW AND CP is Sucrose**	THEN Δ size (nm) is	HIGH (0.75)
33. **IF Velocity is Fast AND CP is Sucrose AND IF %CP is MID AND CP is Sucrose**	THEN Δ size (nm) is	LOW (0.76)
34. **IF Velocity is Slow AND CP is Sucrose AND IF %CP is HIGH AND CP is Sucrose**	THEN Δ size (nm) is	LOW (0.88)
35. **IF Velocity is Slow AND CP is Sucrose AND IF %CP is LOW AND CP is Sucrose**	THEN Δ size (nm) is	HIGH (0.82)
36. **IF Velocity is Slow AND CP is Sucrose AND IF %CP is MID AND CP is Sucrose**	THEN Δ size (nm) is	LOW (0.70)
37. **IF Velocity is Fast AND CP is Trehalose AND IF %CP is HIGH AND CP is Trehalose**	THEN Δ size (nm) is	LOW (0.71)
38. **IF Velocity is Fast AND CP is Trehalose AND IF %CP is LOW AND CP is Trehalose**	THEN Δ size (nm) is	LOW (0.68)
39. **IF Velocity is Fast AND CP is Trehalose AND IF %CP is MID AND CP is Trehalose**	THEN Δ size (nm) is	LOW (0.85)
40. **IF Velocity is Slow AND CP is Trehalose AND IF %CP is HIGH AND CP is Trehalose**	THEN Δ size (nm) is	LOW (0.72)
41. **IF Velocity is Slow AND CP is Trehalose AND IF %CP is LOW AND CP is Trehalose**	THEN Δ size (nm) is	LOW (0.69)
42. **IF Velocity is Slow AND CP is Trehalose AND IF %CP is MID AND CP is Trehalose**	THEN Δ size (nm) is	LOW (0.86)

Table A2.2. Set of combined IF-THEN rules for Δ PDI of the first NFL model. Degree of membership in parentheses.

Rules for Δ PDI		
1. **IF %CP is LOW AND CP is Fructose AND IF Velocity is Fast AND IF %CP is MID-3**	THEN Δ PDI is	LOW (1.00)
2. **IF %CP is LOW AND CP is Fructose AND IF Velocity is Fast AND IF % CP is LOW-1**	THEN Δ PDI is	LOW (1.00)
3. **IF %CP is LOW AND CP is Fructose AND IF Velocity is Fast AND IF %CP is MID-2**	THEN Δ PDI is	LOW (0.92)
4. **IF %CP is HIGH AND CP is Fructose AND IF Velocity is Fast AND IF %CP is MID-3**	THEN Δ PDI is	LOW (0.71)
5. **IF %CP is HIGH AND CP is Fructose AND IF Velocity is Fast AND IF %CP is HIGH-4**	THEN Δ PDI is	HIGH (0.63)
6. **IF %CP is LOW AND CP is Fructose AND IF Velocity is Slow AND IF %CP is MID-3**	THEN Δ PDI is	LOW (0.88)
7. **IF %CP is LOW AND CP is Fructose AND IF Velocity is Slow AND IF %CP is LOW-1**	THEN Δ PDI is	LOW (0.87)
8. **IF %CP is LOW AND CP is Fructose AND IF Velocity is Slow AND IF %CP is MID-2**	THEN Δ PDI is	LOW (0.77)
9. **IF % CP is HIGH AND CP is Fructose AND IF Velocity is Slow AND IF %CP is MID-3**	THEN Δ PDI is	LOW (0.56)

10. **IF %CP is HIGH AND CP is Fructose AND IF Velocity is Slow AND IF %CP is HIGH-4**	THEN Δ PDI is	HIGH (0.78)
11. **IF %CP is LOW AND CP is Glucose AND IF Velocity is Fast AND IF %CP is MID-3**	THEN Δ PDI is	LOW (1.00)
12. **IF %CP is LOW AND CP is Glucose AND IF Velocity is Fast AND IF %CP is LOW-1**	THEN Δ PDI is	LOW (1.00)
13. **IF %CP is LOW AND CP is Glucose AND IF Velocity is Fast AND IF %CP is MID-2**	THEN Δ PDI is	LOW (0.97)
14. **IF %CP is HIGH AND CP is Glucose AND IF Velocity is Fast AND IF %CP is MID-3**	THEN Δ PDI is	LOW (0.62)
15. **IF %CP is HIGH AND CP is Glucose AND IF Velocity is Fast AND IF %CP is HIGH-4**	THEN Δ PDI is	HIGH (0.72)
16. **IF %CP is LOW AND CP is Glucose AND IF Velocity is Slow AND IF %CP is MID-3**	THEN Δ PDI is	LOW (0.94)
17. **IF %CP is LOW AND CP is Glucose AND IF Velocity is Slow AND IF %CP is LOW-1**	THEN Δ PDI is	LOW (0.92)
18. **IF %CP is LOW AND CP is Glucose AND IF Velocity is Slow AND IF %CP is MID-2**	THEN Δ PDI is	LOW (0.82)
19. **IF %CP is HIGH AND CP is Glucose AND IF Velocity is Slow AND IF %CP is MID-3**	THEN Δ PDI is	HIGH (0.54)
20. **IF %CP is HIGH AND CP is Glucose AND IF Velocity is Slow AND IF %CP is HIGH-4**	THEN Δ PDI is	HIGH (0.87)
21. **IF %CP is LOW AND CP is Lactose AND IF Velocity is Fast AND IF %CP is MID-3**	THEN Δ PDI is	LOW (1.00)
22. **IF %CP is LOW AND CP is Lactose AND IF Velocity is Fast AND IF %CP is LOW-1**	THEN Δ PDI is	LOW (1.00)
23. **IF %CP is LOW AND CP is Lactose AND IF Velocity is Fast AND IF %CP is MID-2**	THEN Δ PDI is	LOW (0.90)
24. **IF %CP is HIGH AND CP is Lactose AND IF Velocity is Fast AND IF %CP is MID-3**	THEN Δ PDI is	LOW (0.73)
25. **IF %CP is HIGH AND CP is Lactose AND IF Velocity is Fast AND IF %CP is HIGH-4**	THEN Δ PDI is	HIGH (0.61)
26. **IF %CP is LOW AND CP is Lactose AND IF Velocity is Slow AND IF %CP is MID-3**	THEN Δ PDI is	LOW (0.86)
27. **IF %CP is LOW AND CP is Lactose AND IF Velocity is Slow AND IF %CP is LOW-1**	THEN Δ PDI is	LOW (0.85)
28. **IF %CP is LOW AND CP is Lactose AND IF Velocity is Slow AND IF %CP is MID-2**	THEN Δ PDI is	LOW (0.75)
29. **IF %CP is HIGH AND CP is Lactose AND IF Velocity is Slow AND IF %CP is MID-3**	THEN Δ PDI is	LOW (0.58)
30. **IF %CP is HIGH AND CP is Lactose AND IF Velocity is Slow AND IF %CP is HIGH-4**	THEN Δ PDI is	HIGH (0.76)
31. **IF %CP is HIGH AND CP is Mannitol AND IF Velocity is Fast AND IF %CP is MID-3**	THEN Δ PDI is	LOW (1.00)
32. **IF %CP is LOW AND CP is Mannitol AND IF Velocity is Fast AND IF %CP is MID-3**	THEN Δ PDI is	LOW (0.78)
33. **IF %CP is LOW AND CP is Mannitol AND IF Velocity is Fast AND IF %CP is LOW-1**	THEN Δ PDI is	LOW (0.77)
34. **IF %CP is HIGH AND CP is Mannitol AND IF Velocity is Fast AND IF %CP is HIGH-4**	THEN Δ PDI is	LOW (0.72)
35. **IF %CP is LOW AND CP is Mannitol AND IF Velocity is Fast AND IF %CP is MID-2**	THEN Δ PDI is	LOW (0.67)
36. **IF %CP is HIGH AND CP is Mannitol AND IF Velocity is Slow AND IF %CP is MID-3**	THEN Δ PDI is	LOW (0.91)

37. **IF %CP is LOW AND CP is Mannitol AND IF Velocity is Slow AND IF %CP is MID-3**	THEN Δ PDI is	LOW (0.63)
38. **IF %CP is LOW AND CP is Mannitol AND IF Velocity is Slow AND IF %CP is LOW-1**	THEN Δ PDI is	LOW (0.61)
39. **IF %CP is HIGH AND CP is Mannitol AND IF Velocity is Slow AND IF %CP is HIGH-4**	THEN Δ PDI is	LOW (0.57)
40. **IF %CP is LOW AND CP is Mannitol AND IF Velocity is Slow AND IF %CP is MID-2**	THEN Δ PDI is	LOW (0.52)
41. **IF %CP is HIGH AND CP is Sorbitol AND IF Velocity is Fast AND IF %CP is MID-3**	THEN Δ PDI is	LOW (0.88)
42. **IF %CP is LOW AND CP is Sorbitol AND IF Velocity is Fast AND IF %CP is MID-3**	THEN Δ PDI is	LOW (0.83)
43. **IF %CP is LOW AND CP is Sorbitol AND IF Velocity is Fast AND IF %CP is LOW-1**	THEN Δ PDI is	LOW (0.82)
44. **IF %CP is LOW AND CP is Sorbitol AND IF Velocity is Fast AND IF %CP is MID-2**	THEN Δ PDI is	LOW (0.72)
45. **IF %CP is HIGH AND CP is Sorbitol AND IF Velocity is Fast AND IF %CP is HIGH-4**	THEN Δ PDI is	LOW (0.54)
46. **IF %CP is HIGH AND CP is Sorbitol AND IF Velocity is Slow AND IF %CP is MID-3**	THEN Δ PDI is	LOW (0.72)
47. **IF %CP is LOW AND CP is Sorbitol AND IF Velocity is Slow AND IF %CP is MID-3**	THEN Δ PDI is	LOW (0.68)
48. **IF %CP is LOW AND CP is Sorbitol AND IF Velocity is Slow AND IF %CP is LOW-1**	THEN Δ PDI is	LOW (0.67)
49. **IF %CP is LOW AND CP is Sorbitol AND IF Velocity is Slow AND IF %CP is MID-2**	THEN Δ PDI is	LOW (0.57)
50. **IF %CP is HIGH AND CP is Sorbitol AND IF Velocity is Slow AND IF %CP is HIGH-4**	THEN Δ PDI is	HIGH (0.61)
51. **IF %CP is HIGH AND CP is Sucrose AND IF Velocity is Fast AND IF %CP is MID-3**	THEN Δ PDI is	LOW (1.00)
52. **IF %CP is HIGH AND CP is Sucrose AND IF Velocity is Fast AND IF %CP is HIGH-4**	THEN Δ PDI is	LOW (0.85)
53. **IF %CP is LOW AND CP is Sucrose AND IF Velocity is Fast AND IF %CP is MID-3**	THEN Δ PDI is	LOW (0.77)
54. **IF %CP is LOW AND CP is Sucrose AND IF Velocity is Fast AND IF %CP is LOW-1**	THEN Δ PDI is	LOW (0.75)
55. **IF %CP is LOW AND CP is Sucrose AND IF Velocity is Fast AND IF %CP is MID-2**	THEN Δ PDI is	LOW (0.65)
56. **IF %CP is HIGH AND CP is Sucrose AND IF Velocity is Slow AND IF %CP is MID-3**	THEN Δ PDI is	LOW (1.00)
57. **IF %CP is HIGH AND CP is Sucrose AND IF Velocity is Slow AND IF %CP is LOW-1**	THEN Δ PDI is	LOW (1.00)
58. **IF %CP is HIGH AND CP is Sucrose AND IF Velocity is Slow AND IF %CP is HIGH-4**	THEN Δ PDI is	LOW (0.70)
59. **IF %CP is LOW AND CP is Sucrose AND IF Velocity is Slow AND IF %CP is MID-3**	THEN Δ PDI is	LOW (0.61)
60. **IF %CP is LOW AND CP is Sucrose AND IF Velocity is Slow AND IF %CP is LOW-1**	THEN Δ PDI is	LOW (0.60)
61. **IF %CP is LOW AND CP is Sucrose AND IF Velocity is Slow AND IF %CP is MID-2**	THEN Δ PDI is	LOW (0.50)
62. **IF %CP is HIGH AND CP is Trehalose AND IF Velocity is Fast AND IF %CP is MID-3**	THEN Δ PDI is	LOW (1.00)
63. **IF %CP is LOW AND CP is Trehalose AND IF Velocity is Fast AND IF %CP is MID-3**	THEN Δ PDI is	LOW (0.96)

64. **IF %CP is LOW AND CP is Trehalose AND IF Velocity is Fast AND IF %CP is LOW-1**	THEN Δ PDI is	LOW (0.94)
65. **IF %CP is LOW AND CP is Trehalose AND IF Velocity is Fast AND IF %CP is MID-2**	THEN Δ PDI is	LOW (0.84)
66. **IF %CP is HIGH AND CP is Trehalose AND IF Velocity is Fast AND IF %CP is HIGH-4**	THEN Δ PDI is	LOW (0.69)
67. **IF %CP is HIGH AND CP is Trehalose AND IF Velocity is Slow AND IF %CP is MID-3**	THEN Δ PDI is	LOW (0.88)
68. **IF %CP is LOW AND CP is Trehalose AND IF Velocity is Slow AND IF %CP is MID-3**	THEN Δ PDI is	LOW (0.81)
69. **IF %CP is LOW AND CP is Trehalose AND IF Velocity is Slow AND IF %CP is LOW-1**	THEN Δ PDI is	LOW (0.79)
70. **IF %CP is LOW AND CP is Trehalose AND IF Velocity is Slow AND IF %CP is MID-2**	THEN Δ PDI is	LOW (0.69)
71. **IF %CP is HIGH AND CP is Trehalose AND IF Velocity is Slow AND IF %CP is HIGH-4**	THEN Δ PI is	LOW (0.54)

Table A2.3. Set of combined IF-THEN rules for Δ ZP of the first NFL model. Degree of membership in parentheses.

Rules for Δ ZP		
1. **IF %CP is LOW AND IF CP is Fructose AND Velocity is Fast**	THEN Δ ZP is	LOW (0.51)
2. **IF %CP is HIGH AND IF CP is Fructose AND Velocity is Fast**	THEN Δ ZP is	HIGH (0.67)
3. **IF %CP is LOW AND IF CP is Fructose AND Velocity is Slow**	THEN Δ ZP is	LOW (0.54)
4. **IF %CP is HIGH AND IF CP is Fructose AND Velocity is Slow**	THEN Δ ZP is	HIGH (0.64)
5. **IF %CP is LOW AND IF CP is Glucose AND Velocity is Fast**	THEN Δ ZP is	LOW (0.99)
6. **IF %CP is HIGH AND IF CP is Glucose AND Velocity is Fast**	THEN Δ ZP is	LOW (0.81)
7. **IF %CP is LOW AND IF CP is Glucose AND Velocity is Slow**	THEN Δ ZP is	LOW (0.71)
8. **IF %CP is HIGH AND IF CP is Glucose AND Velocity is Slow**	THEN Δ ZP is	LOW (0.54)
9. **IF %CP is LOW AND IF CP is Lactose AND Velocity is Fast**	THEN Δ ZP is	HIGH (0.56)
10. **IF %CP is HIGH AND IF CP is Lactose AND Velocity is Fast**	THEN Δ ZP is	HIGH (0.74)
11. **IF %CP is LOW AND IF CP is Lactose AND Velocity is Slow**	THEN Δ ZP is	LOW (0.71)
12. **IF %CP is HIGH AND IF CP is Lactose AND Velocity is Slow**	THEN Δ ZP is	LOW (0.54)
13. **IF %CP is LOW AND IF CP is Mannitol AND Velocity is Fast**	THEN Δ ZP is	LOW (0.63)
14. **IF %CP is HIGH AND IF CP is Mannitol AND Velocity is Fast**	THEN Δ ZP is	HIGH (0.55)
15. **IF %CP is LOW AND IF CP is Mannitol AND Velocity is Slow**	THEN Δ ZP is	LOW (0.83)
16. **IF %CP is HIGH AND IF CP is Mannitol AND Velocity is Slow**	THEN Δ ZP is	LOW (0.66)
17. **IF %CP is LOW AND IF CP is Sorbitol AND Velocity is Fast**	THEN Δ ZP is	LOW (0.83)
18. **IF %CP is HIGH AND IF CP is Sorbitol AND Velocity is Fast**	THEN Δ ZP is	LOW (0.66)
19. **IF %CP is LOW AND IF CP is Sorbitol AND Velocity is Slow**	THEN Δ ZP is	LOW (0.80)
20. **IF %CP is HIGH AND IF CP is Sorbitol AND Velocity is Slow**	THEN Δ ZP is	LOW (0.62)
21. **IF %CP is LOW AND IF CP is Sucrose AND Velocity is Fast**	THEN Δ ZP is	LOW (0.77)
22. **IF %CP is HIGH AND IF CP is Sucrose AND Velocity is Fast**	THEN Δ ZP is	LOW (0.59)
23. **IF %CP is LOW AND IF CP is Sucrose AND Velocity is Slow**	THEN Δ ZP is	LOW (0.73)
24. **IF %CP is HIGH AND IF CP is Sucrose AND Velocity is Slow**	THEN Δ ZP is	LOW (0.55)
25. **IF %CP is LOW AND IF CP is Trehalose AND Velocity is Fast**	THEN Δ ZP is	LOW (0.55)
26. **IF %CP is HIGH AND IF CP is Trehalose AND Velocity is Fast**	THEN Δ ZP is	HIGH (0.63)
27. **IF %CP is LOW AND IF CP is Trehalose AND Velocity is Slow**	THEN Δ ZP is	LOW (0.81)
28. **IF %CP is HIGH AND IF CP is Trehalose AND Velocity is Slow**	THEN Δ ZP is	LOW (0.64)

Table A2.4. Set of IF-THEN rules for Δ size of the second NFL model. Degree of membership in parentheses.

Rules for Δ size		
Submodel 1		
1. IF Osmolarity is LOW AND MW_{CP} is LOW	THEN Δ size (nm) is	LOW (1.00)
2. IF Osmolarity is LOW AND MW_{CP} is MID	THEN Δ size (nm) is	HIGH (1.00)
3. IF Osmolarity is LOW AND MW_{CP} is HIGH	THEN Δ size (nm) is	LOW (0.64)
4. IF Osmolarity is MID AND MW_{CP} is LOW	THEN Δ size (nm) is	LOW (0.77)
5. IF Osmolarity is MID AND MW_{CP} is MID	THEN Δ size (nm) is	LOW (1.00)
6. IF Osmolarity is MID AND MW_{CP} is HIGH	THEN Δ size (nm) is	LOW (1.00)
7. IF Osmolarity is HIGH AND MW_{CP} is LOW	THEN Δ size (nm) is	HIGH (0.87)
8. IF Osmolarity is HIGH AND MW_{CP} is MID	THEN Δ size (nm) is	LOW (1.00)
9. IF Osmolarity is HIGH AND MW_{CP} is HIGH	THEN Δ size (nm) is	LOW (1.00)
Submodel 2		
10. IF Speed is Fast AND MW_{CP} is LOW	THEN Δ size (nm) is	LOW (0.77)
11. IF Speed is Fast AND MW_{CP} is MID	THEN Δ size (nm) is	HIGH (1.00)
12. IF Speed is Fast AND MW_{CP} is HIGH	THEN Δ size (nm) is	LOW (0.89)
13. IF Speed is Slow AND MW_{CP} is LOW	THEN Δ size (nm) is	HIGH (0.77)
14. IF Speed is Slow AND MW_{CP} is MID	THEN Δ size (nm) is	LOW (1.00)
15. IF Speed is Slow AND MW_{CP} is HIGH	THEN Δ size (nm) is	LOW (0.81)

Table A2.5. Set of IF-THEN rules for Δ PDI of the second NFL model. Degree of membership in parentheses.

Rules for Δ PDI		
Submodel 1		
1. IF Osmolarity is LOW AND MW_{CP} is LOW	THEN Δ PDI is	LOW (0.67)
2. IF Osmolarity is LOW AND MW_{CP} is MID	THEN Δ PDI is	HIGH (1.00)
3. IF Osmolarity is LOW AND MW_{CP} is HIGH	THEN Δ PDI is	HIGH (0.51)
4. IF Osmolarity is MID AND MW_{CP} is LOW	THEN Δ PDI is	HIGH (0.69)
5. IF Osmolarity is MID AND MW_{CP} is MID	THEN Δ PDI is	LOW (1.00)
6. IF Osmolarity is MID AND MW_{CP} is HIGH	THEN Δ PDI is	HIGH (0.65)
7. IF Osmolarity is HIGH AND MW_{CP} is LOW	THEN Δ PDI is	HIGH (1.00)
8. IF Osmolarity is HIGH AND MW_{CP} is MID	THEN Δ PDI is	LOW (1.00)
9. IF Osmolarity is HIGH AND MW_{CP} is HIGH	THEN Δ PDI is	LOW (1.00)
Submodel 2		
10. IF Speed is Fast	THEN Δ PDI is	LOW (1.00)
11. IF Speed is Slow	THEN Δ PDI is	LOW (0.93)

Table A2.6. Set of IF-THEN rules for Δ ZP of the second NFL model. Degree of membership in parentheses.

Rules for Δ ZP		
Submodel 1		
1. IF Osmolarity is LOW	THEN Δ ZP is	LOW (0.65)
2. IF Osmolarity is HIGH	THEN Δ ZP is	LOW (0.57)

It should be noted that the combination of inputs that led to the highest value of the output are highlighted in blue, while the combination of inputs giving the lowest value are highlighted in red.

STATEMENTS: CONFLICT OF INTERESTS, IMAGE USE, CELL CULTURE AND PUBLISHED CONTENT

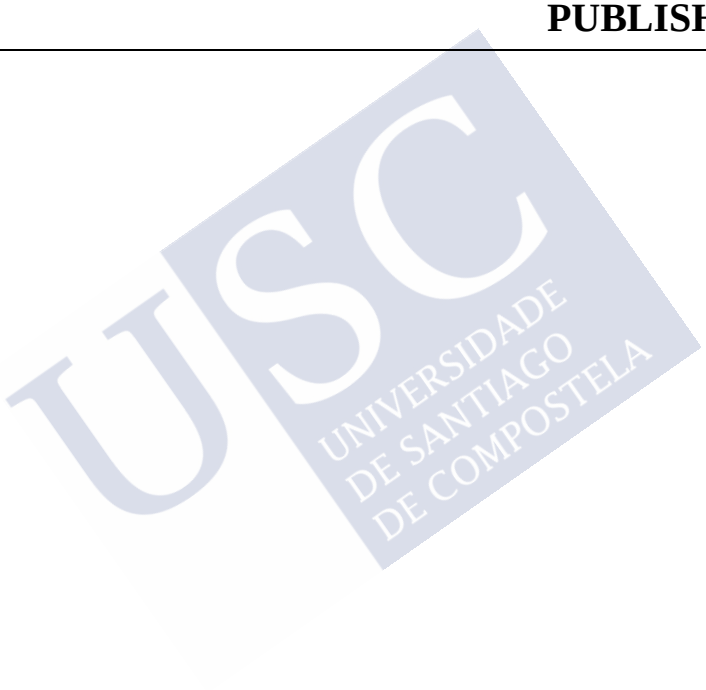

USC
UNIVERSIDADE
DE SANTIAGO
DE COMPOSTELA

CONFLICT OF INTERESTS

The author declares no conflict of interest related with the materials or topics discussed in this work.

IMAGE USE

All the images presented in this manuscript were created by the author of the thesis. In the case of images reused from publications derived from the research developed by the candidate, included outside the published sections, proper citation to the original source can be found at the bottom of the figures.

CELL CULTURE

Cell lines employed in this work were obtained from commercially available resources (American Type Culture Collection, ATCC): THP-1 (ATCC®, TIB-202™) human monocytic cell line, Raw 264.7 (ATCC®, TIB-71™) murine macrophage cell line, Caco-2 (ATCC®, HTB-37™) human colorectal adenocarcinoma cell line. Cells were only used for the research purposes previously specified in this manuscript and were cultured under the conditions recommended by the suppliers.

PUBLISHED CONTENT

Part of this thesis manuscript is a reproduction of publications derived from the research developed by the PhD candidate during her predoctoral period. Published sections along with quality criteria of the publications will be specified below:

List of articles:	1. Introduction-Section B was published as a book chapter. 2. Chapter I was published as a research article. 3. Chapter II was published as a research article.
Title:	1. "Recent advances in solid lipid nanoparticles formulation and clinical applications". 2."Delimiting the knowledge space and the design space of nanostructured lipid carriers through Artificial Intelligence tools". 3. "Rifabutin-loaded Nanostructured lipid Carriers as a Tool in Oral Anti-mycobacterial Treatment of Crohn´s Disease".
Year:	1. 2020. 2. 2018. 3. 2020.
Journal/Book:	1. Nanomaterials for Clinical Applications: Case Studies in Nanomedicines. 2. International Journal of Pharmaceutics. 3. Nanomaterials.
Volume, pages/article number:	1. Pages. 213-247. 2. Volume 553, pages 522-530. 3. Volume 10, article number 2138.

PhD candidate contribution:	1. The contribution of the PhD candidate to this publication consisted in writing the original manuscript corresponding to the sections 1.1. to 1.7, both inclusive, after appropriate scientific literature review. 2. The contribution of the PhD candidate to this publication consisted on work planning, data aquisition, analysis and writing of the original draft. 3. The contribution of the PhD candidate to this publication consisted on work planning and data aquisition, except in the case of TEM and AFM images. In this way, TEM analysis acquisition was performed in UVigo central services, and AFM images were obtained by a contributing author. Besides, the candidate was also responsible for data analysis and writing of the original draft.
Quality indexes:	1. The book "Nanomaterials for Clinical Applications: Case Studies in Nanomedicines" was edited by Costas Demetzos and Natassa Pippa, imprinted by Elsevier, and included in the "Micro and Nano Technology series". Moreover, it was indexed in ScienceDirect. 2. The journal in which Chapter I was published presented an Impact factor of 4.213 in 2018, belonging to quartile 1 in "Pharmacology & Pharmacy" (rank 44/267) and "Pharmacology & Toxicology" (rank 3/276) categories. 3. The journal in which Chapter II was published displayed an Impact factor of 4.324 in 2019, belonging to quartile 1 in "Materials science" category (rank 81/390) and quartile 2 in "Nanoscience & Nanotechnology" (rank 42/103) and "Materials science, multidisciplinary" (rank 89/314) categories.

Ethical considerations:

Introduction-section B and chapter I, have been published as a book chapter and a journal article, respectively, edited by Elsevier. In both cases appropriate permission has been requested, and writen authorization has been obtained.

Chapter II was publised in Nanomaterials, a an open acces MDPI journal. This article has been published under an open access Creative Common CC BY license, and hence, any part of the article may be reused without permission provided that the original article is properly cited. More information relative to MDPI open access information and policy can be found in the following link: https://www.mdpi.com/openaccess.

CHECKLISTS AND PERMISSIONS

USC
UNIVERSIDADE
DE SANTIAGO
DE COMPOSTELA

Checklist for **statistical analysis**

	Yes/No
Type and applicability of test used	
Comparisons of interest are clearly defined	Yes
Name of tests applied are clearly stated.	Yes
All statistical methods identified unambiguously.	Yes
Justification for use of test is given.	Yes
Data meet all assumptions of tests applied (non-normal data sets, small sample sizes)	Yes
Adjustments made for multiple testing is explained.	N/A
Details about the test	
n is reported at the start of the study and for each analysis thereafter.	Yes
Sample size calculation (or justification) is given.	Yes
Alpha level is given for all statistical tests.	Yes
Tests are clearly identified as one or two-tailed.	Yes
Randomization procedures or other ways to eliminate bias in sampling are described.	N/A
Summary of descriptive statistics	
n for each data set is clearly stated	Yes
A clearly labelled measure of center (e.g. mean or median) is given	Yes
A clearly labelled measure of variability (e.g. standard deviation, range, percentiles) is given.	Yes
All numbers following a ± sign are identified as standard errors (s.e.m.) or standard deviations (s.d.).	Yes
Extras	
Any unusual or complex statistical methods are clearly defined and explained.	Yes
Any data exclusions are stated and explained.	N/A
Any discrepancies in the value of n between analyses are clearly explained and justified.	Yes
Data transformations (logarithmic, ….) are explained	Yes
Graphs	
Any distorted effect sizes (e.g. by truncation of y axis) are clearly labelled and justified.	Yes
Error bars in graphs, or confidence intervals, are included, or their absence is explained.	Yes

PhD Student signature

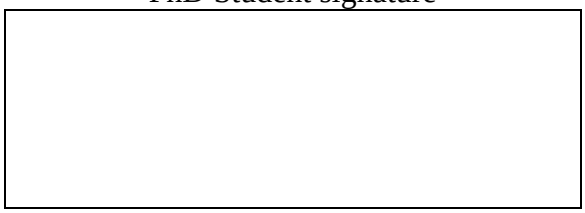

Checklist for recommendations of **Thesis EDI saúde. GENERAL**

Yes-No-N/A		Page
For all Thesis		
Yes	Declaration of potential conflicts of interests	183
Yes	Declaration on the origin and copyright status of non-original figures, with permission if necessary. Include them in the text of each figure	183
Yes	Checklist of statistics adequacy if no other checklists apply.	187
For Thesis involving human experimentation, human samples, or personal data.		
N/A	Declaration on approval by the research ethics committee.	
N/A	Code number of the study.	
N/A	Copy of ethics report	
N/A	Declaration that data are based on anonymous information, and no approval of the ethics committee is needed.	
N/A	If it is an observational study, STROBE checklist.	
For Thesis that include a clinical assay		
N/A	Declaration of its authorization by the Agencia Española de Medicamentos y productos sanitarios.	
N/A	Copy of the authorization	
N/A	CONSORT Checklist	
For Thesis that use embryonic or induced human stem cells		
N/A	Declaration on its authorization	
N/A	Reference of the authorization	
N/A	Copy of the authorization	
For Thesis that include animal experimentation		
N/A	Declaration of its authorization	
N/A	Code number of the authorization of the animal experimentation Project.	
N/A	Register number of the authorized user center if experiments were made in Spain	
N/A	Copy of the capacitation certificate if the experiments were made by the Thesis author.	
N/A	Person, company or service that performed the experiments if applicable.	
N/A	ARRIVE Checklist	

PhD Student signature

ELSEVIER LICENSE TERMS AND CONDITIONS

Dec 18, 2020

This Agreement between University of Santiago de Compostela -- Helena Rouco ("You") and Elsevier ("Elsevier") consists of your license details and the terms and conditions provided by Elsevier and Copyright Clearance Center.

License Number	4971791198823
License date	Dec 18, 2020
Licensed Content Publisher	Elsevier
Licensed Content Publication	Elsevier Books
Licensed Content Title	Nanomaterials for Clinical Applications
Licensed Content Author	Helena Rouco,Patricia Diaz-Rodriguez,Carmen Remuñán-López,Mariana Landin
Licensed Content Date	Jan 1, 2020
Licensed Content Volume	n/a
Licensed Content Issue	n/a
Licensed Content Pages	35
Start Page	213
End Page	247
Type of Use	reuse in a thesis/dissertation
I am an academic or government institution with a full-text subscription to this journal and the audience of the material consists of students and/or employees of this institute?	No
Portion	full chapter
Circulation	10
Format	both print and electronic
Are you the author of this Elsevier chapter?	Yes
Will you be translating?	No
Title	QUALITY-BY-DESIGN APPROACH FOR THE DEVELOPMENT OF LIPID-BASED NANOSYSTEMS FOR ANTI-MYCOBACTERIAL THERAPY
Institution name	University of Santiago de Compostela
Expected presentation date	Feb 2021
Requestor Location	University of Santiago de Compostela Praza Seminario de estudos galegos s/n Santiago de Compostela, 15705 Spain Attn: University of Santiago de Compostela
Publisher Tax ID	GB 494 6272 12
Billing Type	Invoice
Billing Address	University of Santiago de Compostela Praza Seminario de estudos galegos s/n

Santiago de Compostela, Spain 15705
Attn: University of Santiago de Compostela

Total **0.00 EUR**

Terms and Conditions

INTRODUCTION

1. The publisher for this copyrighted material is Elsevier. By clicking "accept" in connection with completing this licensing transaction, you agree that the following terms and conditions apply to this transaction (along with the Billing and Payment terms and conditions established by Copyright Clearance Center, Inc. ("CCC"), at the time that you opened your Rightslink account and that are available at any time at http://myaccount.copyright.com).

GENERAL TERMS

2. Elsevier hereby grants you permission to reproduce the aforementioned material subject to the terms and conditions indicated.
3. Acknowledgement: If any part of the material to be used (for example, figures) has appeared in our publication with credit or acknowledgement to another source, permission must also be sought from that source. If such permission is not obtained then that material may not be included in your publication/copies. Suitable acknowledgement to the source must be made, either as a footnote or in a reference list at the end of your publication, as follows:
"Reprinted from Publication title, Vol /edition number, Author(s), Title of article / title of chapter, Pages No., Copyright (Year), with permission from Elsevier [OR APPLICABLE SOCIETY COPYRIGHT OWNER]." Also Lancet special credit - "Reprinted from The Lancet, Vol. number, Author(s), Title of article, Pages No., Copyright (Year), with permission from Elsevier."
4. Reproduction of this material is confined to the purpose and/or media for which permission is hereby given.
5. Altering/Modifying Material: Not Permitted. However figures and illustrations may be altered/adapted minimally to serve your work. Any other abbreviations, additions, deletions and/or any other alterations shall be made only with prior written authorization of Elsevier Ltd. (Please contact Elsevier's permissions helpdesk here). No modifications can be made to any Lancet figures/tables and they must be reproduced in full.
6. If the permission fee for the requested use of our material is waived in this instance, please be advised that your future requests for Elsevier materials may attract a fee.
7. Reservation of Rights: Publisher reserves all rights not specifically granted in the combination of (i) the license details provided by you and accepted in the course of this licensing transaction, (ii) these terms and conditions and (iii) CCC's Billing and Payment terms and conditions.
8. License Contingent Upon Payment: While you may exercise the rights licensed immediately upon issuance of the license at the end of the licensing process for the transaction, provided that you have disclosed complete and accurate details of your proposed use, no license is finally effective unless and until full payment is received from you (either by publisher or by CCC) as provided in CCC's Billing and Payment terms and conditions. If full payment is not received on a timely basis, then any license preliminarily granted shall be deemed automatically revoked and shall be void as if never granted. Further, in the event that you breach any of these terms and conditions or any of CCC's Billing and Payment terms and conditions, the license is automatically revoked and shall be void as if never granted. Use of materials as described in a revoked license, as well as any use of the materials beyond the scope of an unrevoked license, may constitute copyright infringement and publisher reserves the right to take any and all action to protect its copyright in the materials.
9. Warranties: Publisher makes no representations or warranties with respect to the licensed material.
10. Indemnity: You hereby indemnify and agree to hold harmless publisher and CCC, and their respective officers, directors, employees and agents, from and against any and all claims arising out of your use of the licensed material other than as specifically authorized pursuant to this license.
11. No Transfer of License: This license is personal to you and may not be sublicensed, assigned, or transferred by you to any other person without publisher's written permission.
12. No Amendment Except in Writing: This license may not be amended except in a writing signed by both parties (or, in the case of publisher, by CCC on publisher's behalf).
13. Objection to Contrary Terms: Publisher hereby objects to any terms contained in any purchase order, acknowledgment, check endorsement or other writing prepared by you, which terms are inconsistent with these terms and conditions or CCC's Billing and Payment terms and conditions. These terms and conditions, together with CCC's Billing and Payment terms and conditions (which are incorporated herein), comprise the entire agreement between you and publisher (and CCC) concerning this licensing transaction. In the event of any conflict between your obligations established by these terms and conditions and those established by CCC's Billing and Payment terms and conditions, these terms and conditions shall control.
14. Revocation: Elsevier or Copyright Clearance Center may deny the permissions described in this License at their sole discretion, for any reason or no reason, with a full refund payable to you. Notice of such denial will be made using the contact information provided by you. Failure to receive such notice will not alter or invalidate the denial. In no event will Elsevier or Copyright Clearance Center be responsible or liable for any costs, expenses or damage incurred by you as a result of a denial of your permission request, other than a refund of the amount(s) paid by you to Elsevier and/or Copyright Clearance Center for denied permissions.

LIMITED LICENSE

The following terms and conditions apply only to specific license types:
15. **Translation**: This permission is granted for non-exclusive world **English** rights only unless your license was granted for translation rights. If you licensed translation rights you may only translate this content into the languages you requested. A professional translator must perform all translations and reproduce the content word for word preserving the integrity of the article.

16. **Posting licensed content on any Website**: The following terms and conditions apply as follows: Licensing material from an Elsevier journal: All content posted to the web site must maintain the copyright information line on the bottom of each image; A hyper-text must be included to the Homepage of the journal from which you are licensing at http://www.sciencedirect.com/science/journal/xxxxx or the Elsevier homepage for books at http://www.elsevier.com; Central Storage: This license does not include permission for a scanned version of the material to be stored in a central repository such as that provided by Heron/XanEdu.
Licensing material from an Elsevier book: A hyper-text link must be included to the Elsevier homepage at http://www.elsevier.com . All content posted to the web site must maintain the copyright information line on the bottom of each image.

Posting licensed content on Electronic reserve: In addition to the above the following clauses are applicable: The web site must be password-protected and made available only to bona fide students registered on a relevant course. This permission is granted for 1 year only. You may obtain a new license for future website posting.
17. **For journal authors:** the following clauses are applicable in addition to the above:
Preprints:
A preprint is an author's own write-up of research results and analysis, it has not been peer-reviewed, nor has it had any other value added to it by a publisher (such as formatting, copyright, technical enhancement etc.).
Authors can share their preprints anywhere at any time. Preprints should not be added to or enhanced in any way in order to appear more like, or to substitute for, the final versions of articles however authors can update their preprints on arXiv or RePEc with their Accepted Author Manuscript (see below).
If accepted for publication, we encourage authors to link from the preprint to their formal publication via its DOI. Millions of researchers have access to the formal publications on ScienceDirect, and so links will help users to find, access, cite and use the best available version. Please note that Cell Press, The Lancet and some society-owned have different preprint policies. Information on these policies is available on the journal homepage.
Accepted Author Manuscripts: An accepted author manuscript is the manuscript of an article that has been accepted for publication and which typically includes author-incorporated changes suggested during submission, peer review and editor-author communications.
Authors can share their accepted author manuscript:

- immediately
  - via their non-commercial person homepage or blog
  - by updating a preprint in arXiv or RePEc with the accepted manuscript
  - via their research institute or institutional repository for internal institutional uses or as part of an invitation-only research collaboration work-group
  - directly by providing copies to their students or to research collaborators for their personal use
  - for private scholarly sharing as part of an invitation-only work group on commercial sites with which Elsevier has an agreement
- After the embargo period
  - via non-commercial hosting platforms such as their institutional repository
  - via commercial sites with which Elsevier has an agreement

In all cases accepted manuscripts should:

- link to the formal publication via its DOI
- bear a CC-BY-NC-ND license - this is easy to do
- if aggregated with other manuscripts, for example in a repository or other site, be shared in alignment with our hosting policy not be added to or enhanced in any way to appear more like, or to substitute for, the published journal article.

Published journal article (JPA): A published journal article (PJA) is the definitive final record of published research that appears or will appear in the journal and embodies all value-adding publishing activities including peer review co-ordination, copy-editing, formatting, (if relevant) pagination and online enrichment.
Policies for sharing publishing journal articles differ for subscription and gold open access articles:
Subscription Articles: If you are an author, please share a link to your article rather than the full-text. Millions of researchers have access to the formal publications on ScienceDirect, and so links will help your users to find, access, cite, and use the best available version.
Theses and dissertations which contain embedded PJAs as part of the formal submission can be posted publicly by the awarding institution with DOI links back to the formal publications on ScienceDirect.
If you are affiliated with a library that subscribes to ScienceDirect you have additional private sharing rights for others' research accessed under that agreement. This includes use for classroom teaching and internal training at the institution (including use in course packs and courseware programs), and inclusion of the article for grant funding purposes.
Gold Open Access Articles: May be shared according to the author-selected end-user license and should contain a CrossMark logo, the end user license, and a DOI link to the formal publication on ScienceDirect.
Please refer to Elsevier's posting policy for further information.
18. **For book authors** the following clauses are applicable in addition to the above: Authors are permitted to place a brief summary of their work online only. You are not allowed to download and post the published electronic version of your chapter,

nor may you scan the printed edition to create an electronic version. **Posting to a repository:** Authors are permitted to post a summary of their chapter only in their institution's repository.

19. **Thesis/Dissertation**: If your license is for use in a thesis/dissertation your thesis may be submitted to your institution in either print or electronic form. Should your thesis be published commercially, please reapply for permission. These requirements include permission for the Library and Archives of Canada to supply single copies, on demand, of the complete thesis and include permission for Proquest/UMI to supply single copies, on demand, of the complete thesis. Should your thesis be published commercially, please reapply for permission. Theses and dissertations which contain embedded PJAs as part of the formal submission can be posted publicly by the awarding institution with DOI links back to the formal publications on ScienceDirect.

Elsevier Open Access Terms and Conditions

You can publish open access with Elsevier in hundreds of open access journals or in nearly 2000 established subscription journals that support open access publishing. Permitted third party re-use of these open access articles is defined by the author's choice of Creative Commons user license. See our open access license policy for more information.

Terms & Conditions applicable to all Open Access articles published with Elsevier:

Any reuse of the article must not represent the author as endorsing the adaptation of the article nor should the article be modified in such a way as to damage the author's honour or reputation. If any changes have been made, such changes must be clearly indicated.

The author(s) must be appropriately credited and we ask that you include the end user license and a DOI link to the formal publication on ScienceDirect.

If any part of the material to be used (for example, figures) has appeared in our publication with credit or acknowledgement to another source it is the responsibility of the user to ensure their reuse complies with the terms and conditions determined by the rights holder.

Additional Terms & Conditions applicable to each Creative Commons user license:

CC BY: The CC-BY license allows users to copy, to create extracts, abstracts and new works from the Article, to alter and revise the Article and to make commercial use of the Article (including reuse and/or resale of the Article by commercial entities), provided the user gives appropriate credit (with a link to the formal publication through the relevant DOI), provides a link to the license, indicates if changes were made and the licensor is not represented as endorsing the use made of the work. The full details of the license are available at http://creativecommons.org/licenses/by/4.0.

CC BY NC SA: The CC BY-NC-SA license allows users to copy, to create extracts, abstracts and new works from the Article, to alter and revise the Article, provided this is not done for commercial purposes, and that the user gives appropriate credit (with a link to the formal publication through the relevant DOI), provides a link to the license, indicates if changes were made and the licensor is not represented as endorsing the use made of the work. Further, any new works must be made available on the same conditions. The full details of the license are available at http://creativecommons.org/licenses/by-nc-sa/4.0.

CC BY NC ND: The CC BY-NC-ND license allows users to copy and distribute the Article, provided this is not done for commercial purposes and further does not permit distribution of the Article if it is changed or edited in any way, and provided the user gives appropriate credit (with a link to the formal publication through the relevant DOI), provides a link to the license, and that the licensor is not represented as endorsing the use made of the work. The full details of the license are available at http://creativecommons.org/licenses/by-nc-nd/4.0. Any commercial reuse of Open Access articles published with a CC BY NC SA or CC BY NC ND license requires permission from Elsevier and will be subject to a fee.

Commercial reuse includes:

- Associating advertising with the full text of the Article
- Charging fees for document delivery or access
- Article aggregation
- Systematic distribution via e-mail lists or share buttons

Posting or linking by commercial companies for use by customers of those companies.

20. **Other Conditions**:

v1.10

Questions? customercare@copyright.com or +1-855-239-3415 (toll free in the US) or +1-978-646-2777.

Delimiting the knowledge space and the design space of nanostructured lipid carriers through Artificial Intelligence tools

Author:
Helena Rouco,Patricia Diaz-Rodriguez,Santiago Rama-Molinos,Carmen Remuñán-López,Mariana Landin

Publication: International Journal of Pharmaceutics

Publisher: Elsevier

Date: 20 December 2018

USC
UNIVERSIDADE
DE SANTIAGO
DE COMPOSTELA

nanomaterials

MDPI

Article

Rifabutin-Loaded Nanostructured Lipid Carriers as a Tool in Oral Anti-Mycobacterial Treatment of Crohn's Disease

Helena Rouco [1], Patricia Diaz-Rodriguez [2], Diana P. Gaspar [3], Lídia M. D. Gonçalves [3], Miguel Cuerva [4], Carmen Remuñán-López [5], António J. Almeida [3] and Mariana Landin [1,*]

1 R+D Pharma Group (GI-1645), Strategic Grouping in Materials (AEMAT), Department of Pharmacology, Pharmacy and Pharmaceutical Technology, Faculty of Pharmacy, Universidade de Santiago de Compostela-Campus Vida, 15782 Santiago de Compostela, Spain; helena.rouco@rai.usc.es

2 Drug Delivery Systems Group, Department of Chemical Engineering and Pharmaceutical Technology, School of Sciences, Universidad de La Laguna (ULL), Campus de Anchieta, 38200 La Laguna (Tenerife), Spain; pdiarodr@ull.edu.es

3 Research Institute for Medicines (iMed.ULisboa), Faculty of Pharmacy, Universidade de Lisboa, 1649-003 Lisbon, Portugal; diana.gaspar89@gmail.com (D.P.G.); lgoncalves@ff.ulisboa.pt (L.M.D.G.); aalmeida@ff.ulisboa.pt (A.J.A.)

4 Department of Physical Chemistry, Nanomag laboratory, Universidade de Santiago de Compostela-Campus Vida, 15782 Santiago de Compostela, Spain; miguelcvidales@gmail.com

5 Nanobiofar Group (GI-1643), Department of Pharmacology, Pharmacy and Pharmaceutical Technology, Faculty of Pharmacy, Universidade de Santiago de Compostela-Campus Vida, 15782 Santiago de Compostela, Spain; mdelcarmen.remunan@usc.es

* Correspondence: m.landin@usc.es

Received: 29 September 2020; Accepted: 26 October 2020; Published: 27 October 2020

Abstract: Oral anti-mycobacterial treatment of Crohn's disease (CD) is limited by the low aqueous solubility of drugs, along with the altered gut conditions of patients, making uncommon their clinical use. Hence, the aim of the present work is focused on the in vitro evaluation of rifabutin (RFB)-loaded Nanostructured lipid carriers (NLC), in order to solve limitations associated to this therapeutic approach. RFB-loaded NLC were prepared by hot homogenization and characterized in terms of size, polydispersity, surface charge, morphology, thermal stability, and drug payload and release. Permeability across Caco-2 cell monolayers and cytotoxicity and uptake in human macrophages was also determined. NLC obtained were nano-sized, monodisperse, negatively charged, and spheroidal-shaped, showing a suitable drug payload and thermal stability. Furthermore, the permeability profile, macrophage uptake and selective intracellular release of RFB-loaded NLC, guarantee an effective drug dose administration to cells. Outcomes suggest that rifabutin-loaded NLC constitute a promising strategy to improve oral anti-mycobacterial therapy in Crohn's disease.

Keywords: rifabutin; nanostructured lipid carriers; cell uptake; Caco-2 cells; oral administration; Crohn's disease

1. Introduction

Crohn's disease (CD) is a chronic inflammatory bowel condition with a higher predominance in industrialized countries, principally in Western Europe and North America [1]. The disease is characterized by the presence of outbreaks followed by remission periods [1,2], and although symptomatology is variable, diarrhea, abdominal pain, nausea, vomiting, and weight loss are usually involved [1]. The inflammatory process is usually transmural, involving any region of the digestive tract, affecting distal ileum and colon mainly [1,2].

48. Bain, C.C.; Mowat, A.M. Intestinal macrophages–specialised adaptation to a unique environment. *Eur. J. Immunol.* **2011**, *41*, 2494–2498. [CrossRef] [PubMed]
49. Grès, M.-C.; Julian, B.; Bourrié, M.; Meunier, V.; Roques, C.; Berger, M.; Boulenc, X.; Berger, Y.; Fabre, G. Correlation between oral drug absorption in humans, and apparent drug permeability in TC-7 cells, a human epithelial intestinal cell line: Comparison with the parental Caco-2 cell line. *Pharm. Res.* **1998**, *15*, 726–733. [CrossRef]

USC
UNIVERSIDADE
DE SANTIAGO
DE COMPOSTELA